Analysis of temporal variations of gravimetric tidal parameters

Zur Erlangung des akademischen Grades einer

DOKTORIN DER NATURWISSENSCHAFTEN

der KIT-Fakultät für

Bauingenieur-, Geo- und Umweltwissenschaften
des Karlsruher Instituts für Technologie (KIT)

genehmigte

DISSERTATION

von

Dipl.-Geophys. Eva Luise Schroth

aus Heidelberg

Tag der mündlichen Prüfung: 24.10.2019

Referent: Prof. Dr.-Ing. Dr. h.c. Bernhard Heck
Korreferent: Prof. Dr. rer. nat. Maik Thomas

Karlsruhe (2019)

Abstract

Variations of the tidal parameters with periods of several months to years are observed globally in all tidal wave groups. These variations are caused by small changes of the tidal amplitudes (e.g. $0.1\frac{nm}{s^2}$ for M2) which are significant since superconducting gravimeters (SG) produce data of unprecedented accuracy. The tidal parameters represent the response of the Earth to tidal forcing and therefore, contain information about its elastic properties. However, as the solid Earth is not expected to change its properties within short time scales of months or a few years and numarical effects have been excluded, other causes for the tidal parameter variations like model errors or atmospheric and oceanic loading have to be considered. In this thesis, these causes, especially the influence of loading, are studied quantitatively under the usage of model data describing the physical effects assumed to be responsible for the variations of the tidal parameters.

The influence of loading was investigated by calculating loading time series from ocean models or using the loading time series provided by the Atmospheric attraction computation service (Atmacs) and adding this signal to synthetic body tides. The resulting signal was analysed with moving window tidal analysis (MWA) in the same way as the measured data. If the time series describes the loading realistically the tidal parameters will show similar variations as the tidal parameters obtained from measured data. The synthetic body tides are calculated with the same body tide model that is used in the analysis; therefore, all variations have to be caused by the added loading time series. This approach is called synthetic data MWA in the following.

The main focus of this thesis is on the tidal parameters of the K1 and M2 wave groups.

The tidal parameters of the K1 wave group vary with annual and semi-annual periods. Not only loading but also model errors can cause variations of the tidal parameters, which is shown by the reduction of the variations of the K1 tidal parameters of up to 40% when a more recent model for the Free Core Nutation (resonance period of $T_{FCN} = 431.37$ sidereal days) is used in the analysis.

The S1 harmonic, which is part of the K1 wave group, is influenced by the loading of the S1 radiation tide in the atmosphere. For the same station, corrections of the measured gravity data with Atmacs, which reduces the variation of the K1 tidal parameters by up to 50%, and synthetic data MWA with Atmacs, which cause annual variations of the K1 tidal parameters of the correct order of magnitude, were introduced. These results show that a part of the temporal variations of the tidal parameters is caused by the loading of the atmosphere. Synthetic data MWA with Atmacs and loading calculated with the Ocean model of circulation and tides (OMCT) indicate that there is also an influence of ocean loading.

The annual variation of the tidal parameters of the M2 wave group is probably caused by the loading of an annually varying M2 amplitude in the ocean. This was investigated based on sea surface heights from five nonstationary, nonlinear ocean models, the Atlantic real-time ocean forecast system (ARTOFS, restricted to the North Atlantic), Stormtide, OMCT, the HYCOM global tides model (HGT) and a model for the North Sea (North Sea model, restricted to the North Sea), which potentially describe the annual variation of the M2 ocean tide.

In the synthetic data MWA, three of the five ocean models, ARTOFS, Stormtide and HGT, produce annual variations of the M2 tidal parameters of the correct period and the correct order of magnitude (10^{-4} for the gravimetric factor and $0.01°$ for the phase at the Central European SGs). However, the results differ from each other and from the results obtained from measurements, which shows that the models contain the principle mechanisms but do not yet describe the annual variations of the M2 amplitude realistically.

The annual variation of the M2 tidal parameters obtained with the OMCT model is an order of magnitude lower than the results from measurements. This result is most likely caused by the low spatial resolution of the model grid. The North Sea model does not cause annual variations; there are indications that this is due to a missing forcing of the annual variation of the M2 amplitude at the model boundaries.

An investigation with Stormtide shows that not only the very close coastal area but distant ocean regions contribute significantly to the annual variation of the M2 tidal parameters. Accordingly, the influence of the annual variation of the M2 amplitude on stations has to be studied on a global scale.

Synthetic data MWA with Atmacs and OMCT indicate that the variations of the O1 tidal parameters are caused by influences of the atmosphere and oceans, but further investigations are needed, whereas their influence on the S2 tidal parameters is more evident.

An investigation of another possible model error was made by using recent model values for the higher-degree harmonics in the analysis, but this caused no significant changes of the tidal parameter variations of the Q1, M1, 2N2, N2 and L2 wave groups, possibly affected by higher-degree harmonics. Synthetic data MWA with OMCT show a high similarity of the tidal parameters of 2N2, N2 and L2 obtained with synthetic and measured data. The ocean model has no higher-degree harmonics in its forcing. Therefore, these harmonics are not present in the loading; this means that the loading for the higher-degree harmonics in the measured data has to be much smaller than for degree 2 harmonics with similar frequency.

These results show that the variations of the tidal parameters of many wave groups are caused by loading contributions. In this thesis it is the first time quantitatively shown that the annual variation of the M2 tidal parameters can be explained by ocean loading. The ocean models used here do not (yet) describe the annual variation of the M2 amplitude accurately enough to correct gravity data with the corresponding loading time series, but as SGs are sensitive to the annual variations of the M2 amplitude in the oceans on a global scale in a high temporal resolution, gravity data can provide highly accurate, observational

data of small effects in the oceans. These observations can for example be used as a validation data set for ocean models with respect to annual variation of M2 in the oceans.

Zusammenfassung

Variationen von Gezeitenparametern mit Perioden von einigen Monaten bis mehreren Jahren werden auf dem ganzen Globus beobachtet. Diese werden von kleinen zeitabhängigen Änderungen der Gezeitenamplituden verursacht (z.B. 0.1 $\frac{\mathrm{nm}}{\mathrm{s}^2}$ bei M2), die durch die hohe Genauigkeit von supraleitenden Gravimetern (SG) messbar sind. Die Gezeitenparameter beschreiben die Reaktion der Erde auf die Anregung durch die Gezeitenkräfte und enthalten daher Informationen über ihre elastischen Eigenschaften. Dass die Erde ihre Eigenschaften auf kurzen Zeitskalen von Monaten bis einigen Jahren ändert, ist unwahrscheinlich. Nachdem numerische Effekte ausgeschlossen werden konnten, müssen Modellfehler oder die Auflast von Atmosphäre und Ozeanen als Ursache in Betracht gezogen werden. Diese Ursachen, insbesondere Einflüsse der Auflast, werden in dieser Arbeit quantitativ mit Hilfe von Daten untersucht, die die physikalischen Effekte, die die Variationen der Gezeitenparameter verursachen, potentiell enthalten.

Zur Untersuchung der Auflast als Ursache werden Auflastzeitreihen aus Ozeanmodellen berechnet bzw. die Zeitreihen, die vom Atmospheric attraction computation service (Atmacs) zur Verfügung gestellt werden, verwendet. Diese werden zu synthetischen Gezeiten der festen Erde (Erdgezeiten i. F.) addiert und das resultierende Signal genauso wie die Messdaten in einer gleitenden Gezeitenanalyse (moving window tidal analysis, MWA) analysiert. Falls die Auflastzeitreihe den entsprechenden Auflasteffekt realistisch beschreibt, treten ähnliche Variationen auf wie bei den aus Messdaten bestimmten Gezeitenparametern. Die synthetischen Erdgezeiten werden mit dem gleichen Erdgezeitenmodell, das auch zur Analyse verwendet wird, berechnet. Daher kann die resultierende, aus synthetischen Daten bestimmte Variation der Gezeitenparameter eindeutig der Auflastzeitreihe zugeordnet werden. Dieser Ansatz wird i. F. synthetic data MWA genannt. Das Hauptaugenmerk dieser Arbeit liegt auf den Gezeitenparametern von K1 und M2.

Die Gezeitenparameter der K1-Wellengruppe variieren mit jährlicher und halbjährlicher Periode. Neben den Auflasten können auch Modellfehler Variationen der Gezeitenparameter verursachen, was eine Reduktion der K1-Gezeitenparameter von bis zu 40% zeigt, die mit einem aktuelleren Modell für die Free Core Nutation (Resonanzperiode $T_{FCN} = 431.37$ siderische Tage) erreicht wird.

Die S1-Tide, die innerhalb der K1-Wellengruppe liegt, wird durch die Auflast der atmosphärischen Strahlungsgezeiten beeinflusst. Die Korrektur der Messdaten mit Atmacs, die die Variation der K1-Gezeitenparameter um bis zu 50% reduziert und die synthetic data MWA, die jährliche Variationen in der richtigen Größenordnung erzeugt, werden für die selben SGs durchgeführt und zeigen, dass die Atmosphäre einen Teil der Variationen verursacht. Zusätzlich weisen die Ergebnisse einer synthetic data MWA mit Atmacs und

der aus dem OMCT-Ozeanmodell (Ocean model for circulation and tides) berechneten Auflast auf die Ozeanauflast als Ursache hin.

Eine mögliche Ursache für die jährliche Variation der M2-Gezeitenparameter ist die Auflast der jährlichen Variation der M2-Amplitude in den Ozeanen. Dies wird mit fünf nicht-stationären, nichtlinearen Ozeanmodellen, dem Atlantic real-time ocean forecast system (ARTOFS, beschränkt auf dem Nordatlantik), dem Stormtide-Modell, dem OMCT-Modell, dem HYCOM global tides model (HGT) und einem Modell für die Nordsee (Nordseemodell) untersucht, die potenziell in der Lage sind die Variation der M2-Amplitude im Ozean zu beschreiben.

Für drei der fünf Modelle, ARTOFS, Stormtide und HGT, ergibt die synthetic data MWA zeitliche Variationen der M2-Gezeitenparameter, die die richtige Periode und Größenordnung aufweisen. Allerdings deuten die Unterschiede der Modelle untereinander und zu den Ergebnissen aus Messdaten darauf hin, dass die Modelle die beteiligten Mechanismen zwar prinzipiell beinhalten, aber noch nicht in der Lage sind, die Variation der M2-Amplitude in den Ozeanen realistisch zu beschreiben. Die zeitlichen Variationen der M2-Amplitude, die man mit OMCT erhält, sind eine Größenordnung zu klein, was wahrscheinlich auf die grobe räumliche Auflösung des Modells zurückzuführen ist. Das Nordseemodell erzeugt keine Variationen mit jährlicher Amplitude, möglicherweise weil die jährlichen Variationen an den Modellrändern nicht angeregt werden.

Eine Untersuchung mit Stormtide zeigt, dass neben den nahen Küstengebieten auch entfernte Regionen signifikant zu den zeitlichen Variationen der M2-Gezeitenparameter beitragen. Entsprechend muss der Einfluss der jährlichen Variation der M2-Amplitude im Ozean an einer Station im globalem Maßstab berücksichtigt werden.

Die Untersuchungen mit der synthetic data MWA liefern Hinweise darauf, dass auch die Variationen der O1-Gezeitenparameter von ozeanischen und atmosphärischen Auflasten herrühren könnten, was allerdings weiterer Untersuchungen bedarf, wohingegen der Einfluss der Auflasten auf die S2-Gezeitenparameter offensichtlich ist.

Weitere mögliche Modellfehler, die Variationen der Gezeitenparameter von Q1, M1, 2N2, N2 und L2 verursachen könnten, wurden durch die Verwendung aktueller, theoretischer Werte für Tiden höherer Grade ausgeschlossen, da die Änderung der Werte keine signifikante Änderung der Variationen der Gezeitenparameter der genannten Wellengruppen ergab. Die synthetic data MWA mit OMCT resultiert hingegen in sehr ähnlichen Variationen der Gezeitenparameter von 2N2, N2 und L2 aus gemessenen und synthetischen Daten. OMCT enthält keine Tiden höherer Grade im Antrieb, was bedeutet, dass die Auflast der Tiden höherer Grade in den Messdaten deutlich kleiner sein muss als die Auflast von Tiden 2. Grades mit ähnlichen Frequenzen.

Diese Ergebnisse zeigen, dass die Variationen der Gezeitenparameter vieler Wellengruppen von Auflasteffekten verursacht werden. In dieser Arbeit wird zum ersten Mal quantitativ gezeigt, dass die jährliche Variation der M2-Gezeitenparameter durch Ozeanauflast erklärt werden kann. Die verwendeten Ozeanmodelle beschreiben die jährliche Variation der M2-Amplitude in den Ozeanen (noch) nicht genau genug, um Schweredaten mit den

dazugehörigen Auflastzeitreihen zu korrigieren. Da aber SGs in globalem Maßstab sensitiv für diese Variationen sind, können sie sehr genaue Beobachtungsdaten kleiner Effekte in den Ozeanen liefern. Diese Daten können zum Beispiel verwendet werden um Ozeanmodelle hinsichtlich der jährlichen Variation der M2-Amplitude in den Ozeanen zu validieren.

Contents

Appendices

Chapter 1.

Introduction

The solid Earth deforms due to tidal forces. The tidal signal measured on the Earth therefore contains information about the elastic properties of the Earth. This information about the Earth makes the Earth tide signal interesting for Earth Sciences. The Earth tides can be measured among others in tilt, strain and gravity. The signals are usually investigated with tidal analysis, in which the measured signal is compared to the forcing signal by a least-squares adjustment. A widely used program for tidal analysis is ETERNA (Wenzel, 1996). An amplitude or amplitude factor (depending on the regarded measuring quantity) and phase are estimated. Whereas the amplitude gives the tidal amplitude of the regarded measuring quantity, the amplitude factor shows how much the amplitude is increased or reduced by the response of the solid Earth in the regarded measuring quantity. The phase shows whether the response of the Earth leads or lags the forcing signal. Unfortunately, these tidal parameters, amplitude and phase, cannot be estimated for each tidal frequency because of the restricted frequency resolution (Munk and Cartwright, 1966). Usually, wave groups are used which sum the signals of the tidal frequencies in a defined frequency band under the assumption that the response of the Earth is similar for all frequencies within the wave group.

At the beginning of solid Earth tide research, Earth tide observations helped to reject certain ideas about the structure of the Earth, for instance the concept of an almost completely molten interior. This concept could not explain the observed motion of the Earth's surface (Agnew, 2005). Another effect that could be observed for the first time by Melchior (1966) through its influence on the diurnal tides was the Free Core Nutation (FCN), a resonance of the fluid Earth core. However, smaller effects in the response of the solid Earth (for example the Free Inner Core Nutation, a resonance of the Earth's inner core, only observed with Very Long Baseline Interferometry (VLBI) yet, Mathews et al. 2002) cannot easily be studied, as at some tidal frequencies influences of other phenomena with similar frequencies as the tidal forcing occur and superimpose the solid Earth tide signal. These influences can be induced by the atmosphere (e.g. Volland 1997; Warburton and Goodkind 1977), the oceans (e.g. Farrell 1972; Jentzsch 1997) or hydrology (e.g. Bonatz 1967; Kroner 2001). In recent years, especially these superimposed effects have often been studied in order to correct gravity observations but also in order to investigate these superimposed effects themselves. In the latter case, of course not only tidal frequencies are taken into consideration.

1.1. Previous work on temporal variations of gravimetric factor and phase

The temporal behaviour of tidal parameters is investigated with moving window tidal analysis (MWA). For an MWA, tidal analyses are made for shorter time windows out of a longer data set and the results are displayed over time.

With MWA time-dependent tidal parameters from tilt and strain measurements can be obtained which are used for searching changes in the response of the Earth's crust due to stress-induced changes of the elastic properties in tectonically active fault areas. A numerical study of the influence of an elastic dilatant inclusion on strain and tilt tides was made by Beaumont and Berger (1974). Studies of tidal parameters obtained from measured strain data were made, for example, by Mukai and Fujimori (2001) and Omura et al. (2001). Tidal parameters from measured tilt data were also studied by Westerhaus (1997) and Westerhaus and Zschau (2001). They used time windows of 60 days for MWA of tilt measurements and observed periodic variations of the tidal parameters of M2 with annual period. However, tectonically induced changes of the tidal tilt response are not expected to occur periodically. Other local effects such as a lateral inhomogeneous, poroelastic response due to pore pressure changes in the rock which possibly occur periodic were discussed as possible reason. However, there is no study that could confirm tectonic stresses or other local effects as causes for the periodic variations of the tidal parameters.

Other causes have to be considered. Baker and Alcock (1983) studied temporal variations of tidal parameters obtained from tiltmeters and tide gauges in Great Britain. The tidal parameters from these tilt and tide gauge measurements showed a similar periodicity. Similar observations were made in Canada by Peters and Beaumont (1987). Both studies stated that ocean loading can cause the variations of the tidal parameters. Baker and Alcock (1983) additionally investigated the tidal parameter of K1 and S2 and hypothesised that their variations may be caused by atmospheric loading. These studies indicate that effects whose origin is not the solid Earth tide, but that occur with tidal periods, possibly cause variations of the observed tidal parameters.

In contrast to tilt and strain which can be influenced e.g. by faults or pore pressure changes, gravity measurements are insensitive to such local effects. Gravity is however also influenced by atmospheric and oceanic loading (e.g. Farrell 1972; Jentzsch 1997; Klügel and Wziontek 2009; Warburton and Goodkind 1977). The term loading, in this thesis, denotes the combined gravity effects of deformation of the solid Earth and the Newtonian attraction due to the mass load. At all stations where the temporal behaviour of the gravimetric factor and phase was investigated, variations were observed which were periodic for some tidal frequencies (e.g. Calvo et al. 2014; Meurers 2004; Meurers et al. 2016; Sato et al. 2004; Schroth et al. 2018). The gravimetric factor and phase, especially if they are obtained from superconducting gravimeter (SG) stations located close to each other (e.g. Meurers et al. 2016; Schroth et al. 2018), show similarities which indicate that the gravity at those stations is influenced by the same source.

This thesis focuses on the causes for the temporal variations of the K1 and M2 gravimetric

factors and phases obtained from SG data. Therefore, the variations of the gravimetric factors and phases of K1 and M2 are described in individual chapters and sections, whereas other tidal frequencies are summarised. This structure is used throughout the thesis. In the following the previous work which gives indications for possible causes of these tidal parameter variations are presented in detail.

K1

The K1 gravimetric factor and phase vary with semi-annual and annual periods. There are not many studies which focus on K1, although K1 has the largest amplitude in the diurnal tidal band. The reason is that K1 and the harmonics, which cannot be resolved from K1 in short time windows, are influenced by many different effects, for example by atmospheric and oceanic loading. It is therefore difficult to separate the contribution of the solid Earth from other contributions.

The variation of the K1 gravimetric factor and phase can almost completely be explained by the deviations of the amplitude ratios and phase differences of the five main harmonics (P1, S1, K1, Ψ1 and Φ1, represented by the smaller wave groups) from the expectations of the model on which the tidal analysis is based (Schroth, 2013).

A well-known phenomenon is the FCN resonance (e.g. Zürn 1997) which makes the gravimetric factors and phases in the diurnal band frequency-dependent. The resonance frequency is close to the K1 frequency, and K1 as well as the neighbouring harmonics (see above) are strongly influenced by this effect. During the estimation of the gravimetric factors and phases the frequency dependence of the gravimetric factor and phase caused by the FCN is taken into account by a model. This model is based on the Wahr-Dehant-Zschau model (Dehant, 1987) in which an FCN period of $T_{FCN} = 459.25$ sidereal days (si. d.) is assumed. Recent studies with VLBI estimated a FCN period of $T_{FCN} = (431.18 \pm 0.1)$ si. d. (Krásná et al., 2013). This means that the tidal analysis in ETERNA is based on an outdated FCN model.

Additionally, another effect occurs at the S1 frequency. The S1 frequency corresponds to the solar day. Effects with the same frequency occur in the atmosphere, driven by the heating due to the radiation of the Sun, and can cause gravity changes (radiation tides, e.g. Volland 1997). Atmospheric effects are often taken into account by adjusting the measured air pressure to the gravity measurements (Warburton and Goodkind, 1977), but this does not remove the complete atmospheric signal (Klügel and Wziontek, 2009) and does only account for effects which are represented by the air pressure. An extension of the atmosphere, for example due to heating accompanied by the corresponding change of the density, causes a change in gravity because the atmospheric masses are distributed differently relative to the gravimeter, but the pressure stays the same. These gravity changes possibly cause a deviation of the S1 gravity contribution from the expectations of the model used in the analysis and causes a variation of the K1 gravimetric factor and phase.

An additional influence may arise from the oceans. Ocean loading contributes to all

frequencies in the K1 group. The influence of ocean loading on tilt measurements was studied by Baker and Alcock (1983). They observed a variation of typically 30% of the amplitude of K1 and 15° in the phase. In my opinion, the periods are difficult to estimate as they had only one year of data available. The harmonic analysis of a one-year-long sea surface height (SSH) data set at one of the gauge stations in Great Britain resulted in an S1 amplitude nineteenfold larger than expected from gravitational forcing. Ocean modelling with a barotropic model and meteorological forcing, based on measurements which were evaluated with tide gauge data, shows that an S1 amplitude, larger than expected from astronomical forcing, occurs in large areas of the global oceans (Schindelegger et al., 2016). The additional gravity contributions at the S1 frequency by atmospheric and oceanic loading probably cause an annual variation of the K1 parameters. However, at many stations the variation is dominated by semi-annual periods, or it is a combination of semi-annual and annual periods. The semi-annual period has to be caused by a harmonic in a frequency distance (difference of the frequencies of two tidal harmonics, see also appendix A) of $\frac{1}{0.5 \text{ years}}$. One possibility would be P1, which has a large ocean loading contribution (e.g. Foreman and Neufeld 1991). This additional contribution at the P1 frequency possibly makes the gravity at P1 frequency deviate from the expectations of the model used in the analysis. The influence of the atmosphere is not expected to be large at P1.

The hypotheses for K1 are therefore that the variations of the gravimetric factor and phase are caused by an outdated FCN model as well as loading from the atmosphere and possibly the oceans. Loading from atmosphere and oceans at the S1 frequency can cause an annual variation of the gravimetric factor and phase. Ocean loading at the P1 frequency possibly causes the semi-annual variation.

M2

The influence of ocean loading on gravity measurements is a well-known effect (e.g. Farrell 1972; Jentzsch 1997). The main contribution occurs at the M2 frequency. It is the reason why the M2 gravimetric factor and phase (approx. $\delta = 1.18$ and $\phi = 2°$ in Central Europe) deviate from the expectations from the model on which the tidal analysis is based (approx. $\delta = 1.16$ and $\phi = 0°$). The expected values are reached when the gravimetric factors and phases, estimated from long time series, are corrected with loading calculations based on stationary ocean models (Baker and Bos, 2003). These models, typically used for correcting the loading effects in gravity data, provide amplitudes and phases with high accuracy for about 10 harmonics (Stammer et al., 2014). However, in these models it is assumed that the amplitudes of the regarded harmonics are constant.

The fact that the M2 amplitude in the oceans is not constant and varies with an annual period was already observed in the 1930s by Corkan (1934) in tide gauge data and later by Foreman et al. (1995). Huess and Andersen (2001) observed an annual variation of the M2 amplitude in altimeter data from the North Sea. The effects causing the annual variation of the M2 amplitude were first studied by Kang et al. (2002) and on a global scale by Müller (2012) and Müller et al. (2014). The latter identify a temporally varying loss of energy to turbulent processes and friction through their influence on the barotropic tidal

transport as the responsible mechanism. The tidal transport influences the amplitude of the corresponding tide (e.g. Dietrich et al. 1975).

The annual change of the tidal transport can be caused by annually varying stratification conditions of the ocean water. Under stratified conditions, most likely in summer, the water column is more stable and less energy is dissipated in turbulent processes, while in winter due to the weather conditions the water is well-mixed. Additionally, in the Arctic, the ice coverage and therefore the friction between ice and ocean water changes seasonally. Eddy viscosity and bottom friction can change due to temporally changing water depths. Müller et al. (2014) showed that in an ocean model accounting for barotropic and baroclinic tides with a climatologic atmospheric forcing, amplitudes of the annual variations of the M2 amplitude of several centimetres occur in shelf areas. The comparison with tide gauges and altimeter data showed that the amplitudes of the annual variation of the M2 amplitude from the ocean model are in a realistic range.

The variation of the M2 amplitude can be represented as a time dependence of the M2 amplitude. Instead, Müller et al. (2014) expressed the variation in their study by the amplitude ratio and phase difference of the M2 harmonic and the harmonics with a frequency distance of $\Delta f = \frac{1}{1\text{year}}$ (satellite harmonics). The amplitudes and phases of the satellite harmonics were used for calculating amplitudes and phases of the annual variation of the M2 amplitude which were compared to the measurements (see above). Such a representation is also sometimes used in this thesis. The corresponding harmonics are $\alpha 2$ and $\beta 2$ (names usually used in solid Earth tide context) with the frequencies $f_{\alpha 2} = 1.92953584$ cycles per solar day (cpd) and $f_{\beta 2} = 1.93500115$ cpd. In the ocean tide context they are sometimes also called MA2 and MB2 or H1 and H2.

The influence of the annual variation of the M2 amplitude on tiltmeters in Great Britain through its loading was studied by Baker and Alcock (1983). They observed a similar periodicity in MWA of tide gauge data and tilt measurements. They discuss MA2 ($\alpha 2$, H1) and MB2 ($\beta 2$, H2) as well as MSK2 and MKS2 (compound tides in the oceans), whose amplitudes are larger than expected from gravitational forcing, as the harmonics in the SSH causing the observed variation. It is not clear to me why MSK2 and MKS2 are discussed because those harmonics would cause a semi-annual variation which is not visible in the tilt and tide gauge results they show. However, the annual variations of the M2 tidal parameters in Earth tide measurements (tilt and gravity) were also observed by others (e.g. Sato et al. 2004; Westerhaus 1997). The causes of the temporal variation of the M2 gravimetric factor and phase obtained from SG measurements were studied by Meurers (2004) and Meurers et al. (2016). They also identified the loading of $\alpha 2$ and $\beta 2$ as possible sources of the annual variation of the M2 tidal parameters. In a tidal analysis of a ten-year-long data set they estimate the gravimetric factor and phase of $\alpha 2$ and $\beta 2$, which can be used for calculating the annual variation of the M2 gravimetric factor and phase (as mentioned above for the variation of M2 in the ocean tide). The annual variation calculated from the $\alpha 2$ and $\beta 2$ gravimetric factors and phases fits well to the variation observed in the MWA.

It is hypothesised that the variation of the M2 gravimetric factor and phase is caused by the loading of the annually varying amplitude of M2 in the oceans.

Other wave groups

O1 is often regarded as a frequency which is less affected by atmosphere and oceans than others, as it is purely from lunar origin and therefore not influenced by radiation tides. The ocean loading at diurnal frequencies is also lower than at semi-diurnal frequencies (e.g. Baker and Bos 2003). The variation of the O1 gravimetric factor and phase does not show a clear periodicity.

Schroth et al. (2018) identify several tidal frequencies (Q1, M1, 2N2, N2, L2) which are probably influenced by harmonics of degrees higher than 2. These higher-degree harmonics were identified by the observed variations of their gravimetric factor and phase which occur with 0.56 years and 8.8 years. The solid Earth responds differently to degree 2 and higher-degree harmonics. This is taken into account when analysing the Earth tide registrations. If this model did not describe the response for harmonics of higher-degree correctly, it would cause variations. There are theoretical gravimetric factors and phases available based on different solid Earth models and assumptions (e.g. Dehant 1987; Dehant et al. 1999; Wahr 1981), which give slightly different results for the gravimetric factor and phase of higher-degree harmonics. Conceivable would be that the oceans also respond differently to degree 2 and higher-degree tides, which would affect gravity through their loading.

The S2 gravimetric factor and phase vary with a semi-annual period. At this frequency there is, similar to S1, the influence of the radiation tide of atmospheric origin (e.g. Klügel and Wziontek 2009; Volland 1997); but also the ocean loading of S2 could cause variations as it is 17% (Kantha and Clayson, 2000) larger than expected from gravitational forcing. Thus, the hypothesis for Q1, M1, 2N2, N2 and L2 is that the variation of their gravimetric factor and phase could be caused by an inappropriate description of higher-degree tides in the tidal analysis and by different ocean loading at harmonics of different degree. For S2 the variations can be caused by the loading of the atmosphere and oceans. There is no hypothesis for O1.

In order to distinguish tidal parameters obtained from gravity and tidal parameters obtained from tilt and strain, the term 'gravimetric factor and phase' was used for the tidal parameters from gravity data. As in the following only gravity data are used, the term 'tidal parameters' refers then to tidal parameters obtained from gravity measurements.

1.2. Objectives of this study

Based on the studies summarised above, the issues described below will be addressed in this thesis.

K1

From the results of the studies, described in section 1.1, the following questions arise:

- Is a part of the variation caused by the outdated FCN model used in the analysis? Can the variations be reduced if a better description of the FCN is used?

- Can a part of the variations be explained by atmospheric loading contributions at the S1 frequency? Can the variations be reduced if the contributions from the atmosphere are corrected?

- Is there an evidence that the oceans contribute to the observed variations?

The approaches used for the investigations are described in section 4.2.1. The corresponding studies are given in chapter 7. The atmosphere is characterised by the data sets of the Atmospheric attraction computation service (Atmacs, Klügel and Wziontek 2009) which provide loading time series based on an atmospheric model. For studying the influence of the oceans the Ocean model for circulation and tides (OMCT, Dobslaw et al. 2013; Thomas et al. 2001) and the Stormtide model (Müller, 2012; Müller et al., 2014) are used.

M2

The investigations presented in section 1.1 lead to the following questions:

- Do gravity loading time series computed with SSH from nonstationary ocean models cause annual variations of the M2 gravimetric factor and phase?

- If annual variations are caused by these loading time series are they of the correct order of magnitude compared to the results from measured data? Do they have a similar character?

- Are there evidences why an ocean model shows or does not show annual variations of the M2 amplitude?

- The annual variation of the M2 amplitude in the oceans is large in coastal areas, which is only a small part of the global ocean, whereas the amplitudes in the open oceans are small but these areas cover large regions: Which ocean areas contribute significantly to the variations of the gravimetric factor and phase?

The approaches for these investigations are described in section 4.2.2 and the investigations themselves in section 8. Five ocean models which potentially describe the annual variation of the M2 amplitude in the oceans are used: the Atlantic real-time ocean forecast system (ARTOFS, Mehra and Rivin 2010), the Stormtide model, OMCT, the HYCOM global tides model (HGT, Arbic et al. 2012; Arbic et al. 2010) and the North Sea model (Gräwe et al., 2015).

Other wave groups

Based on the information in section 1.1, the following questions are asked:

- Is there an evidence for atmospheric and oceanic loading as causes for the variations of the O1 gravimetric factor and phase?

- Can the variations for the S2 gravimetric factor and phase be explained by atmospheric loading?

- Does a more recent model for the Earth's admittance (Dehant et al., 1999) reduce the variations which are most likely caused by higher-degree harmonics?

- Does the ocean loading cause variations of the tidal parameters of Q1, M1, 2N2, N2 and L2?

This is studied in chapter 9 with the Atmacs data set and ocean loading calculated with OMCT.

For all the wave groups discussed here, this is the first time the causes for the temporal variations of the gravimetric factor and phase are studied under usage of data that describe the physical effects assumed to cause the observed variations. In case of the atmosphere, correction time series based on atmospheric models are often used when accurate tidal parameters for the solid Earth are required, but their influence on the temporal behaviour of the tidal parameters was never studied. Ocean loading effects are often corrected with stationary models (see section 1.1) which describe a few harmonics very accurately but cannot account for variations of harmonics. This is the first study which uses nonstationary ocean models which potentially contain variations of the amplitudes of certain harmonics and focuses on the temporal variations they probably cause.

The interpretation of the time-dependent tidal parameters and of tidal parameters obtained from short data sets will benefit if the causes of the temporal variations are known. Then the causes can be taken into account. If the solid Earth were of interest, it would be even better when the causing effects could be corrected. Then the tidal parameters for the solid Earth could be derived with a higher precision.

Studying the influence of inappropriate model assumptions is easy if more appropriate models are available, but for the characterisation of the atmospheric and oceanic loading data are needed that describe the mass redistributions in the oceans and atmosphere accurately enough. This leads to another possible use of the MWA. If model data are used for the description of the atmosphere and ocean, as is usually the case, the results of the MWA can be used for the evaluation and validation of the considered model by comparison of the results from the model and the results from measurements.

1.3. Overview on the content of this thesis

The thesis is structured as follows: Chapter 2 introduces the generation of body tides and the mechanism how masses on Earth can influence gravity by their loading. The methods which are used for analysing gravity data (tidal analysis, MWA) and ocean tides (harmonic analysis) as well as for calculating the synthetic body tides and the loading are the topic of

chapter 3. As mentioned in section 1.1, the chapters and sections are ordered according to the regarded tidal frequencies. K1 and M2 are discussed in their own sections, the other wave groups are summarised. This structure is used for chapter 4 in which the potential causes for the temporal variations of the gravimetric factor and phase and the approaches for their investigation are discussed. The data which are used for this investigation are introduced in chapter 5. The results are given in chapters 6 to 9, starting with the results for measured gravity data, followed by K1 (main focus on influence of the atmosphere), M2 (influence of oceans) and other wave groups. A conclusion and an outlook are given in chapters 10 and 11.

Additionally, the accuracy of the loading calculation was studied, which is described in appendix F.

Please take note of the glossary in which important terms are specified and the list of abbreviations, both in appendix A. Appendix B contains a detailed motivation for choosing the value 1.16 as gravimetric factor for the synthetic body tides used for several investigations in this thesis. Additional tables and figures related to chapters 5 to 8 are given in the appendices C to E.

Chapter 2.

Earth tides

An observer on the Earth experiences forces caused by gravitation and movement of the celestial bodies as well as the elastic behaviour of the Earth and mass redistribution on its surface. The sum of these forces is called gravity. The following sections give an introduction to these forces.

2.1. Part of the gravity signal caused by the Earth masses

This part of the gravity signal is the temporally constant part and depends only on the position of the observer on the Earth's surface. It is caused by the gravitational force due to the gravitation of Earth's mass, described by Newton's law, which is given for the point mass M_1 in equation 2.1 (Torge, 1989), and the centrifugal force caused by Earth's rotation.

$$\vec{F}_{grav} = M_1 \vec{b}_{grav} = \gamma M_1 \iiint\limits_{Earth} \frac{\vec{x} - \vec{x}_1}{|\vec{x} - \vec{x}_1|^3} dm \tag{2.1}$$

$\vec{b}_{grav}$ is the acceleration of M_1 caused by the force $\vec{F}_{grav}$, $\gamma = 6.673 \cdot 10^{-11} \frac{\text{m}^3}{\text{kg s}^2}$ (Torge, 1989) is the gravitational constant and $\vec{x}_1$ is the position of the point mass M_1. The extent of the Earth is taken into account through the integration of mass elements dm at the positions $\vec{x}$ within the Earth.
The centrifugal force occurs because of Earth's rotation (in a reference system rotating with the Earth). With the origin of the coordinate system in the centre of mass of the Earth, for M_1 it is given by

$$\vec{F}_z = M_1 \vec{b}_z = -M_1 \vec{\omega} \times (\vec{\omega} \times \vec{d}). \tag{2.2}$$

The centrifugal acceleration of M_1 is represented by $\vec{b}_z$ and the mean angular velocity of the Earth $\vec{\omega}$ with the value $|\vec{\omega}| = 7.292115 \cdot 10^{-5} \frac{\text{rad}}{\text{s}} \,\hat{=}\, 15.0410669 \frac{\text{o}}{\text{h}} \,\hat{=}\, 1.00273779$ cpd (Torge, 1989). $\vec{d}$ describes the shortest distance of M_1 to the rotation axis.
The resulting force is $\vec{F}_g$:

$$\vec{F}_g = M_1 \vec{g} = \vec{F}_{grav} + \vec{F}_z = M_1(\vec{b}_{grav} + \vec{b}_z) \tag{2.3}$$

$\vec{g}$ is called Earth's gravitational acceleration acting on M_1 and depends on its position on the Earth's surface. It is maximal at the geographical poles and minimal at the equator.

2.2. Tides

The gravitational acceleration, described in section 2.1, is caused by the Earth itself, while the dominating time-dependent signals are the tides, which are external forces arising from the existence of other celestial bodies. In this section the tidal forcing and the response of the solid Earth, the body tides, are introduced.

2.2.1. Tidal forcing

Tidal forces arise from the gravitational and centrifugal forces occurring due to the mass of celestial bodies and their movement around each other. In addition to the time dependence mentioned above, there is also a spatial dependence. The description starts with the spatial distribution of tidal forces, followed by the temporal changes that would be observed on the surface of a celestial body.

2.2.1.1. Spatial pattern of tidal forces

A system of two spherical, nonrotating celestial bodies M_E and M_L, shown in Fig. 2.1, is considered.
Here the focus is on the tidal forces, that means the corresponding accelerations caused by M_L on the surface of M_E. Assuming that M_L is distant to M_E, M_L can be treated as a point mass. However, the extent of M_E has to be taken into account. M_L causes a gravitational force, that means acceleration $\vec{b}_0$ on M_E, which is in the centre of mass of M_E equalled by the centrifugal force (acceleration $-\vec{b}_0$) due to movement of the bodies around each other. If the mass of M_E is much larger than the mass of M_L the centre of mass of the system will be inside of M_E and is approximated as the centre of mass O of M_E in Fig. 2.1.
At any other point on M_E, e.g. the observation point P, the same centrifugal acceleration $-\vec{b}_0$ occurs, but the gravitational acceleration depends on distance and position of M_L relative to P. The resulting tidal acceleration $\vec{b}_t$ is:

$$\vec{b}_t = \vec{b} - \vec{b}_0 = \gamma M_L \left(\frac{\vec{r}_E}{|\vec{r}_E|^3} - \frac{\vec{r}_L}{|\vec{r}_L|^3} \right) \tag{2.4}$$

Here $\vec{r}_E$ is the distance vector between P and M_L and $\vec{r}_L$ is the distance vector between O and M_L. The centrifugal acceleration can be represented by the negative gravitational acceleration in O.
This system of two celestial bodies leads to a characteristic pattern of tidal accelerations on the surface of M_E, which is shown by the arrows in Fig. 2.2.
The dashed arrow points towards M_L. At the location on M_E closest to M_L a maximal acceleration acts because the gravitational acceleration is large due to the smaller distance
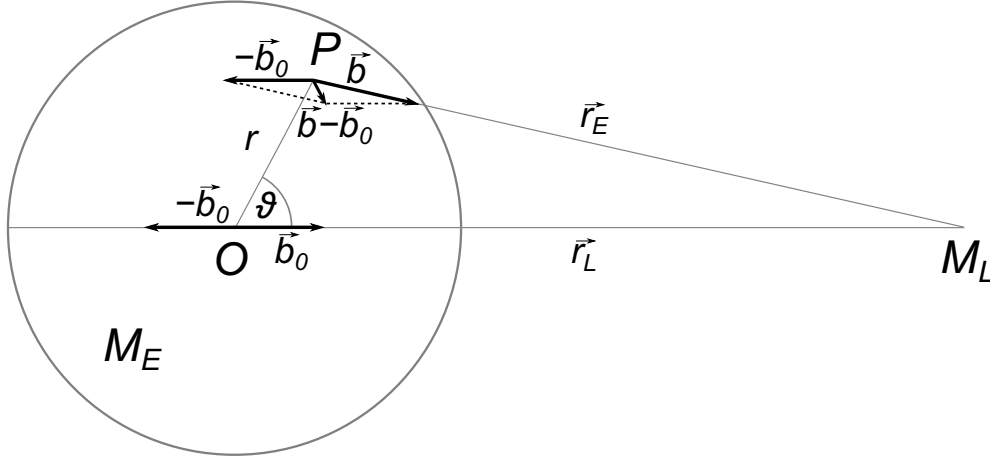
Fig. 2.1. Accelerations due to the gravitational attraction and centrifugal forces as well as tidal acceleration on M_E caused by M_L at the centre of mass O of M_E and an arbitrary observation point P on the surface of M_E. M_L is treated as a point mass. $\vec{r}_E$ is the distance vector of P and $\vec{r}_L$ the distance vector of O to M_L, respectively. r denotes the distance between P and O, ϑ the geocentric zenith distance of M_L and P, $-\vec{b}_0$ the centrifugal and $\vec{b}_0$ the gravitational acceleration in O. Accordingly $\vec{b}$ is the gravitational acceleration in P and $\vec{b} - \vec{b}_0$ the resulting tidal acceleration. After Bartels (1957), modified by Schroth (2013).

to M_L. On the opposite side of M_E the gravitational acceleration is smaller because this point is further from M_L. Here the centrifugal acceleration dominates and results in a maximum acceleration, which points in the opposite direction.

2.2.1.2. Temporal dependence of tidal forces

To introduce a more realistic scenario, it is assumed that M_E rotates around a rotation axis RA. During the period a celestial body is observed at the same position again, any point on M_E passes two maxima and minima which results in semi-diurnal tides. Due to the axis tilt, the extrema an observer, who is fixed at a rotating Earth (and therefore e.g. moves along the red curve in Fig. 2.2), experiences have different amplitudes. Therefore, the tides also have a diurnal component.

The case described above is a vast simplification of the tides on Earth. There are more celestial bodies than just the Moon and the Earth. Other celestial bodies, especially the Sun, have to be taken into account too. The motion of the celestial bodies and their influence on each other has already been described in several publications (e.g. Bartels 1957). In the following, the focus will be on the astronomical elements which are linked to the frequencies of the fundamental processes. All other tidal frequencies can be expressed as combinations
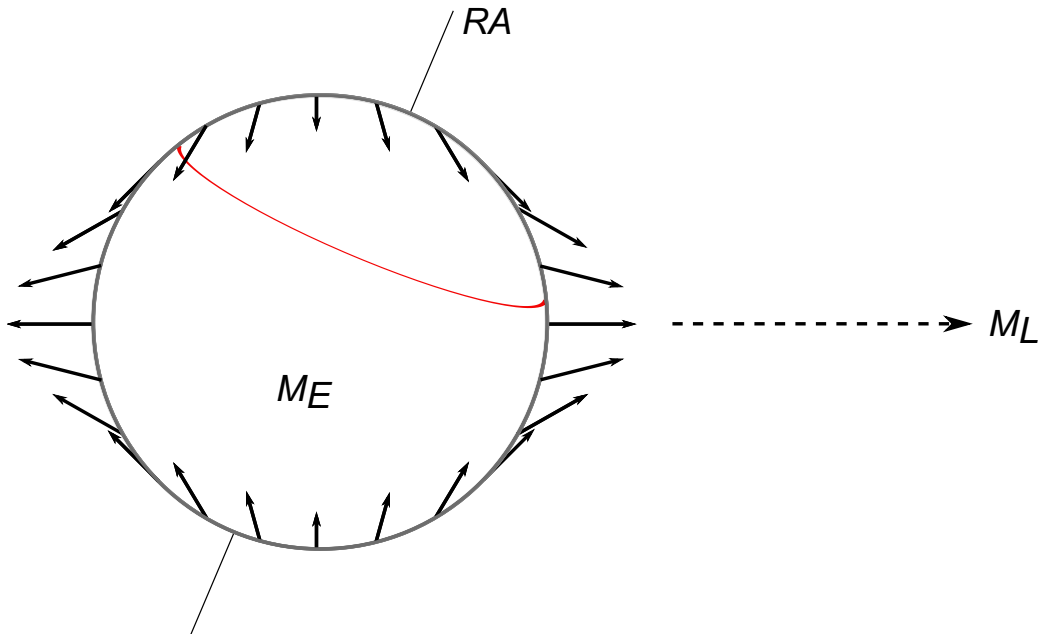
Fig. 2.2. Pattern of tidal accelerations on M_E caused by M_L, represented by the solid arrows. RA is the rotation axis of M_E, the dashed arrow points towards M_L. The red curve represents a possible path of an observer relative to the tidal forces. After Bartels (1957) modified by Schroth (2013).

of them. The astronomical elements and the corresponding frequencies are given in Tab. 2.1 (Wenzel, 1997c).

The corresponding periods are defined as the time spans between two passages of the celestial body (or its perigee or ascending node, respectively) through the meridian of an observer. As all of these objects move with respect to the fixed stars (inertial reference frame), this is usually not an exact 360° cycle of the mean longitude. As the Moon moves along its path around the Earth (and the Sun) during one rotation period of the Earth, it takes 50 min longer than 24 hours until the moon is observed at the same position again. In addition to the undisturbed motion of the celestial bodies they can influence each other which causes additional tidal frequencies (e.g. the evection).

name	f in $\frac{\circ}{h}$	T
mean local lunar time	14.4920521	1.035 d
mean lunar longitude	0.5490165	27.322 d
mean solar longitude	0.0410686	365.242 d
mean longitude of lunar perigee	0.0046418	8.847 a
negative mean longitude of lunar ascending node	0.0022064	18.613 a
mean longitude of solar perigee	0.0000020	20940 a
mean longitude of Mercury	0.1705157	87.968 d
mean longitude of Venus	0.0667570	224.696 d
mean longitude of Mars	0.0218363	1.880 a
mean longitude of Jupiter	0.0034637	11.857 a
mean longitude of Saturn	0.0013957	29.425 a

Table 2.1. Astronomical elements used for the tidal catalogue of Hartmann and Wenzel (1995a,b) (see also section 2.2.2), their frequencies in $\frac{\circ}{h}$ and periods in mean solar days or years (J2000), respectively (Wenzel, 1997c).

2.2.2. Tidal potential

The tidal forces can be derived from the masses and positions of the celestial bodies, the ephemerides. This description of the tidal forces is, for example, used as forcing for the ocean models Stormtide and OMCT, described in sections 5.2.2.2, 5.2.2.4 and 5.2.2.5. For Earth tides, usually tidal potential catalogues are used. All necessary quantities (e.g. acceleration, tilt) can be derived from the tidal potential. The development of the tidal potential has already been described in detail by e.g. Bartels (1957) and Wenzel (1997c). Here, just the general ideas of the development are presented.

The potential for tidal forces can be written as:

$$V = GM_L \left(\frac{1}{|\vec{r}_E|} - \frac{1}{|\vec{r}_L|} - \frac{r \cos \vartheta}{|\vec{r}_L|^2} \right) \tag{2.5}$$

Here the same quantities are used as in section 2.2.1 and Fig. 2.1. r is the distance between O and P and ϑ the geocentric zenith distance of P.

The last term corresponds to the centrifugal force. As it is useful in the following mathematical development (see Bartels 1957 for details), $\frac{1}{r_L}$ is introduced which is spatially constant and has therefore no influence on the corresponding acceleration and makes the potential vanish in O. The term $\frac{1}{r_E}$ in equation 2.5 can be developed into Legendre polynomials, which allows a separation of the distance-dependent parts from the latitude and declination-dependent parts. The Legendre polynomials depend on the geocentric distance ϑ. It can be expressed as longitude and latitude of the observation point and the

geocentric, spherical length of the celestial body causing the potential. This allows the development of the Legendre polynomials into fully normalised spherical harmonics. The potential in equation 2.5 describes the situation of a spherical Earth, which is unrealistic. If the flattening of the Earth is taken into account, additional terms have to be added to the development (Wenzel, 1997c).

For the tidal analysis, the analysis method I used for my investigations, described in section 3.1.1, using a tidal potential catalogue is advantageous. This is a spectral analysis of the tidal potential. The following expression is used by Wenzel (1997c):

$$V = D \sum_{l=1}^{l_{max}} \sum_{m=0}^{l} (\frac{r}{a})^l \Gamma(\theta) \overline{P}_{lm}(\cos\theta) \sum_i (C_i^{lm}(t)\cos(\alpha_i(t)) + S_i^{lm}(t)\sin(\alpha_i(t))) \qquad (2.6)$$

The indices l and m are degree and order of the spherical harmonic development, i the index of sine and cosine terms with degree l and order m. θ is the geocentric, spherical polar distance of the station, D and $\Gamma(\theta)$ are normalisation constants, a is the semi-major axis of the reference ellipsoid and $C_i^{lm}(t)$ and $S_i^{lm}(t)$ are coefficients depending on time t with the unit $\frac{m^2}{s^2}$ per Julian Day (Hartmann and Wenzel, 1995a,b). They are given by:

$$C_i^{lm}(t) = C0_i^{lm} + tC1_i^{lm} \qquad (2.7)$$

$$S_i^{lm}(t) = S0_i^{lm} + tS1_i^{lm} \qquad (2.8)$$

where $C0_i^{lm}$, $C1_i^{lm}$, $S0_i^{lm}$ and $S1_i^{lm}$ are constant. $\alpha_i(t)$, the argument of the sine and cosine functions, is:

$$\alpha_i(t) = m\lambda + \sum_{j=1}^{j_{max}} k_{ij} \cdot E_j(t) \text{ with } k_{i1} = m \qquad (2.9)$$

λ is the geocentric spherical longitude of the observer and k_{ij} is the integer argument number belonging to $E_j(t)$, the astronomical elements which were described in section 2.2.1.2. j_{max} is the number of astronomical elements. The forces of all processes like Earth rotation, movement of planets and so on, are represented as a sum of sine and cosine functions of known frequency and amplitude in the tidal potential catalogue. They can also be expressed as a cosine with amplitude, phase and frequency, a representation which will be used in section 3.1.1. A single cosine function is called harmonic or line.

For my investigations the Hartmann and Wenzel catalogue (Hartmann and Wenzel, 1995a,b) is used. It is based on a development of the tidal potential of the Moon up to degree 6, of Sun up to degree 3 and of the planets Mercury, Venus, Mars, Jupiter and Saturn up to degree 2, which results in a catalogue with 12935 entries.

2.2.3. Response of the solid Earth to tidal forcing

The tidal catalogue describes only the forces caused by the celestial bodies. If the solid Earth behaved perfectly rigid, a gravimeter would directly measure this signal. However,

the elastic properties of the Earth result in a deformation of the Earth's body, which makes
the measured acceleration different to the exciting acceleration. The effect is caused by the
redistribution of the Earth's masses and the corresponding change of the gravitational field
of the Earth as well as the displacement of the station in the gravity field.

A detailed mathematical description of this effect is for example given by R. Wang (1997).
If a nonrotating, spherical Earth (SNREI Earth model, Spherical, Non-Rotating, Elastic,
Isotropic, e.g Dahlen and Tromp 1998) is assumed, the Earth's response has a similar
pattern as the tidal potential and can be expressed in spherical harmonics with the same
degree and order. At the surface of the earth, the response can be described by the Love
numbers h_l and k_l and the Shida number l_l. They only depend on the degree l of the
spherical harmonic. Due to the Free Core Nutation (see section 2.2.4), they can also be
frequency-dependent.

- h_l: describes the radial displacement.

- k_l: describes the gravitational potential of the deformation.

- l_l: describes the tangential displacement.

They depend on the elastic properties of the Earth and can be calculated for specific
Earth models, e.g. for PREM. For second degree, they are $h_2 = 0.6032$, $k_2 = 0.2980$ and
$l_2 = 0.0839$ (Agnew, 2009). This is valid for a spherical Earth. For an elliptical Earth eight
Love numbers are necessary and taking rotation into account makes it even more complex
by coupling the spheroidal displacement fields to the toroidal (Dehant et al., 1999). A
detailed description of the calculation of gravimetric factors based on seismological Earth
models is given by Dehant (1987) and Dehant et al. (1999) and Wahr (1981).

For gravity the radial component and the change in the gravitational potential is relevant.
With h_l and k_l, the gravimetric factor can be calculated:

$$\delta_l = 1 + \frac{2h_l}{l} - \frac{l+1}{l}k_l \tag{2.10}$$

The gravimetric factor is defined as the ratio of the measured acceleration to the exciting
acceleration. For standard Earth models, gravimetric factors are $\delta_2 \approx 1.16$ for $l = 2$ and
$\delta_3 \approx 1.07$ for $l = 3$. This means that the response of the solid Earth to degree 2 forcing
causes a 16% higher amplitude than the amplitude of the forcing signal.

For the description of the measured gravity tides, in addition to the gravimetric factor the
phase ϕ is used which takes into account leads or delays of the measured signal relative
to the forcing. Here the phase is defined with respect to the exciting acceleration at the
observation point, leads (i.e. the response leads the forcing) are positive. For elastic Earth
models the phases are expected to be 0°. The gravimetric factor and phase can be estimated
from measured gravity data with tidal analysis (see section 3.1.1).

The previous part of this section focused on the response of the solid Earth to tidal forcing.
However, also the oceans and the atmosphere have a tidal response. Due to the different
material properties of ocean water, atmospheric air masses and the solid Earth, they respond

differently to tidal forcing. Ocean tides and atmospheric tides are addressed in sections 5.2.2.1 and 5.2.3.1.

2.2.4. Nearly Diurnal Free Wobble (NDFW)/ Free Core Nutation (FCN)

There are oscillations of the Earth's rotation axis which are not necessarily caused by tides but can also influence the acceleration in the tidal frequency band. Therefore, they have to be considered when investigating tides. For this study only the Nearly Diurnal Free Wobble (NDFW, terrestrial frame)/ the Free Core Nutation (FCN, celestial frame) is of relevance (for details, see e.g. Zürn 1997). Both names denote the same effect but in different reference frames. The resonance is due to the differences of the rotation axis of mantle and outer core and depends on the ellipticity of the core-mantle boundary. This results in a restoring force on the core-mantle boundary and a damped wobble of the Earth's rotation axis, with a frequency slightly higher than 1 cpd. It is permanently excited by the diurnal tides. The relocation of the Earth's axis relative to the Earth surface changes the position of an observer in the gravity field and therefore influences tidal observations.

This results in a frequency dependence of the diurnal tidal parameters. The frequency-dependent diurnal gravimetric factor is usually expressed relative to O1, the lunar main harmonic, as shown in equation 2.11.

$$\delta_{n,NDFW}(f) = \delta_n - r_{NDFW} \frac{f - f_{O1}}{f_{NDFW} - f} \qquad (2.11)$$

r_{NDFW} is the resonance factor for the gravimetric factor. The frequencies f, f_{O1} and f_{NDFW} correspond to the harmonic whose gravimetric factor is calculated, to O1 and the NDFW, respectively. n is the index of the regarded harmonic (e.g. number in the tidal catalogue).

2.3. Loading

Gravity changes can also be caused by a redistribution of masses on the Earth, like mass movements in the oceans or the atmosphere, as well as by hydrological effects. Masses change gravity by their direct attraction at a station, but they also deform the Earth's crust and relocate the observation point in the gravity field. The mass has of course to change its position with time to produce a gravity change. This is called loading.

The following paragraph summarises how loading effects on a gravimeter station can be described. The subject is presented in detail by, e.g., Agnew (2009) and Jentzsch (1997) and Farrell (1972). Loading effects can be described by the load Love numbers h'_l, k'_l and l'_l. They are related to the displacement and gravitational deformation potential, as the Love numbers in section 2.2.3 do, but differ from these Love numbers. This is due to different boundary conditions of the problem of surface loads in contrast to the response of the Earth's body to tides.

The load Love numbers can be used to calculate the Green's functions, the response of the

Earth to surface loads. The Green's function for gravity describes the gravity change due to a unit mass as a function of distance from the station.

$$G = \frac{g}{M_E} \sum_{l=0}^{\infty} (l - (l+1)k_l' + 2h_l') P_l(\cos(\nu)) \tag{2.12}$$

The Green's function is also expressed in spherical harmonics. In a spherical model only the degree is of importance because the solution only depends on the distance ν in degree between the mass load and the station. M_E is the mass of the Earth and the value of $\vec{g}$. The first term in equation 2.12 represents the Newtonian attraction of the mass. With this formulation it is assumed that the loading is at height zero. Especially for the atmosphere, the masses close to the observation point are above the station. In this case the attraction has to be formulated differently to the term given in equation 2.12. Agnew (2009) gives a version of the gravitational part with dependence on height under the assumption that the height is small compared to the radius of the Earth.

The gravity change can then be calculated with:

$$\delta b_l = \rho \iint\limits_{oceans} G(\vec{r} - \vec{r}\,')h(\vec{r}\,')\ dA \tag{2.13}$$

The mass is specified by its density ρ and its volume, represented by a cube of height h and the area dA. This has to be integrated over the Earth's surface, taking into account the positions of the station ($\vec{r}$) and of the mass ($\vec{r}\,'$). The density is assumed to be constant, which is not necessarily the case. Otherwise an individual, time-dependent density $\rho(t)$ for every mass has to be used within the integration. The description of the masses causing loading and usually given by ocean or atmosphere models can be found in the section 5.2.2 and 5.2.3.2. The details about the calculation of the ocean loading for this study are given in section 3.2.

Chapter 3.

Methods

This section describes the methods that were used to analyse the measured and synthetic data.

3.1. Methods for the investigation of Earth tides

In the following the methods used for the investigation of Earth tides are introduced.

3.1.1. Tidal analysis

The tidal potential described in section 2.2.2 can be used for the estimation of the tidal parameters introduced in section 2.2.3. This is done with tidal analysis. Here the Hartmann and Wenzel catalogue is used (Hartmann and Wenzel, 1995a,b). The information in this section is mainly taken from the book chapter 'Analysis of Earth tide observations' by Wenzel (1997a). The text follows the description of the same topic presented in my diploma thesis (Schroth, 2013). For the tidal analysis the program ETERNA 3.4 *analyze* is used (Wenzel 1996, modified for Linux). The approach which is described in the following is implemented in ETERNA. The settings which were used in the program are given in this and the following section 3.1.2. They equal the settings given by Schroth et al. (2018) and Schroth (2013). The only difference in case of the latter is the usage of a Boxcar window instead of a the Hann window.

Tidal analysis uses the least-squares method to find the parameters $\boldsymbol{\beta}$, that minimise the squared errors between the model function $\mathbf{f}$, which depends on $\boldsymbol{\beta}$ and the measured data. $\mathbf{f}$ hereafter is called analysis model. As these quantities are no physical vector they are written in bold letters. In a general form the least-squares errors can be expressed by equation 3.1.

$$\sum_{a=1}^{a_{max}} (f_a(\boldsymbol{\beta}) - c_a)^2) = |\mathbf{f} - \mathbf{c}|^2 \tag{3.1}$$

a is the index of the a_{max} measurements – in case of tidal analysis the number of time steps – and c_a is the ath measurement with the corresponding function value f_a of the analysis model. For tidal analysis c_a is the tidal registration and f_a the analysis model, which will

be described in more detail in the following.

The analysis model, used in this study, is given by equation 3.2.

$$f(t) = \underbrace{\sum_{j=1}^{q} \delta_j \sum_{i=a_j}^{e_j} F_i A_i \cos\left(2\pi f_i t + \Phi_i + \phi_j\right)}_{(a)} + \underbrace{\sum_{m}^{m_{max}} R_m F_i z_m(t)}_{(b)} \qquad (3.2)$$

The quantities which are estimated with the least-squares adjustment are the tidal parameters δ and ϕ introduced in section 2.2.3. $z_m(t)$ is one of m_{max} additional time series which will be explained in the following.

The term (a) in equation 3.2 describes the body tides by using the tidal potential, which gives the amplitude of one harmonic of the forcing signal A_i, its frequency f_i and the phase Φ_i. The tidal parameters are not estimated for single harmonics because the frequency resolution is restricted by the signal-to-noise ratio and the length of the time series (Munk and Hasselmann, 1964). They are adjusted for wave groups which are described by the second sum of term (a) in equation 3.2. The index i defines the harmonics included in the wave group, while the index j denotes the number of the wave group. Tab. 3.1 shows the wave grouping used in this study (Wenzel, 1997a). The frequency band is given by f_s and f_e. The name of the wave group is that of the harmonic with the highest amplitude in the frequency band of this wave group.

Within a wave group the amplitude ratios of the single harmonics relative to each other are assumed to be constant. As known from sections 2.2.3 and 2.2.4, the gravimetric factors depend on the degree of the harmonic development and in the diurnal band also on the frequency due to the FCN. This is taken into account based on an elastic Earth model (Wahr-Dehant-Zschau model Dehant 1987). Therefore, the analysis model does not only contain information about the forcing but also a priori information about the Earth's body. The focus of this study is on diurnal and semi-diurnal tides, hence a band-pass filter is applied in *analyze*. Wenzel (1997b) describes the filter as a high-pass, but the spectrum of the filtered data compared to the spectrum of the unfiltered data shows that it has to be a band-pass filter between about 0.8 cpd and about 6 cpd. However, as I am not interested in higher frequencies, this is of no consequence for my results. The ETERNA manual (Wenzel, 1997b) also mentions that the measurements are split at 0.8 cpd, but a spectrum of the filtered data shows also very small contributions between about 0.5 and 0.8 cpd. The filter is represented by F_i in equation 3.2.

The tides are the dominating time-dependent signal in gravity registrations but also other gravity changes are measured and can influence the estimation of tidal parameters if they occur with the same frequencies as the tides. Atmospheric gravity changes can be partly corrected by adjusting the locally measured air pressure to the measurements. Up to 95% of the atmospheric signal can be removed (Klügel and Wziontek, 2009). This is represented by the term (b) in equation 3.2. R_m is the regression factor which is estimated in the adjustment. The filter F_i is also applied to the air pressure time series $z_m(t)$. m is the index of the time series (e.g. air pressure) which is adjusted additionally to the measurement. In

Name	f_s in cpd	f_e in cpd
long	0.001379	0.501369
Q1	0.501370	0.911390
O1	0.911391	0.947991
M1	0.947992	0.981854
K1	0.981855	1.023622
J1	1.023623	1.057485
OO1	1.057486	1.470243
2N2	1.470244	1.880264
N2	1.880265	1.914128
M2	1.914129	1.950419
L2	1.950420	1.984282
S2	1.984283	2.451943
M3M6	2.451944	7.000000

Table 3.1. Definition of wave groups as given by Wenzel (1997b). The first column gives the name of the wave group, which corresponds to the largest line within the group. f_s is the start and f_e the end frequency of the wave group in cpd.

this study only the measured air pressure signal is used, but in general, considering other time series is possible.

The estimation of ϕ_j in equation 3.2 is nonlinear. This is handled by using the sine and cosine representation, which allows a linear estimation of their amplitudes (sine and cosine part). The gravimetric factor and the phase can then be calculated from these amplitudes. Equation 3.2 then can be written as:

$$f(t) = \sum_{j=1}^{q}(X_j CO_j + Y_j SI_j) + \sum_{m}^{m_{max}} R_m F_i z_m(t) \tag{3.3}$$

The quantities X_j, Y_j, CO_j and SI_j are given by the following equations.

$$X_j = \delta_j \cos(\phi_j) \qquad Y_j = -\delta_j \sin(\phi_j) \tag{3.4}$$

$$CO_j = \sum_{i=a_j}^{e_j} F_i A_i \cos(2\pi f_i t + \Phi_i) \tag{3.5}$$

$$SI_j = \sum_{i=a_j}^{e_j} F_i A_i \sin(2\pi f_i t + \Phi_i) \tag{3.6}$$

When X_j and Y_j are adjusted, δ_j and ϕ_j can be calculated.

$$\delta_j = \sqrt{X_j^2 + Y_j^2} \tag{3.7}$$

$$\phi_j = -\arctan(\frac{Y_j}{X_j}) \tag{3.8}$$

The least-squares adjustment directly allows the estimation of standard deviations. For a parameter x, which can be δ, ϕ or the regression factor R, σ_x can be calculated by equation 3.9 (Westerhaus, pers. comm.).

$$\sigma_x = \pm\sqrt{\frac{\sum_{a=1}^{a_{max}} r_a^2}{a_{max} - u}} \sqrt{Q_{aa}} \tag{3.9}$$

σ_x is the standard deviation of the parameter x, r_a is the residual to the corresponding measurement and u is the number of unknowns. The cofactor matrix Q with the main diagonal elements Q_{aa} is given by equation 3.10.

$$Q = (A^T A)^{-1} \tag{3.10}$$

A is the derivative of the linear analysis model in equation 3.3 with respect to the parameters x.

For standard deviations a white noise spectrum is assumed which is usually not true for tidal analysis because among others systematic effects occur (like loading). The standard deviations are too small and they are even smaller when a filter is used in the analysis (up to about eight times smaller) because the residuals are smaller in the filtered case. Wenzel (1997a) suggests a calculation based on red noise, which results in larger standard deviations, insensitive to filtering. However, the benefit of this proposal is discussed controversially; in order to make the comparison with other studies easier the usual definition of the standard deviation is used here.

3.1.2. Moving window analysis

Moving window tidal analysis (MWA, Schüller 1976) takes short time windows out of a longer data set and performs a tidal analysis. The resulting tidal parameters are plotted over the date in the centre of each time window. The resulting graph shows the temporal behaviour of the tidal parameters. Except if noted otherwise, the length of the time window is 90 days. The window is shifted by 2 days, so neighbouring windows have an overlap of 88 days. The analyses by Schroth (2013) showed that these values for length and shift of the window provide are suitable for MWA. Especially the window length is a compromise between the stability of the tidal parameters which requires a long time series and the ability to represent the variation period for which short time series are of advantage. The described procedure was implemented in Matlab (Schroth 2013, with small changes). For the tidal analysis, ETERNA *analyze* is called by the script.

As will be described in section 4.1.1, the window function has an influence on the estimated

tidal parameters (Schüller, 1976, 2015). Therefore, in the MWA a Hann window is used in order to reduce the window-induced variations. A result from such an analysis is exemplarily shown in Figs. 4.1 and 4.2. The tidal parameters are plotted per wave group over time. The thickness of the line represents the standard deviation as output by ETERNA. If not mentioned otherwise, a time axis labelled with year or in a month.year format marks the beginning of the corresponding year or the beginning of the corresponding month, respectively.

The offset/mean value of the curve is the stationary part of the tidal parameter. In the example shown in Figs. 4.1 and 4.2 the two cases that are compared have the same offset. If the difference of the offsets is too large, the mean of the time-dependent tidal parameter is calculated and subtracted in order to make the variation visible. The offset usually matches the tidal parameters estimated with a long time series if the amplitude of the variation is taken into account. The offset can differ from the tidal parameters estimated from the long time series if the time span of the MWA is not a multiple of the variation period. This was also investigated by Schüller (1976).

The length of the time window is kept constant. If there are larger gaps in the data, the time window contains less and less data when it moves into the gap. If the data set becomes too short, the time series of wave groups become linearly dependent. The parameters in this case cannot be interpreted with respect to the Earth. Additionally, their large changes in short time spans before gaps require a large-scale of the y-axis on which the periodic variations of the tidal parameter are not visible. Therefore, I cut out strong variations before gaps. The decision is made by eye. As few parameters as possible are cut out, but as much as necessary to make the variations of the parameters visible. The cutout was always less than one time window. This is of course subjective, but as I interpret only long-periodic behaviour of the tidal parameters which occurs over several years (see section 4.1.1) the influence of slightly too large or too short cutouts is not significant for the interpretation.

3.1.3. Prediction of synthetic body tides

The approach used for this study, described in section 4.2, requires the calculation of synthetic body tides, for which the tidal potential can be used. This is done based on the body tide model. The synthetic body tides are calculated with a modified *predict* (see below) which is part of the ETERNA 3.4 package (Wenzel, 1996). It uses term (a) of equation 3.2 to calculate time series of body tides. The tidal parameters are specified by the user. The calculation is also done with the wave groups defined in Tab. 3.1 (see section 3.1.1). For the synthetic body tides in most cases the gravimetric factors are $\delta = 1.16$, except for K1 with $\delta(K1) = 1.13$ and M3M6 with $\delta(M3M6) = 1.06$, and the phases are $\phi = 0°$ for all wave groups. These values are only approximate values, close to the values given, for example, by Dehant et al. (1999). For the variations only the amplitude ratios and phase differences of the harmonics within the wave group are relevant (see section 4); in this respect, the tidal parameters for solid Earth tides could be chosen arbitrarily (except for $\delta = 0$). They are only important for the mean values of the tidal parameters which are not discussed on an accuracy level that would make more precise, theoretical

values necessary. A more detailed motivation of this choice is given in appendix B.

In section 7.1 it is shown that an FCN model with a resonance period of $T_{FCN} = 431.37$ si. d. fits better to the measured data than the original FCN model with $T_{FCN} = 459.25$ si. d. Therefore, the modified version with $T_{FCN} = 431.37$ si. d. is used, if not noted otherwise.

3.2. Calculation of ocean loading

In this project it was necessary to handle the calculation of ocean loading myself, since existing programs like 'Some Programs for Ocean Tide Loading' (SPOTL, Agnew 2012) have a computation time that is too long. Therefore, equation 2.13, section 2.3, was implemented in Matlab. The main reason for the faster calculation in Matlab is that the values which are the same for every time step, the Green's functions and the areas around the grid points, are calculated and loaded only once. Only the SSH values have to be reloaded for every time step. Additionally, SPOTL requires equidistant grid points; therefore, every time step of the ocean model output used here (see section 5.2.2) except for OMCT has to be interpolated to a finer, equidistant grid (see appendix F.2). The alternative would have been to change the source code of SPOTL. It seemed more efficient to write my own script and ensure it produces similar results as SPOTL (see appendix F.2) rather than understanding and changing the Fortan77 code of SPOTL.

The density of the ocean water for the loading calculation is assumed to be $\rho = 1031 \frac{\text{kg}}{\text{m}^3}$, which is estimated from a density distribution from the ARTOFS model (see section 5.2.2.3). The area around a grid point is approximated by a rectangle. Its sides are calculated as half the distance between the neighbouring grid points on a spherical surface. As the Green's functions are required for certain distances, the given values (Na and Baek, 2011) are interpolated. In appendix F.1.2, the interpolation method is discussed.

Whether there is an influence of these assumptions on the tidal parameters obtained with these loading time series (see section 4.2) is investigated with the tests described in appendix F.

SPOTL takes into account the height of the gravimeter station as well as the coast lines that may intersect grid cells of the ocean model. There also is an interpolation over the grid cell's extent. These effects were neglected in my calculation. Therefore, in appendix F.2 the calculations with my simplified version and with SPOTL are compared to ensure that the influence of the effects discussed above (coast line, station height, etc.) is small at the stations whose results are discussed.

3.3. Harmonic analysis of ocean tides

The harmonic analysis of ocean tides is very similar to the tidal analysis described in section 3.1.1. The harmonic analysis is needed in section 8.1 for the ocean models described in section 5.2.2. ETERNA has the possibility of analysing ocean tides, but it was designed for Earth tide and has disadvantages for the analysis of ocean tides. It does not take into account shallow water tides and there is no possibility to analyse large ocean areas in a reasonable amount of time, at least not without additional resources and changes in the

code.

Therefore, it is much more efficient to use the Tidal Heights Analysis and Prediction program by M. G. Foreman, which is widely used for ocean model analysis. It has the additional advantage that it was used by Müller et al. (2014), and as the same settings are used, the results from the harmonic analysis can be directly compared.

The information in this section about harmonic analysis and especially about the Tidal Heights Analysis and Prediction program is taken from the corresponding manual (Foreman, 2004) and the publication by Foreman and Henry (1989). In the following, the focus is on the differences between the harmonic analysis of ocean tides and the tidal analysis described in section 3.1.1.

The parameters which are estimated for the oceans are the amplitude in metres and the Greenwich phase of a certain harmonic. In contrast to the phase lead estimated in the solid Earth tidal analysis (local phase), the Greenwich phase lag is not estimated relative to the local potential, but the potential in Greenwich. This means that the location at which the analysed time series was obtained is not needed in the analysis (it is of relevance when the Greenwich phase is converted to the local phase).

For the harmonic analysis, 146 harmonics can be used in the program which contain 45 main harmonics of astronomical origin and 101 shallow water harmonics. As not every harmonic can be resolved, a concept called 'constituent clusters' is used. Similar to the wave groups on which the tidal analysis is based, the constituent cluster is based on the assumption that harmonics with similar frequency have a similar response. Therefore, the amplitude ratios of the harmonics as predicted by the tidal potential catalogue are assumed to be constant also for the amplitudes of the tidal harmonics in the SSH. For the constituent cluster, harmonics with the same first three integer argument numbers (which correspond to the Doodson numbers, Doodson 1921) mentioned in section 2.2.2 are combined. It is assumed that the constituent cluster i can be represented by a single cosine:

$$SSH_{cc,i}(t) = \underbrace{m_i A_i'}_{=A_{cc,i}'} \cos(2\pi f_i t - \Phi' - \underbrace{\phi_i' + \epsilon_i}_{=\phi_{cc,i}'}) \quad (3.11)$$

with:

$$m_i = \sqrt{(1 + \sum_k I_{ik}\frac{A_k'}{A_i'}\cos(2\pi\Delta f_{ik}t + \Delta\Phi_{ik}))^2 + (\sum_k I_{ik}\frac{A_k'}{A_i'}\sin(2\pi\Delta f_{ik}t + \Delta\Phi_{ik}))^2}$$

$$(3.12)$$

$$\epsilon_i = \arctan(\frac{\sum_k I_{ik}\frac{A_k'}{A_i'}\sin(2\pi\Delta f_{ik}t + \Delta\Phi_{ik})}{1 + \sum_k I_{ik}\frac{A_k'}{A_i'}\cos(2\pi\Delta f_{ik}t + \Delta\Phi_{ik})}) \quad (3.13)$$

$SSH_{cc,i}$ is the SSH variation of the regarded constituent cluster. A_i', ϕ_i' and Φ_i' are the true amplitude, the Greenwich phase lag and the phase of the main harmonic, respectively. The prime notation indicates that these are different quantities than the acceleration amplitudes

in section 3.1.1. Only the amplitude $A'_{cc,i}$ and the phase $\phi'_{cc,i}$ of the constituent cluster are estimated. They are corrected by the amplitude correction factor m_i and the phase correction ϵ_i accounting for the satellite harmonics in order to estimate A'_i and ϕ'_i of the main harmonic. They are also called nodal modulation corrections. k_{max} is the number of satellite harmonics, the corresponding quantities are the same as for the main harmonic, but denoted with index k. The elements of the interaction matrix I_{ik} describes the interference of the satellite harmonic with the main harmonic. Δf_{ik} is the frequency distance between the satellite harmonic k and the main harmonic i and $\Delta\Phi_{ik}$ the corresponding difference of the phases.

Another difference to the tidal analysis in section 3.1.1 is the selection of harmonics taken into account in the analysis. Two harmonics with frequencies f_1 and f_2 have to fulfil the condition provided in equation 3.14.

$$|f_1 - f_2|T \geq c_r \tag{3.14}$$

T is the length of the regarded time series. The criterion's coefficient c_r is 1 by default which corresponds to the Rayleigh criterion. The Rayleigh criterion is used here because it was set in the analysis by Müller et al. (2014) (M. Müller, pers. comm.) to whose results those of this thesis are compared. However, as discussed by Munk and Hasselmann (1964) the Rayleigh criterion does not apply to harmonic and tidal analysis, so c_r can be chosen differently.

3.4. Fourier transform with *foutra*

For the calculation of spectra the program *foutra*[1] by T. Forbriger is used. *foutra* is introduced here because it uses an unusual, but useful normalisation of the amplitudes in the spectrum. The amplitude of an harmonic signal in a fast Fourier transform (FFT), if it is normalised to the duration of the time window, depends on the Fourier transform of the window function and the time-domain amplitude of the harmonic signal (divided by 2). Assuming that side lobes can be neglected, the FFT amplitude of the signal of interest can be normalised with the FFT amplitude of the window function. The amplitude of the harmonic signal in the spectrum then has the same amplitude as the time domain signal.

---

[1] https://git.scc.kit.edu/Seitosh/Seitosh/wikis/src_ts_wf_foutra (11.07.19)

Chapter 4.

Temporal variations of tidal parameters

In this chapter it is discussed how temporal variations of tidal parameters are generated. Possible causes of the variations of the K1 and M2 tidal parameters as well as the concept of their investigation is presented in detail. The same issue for other wave groups are summarised.

4.1. Potential causes for temporal variations of tidal parameters

There are technical reasons why tidal parameters could vary. As the main focus of this study is on the variations caused by the system Earth, it has to be ensured that the observed variations are not caused by technical issues of the instruments, the preprocessing or deficiencies of the analysis method. This is discussed in the first part of this chapter. How tidal parameter variations can be caused by the Earth is described in the second part.

4.1.1. Technical causes

As an example for temporal variations of tidal parameters, Figs. 4.1 and 4.2 show the variations for twelve wave groups in light green, obtained from the data of the SG at the Black Forest Observatory (BFO) using the standard MWA, described in section 3.1.2.
The tidal parameters of the different wave groups vary with a different periodicity. The amplitude and the phase of one wave group usually show the same periodicity. This was also observed for all other stations I analysed (Schroth et al., 2018).
In the following it is shown that these variations cannot originate from technical causes.
A calibration factor changing with time could cause temporal variations of the tidal parameters. This would affect all wave groups and would most likely be different for all SGs. Meurers et al. (2016) mention a trend in the gravimetric factor of M2 at the station Bad Homburg, which is also observed here (see Fig. 6.2 in chapter 6). The results of Schroth et al. (2018) show that this trend occurs only in the gravimetric factor of M2. Therefore, this trend cannot be caused by a temporally varying calibration factor. Another effect that would cause a temporal variation of the tidal parameters is the nonlinearity of the gravimeter response. This would lead to certain spectral components in the residuals. A
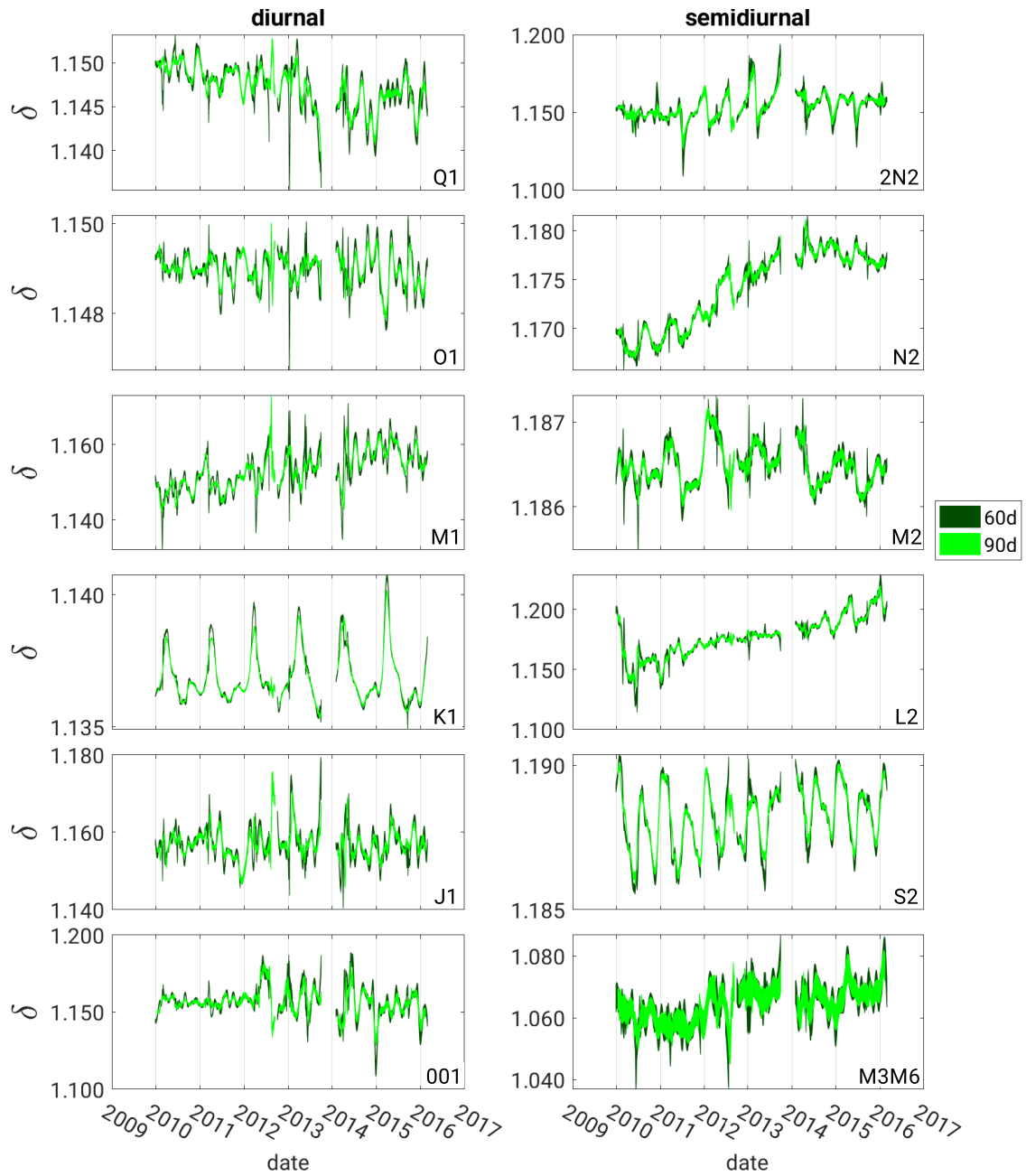
Fig. 4.1. Gravimetric factors for BFO station in light green obtained with the standard MWA described in section 3.1.2 and in dark green obtained with an MWA with the same settings but a window length of 60 days.
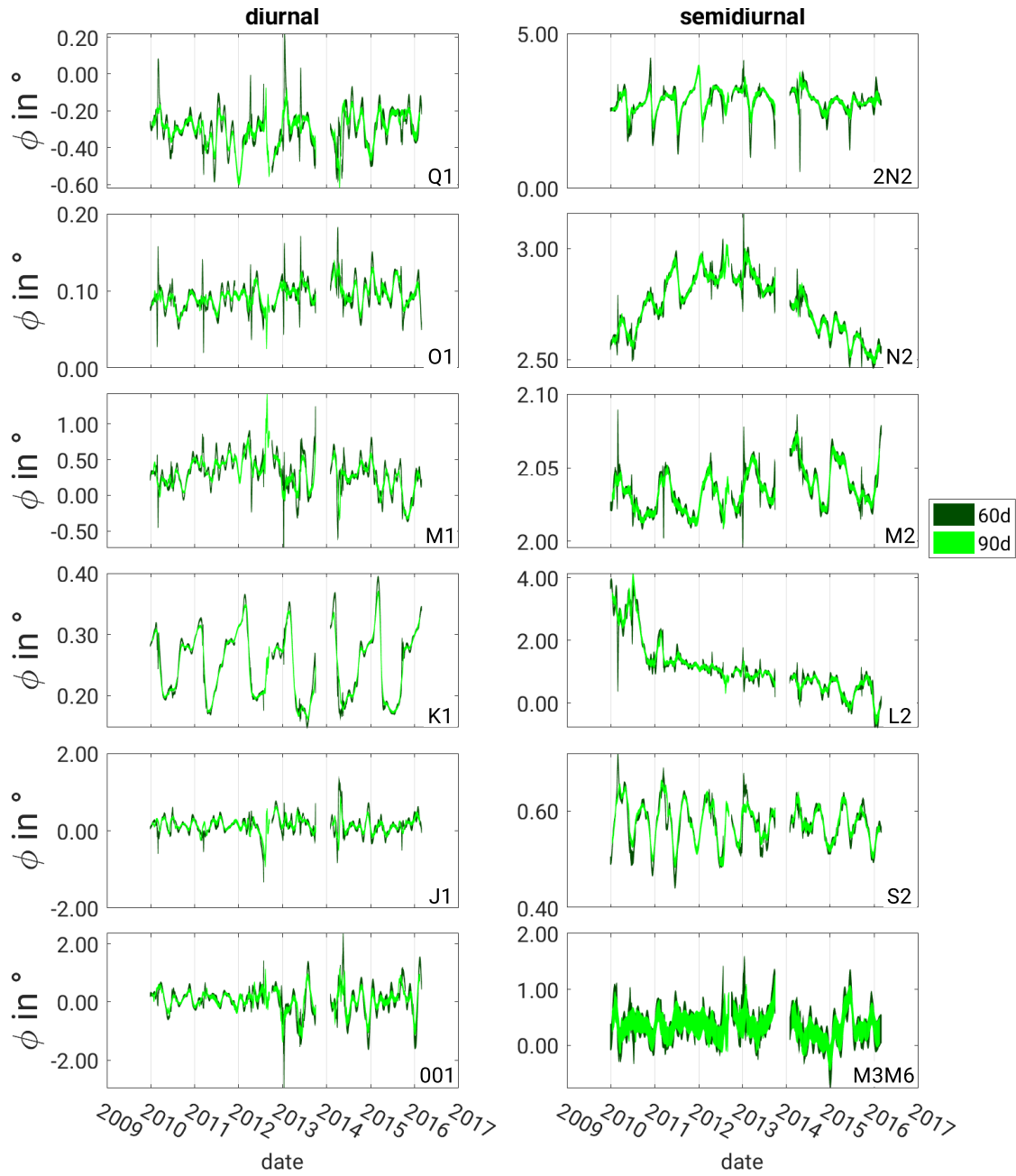
Fig. 4.2. Phase in degree for BFO station in light green obtained with the standard MWA described in section 3.1.2 and in dark green for an MWA with the same settings but a window length of 60 days.

synthetic test by T. Forbriger (pers. comm.) showed at which frequencies these components would occur. They were not present in spectra of the residuals obtained from tidal analyses of measured data. Besides, the variations of the tidal parameters are similar for a lot of stations (e.g. Fig. 6.1 or Schroth et al. 2018). If this was caused by a nonlinear response of the SGs or a change of their gain factors, both effects would have to occur similarly for all SGs. This would be a serious disadvantage of the SGs' construction. The fact that the discussed effects occur similarly at all SGs, can also be excluded by comparing the results of the SG with results from a co-located spring gravimeter, which has a fundamentally different construction. The temporal variations of the tidal parameters obtained with the SG and the spring gravimeter at the same station are similar (e.g. Riccardi et al. 2011, the differences in some parts of the results observed there were due to an instability of the spring gravimeter's calibration). This means that the variations cannot be explained by a nonlinear response or a changing gain factor.

The preprocessing can cause variations of the tidal parameters because steps which were not completely removed and the filling of gaps with inappropriate model tides can influence the tidal parameters (Schroth, 2013). These influences should only occur as long as the disturbance (step or filled gap) is in the actual time window which means that the disturbance will occur with a length equal to the length of the time window. Therefore, I do not interpret short-term variations.

The preprocessing can also produce signals that occur over a longer time-span of several years (like trends, Bützler 2018), but this is far from the diurnal and semidiurnal frequency range regarded in this study. However, there are preprocessing steps that influence the MWA results, as the example in Figs. 4.3 and 4.4 shows.

Both data sets are from the SG at Onsala, but they were differently preprocessed by the station operators at the Onsala Space Observatory (OSO) and IGETS (see also section 5.1). There are many small short-term variations in the results from the OSO data set. Disturbances were probably removed differently during preprocessing. A striking feature is the difference in the offsets of the tidal parameters. The tidal parameters of the wave group M2 obtained with the IGETS data set are about $8 \cdot 10^{-3}$ smaller in the gravimetric factor and about 0.03° lower in the phase. The time lags are different in both data sets, but the time lag does not influence the gravimetric factor. This is tested by running an MWA of the IGETS data with the time lag $\Delta t = 9.07$ s given in the OSO data set. The gravimetric factor stays the same, but the phase is shifted and then fits well to the results obtained with the OSO data set. The different mean values for the gravimetric factors indicate that the tidal amplitudes were changed during preprocessing. It is conceivable that this is caused by inappropriate filtering or some kind of scaling of the amplitudes, but this was probably not intended by the person who preprocessed the data, as the analysis result should not be influenced by the preprocessing. However, the temporal variations mainly differ in the short-term variations mentioned above. As the focus of this study is on variations with periods of half a year to several years, the differences are not relevant here. The stationary part of the tidal parameters from Onsala is not discussed.

Deficiencies of the analysis method can also cause temporal variations of the tidal parameters. Cross-talk can occur if there is a trade-off between model parameters. This can lead to a
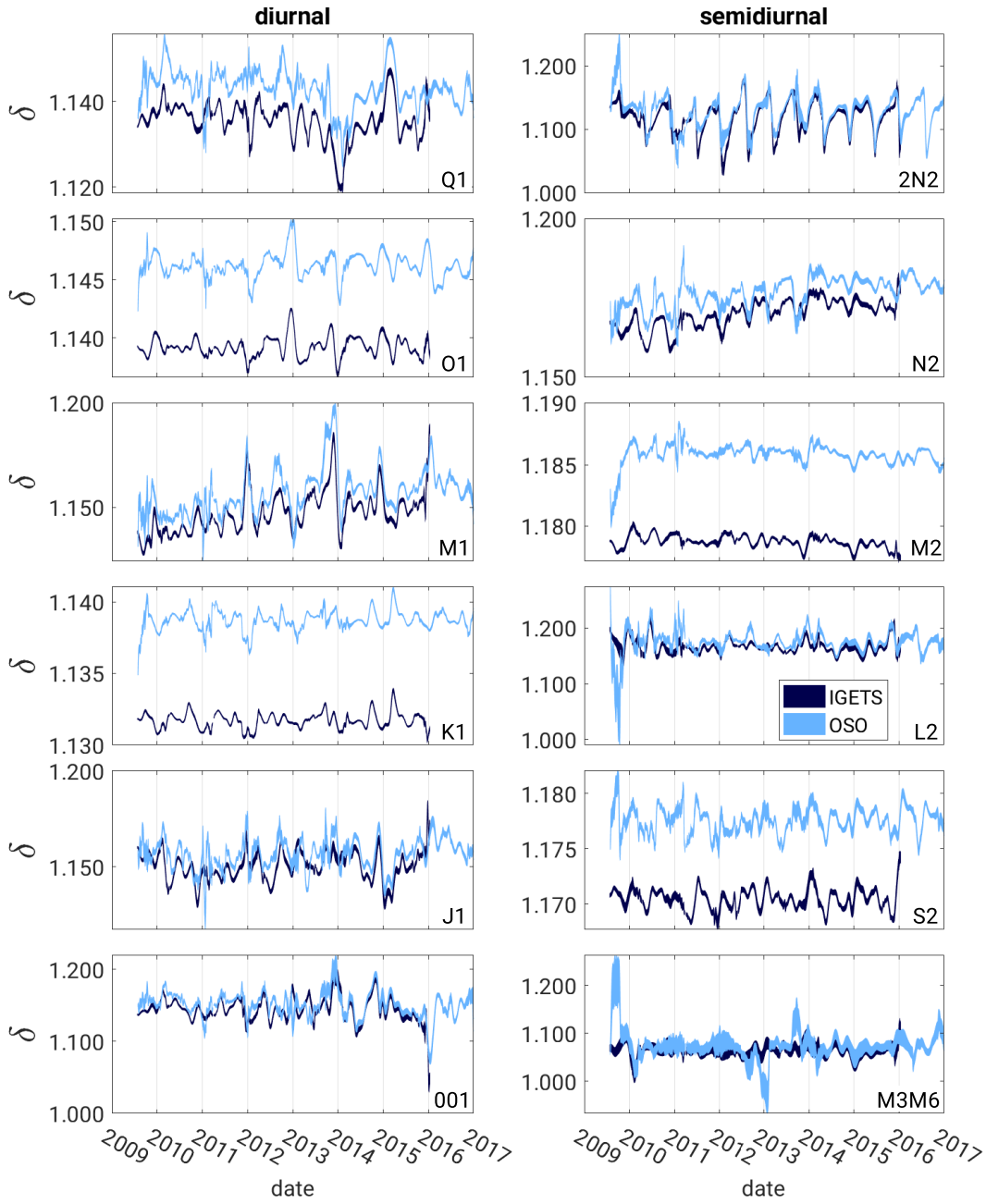
Fig. 4.3. Gravimetric factors for Onsala station in light blue obtained with data preprocessed by the station operators at Onsala Space Observatory (OSO) and in dark blue obtained with the IGETS data set.
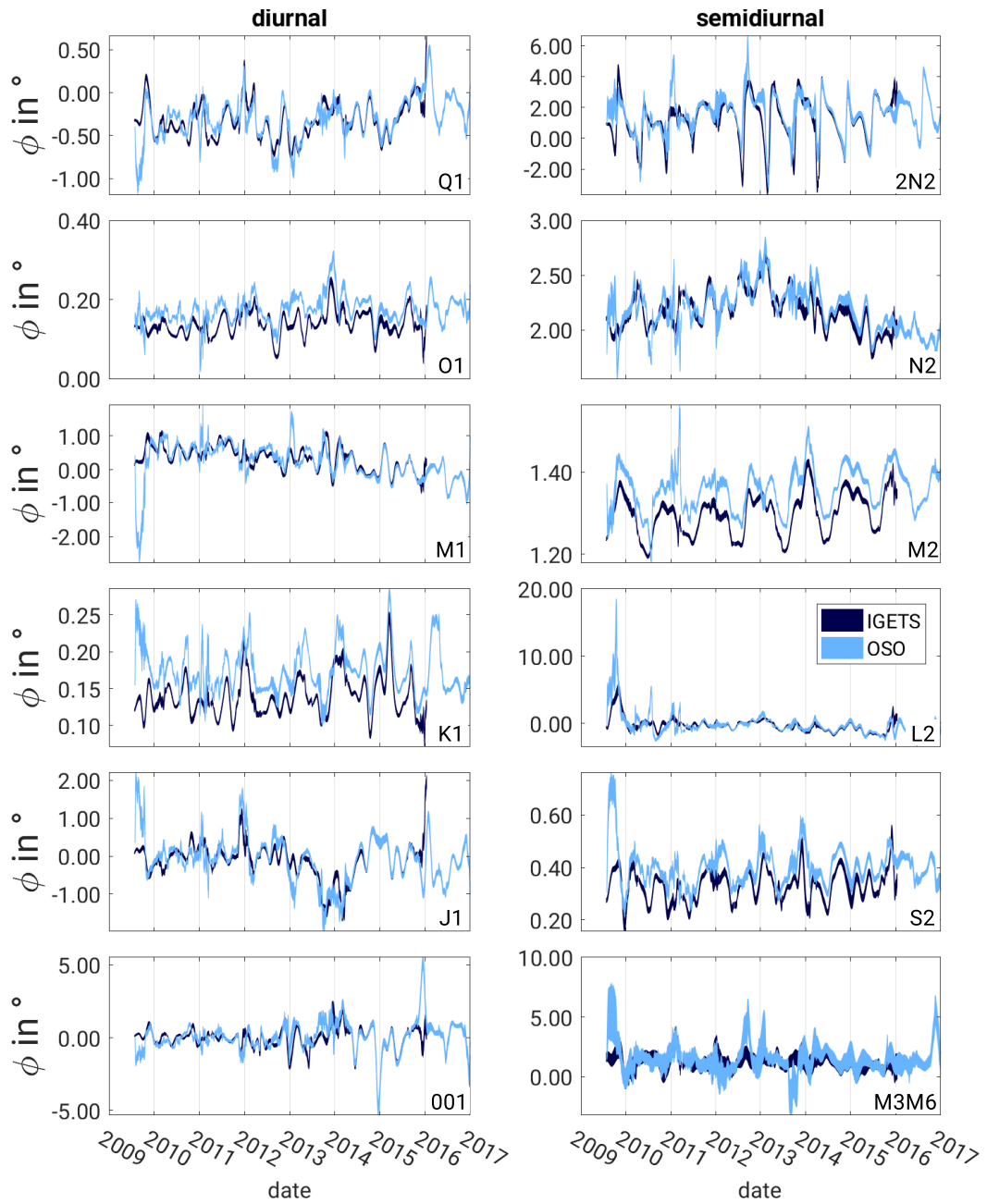
Fig. 4.4. Phase in degree for Onsala station in light blue obtained with data preprocessed by the station operators at Onsala Space Observatory (OSO) and in dark blue obtained with the IGETS data set.

linear dependency of the model parameters and an increased sensitivity to noise.

The window function, a boxcar in the simplest case, can cause spectral leakage (Schüller, 1976) and in an MWA analysis produce variations of the tidal parameters.

These effects can be identified by using windows of different lengths. Variation periods which change with the window length are an indication for deficiencies of the analysis whereas variations that stay the same should be caused by the properties of the measured time series. Of course, it has to be taken into account that a variation of a certain length can only be represented by a window which is shorter than the period of the variation. Otherwise, the variation will be smoothed over a longer period, depending on the time window.

Figs. 4.1 and 4.2 provide an example for tidal parameters obtained with MWA that are performed with the same settings except for the length of the time window. The results with a 90 d window are shown in light green and with a 60 d window in dark green. The variation frequencies are independent from the window length. Therefore, the variations can be discussed with respect to effects of the Earth. Variations caused by the window function are already reduced by the usage of a Hann window. The amplitude of the variation with the 90 d window is slightly smaller because the longer window averages over a longer time span.

The peaks which occur for example in the gravimetric factors of Q1 and O1 at the beginning of 2013 obtained with the 60 d window are caused by gaps in the data set. They have a stronger effect on the results obtained with the shorter window because it contains less data anyway. If the gaps are too large, the parameters become linearly dependent.

4.1.2. Generation of the variations of the tidal parameters

In this section the general mechanism causing the temporal variations of the tidal parameters is described.

Temporal variations of tidal parameters caused by the Earth show up when the temporal behaviour of the analysed acceleration signal differs from the expected time dependence. This can happen if inappropriate assumptions about the solid Earth are made or if additional signals with frequencies similar to the tides occur which are not taken into account in the analysis model (see end of this section and chapter 1).

There are two different ways to describe such variations: They can be regarded as temporal variation of the amplitude of a harmonic or they can be expressed by side lines of the main frequencies (satellite harmonics). The amplitudes of these satellite harmonics are constant. For example, an annual variation of the amplitude of the main harmonic with the frequency f_M can be expressed by satellite harmonics with frequencies $f_{sl} = f_M \pm \frac{1}{1 \text{ year}}$. This is in some way always used in tidal analysis for the representation of the tidal forces, expressing the time dependence of the acceleration as a sum of harmonics.

The acceleration signal of a wave group shows a beat character because harmonics with similar frequencies are summed. As mentioned in section 3.1.1 the amplitude ratios and phase differences within a wave group are assumed to be constant. If the time dependence of the measured acceleration is different from what the harmonics in the wave group express,

there will be a small tidal signal remaining in the residuals which cannot be explained by the analysis model. The tidal parameters for the wave group will then be chosen in such a way that they produce the smallest residuals over the whole time series. In the MWA the adjustment then depends on the actual time window. If the window is shorter than the time dependence which is not fully described by the analysis model, and especially shorter than half of the variation period, the tidal parameters will be scaled depending on the position of the time window relative to the unexplained time dependence of the acceleration signal. Therefore, a variation of the tidal parameters occurs with the beat frequency of the harmonics that are not correctly explained by the analysis model. For illustration a simple case is shown in Fig. 4.5.
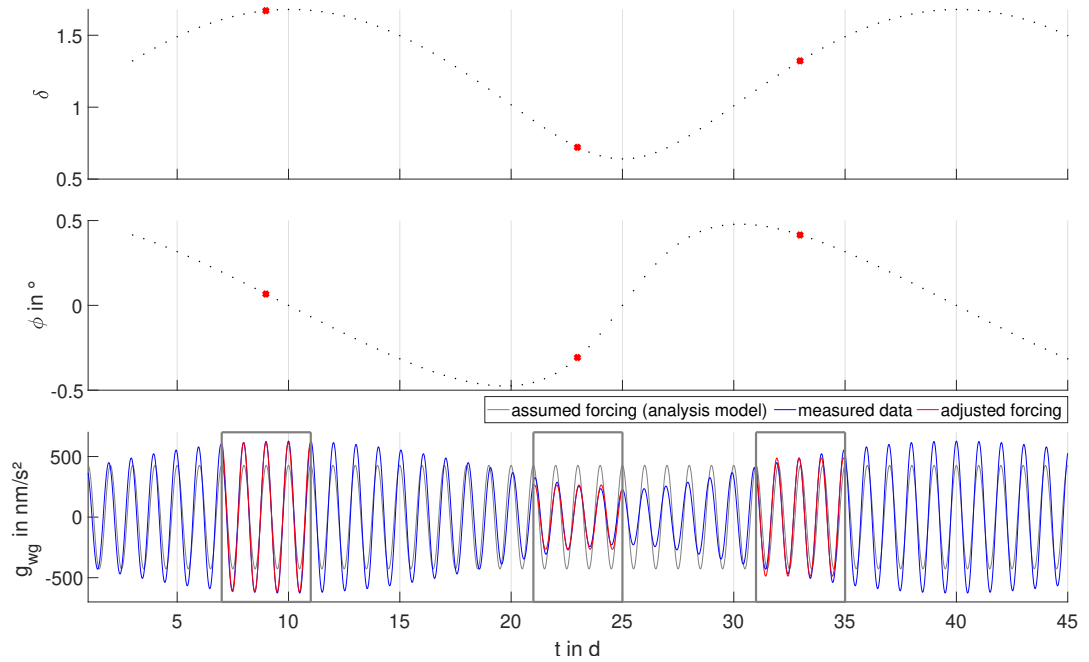
Fig. 4.5. Illustration of the generation of temporal variations of tidal parameters. The upper and the central panel show the resulting gravimetric factor δ and the phase Φ. The lower panel shows the corresponding gravity time series, the model time series in grey based on the analysis model multiplied with the gravimetric factor $\delta = 1.16$, the 'measured' data in blue (please note that these are also synthetic data, representing the measured data in this illustration) and the fitted model data in red for three exemplary time windows. The larger red dots in the two upper panels visualise the corresponding tidal parameters.

The data set representing the measured data was calculated as a sum of two harmonics with the amplitudes $A_1 = 368 \ \frac{\text{nm}}{\text{s}^2}$ and $A_2 = 200 \ \frac{\text{nm}}{\text{s}^2}$ and phases of $\phi_1 = 0°$ and $\phi_2 = 120°$. The frequencies are $f_1 = 1$ cpd and $f_2 = 1$ cpd $- \frac{1}{1 \text{ month}} = 0.966667$ cpd. The corresponding acceleration is the blue beating signal in Fig. 4.5 (lower panel). These values were chosen in a way that the curves in the lower panel of Fig. 4.5 are distinguishable from each other.

In the analysis a cosine with A_1, ϕ_1 and f_1 is assumed as model. In Fig. 4.5 this signal is multiplied by 1.16, the theoretical gravimetric factor for Earth models (see section 2.2.3). As the amplitude of this 'model acceleration' is constant the temporal behaviour of the acceleration caused by the analysis model differs from the behaviour of the 'measured' acceleration. In a realistic case both signals would have a beat character with slightly different envelopes. For the MWA, the regression (corresponding function in Matlab) was performed with a window length of 10 days, shifted by 1 day.

Three time windows are discussed exemplarily. In the first time window in Fig. 4.5 the beat amplitude of the 'measured' signal is almost at its maximum, but the expected model signal is much lower. Both signals are almost in phase. This means for the tidal parameters that the gravimetric factor has to be much larger than 1.16 in order to explain the 'measured' signal whereas the phase is close to zero. In the second time window the 'model' signal has a larger amplitude than the 'measured' signal and thus the gravimetric factor is smaller than expected. The 'measured' signal lags the theoretical and causes a negative phase (leads are positive, see section 3.1.1). The amplitude of the 'model' signal in the third window is only slightly smaller than the amplitude of the 'measured' signal, thus the gravimetric factor is only slightly increased. This time the 'measured' data lead the 'model' data which causes a positive phase.

In this example all amplitudes of harmonics are assumed to be constant but they can of course also vary with time, as deviations from the body tide model can be caused by the atmosphere or oceans, which do not have to behave perfectly harmonic. If this is the case, the monthly variation of the tidal parameters in Fig. 4.5 would not be as smooth.

A not perfectly harmonic behaviour can be better represented by an MWA for which the amplitudes are assumed only to be constant within a time window, whereas a tidal analysis in which the amplitudes of the satellite harmonics are estimated will keep the amplitudes constant over the whole time series. Therefore, MWA is more suitable for this study.

In this context the term beat does not denote just a superposition of two cosine functions (harmonics). As several harmonics are summed in one wave group the temporal dependence of the acceleration signal can be more complex. Therefore the variation of the tidal parameters can be complex as well.

The causes for the variations that are studied in the following chapters are already discussed in detail in the introduction (see chapter 1). Here, a summary is given.

K1:

- An outdated FCN model with a resonance period of $T_{FCN} = 459.25$ si. d. (Dehant, 1987) is assumed in the analysis model instead of a model with values close to the observed $T_{FCN} = 431.18 \pm 0.1$ si. d. (Krásná et al., 2013).

- The large gravity contributions of the radiation tides at the S1 frequency cannot be represented by the measured air pressure (Klügel and Wziontek, 2009; Volland, 1997). The data are not corrected for these contributions when the influence of the atmosphere is taken into account by fitting the measured air pressure to the data

(see section 3.1.1).

- The radiation tides can also influence the oceans (Baker and Alcock, 1983). A baro-tropic ocean model with meteorological forcing based on measurements predicts S1 amplitudes which are tenfold higher than the amplitudes expected due to astronomical forcing (Schindelegger et al., 2016). The loading of these signals can cause variations of the tidal parameters.

M2:

The annual variation of the M2 tidal parameters is probably caused by the loading of an annual variation of the M2 amplitude in the oceans (Meurers, 2004; Meurers et al., 2016). The annual variation of the M2 amplitude was observed in tide gauge data (Baker and Alcock, 1983; Corkan, 1934) and in some regions in altimeter data (Huess and Andersen, 2001; Müller et al., 2014). The mechanisms causing the variation in the oceans were studied by Müller et al. (2014) and Müller et al. (2012).

Others:

- There is no indication for effects causing the variation of O1.

- The higher-degree harmonics deviate from the expectations of the analysis model which can be responsible for the variations of Q1, M1, 2N2, N2 and L2. Theoretical tidal parameters calculated by Dehant et al. (1999) are slightly different from the values used in ETERNA (Dehant, 1987). Another possible cause can be ocean loading.

- A large influence of radiation tides from the atmosphere (Klügel and Wziontek, 2009; Volland, 1997) and the oceans (Kantha and Clayson, 2000) occur at the S2 frequency. Like in the case of S1 the radiation tides in the atmosphere cannot completely be represented by the air pressure. The radiation tide at the S2 frequency in the oceans causes higher S2 amplitudes than expected from astronomical forcing which can cause variations of the tidal parameters as well.

4.2. Concept of investigation

There are two possibilities how to investigate the influence of the effects mentioned in the previous section (see also chapter 1). For both cases it is necessary to have a time series that characterises the gravity signal caused by the discussed loading effect. The first option is the correction of the measured data with these gravity loading time series. If the loading time series describes the loading realistically, the advantage is that the results can be directly interpreted with respect to the solid Earth. A precise description of the

regarded loading effect is not always available which has in this case the disadvantage that the loading time series adds noise to the measured gravity signal.

The second option is to add the loading time series that describes the loading effect to synthetic body tides. If the body tides (without any loading) are analysed with the same wave grouping as used for their calculation, the gravimetric factor and phase from MWA are constant (Schroth, 2013). If a variation in the analysis of the sum of the body tides and the time series of the loading of an external gravity effect appears, the variation has to be caused by the loading time series. Loading time series containing signals which are not present in the measured data will cause time-dependent tidal parameters different from the results obtained with measurements. If there are similarities, it is likely that the same effects cause the variations in the results from synthetic and measured data. In the following chapters the approach described above is called 'synthetic data MWA'. In this thesis I focus on a visual comparison of the order of magnitude of the variations and the character of the variations. The latter is defined by the occurrent periods in the variation. Other methods, like coherence or correlation, have a frequency resolution that is too low for the estimation of the similarity of the results obtained from measured and synthetic data for many of the data sets used here. As described in section 3.1.1, the standard deviation is not a proper measure of the tidal parameter's accuracy and is in general too low. Therefore, if parameters differ by less than one standard deviation, they are regarded as the same; but if their difference is larger it does not necessarily mean that the difference is significant. In the latter case the differences are discussed with respect to the amplitude of the variation of the tidal parameters obtained from observations.

In contrast to the correction of the measured data with the loading time series, synthetic data MWA has the advantage that the source of the variations can be clearly distinguished. Variations of the tidal parameters obtained with the synthetic data MWA can only be caused by the loading time series.

In the following, it is discussed in detail how the approaches described above are used for investigating the temporal variations of the tidal parameters of K1, M2 and the other wave groups.

4.2.1. K1

The influence of the outdated FCN model can easily be estimated by replacing the outdated ($T_{FCN} = 459.25$ si. d., Dehant 1987) by a more recent model ($T_{FCN} = 431.37$ si. d., Dehant 1987) in ETERNA. The measured data can then be analysed with both FCN models. The model which produces the smaller variations of the tidal parameters explains the measured data better.

The next step is to determine which harmonic in the frequency band of the K1 wave group causes the main contribution. The harmonics with the largest amplitudes are P1, S1, K1, $\Psi 1$ and $\phi 1$. They can be used for subdividing the large K1 wave group into five smaller wave groups (then also a K1 wave group exists but it covers a smaller frequency band, see Tabs. D.1 to D.3). Schroth (2013) shows that the FCN model does not have much influence on the synthetic body tides if they are calculated with individual tidal parameters for each

of the smaller wave groups. This is used for calculating synthetic body tides in which the amplitude ratio of one of the small wave groups and K1 is set equal to the ratio of this wave group and K1 in the measured data (estimated with tidal analysis). The variation of the K1 tidal parameters obtained in MWA then shows how large the contribution of this tidal parameter is.

The result of the synthetic test indicates that the S1-to-K1 ratio has a strong influence on the K1 tidal parameter variation. As mentioned in the introduction (see chapter 1), S1 is influenced by the radiation tides in the atmosphere which cannot completely be corrected by the adjustment of the measured air pressure signal (see section 3.1.1). A better description of the atmospheric loading is needed. The Atmacs data set (Klügel and Wziontek, 2009) is used (see section 5.2.3.2). Atmacs is chosen because the loading of the air masses close to the station is calculated as Newtonian attraction and deformation of the Earth's crust (Klügel and Wziontek, 2009) whereas the representation of the local air masses by a Bouguer plate is used in the adjustment of the measured air pressure time series and other correction products (e.g. Boy et al. 2009). The latter method is, of course, based on the air pressure (measured or modelled) which cannot represent the effects occurring at the S1 frequency completely.

The atmospheric models describe the real atmosphere sufficiently well (in terms of reducing the residuals that remain after the tidal analysis, e.g. Boy et al. 2002; Klügel and Wziontek 2009), therefore, it is in some cases possible to correct the gravity data with Atmacs. If the atmospheric gravity time series describes the effects in the atmosphere at the S1 frequency correctly, the annual variation of the K1 parameter should be reduced.

The Atmacs time series are also used for synthetic data MWA. For stations where the correction of the measured data worked, well the variations of the tidal parameters obtained with synthetic data MWA should be similar to the results obtained from measurements.

The ocean loading contribution at S1 and other frequencies in the K1 wave group cannot be investigated with stationary ocean models. Those models typically used for correcting for ocean loading in gravity measurements consist of temporally constant amplitudes and phases for about 10 constituents. S1 is usually not included. Therefore, the ocean models for the investigation of the annual variations of the M2 tidal parameters (see sections 4.2.2 and 5.2.2) are used here as well. In this case only the synthetic data MWA is used because the models probably do not describe the real ocean precisely enough for correcting the measured gravity signal.

4.2.2. M2

To investigate the influence of the variation of M2 in the oceans it is necessary to use a data set which potentially contains it. Stationary ocean models cannot account for the variation as they usually only give amplitudes and phases for the largest harmonics. Nonlinear, time-stepping ocean models which account for barotropic and baroclinic tides (see section 5.2.2.1) as well as currents and other relevant effects like the mixing of the ocean water and friction effects (see chapter 1.1) might be able to describe these variations.

The ocean models used here are described in section 5.2.2. They are not as precise for the

barotropic tides as the stationary models, but in contrast potentially describe the annual variation of the M2 amplitude. First, the SSH is analysed to see whether it contains an annual variation of the M2 amplitude.

Then the SSH is used for calculating a synthetic time series of ocean loading which is subsequently added to synthetic body tides. As mentioned at the beginning of section 4.2, the results of synthetic data MWA of these data will show the variations caused by the ocean models. Similarities with results from measurements are a good reason for denoting the variations of the M2 amplitude in the oceans as the cause for the variations of the M2 tidal parameters estimated from gravity measurements. For this comparison the order of magnitude of the variation of the tidal parameters (between 10^{-4} and 10^{-3} for the gravimetric factor and $0.01°$ to $0.1°$ for the phase, depending on the station) and the periods are compared. It is not expected that the loading from the models is able to describe the variation of the tidal parameters precisely.

A comparison of the stationary parts (mean values, see section 3.1.2) of the time-dependent tidal parameters estimated with measured and synthetic data is a measure of how well the stationary M2 amplitude is described by the ocean model. The models used here are not expected to explain the offset of the measured data as good as the stationary ocean models; but if they describe the stationary M2 amplitude realistically, their contribution should at least have the correct sign. This means, if the tidal parameters estimated from measurements are larger than the values predicted by the body tide model, the ocean loading contribution of the models should also increase the tidal parameters obtained with the synthetic data.

The results of the harmonic analysis can be used for finding the regions which contribute significantly to the loading and annual variation of the tidal parameters. This is done by calculating the loading only for grid points whose maximal gravity contribution exceeds a certain threshold. In comparison to the results obtained with the whole ocean model, this investigation shows how many grid points are needed to get results which are close to the results of the total model. Plotting the necessary grid points in a map shows from which area significant contributions originate.

4.2.3. Other wave groups

At the O1 frequency, there is no indication for a certain cause generating the temporal variations of the O1 tidal parameters that would be more likely than another. However, this wave group is often studied in tidal research as it has the second largest amplitude in the diurnal band and is not, like K1, influenced by many other effects (see chapter 1). Therefore, it is checked whether there is an influence of atmosphere or oceans visible in the O1 tidal parameters.

Even if the changes of the amplitude ratios of the theoretical tidal parameters of Dehant et al. (1999) relative to the values ETERNA uses (Dehant, 1987) are too small to explain the variations of the observed tidal parameters of Q1, M1, 2N2, N2 and L2, their influence is tested by changing the values for the theoretical tidal parameters in the ETERNA code. The results for the mentioned wave groups are compared to the results obtained with the

original version (with changed FCN model, see section 7.1) in order to see whether there is a significant influence of the model assumptions. As they will probably not explain the observed variations completely, the ocean loading is tested as a possible cause. Similar to the approach described in section 4.2.2 synthetic data MWA with ocean models are used for checking whether similar periodicities and amplitudes of the same order of magnitude are observed.

The same approach is used for S2. Because of the likely influence of the atmosphere, this is done in combination with the Atmacs time series, similar to the investigations described in section 4.2.1. Also, the correction of measured data with Atmacs, mentioned there, is studied.

Chapter 5.

Data and models

In this chapter the data used for the study are presented.

5.1. Superconducting gravimeter data

For this study, data from superconducting gravimeters are used. The technical details of SGs are not discussed here; the reader is referred to, for instance, the description by Hinderer et al. (2007). All of the measured SG data sets were downloaded from the International Geodynamics and Earth Tide Service (IGETS) database[2] (Voigt et al., 2016). Preprocessed hourly data are used. The station names and the length of their time series are listed in Tab. 5.1. From BFO and Onsala additional data sets were provided by the station operators. Both data sets from BFO (from IGETS and from the station operators) are combined because they cover different time periods. The data sets from Onsala cover the same period but were preprocessed differently (see section 4.1.1). The additional data set provided by the station operators was not available at the beginning of the study, therefore the IGETS data set was used for the investigations of the influence of the atmosphere (see chapter 7). For the comparisons with the results of the synthetic data MWA with time-dependent ocean loading (see chapter 8), the data set provided by the station operators was used.

The selection of stations was based on the length and the quality of the data and the location of the station. Their locations are shown in Fig. 5.1. For dual-sphere instruments (marked with an asterisk in Tab. 5.1) the data from the lower sensor are used, as they are usually insensitive to magnetic disturbances as opposed to the upper sensors (Zürn et al., 2008). In 2010 the SG in Wettzell was exchanged, therefore two entries are listed in Tab. 5.1. With the MWA of the data from Wettzell, it was possible to identify periods in the data set in which the time lag and the calibration factor given in the header of the data files are wrong. This was also observed by Meurers et al. (2016). The misleading term 'calibration factor' is used in the ETERNA manual (Wenzel, 1997b). This factor is multiplied with the gravity time series. If the calibration factor of the SG is precisely known and applied correctly to the raw data, the 'calibration factor' in the header of the data file should be 1.0.

The values of the time lag and the 'calibration factor' at Wettzell were corrected (P. Wolf,

---

[2] https://isdc.gfz-potsdam.de/igets-data-base/ (10.07.2019)

station		length
BF: Black Forest Observatory*, Germany		2009-2016
BH: Bad Homburg*, Germany	CD030*	2004-2006
	SG044*	2006-2015
CA: Cantley, Canada		1997-2013
CB: Canberra, Australia		1997-2015
CO: Conrad, Austria		2007-2013
KA: Kamioka, Japan		2004-2013
MC: Medicina, Italy		2004-2015
MB: Membach, Belgium		1997-2011
MO: Moxa*, Germany		2000-2014
OS: Onsala, Sweden	SG054 OSO	2009-2018
	SG054 IGETS	2009-2016
PE: Pecny, Czech Republic		2006-2014
ST: Strasbourg, France		1997-2013
SU: Sutherland*, South Africa		2000-2014
SY: Syowa, Antarctica		1998-2001
TC: TIGO Concepci'on		2003-2013
WE: Wettzell, Germany	CD029*	1998-2010
	CD030*	2010-2015

Table 5.1. SG data sets. Name and abbreviation of the station and length of the data set. Dual-sphere instruments are marked with an asterisk.

H.Wziontek, pers. comm., Wziontek 2016), but then still steps occurred that seemed to be cause by changes of the 'calibration factor' or time lag. Therefore, the values were chosen such that the curves of the tidal parameters contain as few and as small steps as possible. This does not necessarily mean that these values are the true ones. Tab C.1 in appendix C shows the original and corrected values.

Also, at Bad Homburg an offset between the results obtained from the two different SGs occur. The headers indicate that they were preprocessed by different persons. As the data sets are used separately in my study, there is no further investigation of this issue. It is small enough (see Fig. 6.2) to be of no relevance for the interpretation of the stationary part of the tidal parameters and it does not influence the temporal variations anyway.
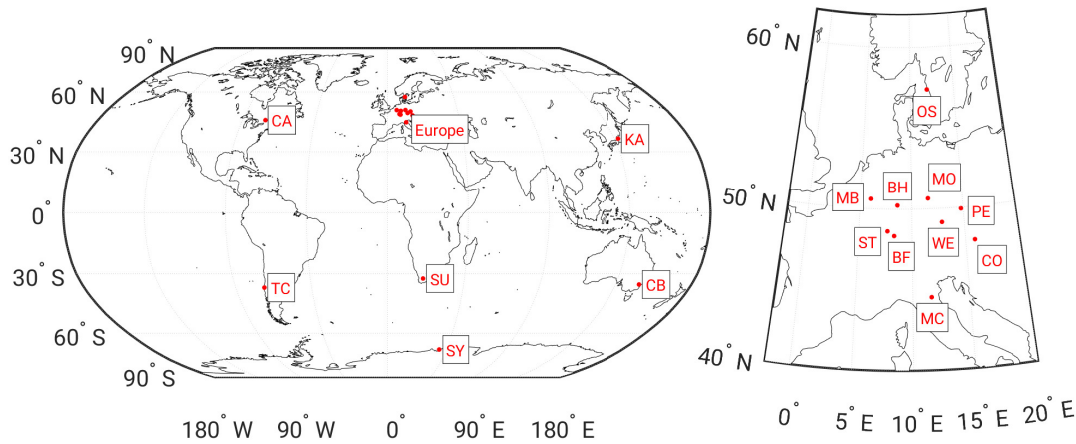
Fig. 5.1. Locations of the SG stations. Left: global stations, CA: Cantley, Canada; CB: Canberra, Australia; KA: Kamioka, Japan; SU: Sutherland, South Africa; SY: Syowa, Antarctica; TC: TIGO Concepcion. Right: European stations, BF: Black Forest Observatory (BFO), Germany; BH: Bad Homburg, Germany; CO: Conrad, Austria; MB: Membach, Belgium; MC: Medicina, Italy; MO: Moxa, Germany; OS: Onsala, Sweden; PE: Pecny, Czech Republic; ST: Strasbourg, France; WE: Wettzell, Germany.

5.2. Synthetic data

The following sections contain information about the used synthetic data sets. The synthetic Earth tides are described first, followed by an overview of the ocean models and the atmospheric loading.

5.2.1. Synthetic body tides

The synthetic body tides are calculated as described in section 3.1.3. Using exactly the same wave groups for calculating synthetic body tides as in the analysis, it is assured that no variations in the results are caused by the synthetic body tides. The tidal parameters $\delta = 1.16$ and $\varphi = 0°$ were assumed for Q1, O1, M1, J1, OO1, 2N2, N2, M2, L2 and S2. For K1, δ was set to 1.13; for M3M6, δ was set to 1.06. The parameters given above were assumed for all analyses with oceanic data used in chapter 8. In chapter 7 the gravimetric factor for K1 was accidentally also set to 1.16. As this is not relevant for the variation and the mean values are not discussed in the context of K1, I desisted from redoing the analyses with $\delta = 1.13$.

5.2.2. Ocean models

In the following sections the different ocean models used for the study are depicted. The description of the essential equations is followed by a comparative overview of the properties

of the ocean models. In sections 5.2.2.3 to 5.2.2.7 the main properties of the ocean models are described.

5.2.2.1. Description of the motion of ocean water

The motion of ocean water is driven among others by the tidal forcing, atmospheric forcing like winds and buoyancy, e.g. due to heating/cooling and precipitation/evaporation, Earth tides and earthquakes. For my purpose the tidal forcing is important but also the atmospheric forcing. The latter forces the general ocean circulation which interact with the tides. It cannot be excluded that short-term, transient signals like tsunamis show up in SG measurements but it is unlikely that they influence tidal parameters significantly.

The shallow water equations describe the motion caused by the forcing mentioned above. The volume conservation (corresponds to mass conservation, see section 5.2.2.2) and momentum equations for one layer (barotropic) are:

$$\frac{\partial \vec{v}}{\partial t} + \vec{v} \, \vec{\nabla} \cdot \vec{v} + \vec{f} \times \vec{v} = -g\vec{\nabla} h + \vec{b}_{ev} + \vec{b}_{bf} + \vec{b}_{id} + \vec{b}_{SAL} + \vec{b}_{td} + \vec{b}_{tides} + \vec{b}_{atmos} + \dots \quad (5.1)$$

$$0 = \frac{\partial h}{\partial t} + \vec{\nabla} \cdot ((H + h)\vec{v}\,) \quad (5.2)$$

Describing the oceans by a system of equations like 5.1 and 5.2 requires assumptions. There could be phenomena which are not taken into account in any case and which could be formulated differently in their mathematical description. Because of this, the terms $\vec{b}_{xxx}$ are represented in this generalised form. The eddy viscosity term (ev) parameterises dissipation of energy due to internal friction, the bottom friction (bf) describes the friction at the sea floor and the ice drag (id) friction at sea ice. The excess of mass during a high tide attracts the surrounding masses. At the same time the mass deforms the Earth's crust. The self-attraction and loading (SAL) term takes these effects into account. Interaction of currents with topography is described by the topographic drag (td), while *tides* and *atmos* describe the tidal and the atmospheric forcing, respectively. The points denote that this equation does not make a claim on completeness. Other effects could possibly be taken into account. $\vec{v}$ is the velocity of the current, t the time, g the absolute value of the Earth's gravitational acceleration, $\vec{f} \times \vec{v}$ describes the Coriolis force and h the sea surface height (SSH) relative to H, the undisturbed sea level. Usually, the equations for salinity and temperature complete this set of equations.

Equations 5.1 and 5.2 describe an ocean with only one layer. The barotropic tides, the direct response of ocean water to tidal forcing, exist in this system but other important effects depend on the variation of physical properties of the water, e.g. the temperature, with depth. With these equations, it is also not possible to describe the stratification of the water which is important for the annual variation of the M2 amplitude (Müller, 2012; Müller et al., 2014), as described in section 4.1. A correct description of a layered ocean is also necessary for the correct description of internal waves. Internal or baroclinic waves occur within the water column and have only small amplitudes at the surface. They are

important for the mixing of the water column and are generated, for example, by interaction of currents or tidal flow with topography and shelves or with each other. A significant part of energy of the barotropic tides is converted to baroclinic tides (e.g. Baines 1982). In regions where large internal tides occur an interaction between the internal M2 tide and the annual variation of the M2 amplitude in the oceans is possible (Müller et al., 2014).

5.2.2.2. Properties of the ocean models

All ocean models available for this study use a version of the equations described in section 5.2.2.1. They take into account different phenomena and use different assumptions. Tab. 5.2 lists some properties of the ocean models, but cannot reflect all differences in detail. The information is taken from several publications (Arbic et al., 2012; Arbic et al., 2010; Dobslaw et al., 2013; Gräwe et al., 2015; Mehra and Rivin, 2010; Müller et al., 2014; Thomas et al., 2001) and from personal communication (M. Müller, B. K. Arbic, J. F. Shriver, J. Saynisch, U. Gräwe, A. Mehra and L. Liu). The full names of the models are given in sections 5.2.2.3 to 5.2.2.7. The lengths and dates of the time series were determined by the available data, except for OMCT and the North Sea model. In case of OMCT, the data sets were specifically calculated for this study; in case of the North Sea model, of which a very long data set is available, a suitable period based on the availability of measured SG data was chosen.

Two different representations are used for the tidal forcing. The ephemerides describe the position of a celestial body, which allows the calculation of the tidal effects this celestial body is causing on Earth. This is used as forcing for Stormtide and OMCT. The second possibility is the usage of harmonics, e.g. from a tidal catalogue (see section 2.2.2). The number of harmonics used by ARTOFS and HGT are given in Tab. 5.2 and they are specified in sections 5.2.2.3 and 5.2.2.6. For the North Sea model see section 5.2.2.7.

A widely used assumption for ocean modelling is the Boussinesq approximation (Mellor, 1996). It was applied in all five models. It replaces the mass conservation by a volume conservation (see equation 5.2).

Measured data are sometimes used to obtain results closer to real oceans. This can be done by assimilation or nudging. In case of this study, I do not distinguish between both concepts and therefore, I focus on the fact that observational data are used.

The ocean models are already described in detail by their developers (see citation in sections 5.2.2.3 to 5.2.2.7). The focus of the following sections is on the most important details for this study.

5.2.2.3. Atlantic real-time ocean forecast system (ARTOFS)

A description of the model is given by Mehra and Rivin (2010). It is a regional model which covers the North Atlantic from approximately 25°S to 72°N and from 98°W to 16°E. The spatial resolution varies over the grid. It is the highest in the Gulf of Mexico and the lowest at the African coast. In the North Sea it has still a resolution of about 9 km which is in

	ARTOFS	Stormtide	OMCT	HGT	North Sea
period	2008-2017	'prototype year' 1954-1956 **	2001-2015	2006-2010	2009-2013
region	North Atlantic	global	global	global	North Sea
spatial res.	0.03°-0.1°	0.06° 0.1°	1.0°/1.875°	0.03° 0.08° ***	0.0333° 0.0556° ***
temporal res.	1h	arbitrary 1h	2h/3h	1h	1h
vert. layers	26*	40	20/13	32	42
tidal forcing	8 harmonics	ephemerides	ephemerides	8 harmonics	-
meteo. forcing	ws, wv, p fw, pr, hu T, rf	ws, wv pr, hu rf, T, h(c)	ws, p fw T	ws, wv, p pr, ev T, h	ws, p fw, pr, hu T,cc
output	SSH	A, ϕ SSH	SSH, OBP	SSH (total, nonsteric)	SSH
nudging	yes	yes	yes	no	no

Table 5.2. Properties of the ocean models. ws: wind stress; wv: wind speed; p: pressure; h: heat flux; fw: fresh water flux; T: temperature; pr: precipitation; ev: evaporation; rf: radiation flux; hu: humidity; cc: cloud coverage; (c): climatologic, SSH: sea surface height; OBP: ocean bottom pressure; A, ϕ: amplitudes and phases for lines.*: 21 isopycnal, 5 z-level.; **: there are two different types of output available, please see section 5.2.2.4 for details; ***: resolution is different in latitude and longitude direction.

the same order of magnitude as the resolution of the global models Stormtide and HGT (see Tab. 5.2).

It is close to the HGT model (B. K. Arbic, pers. comm., see section 5.2.2.6) but, in contrast, nudges measured data for sea surface temperature from radiometers and satellites, sea surface height via sea level anomalies from altimeter data and temperature and salinity profiles from ARGO floaters. From all the available models it uses most measurements. Tidal forcing is described by the eight major diurnal and semidiurnal lines (Q1, O1, P1, K1, N2, M2, S2, K2). At the open boundaries it is driven by the same lines from the TPX06 model (Egbert and Erofeeva, 2002).

Hourly SSH values are used for the calculation of ocean loading. An example is shown

in Fig. 5.2. The date 01.01.2010, 03:00 was chosen because it is one of the time steps which is available for all models. The data were downloaded from http://data.nodc.noaa.gov/opendap/ncep/rtofs/ in spring 2015. Unfortunately, this website is no longer available, but the data can still be accessed via https://data.nodc.noaa.gov/thredds/catalog/ncep/rtofs/ (last access: 11.09.2018).
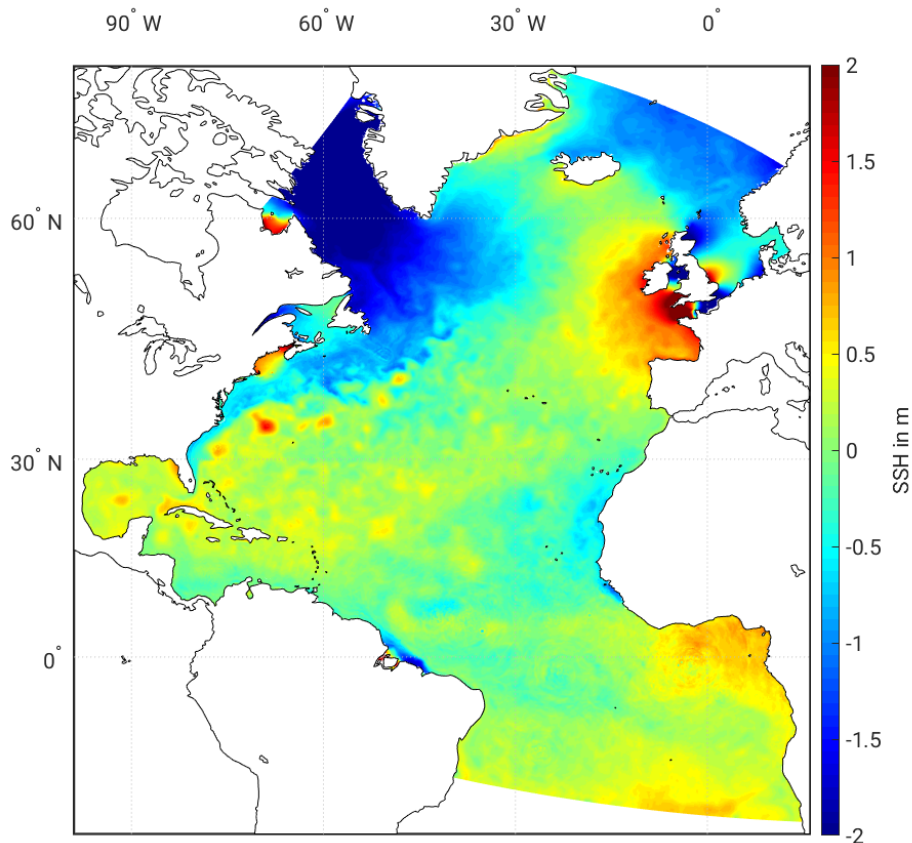
Fig. 5.2. Sea surface height (SSH) from the ARTOFS model at 01.01.2010, 03:00.

5.2.2.4. Stormtide

Stormtide is the only model which was used for the investigation of the annual variation of the M2 amplitude in the oceans (Müller, 2012; Müller et al., 2014). This was done by the harmonic analysis of SSH, described in section 3.3. Amplitudes and phases for harmonics in a frequency distance of $\pm\frac{1}{1a}$, called MA2 and MB2 or $\alpha2$ and $\beta2$, were estimated (Müller et al., 2014). Amplitudes and phases of $\alpha2$ and $\beta2$ were used to calculate the amplitudes and phases for an annual variation of the M2 amplitude, shown in Figs. 8.1 and 8.2 in section 8.1. The SSH with M2 frequency h_{M2} is calculated with the amplitude A_{M2} and the phase ϕ_{M2} of M2 and the amplitude A_v and the phase ϕ_v of the annual variation (Müller

et al., 2014):

$$h_{M2}(t) = (A_{M2} + A_v \cos(\omega_v t - \phi_v)) \cos(\omega_{M2} t - \phi_{M2}) \tag{5.3}$$

The amplitude A_v and the phase ϕ_v are estimated from the amplitudes $A_{\alpha 2}$, $A_{\beta 2}$ and phases $\phi_{\alpha 2}$, $\phi_{\beta 2}$ of the two harmonics with a frequency distance of $\Delta f = \pm \frac{1}{1a}$ to the M2 frequency. They can be estimated in a harmonic analysis of SSH. A_v and ϕ_v are calculated with equations 5.4 and 5.5 (M. Müller, pers. communication).

$$A_v = \sqrt{A_{\alpha 2}^2 + A_{\beta 2}^2 + 2A_{\alpha 2}A_{\beta 2}\cos((-\phi_{\beta 2} + \phi_{M2} + \Delta\phi_{AS\beta}) - (\phi_{\alpha 2} - \phi_{M2} + \Delta\phi_{AS\alpha}))} \tag{5.4}$$

$$\phi_v = \arctan\frac{A_{\alpha 2}\sin(\phi_{\alpha 2} - \phi_{M2} + \Delta\phi_{AS\alpha}) + A_{\beta 2}\sin(-\phi_{\beta 2} + \phi_{M2} + \Delta\phi_{AS\beta})}{A_{\alpha 2}\cos(\phi_{\alpha 2} - \phi_{M2} + \Delta\phi_{AS\alpha}) + A_{\beta 2}\cos(-\phi_{\beta 2} + \phi_{M2} + \Delta\phi_{AS\beta})} \tag{5.5}$$

$\Delta\phi_{AS\alpha} = -177.5°$ and $\Delta\phi_{AS\beta} = 2.45°$ (M. Müller, pers. communication) are the differences between the astronomical arguments of M2 and α_2 or β_2, respectively. The output is available as amplitudes and phases of the largest eight diurnal and semidiurnal harmonics (Q1, O1, P1, K1, N2, M2, S2, K2) as well as an annual variation of M2 amplitude. The phases are given in months, which is the time when the maximum in the annual variation of the M2 amplitude occurs. The amplitudes and phases were estimated from SSH in the years 1954 to 1957. Additionally, the SSH values, from which the amplitudes and phases were estimated, were available for this study. The data from 1954 to 1956 are used here. The data from 1957 are not available in the same data format as the data from the other years. As the forcing is climatologic, the results are not expected to differ much from year to year and I considered 3 years as long enough for the loading calculations and the synthetic data MWA.

While for the other ocean models re-analysis are used to describe the meteorological forcing, here the forcing is climatologic. The tidal forcing is described by the tidal potential of second degree calculated based on ephemerides. The model uses nudging for the sea surface temperature and salinity (Steele et al., 2001).

5.2.2.5. Ocean model for circulation and tides (OMCT)

The OMCT model has the lowest spatial resolution compared with the other models (Dobslaw et al., 2013; Thomas et al., 2001). Two versions exist with 1.875° and 1.0° resolution, respectively, which differ also in other properties. They are forced, like Stormtide, with the tidal potential of second degree calculated based on ephemerides. The output is given as distribution of SSH and ocean bottom pressure (OBP) every 3h for the 1.875° and every 2h for the 1° resolution. For my analysis it was necessary to interpolate the OMCT gravity time series to hourly values. Linear interpolation is used. The influence of the interpolation on the tidal parameters is discussed in appendix F.3.

For the ocean loading, equation 2.13 has to be adjusted:

$$\delta b_l = \int G \underbrace{\rho(t)h}_{=\frac{P}{g}} \, dA \tag{5.6}$$

Here, P is the OBP and g the value of the Earth's gravitational acceleration. In contrast to the density ρ in equation 2.13, the density $\rho(t)$ in equation 5.6 is not constant. The OBP represents the mass of the complete water column and the column of the overlaying atmosphere. In contrast to the SSH, this includes density variations that change the mass of the water column but not the SSH and it contains information about the atmosphere as well.

First tests were made with the Earth's gravitational acceleration $g = 9.81 \frac{\text{m}}{\text{s}^2}$ independent from the position. Before the loading signal was added to the synthetic body tides, the mean value of about -1000000 $\frac{\text{nm}}{\text{s}^2}$ had to be removed because the data format in ETERNA does not allow values higher than 999999.999. The constant part of the loading signal does not affect the results anyway.

The differences of the results calculated with OBP compared to those calculated with SSH were small for M2 (see section 8.2.3.1 for details). Therefore, I refrained from using OBP and concentrated on the calculation with SSH. The significant differences in the results for K1 and S2 of these first tests mentioned above are discussed in sections 7 and 9.

Several SSH data sets with differences were calculated for this study by J. Saynisch. As the changes of the properties were made dependent on the result of each previous study the reasons for the changes are given in section 8.2.3.2. Tab. 5.3 gives an overview on these data sets. Changes were made regarding the ice drag, because Müller et al. (2014) pointed

property	1.875°, 3h length	1.0°, 2h length
original	2001-2013	2010-2013
ice drag	2010-2015	2010-2012
strong nudging	2010-2013	-
weak nudging	2010-2013	-

Table 5.3. Properties of the different OMCT data sets. The first column gives the property that was changed, the 2. and 3. column the length of the data set for the two versions of OMCT.

out as a reason for the variability of the M2 amplitude in Arctic regions. In the original version the water could transfer momentum to the ice, but not the other way round. This means, for example, that the water was not slowed down by slower sea ice. The formulas given by Müller et al. (2014) were used (J. Saynisch, pers. communication).

With the strong nudging (tenfold larger than the weak nudging) the model was forced to

follow the expected, climatologic values from the World Ocean Atlas[3], while in case of the weak nudging the model could develop more independently. Fig. 5.3 shows an example of the SSH and OBP from the original model version at 01.01.2010, 03:00. The differences are obvious especially for the SSH. The OBP is dominated by the depth of the ocean basins but there are also differences visible.

5.2.2.6. HYCOM global tides model (HGT)

The HGT model is described by Arbic et al. (2012) and Arbic et al. (2010). In comparison to the global models it has the highest horizontal resolution but less vertical layers than Stormtide. The distance of the grid points varies slightly over the grid. It is driven by the eight largest diurnal and semidiurnal lines (Q1, O1, P1, K1, N2, M2, S2, K2). The output is available as hourly snapshots of the total and the nonsteric SSH, which are shown in the top and in the middle panel of Fig. 5.4. Steric effects are caused by thermal expansion or contraction. The change of volume, which causes changes in the SSH, is accompanied by the correspondingly varying density. The mass which is crucial for the loading does not change. If the total SSH for the loading calculation is used and the density is assumed to be constant, a change in the SSH is directly interpreted as variation in mass. By comparing the results of total and nonsteric SSH, the influence of this effect can be estimated.
As can be seen in the middle of Fig. 5.4, the nonsteric SSH shows a large-scale pattern. It represent the barotropic tides, while the steric SSH shows small-scale features, related to the baroclinic tides.

5.2.2.7. North Sea model

The North Sea model (Gräwe et al., 2015) is a local model with a high spatial resolution. It is restricted to the North Sea between about 5°W and 13°E and between about 48°N and 61°N. It has the highest spatial resolution of all the ocean models used here. No astronomical forcing is used, because the tides coming in from the boundaries, like at the English Channel, dominate the tidal patterns in the North Sea. They are taken from the OSU tidal data inversion model (Egbert et al., 2010). The lines which were used are the largest diurnal and semidiurnal tides (Q1, O1, P1, K1, N2, M2, S1, K1), the quarter-diurnal M4 and the nonlinear tides MS4 and MN4. The output is given as hourly distributions of SSH. An example is shown in Fig. 5.5.

5.2.3. Atmosphere

The atmospheric masses also have an influence on gravity measurements. Hereafter, atmospheric signals, which are important for gravity, are discussed. In the second part of the section the data from Atmacs are described.

---

[3] https://www.nodc.noaa.gov/OC5/indprod.html (04.07.2019)
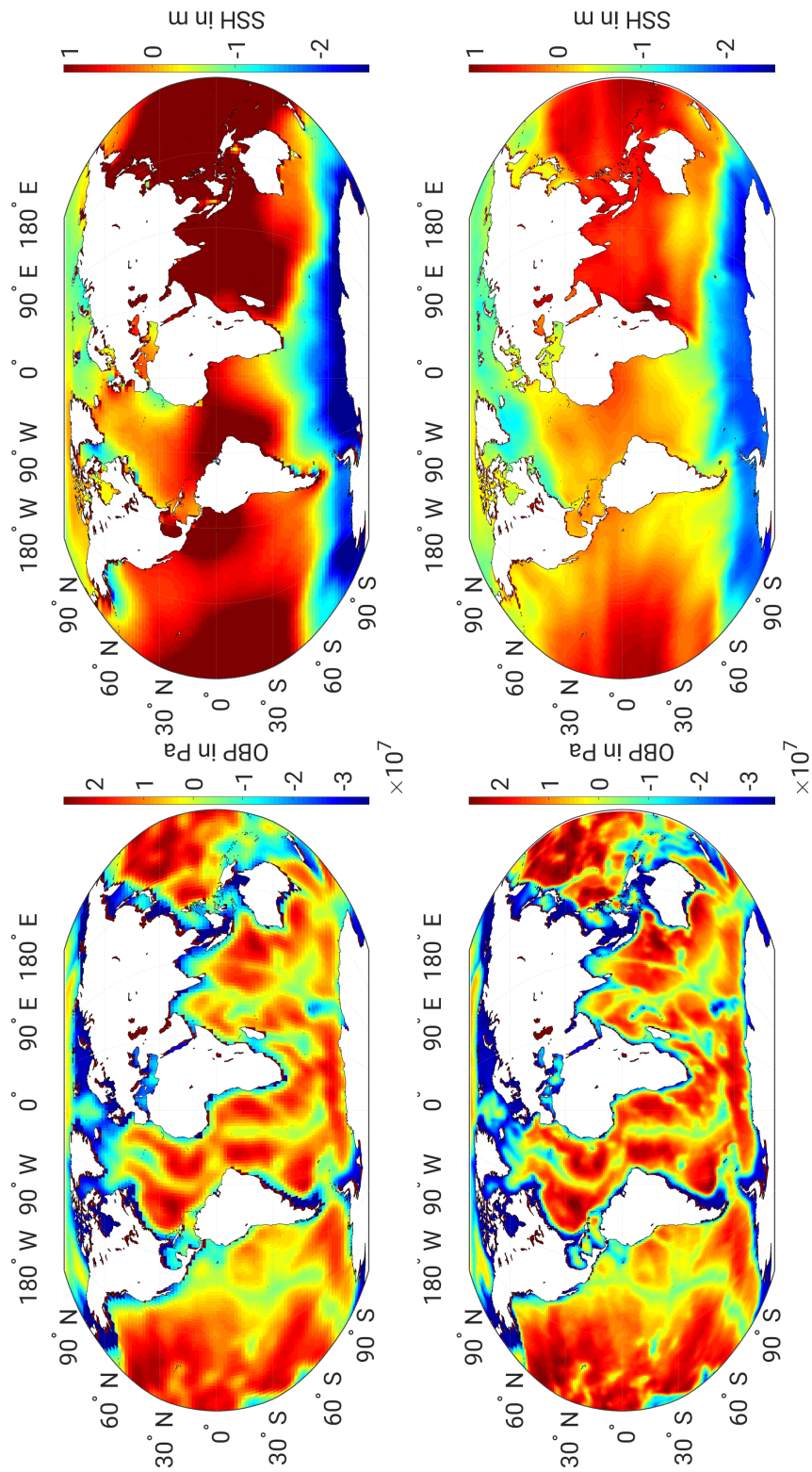
Fig. 5.3. SSH (top) and OBP (bottom) at 01.01.2010, 03:00; 1.875° resolution (left) and 1° resolution (right). The mean value was removed in each case.
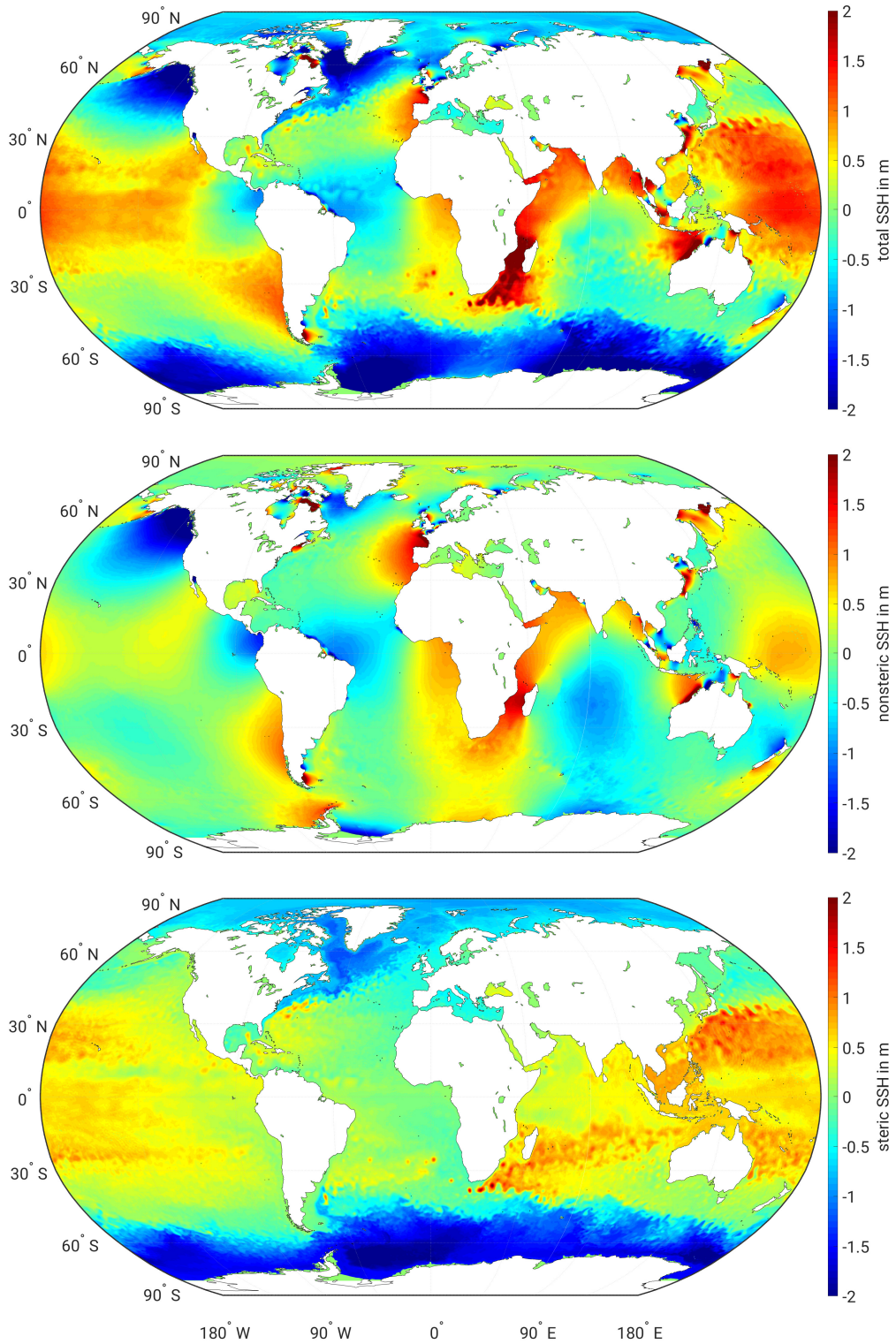
Fig. 5.4. Top: total SSH in metres from the HGT model at 01.01.2010, 3:00, middle: nonsteric SSH, bottom: steric SSH.
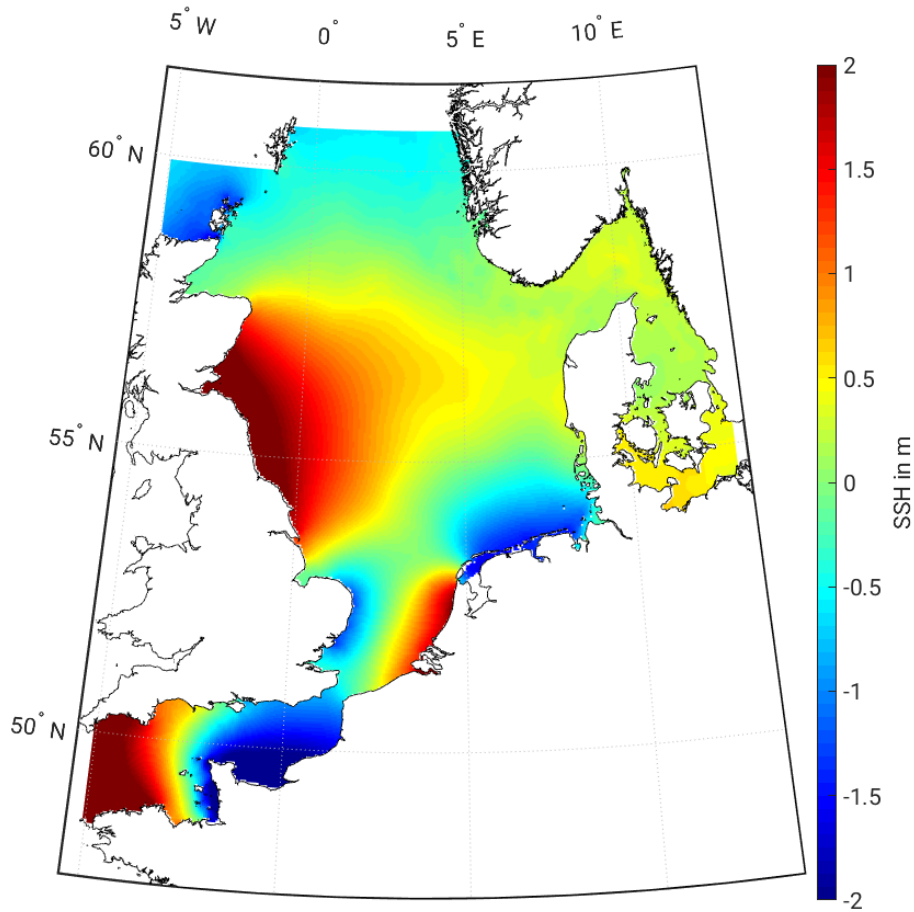
Fig. 5.5. SSH in metres from the North Sea model at 01.01.2010, 3:00.

5.2.3.1. Atmospheric gravity signals

The gravitational effects of tidal forcing in the atmosphere are relatively small (Volland, 1997). There are on one hand similarities to ocean tides, for example because of the interactions of the tides with currents and internal tides in the atmosphere, but on the other hand there are large differences because the motion of the ocean water is bordered by the continents, in contrast to the air masses. A detailed description of atmospheric tides is given for example by Volland (1997). The focus here will be on radiation or thermal tides, because they probably are the cause for some of the variations discussed in sections 7.3 and 9.3. They are much larger than the tidal signals and mainly driven by the heating of the Sun. Therefore, they occur with solar frequencies like S1 and S2.
As described in section 2.3 the gravity effect of loading is a combination of deformation of the Earth's crust and direct attraction. In contrast to the oceans, whose masses are located

below the instrument in any case, the atmospheric masses on a local scale are above the gravimeter.

5.2.3.2. Atmospheric attraction computation service (Atmacs)

There are different institutions offering an atmospheric gravity correction for SG time series. The reason why Atmacs is used is the calculation of the attractional part with Newton's law for all atmospheric masses defined by the model. This approach should be able to represent the radiation tides more realistically than the Bouguer assumption which is used for the adjustment of locally measured air pressure to the SG data and also for other correction products.

Atmacs is operated by the Federal Agency for Cartography and Geodesy (Klügel and Wziontek, 2009). It provides time series of the atmospheric gravity effect for many IGETS stations. The calculation is based on the models of the German weather service (DWD), which was the regional LM/COSMO-EU model (Steppeler et al., 2003) until 30.11.2016 and ICON-EU[4] since 14.01.2016, and the global model GME (Majewski et al., 2002) until 22.12.2015 and ICON384 since 04.12.2014. The recently introduced models have a higher resolution than the older ones. ICON-EU has a triangular grid in contrast to the square cells of COSMO-EU. Most of the SG data sets (see Tab. 5.1) lie within the COSMO period. Hereafter, I do not discuss the details of COSMO and ICON, as I do not directly work with the models and do not compare with other models. For details see citations, mentioned above and the website of Atmacs[5]. The loading calculation is described in section 2.3.

Estimation of density from the atmospheric models For loading and atmospheric attraction the atmospheric masses have to be estimated. This is done with density and volume. The density is approximated using the atmospheric model. Assuming that the air behaves like an ideal gas, the density ρ can be estimated for each layer of the model by

$$\rho = \frac{p_{bot} + p_{top}}{2RT_v}. \tag{5.7}$$

p_{bot} and p_{top} are the pressure values at the bottom and the top of the layer, $R = 287 \frac{\text{J}}{\text{kg K}}$ is the gas constant and T_v the virtual temperature. This is the temperature at which dry air has the same density as wet air at a specific temperature. p_{top} can be calculated depending on p_{bot}:

$$p_{top} = p_{bot} e^{\frac{-g(z_{top} - z_{bot})}{RT_v}} \tag{5.8}$$

z_{bot} and z_{top} are the heights of the bottom and the top of a layer.

---

[4] https://www.dwd.de/EN/research/weatherforecasting/num_modelling/01_num_weather_prediction_modells/icon_description.html (04.07.2019)

[5] http://atmacs.bkg.bund.de (04.07.2019)

Calculation of the Newtonian attraction   The Newtonian attraction is calculated for different distances ranges from the station with different approaches.

The proximity of the SG station, usually nine neighbouring grid points (of the atmospheric model), is replaced by a cylinder. It covers the same area as the original grid points and is divided into layers, which correspond to the layers in the atmospheric model. The gravity effect of a disc can be calculated analytically and uses the estimation of the density as described in the previous paragraph.

For a region around the station, which extends from the local model to about 10° to 20° distance from the SG station, the same estimation for density is used. The grid cells are treated as point masses. The distance between the SG and the point mass is calculated from the geometry.

The rest of the model (the global part) was calculated in a 2D approximation, which means that the height of the grid points of the atmospheric model was neglected. Since 2008, the same approach as for the regional part described above is used.

Crustal deformation   The calculation of deformation part is described in section 2.3; it is also used for the loading of the atmosphere. However, the Green's functions have to account only for the loading and not for the attractional part. They are based on the PREM model. For interaction of atmosphere and oceans, an inverted barometer behaviour of the oceans is assumed.

Chapter 6.

Results from measured data

As described in section 4.2, the results of the investigation of synthetic data are compared to results obtained from measurements. The latter are presented in this chapter, with a focus on the K1 and M2 tidal parameters. For the results of the other wave groups (see Schroth et al. 2018).

K1

Fig. 6.1 shows as an example the results of the K1 wave group for some European stations. The upper panel contains the gravimetric factors and the lower panel the phases. The MWA was done as described in section 3.1.2.
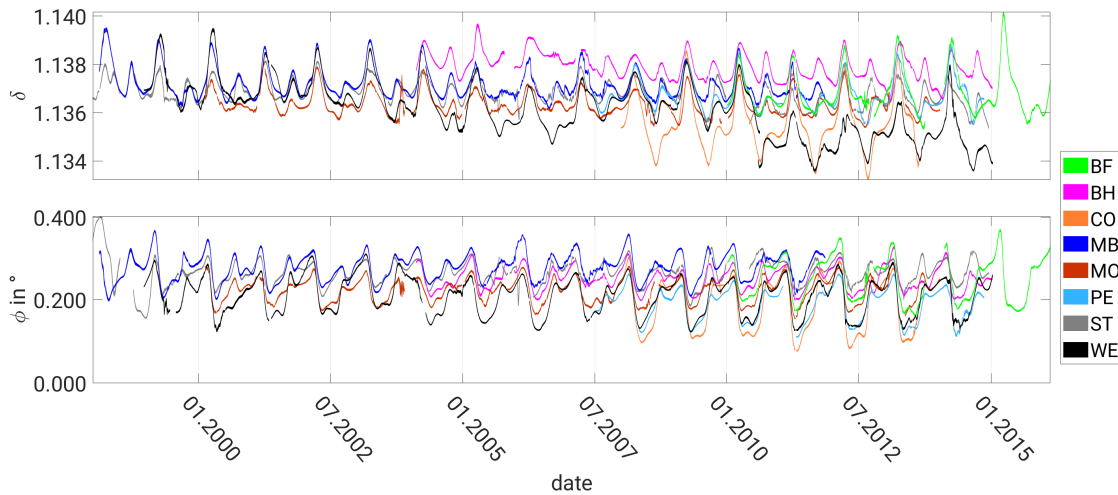
Fig. 6.1. Variation of the K1 tidal parameters for eight European stations. The upper panel shows the gravimetric factors, the lower panel the phase leads in degree. BF: BFO, Germany, BH: Bad Homburg, Germany, CO: Conrad, Austria, MB: Membach, Belgium, MO: Moxa, Germany, PE: Pecny, Czech Republic, ST: Strasbourg, France, WE: Wettzell, Germany.

The variation is a combination of annual and semiannual periods. At some stations for example Strasbourg and Bad Homburg the semiannual variation dominates, whereas for example at BFO or Conrad the annual variation is large. The amplitude of the variation is approx. $0.8 \cdot 10^{-4}$ for the gravimetric factor and about $0.07°$ for the phase. For other stations the same periodicity and the same order of magnitude are observed (Schroth et al., 2018). Especially for the European stations which are located relatively close to each other, the variations look similar.

The stationary parts of the tidal parameters are close to each other and also close to the expected value of about $\delta_{K1} = 1.134$ and $\phi_{K1} = 0°$ (Dehant et al., 1999).

A step is visible in the results from Wettzell which is caused by the usage of two different SGs and problems with the 'calibrations factors' and time lags in the data files, as described in section 5.1. It is the same for the M2 tidal parameters, shown in Fig. 6.2.

M2

The tidal parameters of M2 show an annual variation, as shown in Fig. 6.2. For the Central European stations the variation of the gravimetric factor is about $5 \cdot 10^{-4}$ and of the phase about $0.02°$ (Schroth et al., 2018). There is a close similarity in the variations of the tidal parameters whereas the stationary part differs stronger from the expected value of about $\delta_{M2} = 1.16$ and $\phi_{M2} = 0°$. This is due to ocean loading. Baker and Bos (2003) calculate tidal parameters corrected for ocean loading for several stationary ocean models at some of the stations shown here and others used later in the study. Their observed tidal parameters are quite close to the stationary part of my results and the corrected tidal parameters are
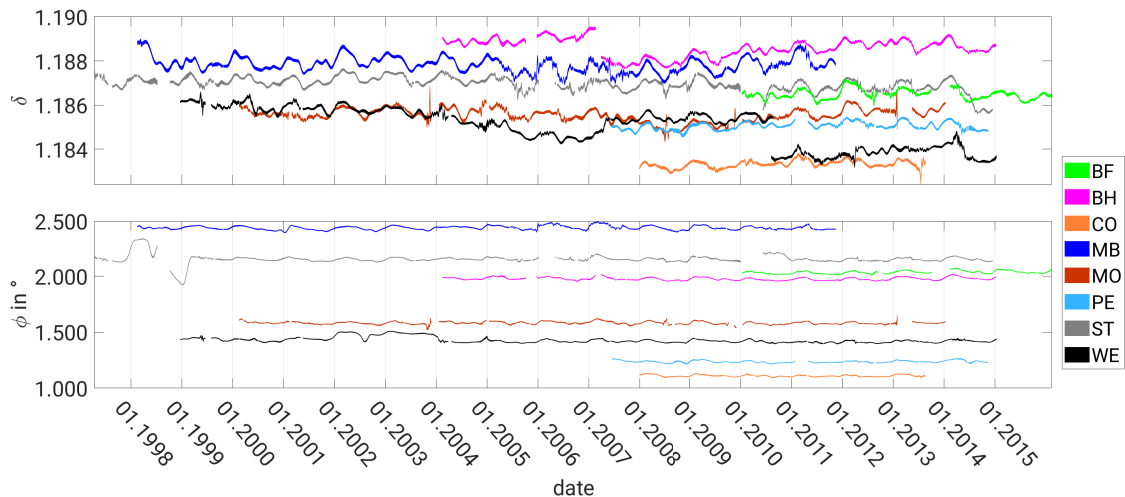
Fig. 6.2. Variation of the M2 tidal parameters for eight European stations. The upper panel shows the gravimetric factors, the lower panel the phase leads in degree. The same stations as in Fig. 6.1 are used.

close to the expected values. Therefore, it is reasonable to regard stationary ocean loading as reason for the tidal parameters deviating from the expected body tide model values.

The gravimetric factor from Bad Homburg (pink curve in Fig. 6.2) seems to increase with time. This is not observed for the phase. In Fig. 6.2 the range of the axis is too large, so even if a trend existed, it would not be visible there. However, the results from Bad Homburg plotted separately (Schroth et al., 2018) show that there is no trend in the phase. The shape of the curves may imply a long-periodic variation but the data set is too short to be sure. However, this also shows, as already mentioned in section 4.1.1, that the variation of the gravimetric factor is probably not due to a varying gain factor.

Chapter 7.

Temporal variations of K1 tidal parameters

In this section, the influence of using a more recent FCN model in the tidal analysis on the variations of the K1 tidal parameters is discussed, followed by a synthetic test in order to find out which harmonic contributes most to the remaining variation. As pointed out in chapter 1 and section 4.1.2, the loading of atmosphere and oceans are possible causes for the variations of the K1 parameters. The investigation with oceanic and atmospherical models is described in the later parts of this chapter. The variation of the K1 tidal parameters is called 'VK1' in the following. If I refer specifically to the variation of the gravimetric factor or the phase, the term is written out.

7.1. Variations caused by an outdated Free Core Nutation model

As mentioned in section chapter 1 and 4.1.2, the FCN model used in the Wahr-Dehant-Zschau model (Dehant, 1987) is outdated with respect to the FCN frequency inferred from VLBI (Krásná et al., 2013). Dehant et al. (1999) suggest theoretical tidal parameters whose calculation is based on more recent Earth models including a more recent FCN model. The value for the FCN period of $T_{FCN} = 431.37$ si. d. differs slightly from the value estimated by Krásná et al. (2013) which is $T_{FCN} = 431.18 \pm 0.1$ si. d. The difference is significant with respect to the accuracy of the VLBI methods. However, as there are most likely other effects influencing the gravity in the frequency band of K1 (see sections 7.3 and 7.4), tidal analysis does not yet reach the same level of accuracy. This is supported by the lower accuracy of the FCN period of about two sidereal days when the estimation is based only on tidal displacements from VLBI (Krásná et al., 2013).

In the following the frequency dependence of the gravimetric factor for both FCN models described above is compared with tidal parameters obtained in a tidal analysis of a long time series (approx. two years). The comparison is shown in Fig. 7.1. The calculation of the black curve is based on an FCN period of $T_{FCN} = 459.25$ si. d. (Wahr 1981, Wahr-Dehant-Zschau model, WDZ in the following) and the calculation of the red curve on $T_{FCN} = 431.37$ si. d. (D1999 in the following). The blue gravimetric factors with their
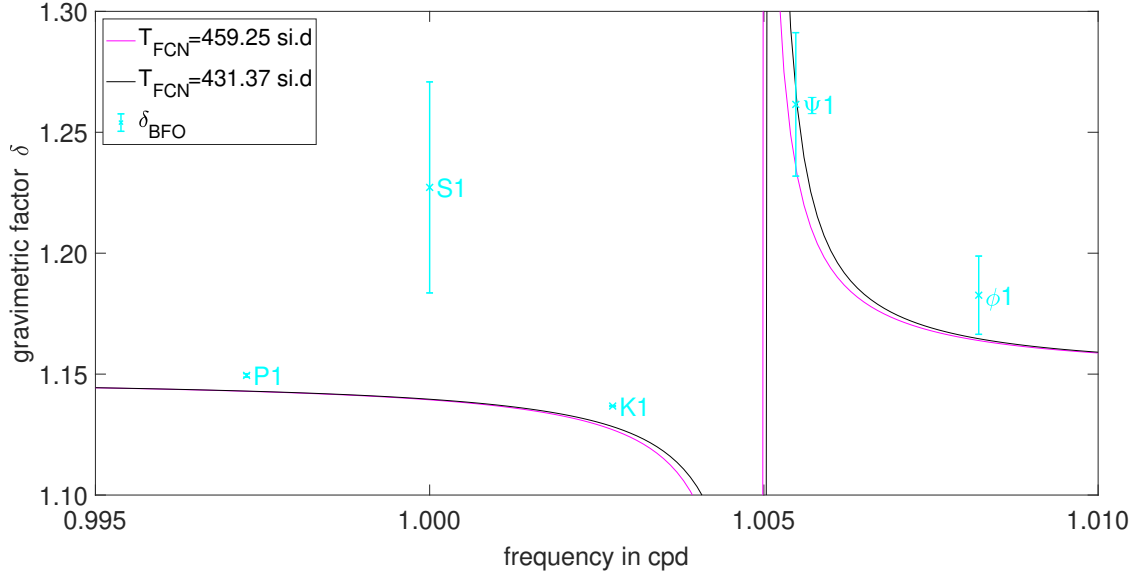
Fig. 7.1. Gravimetric factors computed with the outdated FCN model $T_{FCN} = 459.25$ si. d. in pink, with the more recent FCN model $T_{FCN} = 431.37$ si. d. in black and obtained from measurements at BFO in cyan together with their standard deviation. Frequency values taken from the Hartmann and Wenzel catalogue (Hartmann and Wenzel, 1995a,b).

standard deviation are obtained from a tidal analysis with 22 wave groups as suggested by Wenzel (1997b) for a data set longer than one year. The definition of the wave groups is given in Tab. D.1 in appendix D. The large (in terms of covered frequency range) K1 group (called K1$_{MWA}$ group in the following) used in the MWA is subdivided in five smaller wave groups. As the FCN model is only used for the scaling of the harmonics within the wave groups, the influence on the tidal parameters for the five sub-groups is weaker than in the case of the K1$_{MWA}$ group. The estimation of tidal parameters for more wave groups of which each covers a smaller frequency range is less influenced by the FCN model than the estimation of tidal parameters for one K1$_{MWA}$ group (Schroth, 2013). The gravimetric factors deviate from both assumed models by more than one standard deviation, except for $\Psi1$. This indicates that the VK1 cannot completely be explained by an outdated WDZ model. However, especially the gravimetric factor of $\Psi1$ matches the D1999 curve very well and also the other parameters are closer to the D1999 than to the WDZ model. This indicates that the more recent D1999 model can be of benefit for the reduction of the VK1. In the next step, the influence of the D1999 model on the MWA are investigated and compared to the results obtained with the original WDZ model. The values used in ETERNA 3.4 are replaced by the values given by Dehant et al. (1999). In ETERNA, the description of the frequency dependence of the gravimetric factors is represented by equation 2.11. Tab. 7.1 shows the new and the replaced values of the resonance factor r_{FCN}, the NDFW resonance frequency f_{NDFW} and the FCN period T_{FCN}, respectively. MWA are performed with the

original WDZ version and the more recent D1999 version of the FCN model. All settings are used, as described in section 3.1.2. Fig. 7.2 shows the comparison for the stations BFO, Cantley, Strasbourg and Sutherland. The black curves are the results obtained with the D1999 model; the green curve represents the results obtained with the WDZ model. In most cases the usage of the D1999 FCN model reduces the VK1. The reduction depends on the station and is largest for Strasbourg, where it is up to 40% for the phase after 07.2007. For BFO it reaches about 10% and is very small for Cantley and Sutherland. In some parts of the curves the VK1 at Cantley and Sutherland is slightly increased. At these stations probably larger loading effects occur that are the dominating cause for the VK1. Larger loading contributions are indicated by the VK1 which is for example at Sutherland about fivefold larger than at the European stations. The part of the VK1 which is caused by the FCN model is small compared to that contributions.

The FCN model does not only influence the MWA. It can affect the results of a tidal analysis of a long (several years) data set. The influence of the FCN model is smaller if the tidal parameters can be estimated for more wave groups of which each covers a smaller frequency band (sub-groups), as mentioned above. The influence of the FCN models (WDZ and D1999) on the K1 tidal parameters is investigated with tidal analyses of a long time series using a K1$_{MWA}$ in the MWA and five finer wave groups that subdivide the K1$_{MWA}$ group (see Tab. D.1 in appendix D). Fig. 7.3 shows the tidal parameters of four different tidal analyses of a data set from BFO about two years long. The gravimetric factors shown in Fig. 7.3 were obtained for the finer wave groups with the WDZ (blue) and the D1999 (black) FCN model. Instead of filtering, tidal parameters for the long-periodic tides and a drift polynomial were estimated (Wenzel, 1997a,b). For the dark and light green results shown in Fig. 7.3 the same settings as for the MWA are used. The results for all wave groups in the four analyses are given in Tabs. D.2 and D.3 in appendix D.

The results shown in blue and black in Fig. 7.3 are very similar, which matches the expectation that the FCN model has only a small influence on the tidal parameters if small sub-groups are used. The standard deviations obtained with the WDZ FCN model are about twice as large as the standard deviations obtained with the D1999 model. The same observation is made for the tidal analyses which used the MWA settings shown in the right panel of Fig. 7.3, although the standard deviations in this case are much smaller due to filtering (see section 3.1.1). This indicates that the D1999 FCN model reduces the residuals and explains the measured data better. Especially short data sets are often analysed with settings like in the MWA. From the results described above it is concluded that for short data sets the D1999 FCN model should be used.

Both gravimetric factors obtained with the MWA settings differ significantly from the results with the finer wave grouping. They deviate from each other even more. The difference between the D1999 results obtained with the different wave grouping indicates that there are other effects, probably loading, that change the amplitude ratios and phase differences with respect to the analysis model and cause the VK1.

The results in this section show that a part of the VK1 can be explained by the outdated WDZ FCN model. The D1999 model produces smaller variations and fit the measured data better; but the reduction of the VK1 is different from station to station. However, even

	r_{NDFW}	f_{NDFW} in cpd	T_{FCN} in si. d.
Dehant 1987/WDZ	-0.000625	1.0049153	459.25
Dehant et al. 1999/D1999	-0.000627	1.0050623	431.37
Krásná et al. 2013		1.0050635	431.18 ± 0.1

Table 7.1. Resonance factor r_{NDFW}, NDFW resonance frequency f_{NDFW} in cpd and FCN period T_{FCN} in sidereal days. The more recent values for the resonance factor were taken from Tab. 14 (Dehant et al. 1999, δ_0 for FCN in the nonhydrostatic inelastic case) and the resonance frequency from Tab. 13 (Dehant et al. 1999, λ_{FCN} also for the nonhydrostatic inelastic case). Please note that the frequency given by Dehant et al. (1999) is normalised. The ratio λ_{FCN} was multiplied with the Earth rotation frequency $|\vec{\omega}| = 1.00273779$ cpd to receive f_{FCN} and f_{NDFW}, respectively. Both parameters had to be rounded to the available digits in ETERNA.
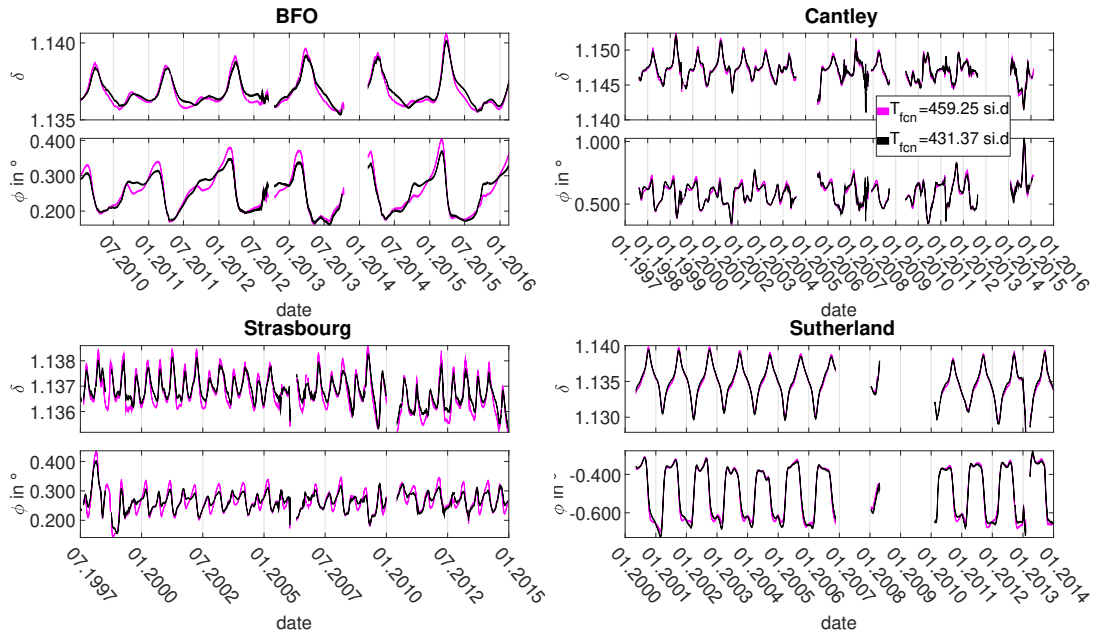
Fig. 7.2. Tidal parameters obtained from measurements at BFO, Cantley, Strasbourg and Sutherland with MWA as described in section 3.1.2, with WDZ $T_{FCN} = 459.25$ si. d. in pink and the D1999 model $T_{FCN} = 431.37$ si. d. in black.

Fig. 7.3. Left: Gravimetric factors and their standard deviations for the wave groups P1, S1, K1, Ψ1 and Φ1 with two different types of tidal analysis. The cyan (WDZ(=old) FCN) and the blue (D1999(=new) FCN) gravimetric factors were obtained with 22 wave groups and a drift polynomial and the pink (WDZ) and black (D1999) with the settings used for the MWA (see section 3.1.2). Right: Small frequency band around K1, K1 gravimetric factors from the analyses described before.

with the D1999, a VK1 remains for which other causes have to be found.

7.2. Contributions to the variation caused by the different harmonics within the K1 group

As can be seen in Fig 7.2, there is still a VK1 left which cannot be explained by replacing the WDZ FCN model. Schroth (2013) shows that the VK1 can almost completely be explained by the amplitude ratios and phase differences of the harmonics within the $K1_{MWA}$ group (represented by 5 smaller wave groups that subdivide the $K1_{MWA}$ group, see section 7.1). On the one hand, Fig. 7.1 shows that the S1 gravimetric factor (and the phase lead, see Tab. D.3 in appendix D) deviates strongly from the expectations of the FCN model ($\phi = 0°$ expected). On the other hand, the amplitude of S1, $A(S1) = 3.39\frac{nm}{s^2}$, is very small; therefore, the absolute S1 amplitude ($\delta(S1) \cdot A(S1)$) and the difference to the expected S1 amplitude is small compared to the total signal of the $K1_{MWA}$ group. In contrast, the tidal parameters of P1 differ only slightly from the analysis model, but the amplitude $A(P1) = 143.60\frac{nm}{s^2}$ is larger, so the difference to the expectations is larger. This is shown in Fig. 7.4. The question which arises from this observation is which harmonic contributes more to the VK1. The difference between expected and estimated amplitudes in Fig. 7.4 is
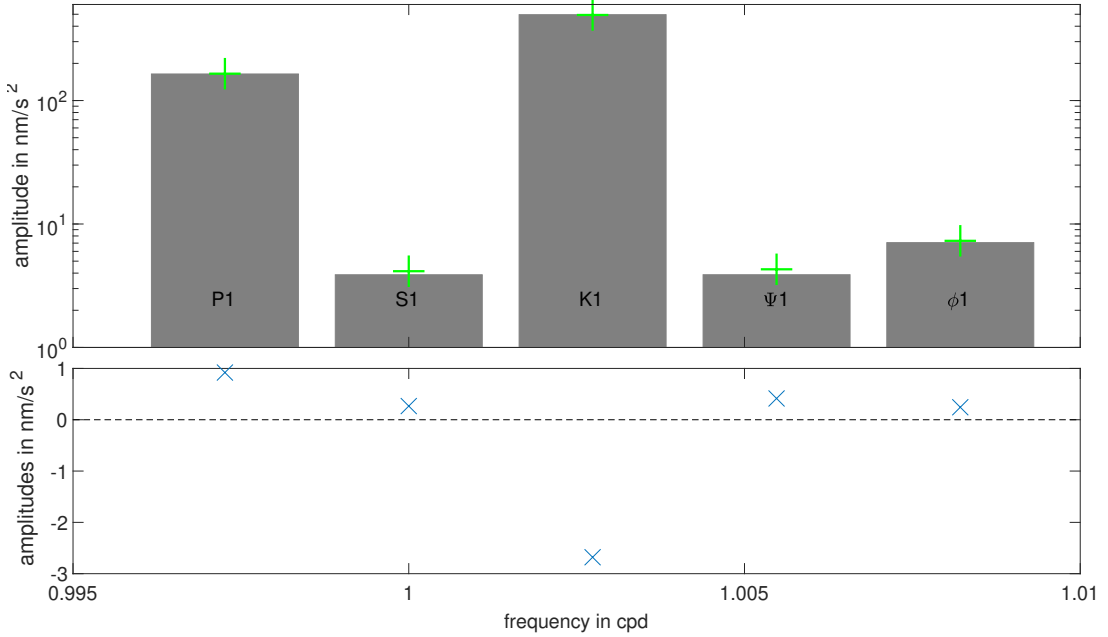
Fig. 7.4. Top: Amplitudes of the P1, S1, K1, Ψ1 and ϕ1 at BFO in $\frac{nm}{s^2}$ in grey as predicted by the body tide model and in green from tidal analysis. Bottom: Difference between both amplitudes. Please note that the upper panel has a logarithmic scale.

the largest at P1 and K1 frequencies. Hence, the expectation could arise that the P1-to-K1 amplitude ratio produces the largest variations. However, also the phases have to be taken into account. Please note that in this section whenever 'wave groups' are mentioned, the five smaller sub-groups are meant. The large K1 group that includes them all is denoted K1$_{\mathrm{MWA}}$.

It is assumed that the amplitude ratio and phase difference of K1, because of its high amplitude, to the other harmonics is crucial for the VK1. Then S1 and Ψ1 are expected to produce an annual and P1 and ϕ1 a semi-annual variation. In order to distinguish the different contributions, synthetic data sets have been prepared (see section 3.1.3) in which the harmonics follow exactly the body tide model, except for one wave group. The tidal parameters of this wave group are given by:

$$\delta(f) = \delta_{model}(K1)\frac{\delta_o(f)}{\delta_o(K1)} \tag{7.1}$$

$$\phi(f) = \phi_o(f) - \phi_o(K1) \tag{7.2}$$

$\delta(f)$ is the gravimetric factor at frequency f (here the P1, S1, Ψ1 or ϕ1 frequency) and $\frac{\delta_o(f)}{\delta_o(K1)}$ is the ratio between the observed gravimetric factor at frequency f and the observed K1 gravimetric factor. $\phi_o(f)$ and $\phi_o(K1)$ are the observed phase leads of the harmonics
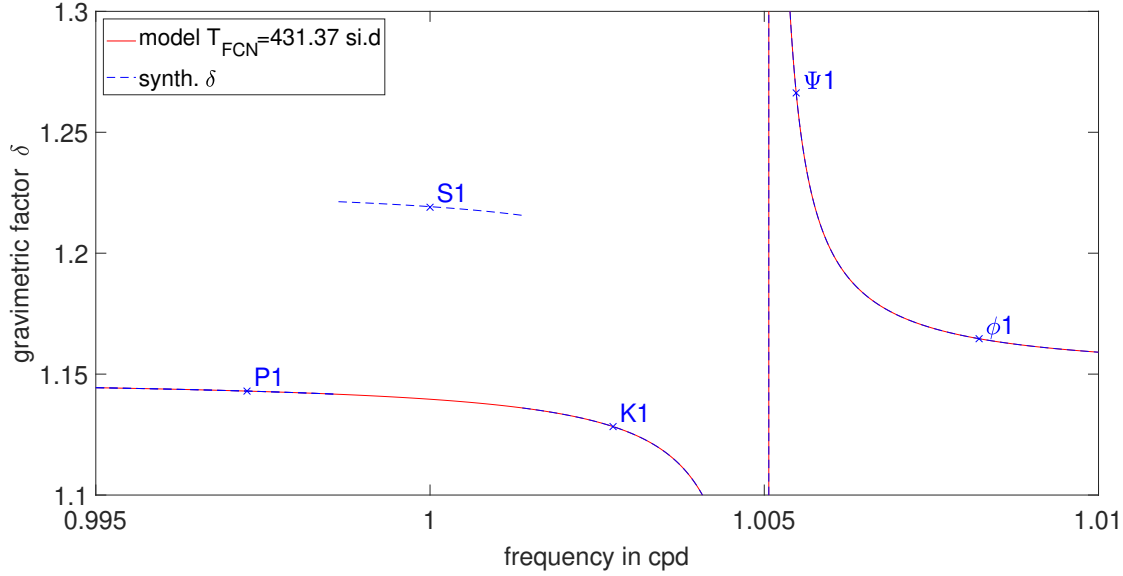
Fig. 7.5. Gravimetric factors computed with the D1999 FCN model $T_{FCN} = 431.37$ si.d in red and synthetic gravimetric factors used for the calculation of synthetic tides at BFO in blue (in contrast to Fig. 7.1 the tidal analysis with the D1999 FCN model was used). In this example all gravimetric factors follow the FCN model, except for the wave group S1. It has the same amplitude ratio to K1 as estimated in the tidal analysis.

at frequencies f and K1. The observed values of the tidal parameters are the results of the tidal analysis already mentioned in section 7.1 (see Tabs. D.2 and D.3 in appendix D). As the mean value is not discussed here, $\delta_{model}(K1)$ can be chosen arbitrarily (except for $\delta_{model}(K1) = 0$). However, the predicted value of $\delta_{model}(K1) = 1.1345$ (Dehant et al., 1999) is used.

Fig. 7.5 shows for BFO, as an example, the model for S1 which is used for the calculation in comparison to the analysis model. All harmonics, S1 and its satellites, deviate from the analysis model, which is indicated by the section of the blue line around S1 in Fig. 7.5. Schroth (2013) shows that the satellite harmonics are of insignificant influence.

A synthetic data set was calculated for all four wave groups with tidal parameters based on equations 7.1 and 7.2, from 27.11.2009 to 31.12.2013. These data sets were analysed with MWA as described in section 3.1.2. The results are shown in Fig. 7.6. All four wave groups cause variations. As expected, the deviation of S1 and $\Psi1$ tidal parameters from expectations of the analysis model cause annual variations, whereas the variations caused by $P1$ and $\phi1$ are semi-annual. For BFO S1 contributes most to the variation of the $K1_{MWA}$ tidal parameters. The annual variation caused by S1 is about $\Delta\delta(K1_{MWA}) = 8.5 \cdot 10^{-4}$ and about $\Delta\phi(K1) = 0.035°$. The second largest contribution is from P1, the variations caused by $\Psi1$ and $\phi1$ are very small. In principle, the contributions could be completely different at every station, but ocean loading is a global phenomenon, which probably influences
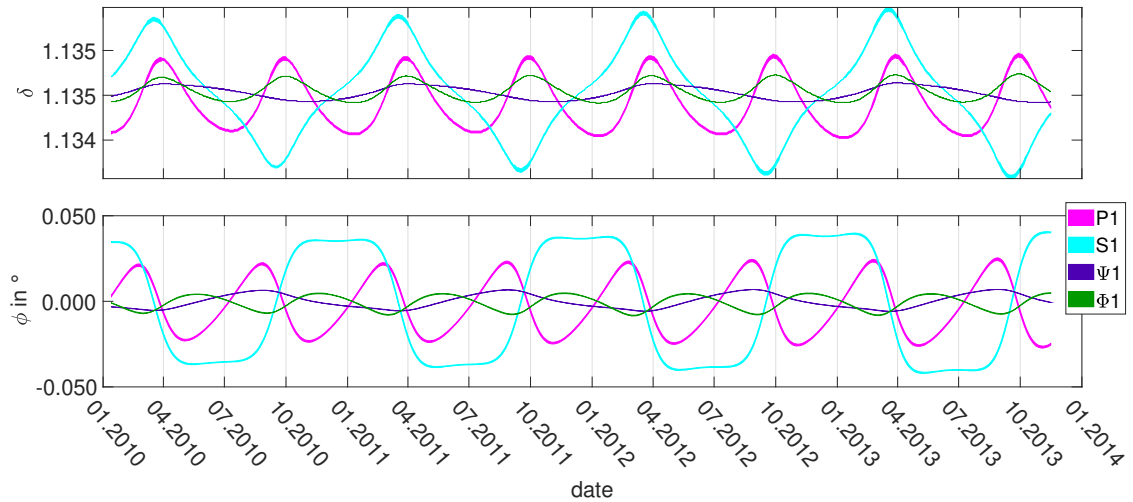
Fig. 7.6. VK1 caused by a deviation of one wave group from the analysis model. The specific wave group is given in the legend. Please note that the thickness of the $\Psi 1$ and $\phi 1$ line does not reflect the standard deviation because they are smaller than the available digits in ETERNA. The line was plotted thicker for a better visibility.

all harmonics in the K1 group (not necessarily in a similar way). On a global scale, the atmosphere influences all SGs in the same way; although the local atmosphere does not behave perfectly the same at all stations the principal phenomena are the same and occur with the same frequencies (e.g. heating of the Sun). That this is a valid assumption is supported by the K1 tidal parameters from the European station, given in Fig. 6.1 in chapter 6, which show similar variations. Based on this assumption it is concluded that the main contribution to the VK1 comes from P1 when the variation is mainly semi-annual, and from S1 when the variation is mainly annual. In order to show that the variations caused by the single wave groups deviating from the analysis model represent the VK1 correctly, the variations in Fig. 7.6 are summed. Fig. 7.7 shows the sum in comparison to the temporal variations of the tidal parameters estimated from measured data. The VK1 are similar which shows that the VK1 obtained from measurements are represented correctly by the variations caused by the single harmonics in the synthetic test. The deviation of the amplitude ratios and phase differences are probably due to environmental effects (see section 4.2.1) whose influence on the VK1 are studied in the following sections. Environmental effects do not behave perfectly harmonic which results in the small differences between the VK1 obtained in the synthetic test and the VK1 obtained from measurements.

7.3. Variations caused by the atmosphere

A well-known phenomenon is the strong gravity effect of S1 in the atmosphere (radiation tide, see section 5.2.3.1). It cannot completely be removed by the correction with the
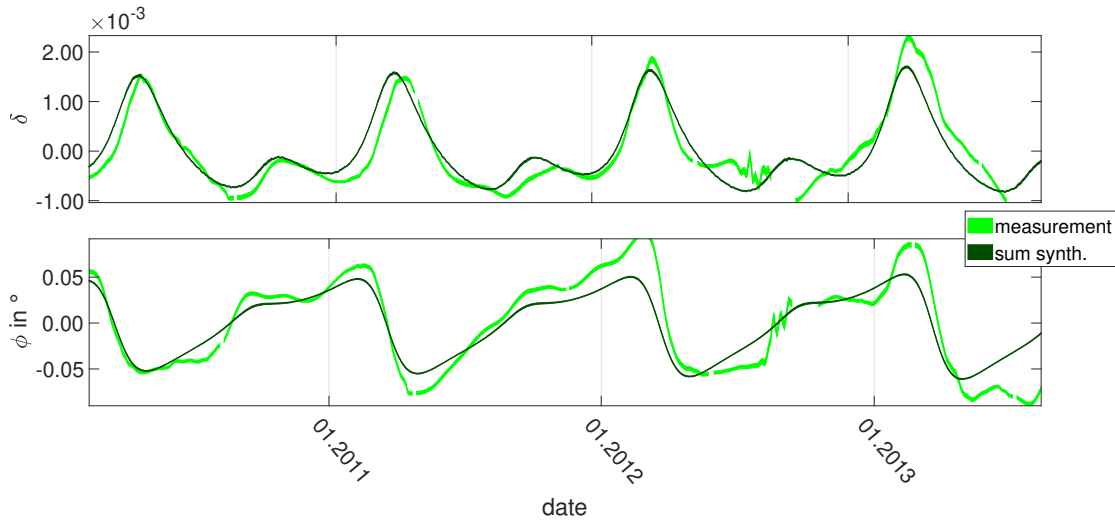
Fig. 7.7. Variation of the K1 tidal parameters from BFO data in light green and the sum of the variations shown in Fig. 7.6 in dark green. The offset was subtracted in both cases.

measured air pressure. The S1 radiation tide can be a reason why the S1-to-K1 amplitude ratio and phase difference deviate from the expected values and are a main contribution to the VK1, as shown in section 7.2. The influence of the atmosphere is studied with the Atmacs model (see sections 5.2.3.2 and 4.2.1).

Two different methods were used: First the measured data are corrected with the model time series. If the Atmacs gravity time series explains the atmospheric gravity signal more realistically than the correction with the measured air pressure, the VK1 should be reduced. The second step is to add the Atmacs time series to synthetic body tides. The tidal parameters obtained with measured and synthetic data will show similarities if the Atmacs model describes the atmosphere realistically. As described in section 4.2, synthetic data MWA, can be used for distinguishing the VK1 which are caused by the Atmacs gravity signal and by the measured data.

7.3.1. Correction of measured gravity with the Atmacs time series

In this section the results of MWA of measured data corrected with Atmacs (see section 4.2.1) are shown. This is done for the stations BFO, Bad Homburg, Canberra, Kamioka, Medicina, Metsahovi, Moxa, Onsala, Strasbourg, Sutherland and Wettzell. The European stations are located close to each other and are therefore probably affected by the same phenomena. The other stations are chosen to compare the European stations with those from other continents.

There are two possibilities for correcting the measurements with the Atmacs time series:

- *Direct method*: The Atmacs time series can be used directly for the correction of the measured gravity data which means that the Atmacs time series is subtracted from

the measured data before the MWA.

- *Replacement method*: The model air pressure is replaced by the measured air pressure. As mentioned in section 3.1.1 the measured air pressure can represent up to 95% of the atmospheric gravity signal (Klügel and Wziontek, 2009). The modelled air pressure will probably not be as accurate as the measured one because, for example, very local effects are not covered by the grid of the atmospheric model. The replacement of the modelled by the measured air pressure is done by subtracting the modelled air pressure multiplied by a factor r_p, which has a similar meaning as the regression factor R_m (see section 3.1.1), from the Atmacs gravity time series. The measured air pressure is then added with the same factor r_p. The factor r_p is, like the regression factor R_m, given in $\frac{\text{nm/s}^2}{\text{hPa}}$. In the description of Atmacs[6] it is recommended to use an r_p which is typical for the station. Here, the factor r_p is estimated in a grid search. A time series of at least 1 year is chosen and corrected with the Atmacs time series in which the modelled air pressure was replaced by the measured one with different factors r_p. The r_p which produces the smallest RMS residual is used for the correction. R_m is usually about 3.2 $\frac{\text{nm/s}^2}{\text{hPa}}$ for most stations, therefore the parameter range tested in the grid search is 2.8 $\frac{\text{nm/s}^2}{\text{hPa}}$ to 3.7 $\frac{\text{nm/s}^2}{\text{hPa}}$ (except for Kamioka, see below). The grid search is made for two different time series in different years which had consistent results in all cases. All stations mentioned above are analysed except for Medicina, Metsahovi and Moxa.

The factors r_p which are used for the *replacement method* are given in Tab. 7.2. For Kamioka the factor r_p is extraordinarily small. In the first grid search it was obvious that the minimum RMS residual was not reached (by plotting the RMS residual over r_p), therefore the range of possible values was extended towards smaller values. Both approaches, the *direct* and the *replacement method* are used and compared.

Fig. 7.8 shows the tidal parameters for the stations mentioned above, except for Medicina, Metsahovi and Moxa for which only the *direct method* was used. The results of the latter stations are given in Fig. D.1 in appendix D. As described in section 5.1, the mean values of the tidal parameters at Wettzell are uncertain because of the uncertain sensitivities and time lags. In this test, they were accidentally set differently in the MWA with the locally measured air pressure and the both MWA with the Atmacs time series. As the mean values are not of interest in this case, they have therefore been subtracted, instead of rerunning the whole analysis. Here, the IGETS data set from Onsala was used.

In almost all cases the usage of the *direct method* increases the VK1, except for Kamioka. This unexpected observation for Kamioka is discussed below. For the other stations, the increase is probably due to the inaccurate description of the local atmosphere by the atmospheric model. If the *replacement method* is used, the benefit of the correction with Atmacs differs from station to station. Whereas for some stations the reduction is obvious,

---

[6] http://atmacs.bkg.bund.de/docs/computation.php (06.12.2018)
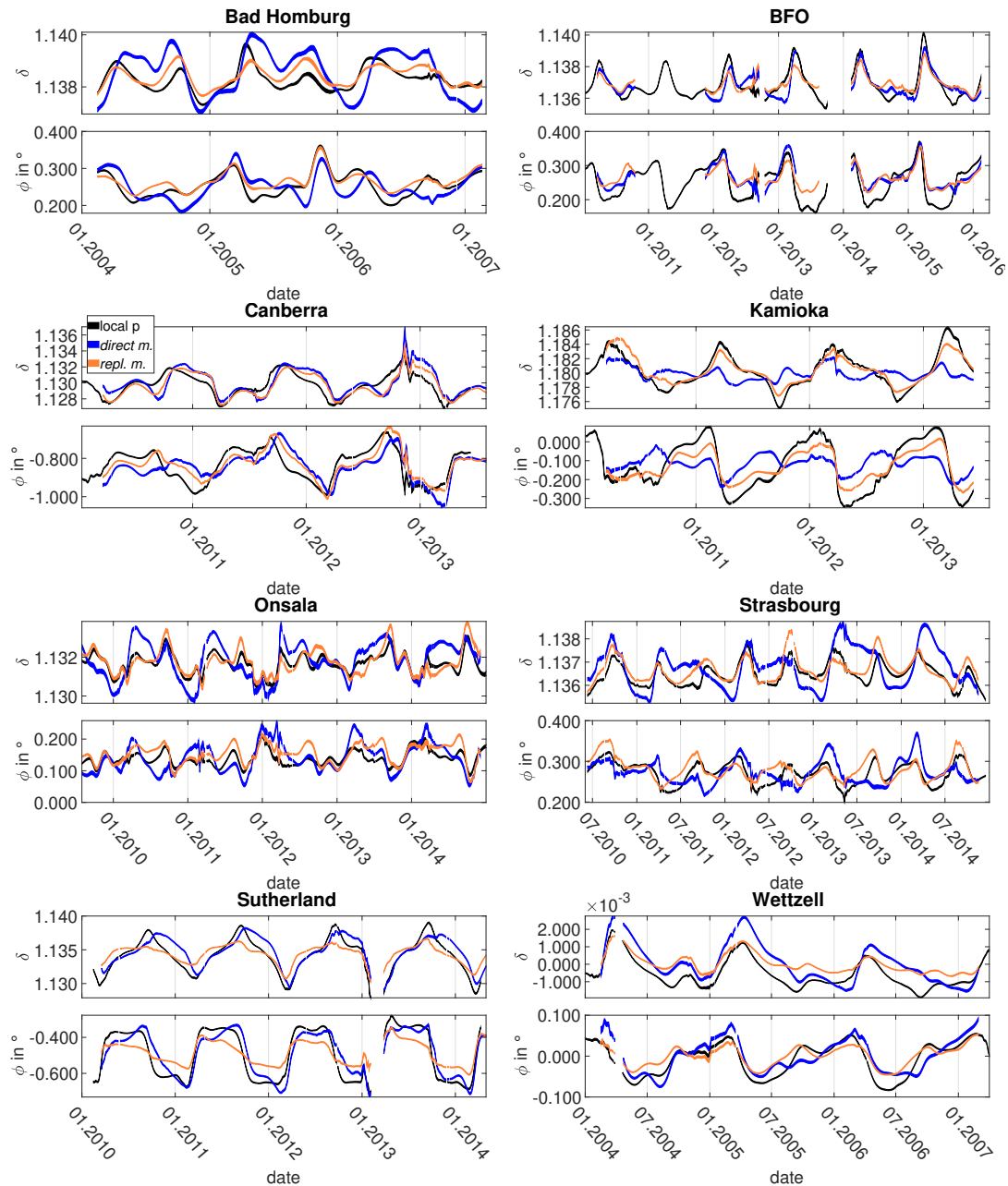
Fig. 7.8. Tidal parameters of wave group K1 at Bad Homburg, BFO, Canberra, Kamioka, Onsala, Strasbourg, Sutherland and Wettzell. The black curves are the tidal parameters of the measured data with the locally measured air pressure adjusted to the data. The blue curve shows the results when the SG data are corrected with the Atmacs model before the MWA and the orange curve when the data are corrected with Atmacs combined with the measured air pressure. At Wettzell the mean values are subtracted from all curves.

station	years	r_p in $\frac{\mathrm{nm/s^2}}{\mathrm{hPa}}$
Bad Homburg	2004/2006	3.30
BFO	2010/2015	3.45
Canberra	2010/2014	3.20
Kamioka	2011/2012	1.80
Onsala	2010/2014	3.50
Strasbourg	2009/2013	3.20
Wettzell	2005/2008	3.30

Table 7.2. Factors r_p in $\frac{\mathrm{nm/s^2}}{\mathrm{hPa}}$ for different stations and the two different years of which the data were used for the estimation of r_p.

for example in Strasbourg, it is not clear whether a reduction or an increase predominates. In order to compare the VK1 for the different cases the variance of the tidal parameters for the different stations and methods of using Atmacs is calculated. The results are given in Tab. 7.3. The variance is reduced for all stations except for Onsala. Here the usage of Atmacs increases the variance for both methods. This can also be seen in Fig. 7.8 and is probably due to the influence of the nearby ocean whose interaction with the atmosphere is not well represented in Atmacs (T. Klügel, pers. comm.). The reduction of the variance is very small for the gravimetric factor at Canberra, compared to other stations. The atmospheric model of the DWD which is used for the Atmacs calculations has different resolutions depending on the distance of an area to Germany. The lowest resolution is outside of Europe. Therefore, it is likely that the model does not represent the topography in hilly regions, like the area around Canberra, accurately enough. The local topography is important for the correct description of local effects. The average grid spacing is 20 km (even more for older versions). Therefore, local effects depending on the topographic conditions are probably not covered by the model. In Sutherland the model has the same coarse grid and in contrast to Canberra, the variance is strongly reduced. The station is located on a plateau where the topography is not as rapidly changing as in mountain regions. It would be necessary to study the influence of the atmosphere at both stations in detail to check if the different topographic conditions cause these results which is not topic of this thesis.

The highest reduction is achieved at Kamioka. As mentioned above the results for Kamioka are exceptional. The factor r_p which is used for replacing the modelled by the measured air pressure is only about half of those of other stations. The VK1 is about 50% larger (estimated from the variation amplitude) if the measured air pressure is used. This means that the measured air pressure does not represent the local atmosphere as precisely as the modelled air pressure. An additional test, namely an MWA in which the model air pressure instead of the measured air pressure is fit to the data, is performed. The results are shown together with the results from Fig. 7.8 in Fig. 7.9. A large reduction of the VK1

station		local p	*direct m.*	*repl. m.*	reduction
BF	$v_\delta \cdot 10^7$	9.70	8.90	3.80	60.8%
	$v_\phi \cdot 10^3$ in $(\circ^2)$	3.34	1.91	1.23	63.2%
BH	$v_\delta \cdot 10^7$	2.00	7.40	1.30	35.0%
	$v_\phi \cdot 10^3$ in $(\circ^2)$	1.10	1.23	0.59	46.4%
CB	$v_\delta \cdot 10^7$	25.90	26.80	25.10	3.0%
	$v_\phi \cdot 10^3$ in $(\circ^2)$	7.08	5.48	5.74	18.9%
KA*	$v_\delta \cdot 10^7$	58.20	7.60	36.80	86.9%
	$v_\phi \cdot 10^3$ in $(\circ^2)$	16.80	2.22	6.12	86.8%
OS	$v_\delta \cdot 10^7$	3.00	8.50	4.30	-43.3%
	$v_\phi \cdot 10^3$ in $(\circ^2)$	0.68	1.99	0.92	-35.2%
ST	$v_\delta \cdot 10^7$	3.2	7.2	2.4	25.0%
	$v_\phi \cdot 10^3$ in $(\circ^2)$	0.84	0.82	0.71	15.5%
SU	$v_\delta \cdot 10^7$	65.50	43.30	16.20	75.3%
	$v_\phi \cdot 10^3$ in $(\circ^2)$	19.60	13.86	4.27	78.2%
WE	$v_\delta \cdot 10^7$	6.1	11.80	2.70	55.70%
	$v_\phi \cdot 10^3$ in $(\circ^2)$	1.63	1.67	0.58	64.4%

Table 7.3. Variance of the time-dependent tidal parameters shown in Fig. 7.8, multiplied by 10^7 and 10^3. The term 'local p' means that the atmospheric loading is taken into account by adjusting the measured air pressure to the data during the analysis. In case of *direct m.* (=*direct method*) the SG registrations are corrected in advance with the Atmacs time series and *repl. m.* (=*replacement method*) means that the model air pressure in Atmacs is replaced by the measured air pressure and SG data are corrected before the analysis. The reduction of the variance is calculated for the *replacement method* relative to the 'local p' result, except for Kamioka (*). There the measured air pressure does not represent the atmosphere correctly and the modelled air pressure is used instead.

occurs when the model air pressure is used. This is most likely because the air pressure is measured in the mine where the gravimeter is placed and a ventilation system is running (Y. Tamura, pers. comm.).

Therefore, at Kamioka the model air pressure is a better representation of the local atmosphere than the measured air pressure. In the following parts of this chapter, the measurement results shown for Kamioka are results obtained with the *direct method*. In chapter 8, the measured air pressure is used for correcting the data. The ventilation system does probably not cause gravity changes with the M2 frequency and the Atmacs time series contains noise in this frequency band which influences the parameter estimation.
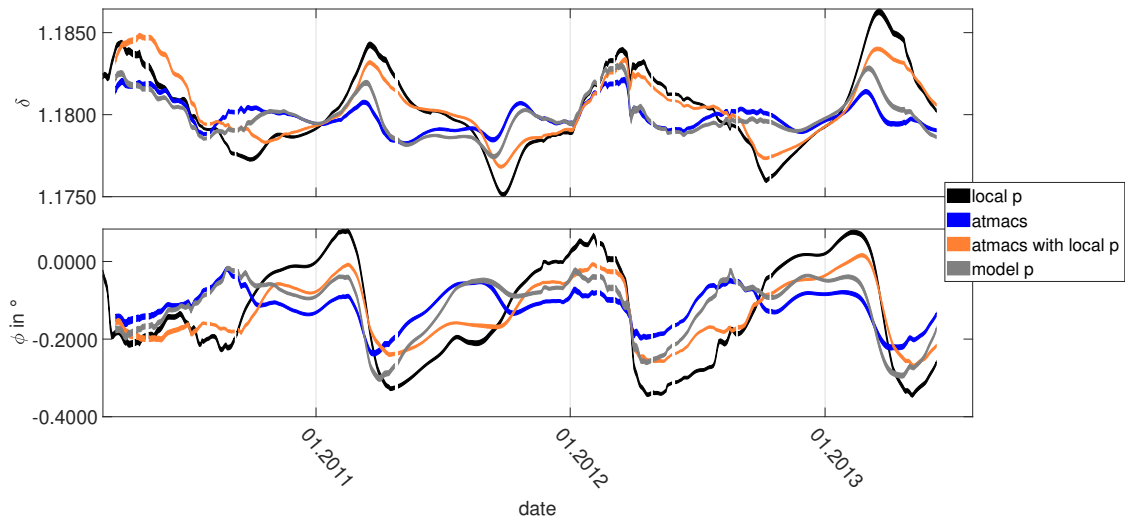
Fig. 7.9. VK1 at Kamioka. The same colours are used as in Fig. 7.8; the result of the MWA with the adjustment of the model air pressure is added in grey.

Even if Canberra is not counted due to the small reduction in the gravimetric factor, there are six stations out of eight where the usage of Atmacs in combination with the measured air pressure reduces the VK1. Especially for Bad Homburg, BFO, Strasbourg and Wettzell the VK1 changes its character from annual to a semi-annual behaviour. This indicates that Atmacs explains parts of the S1 signal in the atmosphere better than the measured air pressure does. In some cases the correction seems to increase the VK1, for example in the second half of 2012 at Strasbourg (see Fig. 7.8). This can happen when the annual variation, which is reduced by the correction with Atmacs, had cancelled out a semi-annual amplitude.

The reduction of the VK1 obtained with the D1999 FCN model with respect to the MWA with the original WDZ FCN model was not compared for all stations. However, comparing the variation amplitudes for both tidal parameters at Strasbourg, Sutherland and BFO the usage of the D1999 FCN model and Atmacs in combination with the measured air pressure reduces the VK1 by at least 50% and reaches even about 70% for the phase at Strasbourg at the beginning of 2012, as shown in Fig. 7.10 However, the reduction is not as large for the complete time series. There are parts of signal that can be explained by neither the solid earth tides nor the FCN model or Atmacs.

With this test, the correction of measured data with Atmacs, it is not possible to distinguish whether the observed reduction is caused by a better representation of the local effects (see section 5.2.3.2) or by the consideration of the global atmosphere in Atmacs. However, this investigation shows that at least a part of the additional signal at the S1 frequency is caused by the atmosphere.
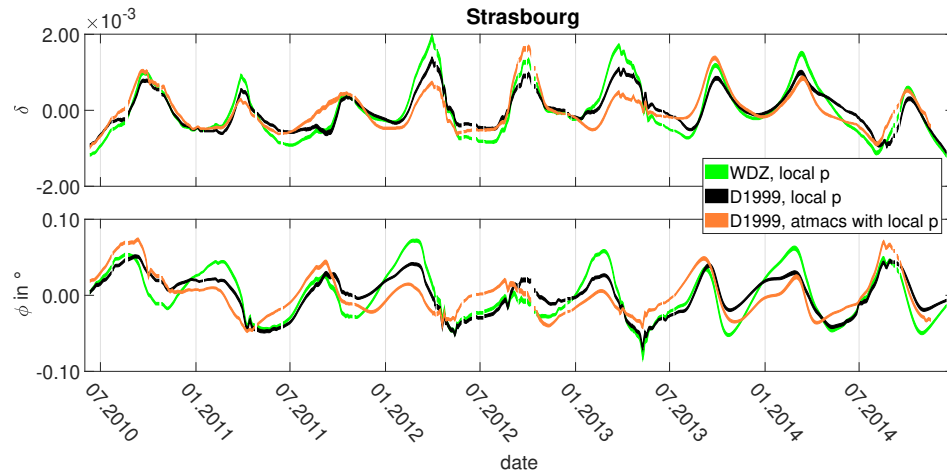
Fig. 7.10. VK1 at Strasbourg. The green curve is obtained with an MWA based on the WDZ model, the black curve with an MWA based on the D1999 model and the orange curve with an MWA based in the D1999 model of data corrected with Atmacs and the locally measured air pressure (same curve as in Fig. 7.8).

7.3.2. Analysis of the Atmacs time series with synthetic data MWA

The correction of the measured SG data with time series based on models like Atmacs have the disadvantage that the origin of unexplained parts of the analysed time series cannot be identified. They may result from noise in the measurements or inaccuracy of the Atmacs time series. Therefore, the synthetic data MWA described in section 4.2 is used. The synthetic Earth tides used for the synthetic data MWA are calculated for the same model used for the analysis; therefore, all variations have to be caused by Atmacs which is added to the synthetic Earth tides. In contrast to the description in section 5.2.1, the gravimetric factor of the K1 group was accidentally set to 1.16. This does not influence the VK1 but makes the comparison with the gravimetric factors obtained from measurements difficult which have a mean value of approx. 1.13. In order to compare with the VK1 from measurements, the mean value of each time-dependent tidal parameter has to be subtracted. There is no special reason behind the fact that the selection of stations and the length of the data set differs slightly from the selection used in the test in section 7.3.1.

There are three different possibilities of calculating the synthetic data sets and of analysing them. The names of the methods given below are used in the following for these possibilities. The term 'local p' denotes the standard MWA of measured data with adjustment of the measured air pressure as described in section 3.1.2.

- *atmacs*: The Atmacs time series is added to synthetic Earth tides and the model air pressure is subtracted with the factor r_p (see Tab. 7.2). No air pressure adjustment is

used in this case.

- *atmacs with model p*: Another way to produce a synthetic data set is to add Atmacs to the synthetic Earth tides, without subtracting the modelled air pressure and fitting it to the data during the analysis. This was done for a selection of stations (see Fig. 7.11).

- *atmacs with local p*: The third possibility is similar to *atmacs with model p*; but here the modelled air pressure is replaced by the measured air pressure with the factor r_p (*replacement method*, see section 7.3.1) and the measured air pressure is fit during the synthetic data MWA. This was done for all stations except for Kamioka due to the problem with the measured air pressure (see section 7.3.1). For Moxa no factor r_p was adjusted, a typical factor of 3.3 $\frac{\text{nm/s}^2}{\text{hPa}}$ is assumed.

If the fitting of the pressure signal during the analysis worked perfectly, it would only affect the part of the synthetic time series that is represented by the pressure signal; therefore, all three solutions should be identical. Differences indicate that also other parts of the signal influence the fitting of the pressure time series. The results for the three methods are shown in Fig. 7.11. The VK1 estimated with the synthetic data MWA based on the three methods for using Atmacs have the same order of magnitude as the results from measurements. For those stations whose parameters are strongly reduced when the measured data are corrected with Atmacs (see section 7.3.1) the results from the synthetic data MWA also show stronger similarities to the measured data, for example at Wettzell. At stations where the correction with Atmacs did not have a benefit, the character of the parameters estimated from the synthetic data MWA differs from the results obtained from measurements, e.g. at Onsala. The results are consistent in this respect. For all stations the dominating frequency in the VK1 obtained from synthetic data MWA is annual whereas all stations except for Sutherland show also a clear semi-annual variation. This explains why for some stations, for example at Strasbourg or Bad Homburg, every second maximum in the tidal parameters obtained with the synthetic data MWA fits well to the results from measurements, while the other maxima are not explained. This is also in agreement with the observations in section 7.3.1 of the reduction of an annual component in the VK1.

The synthetic data MWA allows to distinguish the origin of certain signals. In the first half of 2012 a local minimum in the tidal parameters adjusted from the measured data at Wettzell occurs (see Fig. 7.11 lowest panel on the right side, black curve). This can also be seen in the results from synthetic data computed with *atmacs with local p* (orange curve), but not in the tidal parameters obtained from the other synthetic data sets (cyan and blue curves). This means that the air pressure time series is the origin of this short-term VK1. The results obtained with the three methods of adding Atmacs to synthetic body tides and analysing the total signal differ only slightly from each other, but the difference is significant with respect to the standard deviations. However, the differences between the results obtained with synthetic data (all three methods) and measured data are much larger. Only for Strasbourg the differences between the *atmacs* method and the methods with an adjustment of pressure time series (*atmacs with model p* and *atmacs with local*
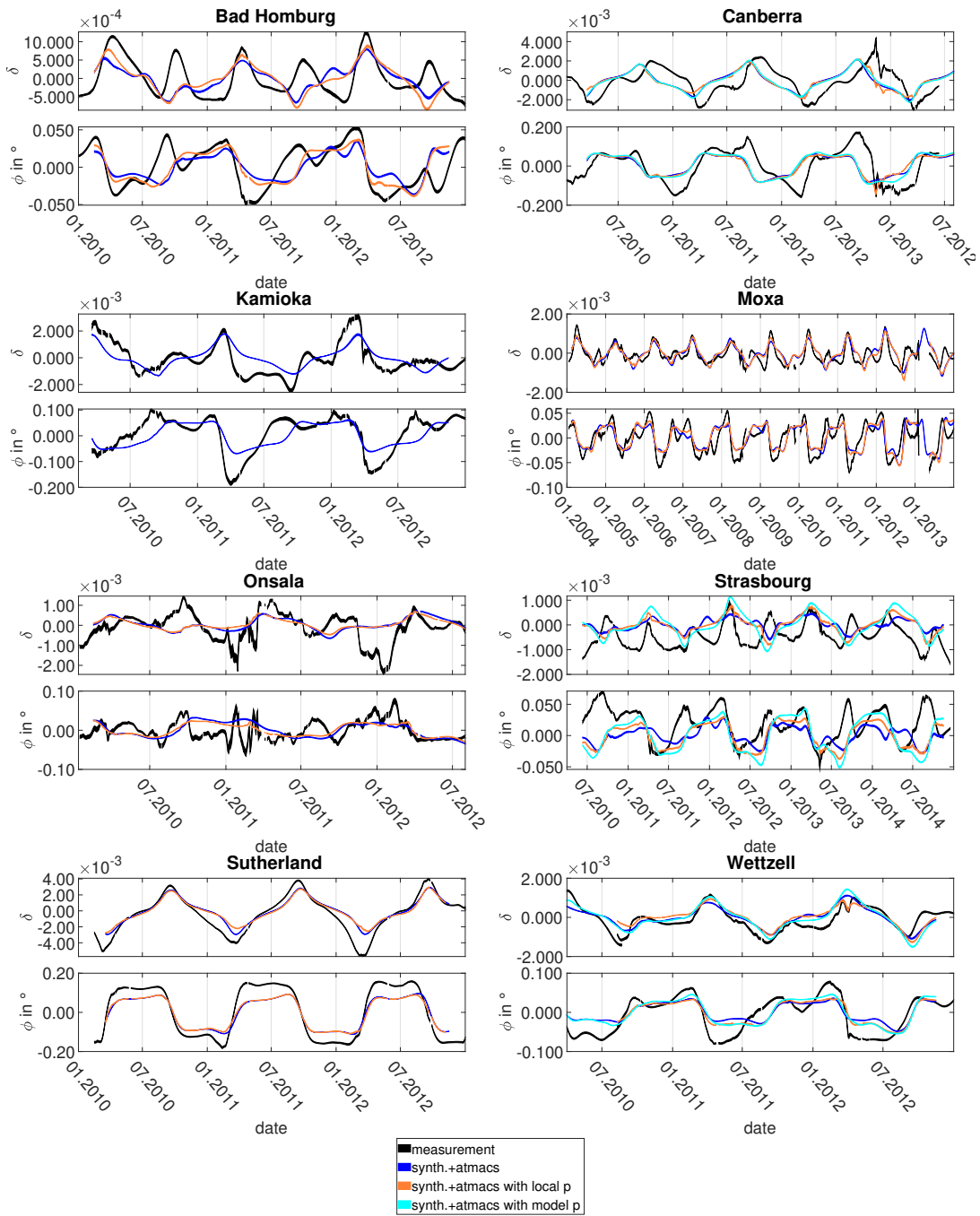
Fig. 7.11. Tidal parameters of wave group K1 at Bad Homburg, Canberra, Kamioka, Moxa, Onsala, Strasbourg, Sutherland and Wettzell. The black curves were obtained from measured data with the locally measured air pressure adjusted to the data. The blue curves result form a MWA with *atmacs*. The orange curves are obtained with *atmacs with model p*. The cyan curves are the results with the *atmacs with local p* method.

p) show larger differences (see Fig. 7.11 third panel on the right side). Especially in the phase the variation is twice the variation obtained with the methods using an air pressure adjustment.

This shows that at most of the stations the adjustment of the air pressure has only a small influence on the tidal parameters (as is desired) whereas in Strasbourg the tidal parameters of K1 are affected by the air pressure adjustment. Then, also the meteorological parameter (see section 3.1.1) has to vary. Fig. 7.12 shows the meteorological parameters estimated in the synthetic data MWA of the results shown in Fig. 7.11 from Strasbourg. The meteorological parameters which are estimated with the synthetic data MWA have an
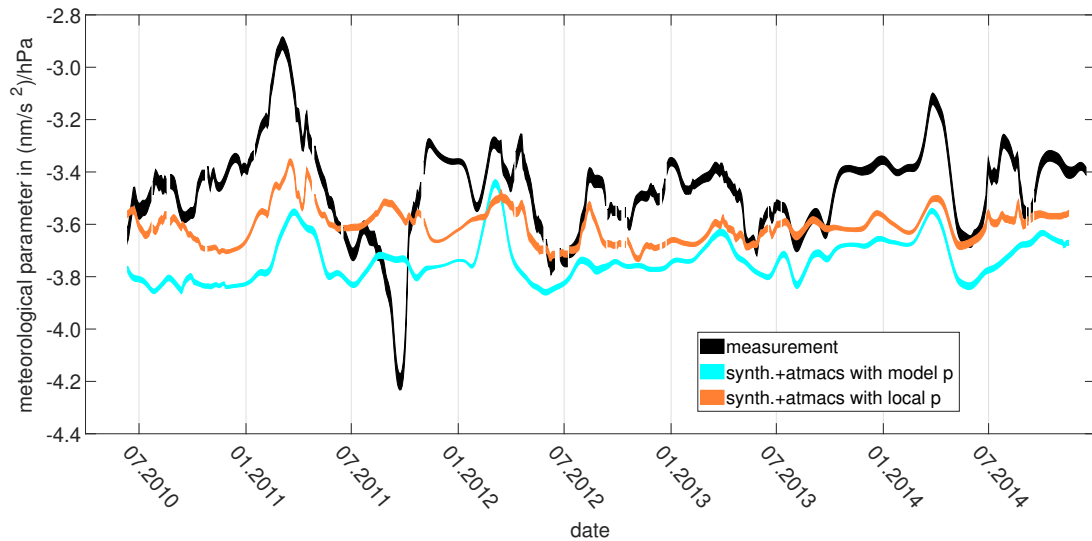
Fig. 7.12. Variation of the meteorological parameter for the MWA results of Strasbourg shown in Fig. 7.11. The black curve results from the adjustment of the measured air pressure to the the measured gravity data. The orange curve was obtained in the synthetic data MWA of the *atmacs with model p* data set and the cyan curve with the *atmacs with local p* data set.

annual and semi-annual variation which is stronger in the years 2010 to 2012. The variation of the meteorological parameter estimated for the measured data is twice as large as the variation of the parameters from synthetic data MWA and, in contrast, dominated by an annual period. There are some features, for example the maximum at the beginning of 2011, which is present in all three curves. This means that the effect causing this maximum is present in the measured air pressure as well as the Atmacs time series. This is an effect in the atmosphere which is also represented by Atmacs.

In Fig. 7.12, the adjustments of the measured air pressure to measured (*local p*) and synthetic data (*atmacs with local p*) show similarities in single short-term features, e.g. the location of the two maxima at the beginning of 2011, which are not observable with *atmacs*

with model p. This means that this effect is only present in the measured air pressure. The adjustment varies with time because parts of the global Atmacs time series or the Earth tide signal can be explained by the measured or modelled air pressure if the meteorological parameter and/or the tidal parameters are adjusted slightly differently. This happens if a changing adjustment leads to a smaller RMS residual. The differences between the VK1 in Fig. 7.11 show that this effect is insignificant compared to the unexplained part of the VK1 obtained from measurements.

7.4. Variations caused by the oceans

Although a significant reduction of the VK1 is achieved with the new FCN model and the correction with Atmacs, there is still an unexplained variation left. Another phenomenon that influences the gravity in the complete tidal band is the loading of the ocean tides. If the oceans behaved like the solid Earth, the mean value would be changed but no temporal variations would occur (see section 4.1.2). Baker and Alcock (1983) discuss, among others, the variations of the K1 amplitudes observed in tide gauge data and show that especially the amplitudes of S1, but also $\psi1$ and $\phi1$, deviate from the amplitudes which are expected from forcing. Schindelegger et al. (2016) studied the S1 harmonic in the oceans with hydrodynamic modelling (see chapter 1.1). The results show that the amplitude of S1 can reach several centimetres instead of a few millimetres. The latter is expected based on the assumption that S1 behaves like its neighbouring harmonics P1 and K1. Then, the S1 amplitudes and phases can be derived from their amplitudes and phases. The study by Schindelegger et al. (2016) indicates that this is not the case. The loading of these ocean tide harmonics can also lead to a variation of the K1 tidal parameters, because the amplitude ratios and phase differences of S1 relative to the other harmonics in the wave group differ from the expected ratios of the analysis model (see section 4.1.2). Additionally, as mentioned in section 4.2.1, there can also be a contribution at the P1 frequency that will cause a semi-annual variation, if the oceans do not behave perfectly similar at P1 and K1 frequencies.

From the five ocean models which are available, I decided to use OMCT. It is a global model and driven by ephemerides which is of advantage because S1 is taken into account in the forcing. This is not the case for ARTOFS and HGT. The North Sea model and ARTOFS are restricted to certain regions. Stormtide is also driven by ephemerides, but the amplitude and phase representation does not contain S1 and the SSH were calculated from 1954 to 1957 when no SG measurements and no Atmacs calculations were available. OMCT has the disadvantage of a low spatial resolution. The results in section 8.2.3 show that OMCT does not represent the annual variations of the M2 tidal parameters. The spatial resolution, especially the vertical, is probably not high enough to resolve the effects causing the annual variations of the M2 amplitudes. As Schindelegger et al. (2016) use a barotropic model and obtain S1 amplitudes which are comparable to S1 amplitudes from tide gauges, other processes than in the case of M2 must be involved in the generation of the higher S1 amplitudes. Therefore, the vertical resolution of the OMCT model is probably not important in this case.

The calculation of the ocean loading is described in section 3.2. For considering the atmosphere, the *atmacs* method is used (see section 7.3.2) as the three methods of including Atmacs do not differ much for most of the stations (see section 7.3.2). The ocean is taken into account by adding the ocean loading time series calculated with the 1° OMCT version with changed ice drag (see section 5.2.2.5). The calculation based on SSH (ocean bottom pressure, OBP, is also available, see section 8.2.3.1) is used because the time series were already available from the study of M2 described in section 8.2.3. Besides, the OBP time series contain the contribution of the atmosphere above the ocean areas. This atmospheric contribution would be contained twice if the OBP from OMCT was used for the synthetic data MWA together with Atmacs.

The synthetic data set is analysed with synthetic data MWA (see sections 3.1.2 and 4.2). The results for five of the eight stations analysed in section 7.3.1 are given in Fig. 7.13. For most of the stations the results with OMCT do not differ much from the results obtained only with *atmacs*. The exception is Onsala where the variation caused by OMCT is about fourfold larger than the variations obtained from measurements. The SG at Onsala is located very close to the coast and the Kattegat and Skagerrak regions have complex coastlines which are probably not well represented by the 1° grid of OMCT. The results for the M2 tidal parameters in section 8.2.3 and appendix F.2 show that, in general, OMCT predicts amplitudes too large for Onsala.

For Bad Homburg, Sutherland and Wettzell the usage of OMCT brings a small semi-annual component to the VK1 which is also observed for the results from measurements. The difference between the variations observed with measured and synthetic data is of course large. As mentioned in section 4.2.1, the ocean models are probably not precise enough to describe the oceans realistically. However, the combination of Atmacs and OMCT for these three stations leads to similar frequencies of the VK1 which indicates that the oceans also have an influence on the tidal parameters of K1, especially causing a semi-annual component. However, the S1 amplitude does not have a large influence in this case.

The VK1 for Kamioka is not as large as for Onsala, but the usage of OMCT does not bring any benefit regarding the similarities of tidal parameters obtained with measured and synthetic data. In contrast to the other three stations the OMCT model does not seem to characterise the ocean loading at Kamioka realistically. With OMCT the VK1 from synthetic data MWA do not reach the amplitudes observed for the measured data.

However, the synthetic data MWA with the Stormtide model (*atmacs* is not used here, see sections 5.2.2.4 and 8.2.2 for details) indicates that the contribution from the oceans is larger than predicted by OMCT. The K1 tidal parameters are for BFO shown in Fig. 7.14. The amplitude of the gravimetric factor is about $7.6 \cdot 10^{-4}$, which is about half of the variation observed for measurements, and the variation of the phase is about 0.02°, which is a third of the phase variation from measured gravity. In contrast to the observations made with OMCT it is dominated by an annual period, but also contains a semi-annual component. As the data are calculated for a period where no SG measurements and no Atmacs calculations are available, there is no possibility for a direct comparison with results from measurements.

This study shows that the oceans can contribute significantly to the VK1, even if it is not
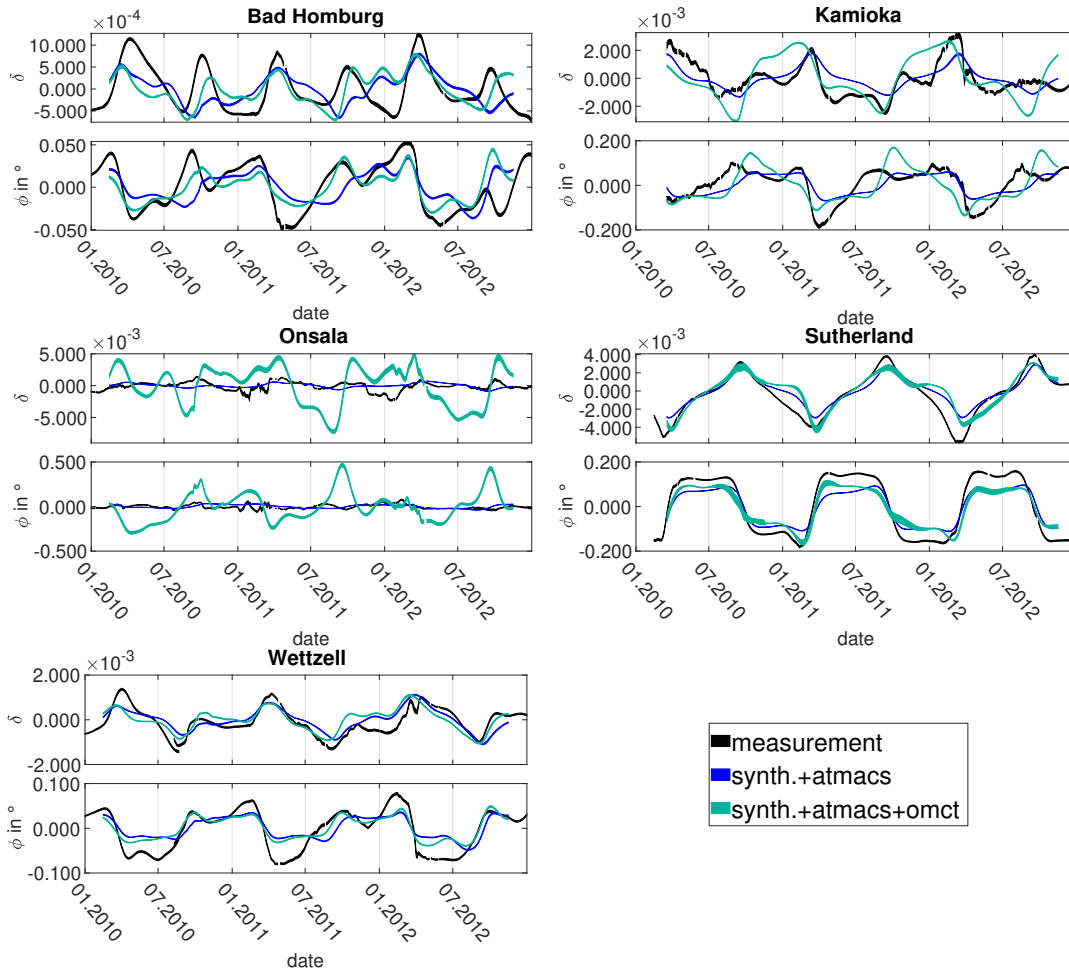
Fig. 7.13. Tidal parameters of wave group K1 at Bad Homburg, Kamioka, Onsala, Sutherland and Wettzell. The black curves represent the tidal parameters of the measured data with the locally measured air pressure adjusted to the data. The blue curve shows the results when the Atmacs time series was added to the synthetic data set and the modelled air pressure was subtracted with the factor r_p. The green curve results from an MWA of synthetic Earth tides to which the Atmacs time series without the modelled air pressure (like the blue curve) and the gravity loading of the OMCT model was added.
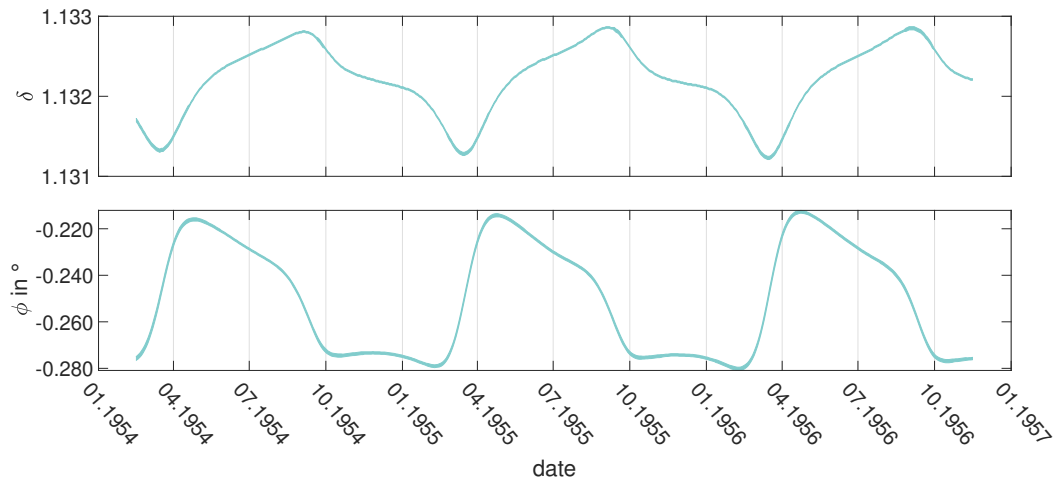
Fig. 7.14. Variation of the K1 tidal parameters obtained with loading calculated based on the SSH from the Stormtide model at the station BFO. The upper panel shows the gravimetric factor and the lower panel shows the phase in degree.

possible to obtain similar VK1 with the ocean models available here.

7.5. Summary of this chapter

In this chapter it is shown that a part of the K1 parameter variations can be explained by the outdated WDZ FCN model ($T_{FCN} = 459.23$ si. d.) used in the ETERNA 3.4 program. The usage of the D1999 model ($T_{FCN} = 431.37$ si. d.) reduces the variations by up to 40% with respect to the variations observed with the WDZ version, depending on the station. With a synthetic test it is shown that the main part of the variation of the K1 tidal parameters at BFO is caused by the deviation of the S1-to-K1 amplitude ratio and phase difference from the expectations of the analysis model. The second largest contribution is caused by the P1-to-K1 amplitude ratio and phase difference.

The atmosphere contributes a lot at the S1 frequency. Correcting for the atmospheric loading with Atmacs in combination with the measured air pressure reduces the variation of the K1 tidal parameters significantly for most of the stations and reaches up to 50% in the gravimetric factor of Wettzell. In comparison to the original ETERNA version with the outdated FCN model (WDZ), the usage of the more recent FCN model (D1999) and the correction with Atmacs reduces the variation of tidal parameters by at least 50% for most of the stations used here and reaches a 70% reduction in the phase of Strasbourg.

Synthetic data MWA with the Atmacs time series supports the results obtained with the correction of the measured time series. It shows that the atmospheric signal causes an annual variation while the semi-annual variation seems to have a different origin. Atmacs is able to describe S1 contributions from the atmosphere which are not described by the

measured air pressure. A part of the variations of the tidal parameters of K1 are obviously caused by the atmosphere.

A part of the semi-annual variations and also a part of the annual variation are probably caused by ocean loading which is shown by MWA of synthetic Earth tides to which Atmacs and the OMCT ocean loading time series were added. For three of the investigated stations, although the calculation for OMCT does not represent the ocean loading realistically, the frequencies of the variations are closer to the frequencies observed from measured data. However, OMCT mainly adds a semi-annual contribution to the synthetic data MWA results, whereas a synthetic data MWA with Stormtide SSH (without Atmacs) is dominated by annual variations. This issue needs further investigation.

Which of the above mentioned periods dominate the variation of the K1 tidal parameters varies from station to station. They all have in common that, if the Atmacs correction is of benefit, the annual period in the variation is reduced.

Chapter 8.

Temporal variations of M2 tidal parameters

The loading of the harmonics $\alpha 2$ and $\beta 2$ in the oceans which have higher amplitudes than expected from astronomical forcing can cause the annual variations of the M2 tidal parameters (AVM2) (see chapter 1 and section 4.2.2). In this chapter, the influence of these harmonics is investigated with the concept of synthetic data MWA of the ocean loading calculated for the ocean models (see section 5.2.2), as described in section 4.2.2. In the first part, harmonic analyses of the SSH from the ocean models show whether the available ocean models produce annual variations of the M2 amplitude and how the amplitudes and phases of the variations are spatially distributed. The results of the temporal variations caused by the different ocean models are discussed and compared in the second part of the chapter. At last, the contribution of different ocean areas to the total result is investigated. Studies of the accuracy of the loading calculation are shown in appendix F. Please note that the abbreviation 'AVM2' is only used for 'annual variation of the M2 tidal parameters'. If the variation only of one the tidal parameters, e.g. the annual variation of the gravimetric factor or variations with other periods are meant, the abbreviation is not used. For the annual variation of the M2 amplitude and phase in the SSH 'AVM2ssh' is used.

8.1. Annual variation of the M2 amplitudes and phases in the ocean models' SSH

In order to investigate whether the available ocean models show an AVM2ssh, harmonic analyses of the SSH data (see section 3.3) are made. The result for Stormtide was provided by M. Müller. His settings for the 'Tidal Heights Analysis and Prediction' program which were used for his analysis of Stormtide (Müller et al., 2014) and his Matlab script for the calculation of the amplitude and phase of the AVM2ssh are used. The latter is based on equations 5.4 and 5.5. The results for the annual variations are shown in Figs. 8.1 to 8.2 for ARTOFS, Stormtide and OMCT. Due to the high resolution of the HGT model it took some time to analyse this model. As this was not finished until the hand-in of this thesis, the results are shown in Fig. E.1 in appendix E.1 together with a description of the analysis approach in this case.

The results for the stationary part of M2 are shown in Figs. E.3 to E.6 in appendix E.2 in comparison to the M2 amplitudes and phases from the stationary HAMTIDE model[7] (Taguchi et al., 2014). HAMTIDE is chosen because the results for the stationary part of the tidal parameters for this model are close to the results from measurements (see section 8.2.6.2). However, most of the results for the other stationary models are within the level of accuracy estimated there; therefore, most of the other models would suit equally well for this comparison.

The analysis was done for the OMCT data set with the changed ice drag on a 1° grid (see section 5.2.2.5). As the different data sets (see section 5.2.2.5) show only very small differences in the results of the MWA, this data set is chosen as an example (see section 8.2.3.2). The results of the harmonic analyses of the other model versions probably look very similar. The data set provides SSH values with 2 h resolution. As the analysis program required hourly time steps, the data were interpolated linearly to hourly values with the time interpolation function of the *Climate Data Operators*[8] (CDO, Schulzweida 2018).

For all four models, amplitudes of the AVM2ssh in the expected order of magnitude (several centimetres in certain shelf areas, Müller et al. 2014), shown in Figs. 8.1 and E.1 in appendix E.1), are observed. The amplitude of the AVM2ssh is, in general, similarly distributed. The AVM2ssh from ARTOFS and HGT have higher amplitudes than the AVM2ssh from Stormtide. For the OMCT data set, the amplitudes are slightly differently distributed than for Stormtide. At some regions, for example at the Russian coast, the amplitudes of the AVM2ssh are much smaller compared to the amplitudes in this region in Stormtide (few millimetres instead of several centimetres).

The phase lags for the four models show differences. There are general patterns that can be found in all four models, e.g. amphidromic points and areas in the model where the same phases occur, but the phase tends to different dominating values, which can be seen by the dominating colours in Fig. 8.2. Whereas the phases obtained for OMCT show mainly purple colours which means 10 months, Stormtide is dominated by phases of about 8 months. Both, ARTOFS and HGT show smaller values between 2 to 4 months. However, the difference in the phase is not just a shift as can be seen for example at the North American coast where Stormtide shows a region with values of about 2 months, whereas for OMCT these regions shows values of 0 months to 1 month. Noticeable is the fine structure in the phase of the AVM2ssh from HGT and ARTOFS (fast variations of the phase in small areas). This structure is not as prominent for Stormtide. This difference between the phases of the AVM2ssh in Stormtide and HGT and ARTOFS can be caused by the different grid resolutions. The latter two models have a finer grid than Stormtide and therefore shall represent small-scale patterns better. In HGT, these small-scale variations have a dimension of approx. 10 grid cells. The same area is represented by only three grid cells in Stormtide. Additionally, the distribution of the these small-scale patterns in the amplitude of the AVM2ssh shows similarities to the distribution of the M2 internal tides in this model (Arbic et al., 2010), e.g. in the region East of Indonesia. Further studies will be necessary to decide

---

[7] https://icdc.cen.uni-hamburg.de/1/daten/ocean/hamtide.html (03.05.2019)
[8] https://code.mpimet.mpg.de/projects/cdo/ (05.07.2019)
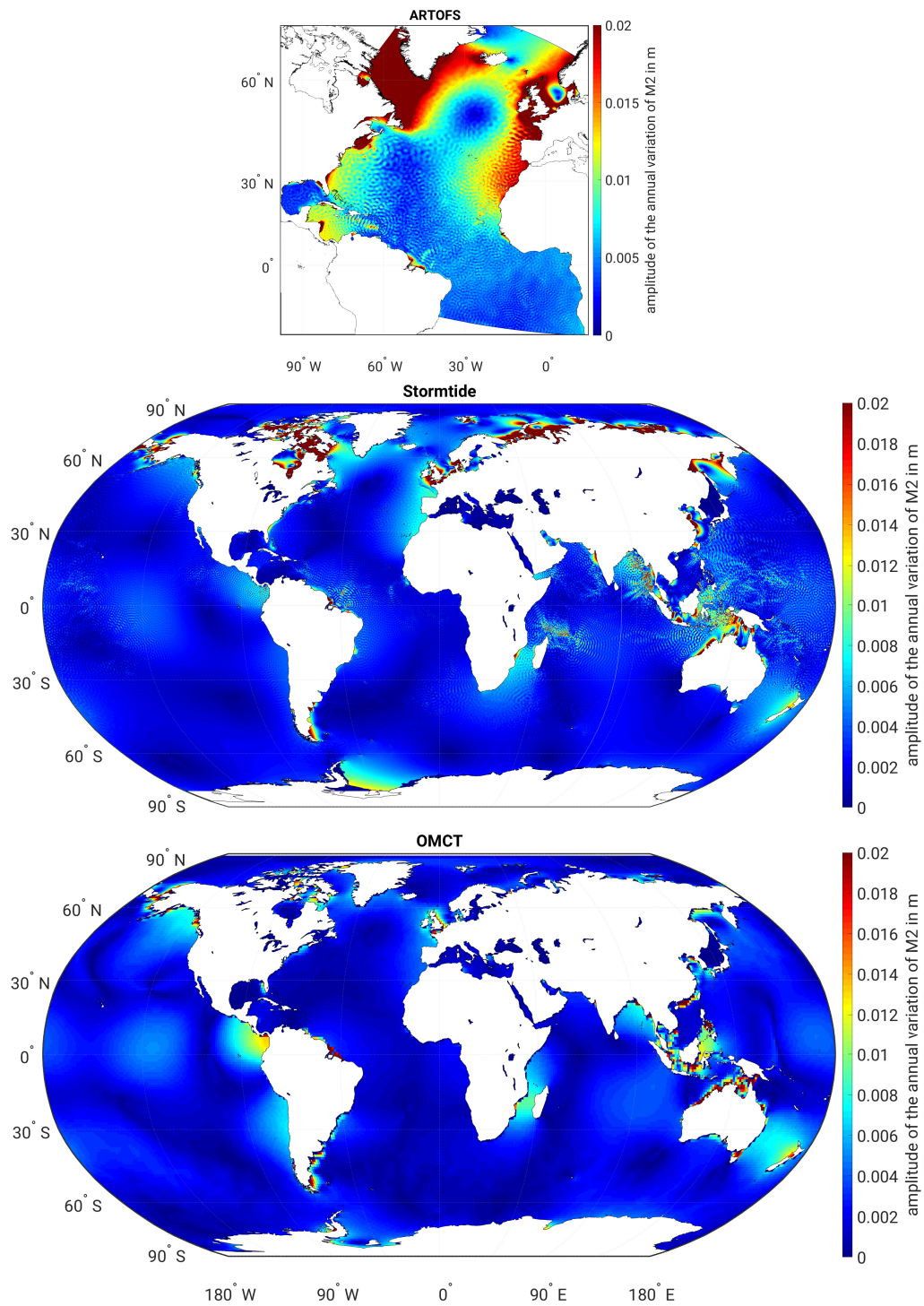
Fig. 8.1. Amplitudes in metres of the annual variation of the M2 amplitude from ARTOFS (top), Stormtide (centre) and the OMCT data set with changed ice drag (bottom). The maximum amplitude can reach about 30 cm in a very small area. To make the patterns at other coastlines and the open ocean visible, the colour scale was clipped at a maximum of 2 cm.
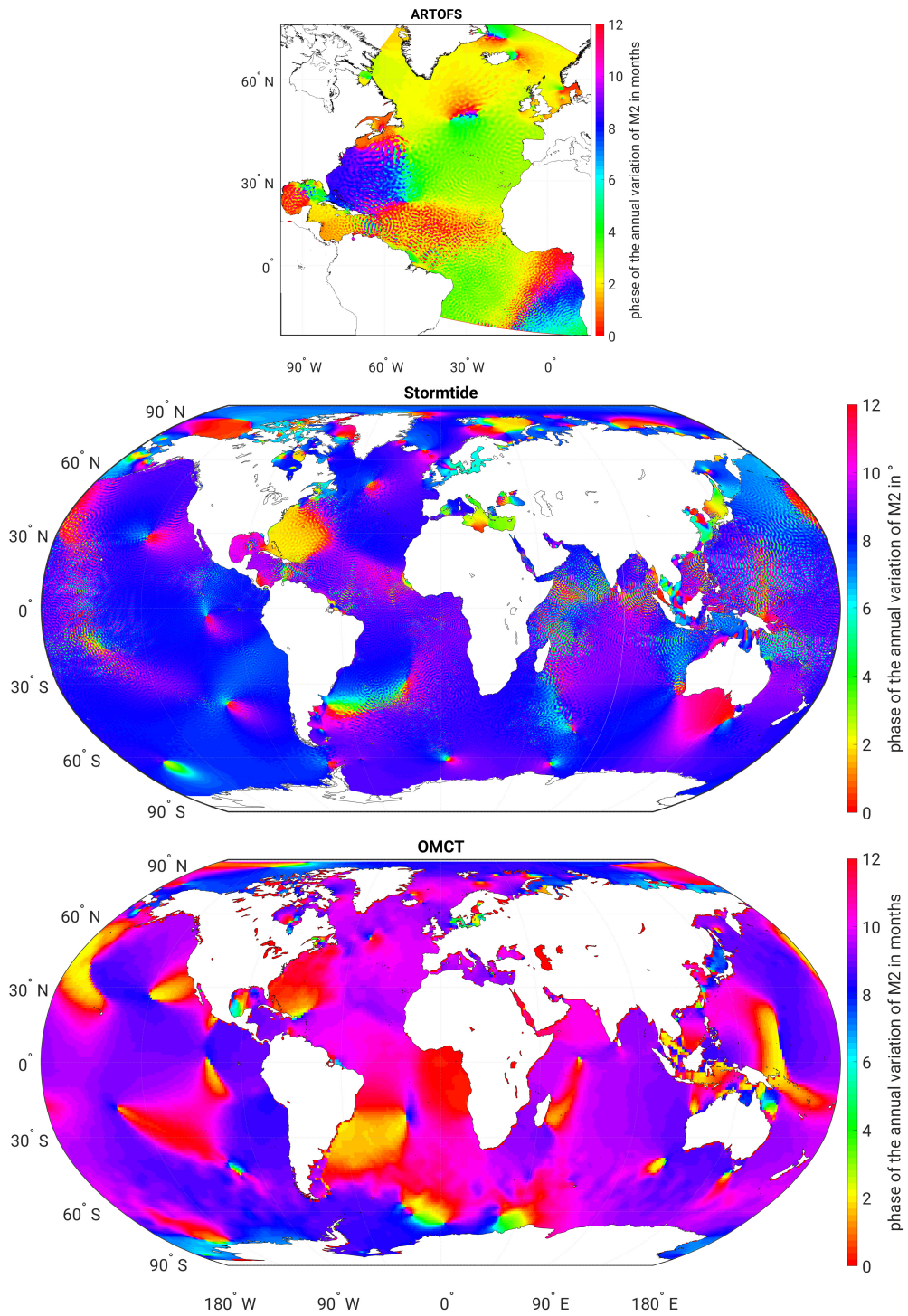
Fig. 8.2. Greenwich phases in months of the annual variation of the M2 amplitude from ARTOFS (top), Stormtide (centre) and the OMCT data set with changed ice drag (bottom).

whether both effects, the AVM2ssh and the internal M2 tide are coupled.

In order to compare the North Sea model with the other ocean models, the AVM2ssh in the North Sea region is shown for all five models in Figs. 8.3 and 8.4.

The amplitudes of the annual variation obtained for ARTOFS, Stormtide, HGT and the North Sea model look similar in distribution and value of the amplitude, whereas OMCT also shows amplitudes of a similar order of magnitude, but they have only half the value of the amplitudes from Stormtide and are differently distributed. Similar to the observation made for the whole model, the amplitudes from HGT and ARTOFS are larger than the amplitudes for Stormtide. For ARTOFS, Stormtide and HGT, the observations made for the whole model also hold for the phase in the North Sea. There is a similarity in the general pattern (e.g amphidromic points), but the values are different. The North Sea model fits to these observations, as it shows a similar distribution for the amplitude of the AVM2ssh and a phase which shows differences to the other models, but has comparable patterns (amphidromic points, etc.). Due to the coarse gird, the phase from OMCT in the North Sea does not show a structure as fine as the phase of the other models. However, like the other models it produces smaller values of the phase in the Kattegat and the Skagerrak than in the rest of the North Sea.

This shows that all five ocean models predict annual variations of the M2 amplitude. As ARTOFS, Stormtide, HGT and the North Sea model show similar results in the harmonic analysis and as mentioned above Stormtide was compared to results from measurements, these models are probably not too far from reality. For OMCT the pattern of the amplitudes and phases differs from the results of the other models, especially in small-scale patterns, and in the North Sea the amplitudes have only half the value of the other models.

Whether the loading of these models leads to an AVM2 is investigated in the following with synthetic data MWA.

8.2. Results of synthetic data MWA with the different ocean models

In this section the results for the different ocean models (see section 5.2.2) are presented and compared. The synthetic data MWA is applied as described in section 4.2. The influence of the atmosphere at the M2 frequency is small and it was already shown that the observed variations of the tidal parameters are not caused by atmospheric effects (Meurers, 2004; Schroth, 2013). Therefore no atmospheric data is added to the synthetic data. In the of measured data atmospheric effects are corrected with measured air pressure.

For all global models the same stations are used for the investigation. The SG stations in Central Europe are located relatively close (in the range of hundreds of km) to each other which allows to see the spatial variation of the loading signal on small scales. The AVM2 obtained from measured data at these stations are very similar (see chapter 6) which also should be reflected by the results from synthetic data MWA. The stations BFO, Bad Homburg, Membach, Moxa, Onsala, Strasbourg and Wettzell are considered. For the global pattern one station on each continent is used: Cantley, Canberra, Kamioka, Sutherland,
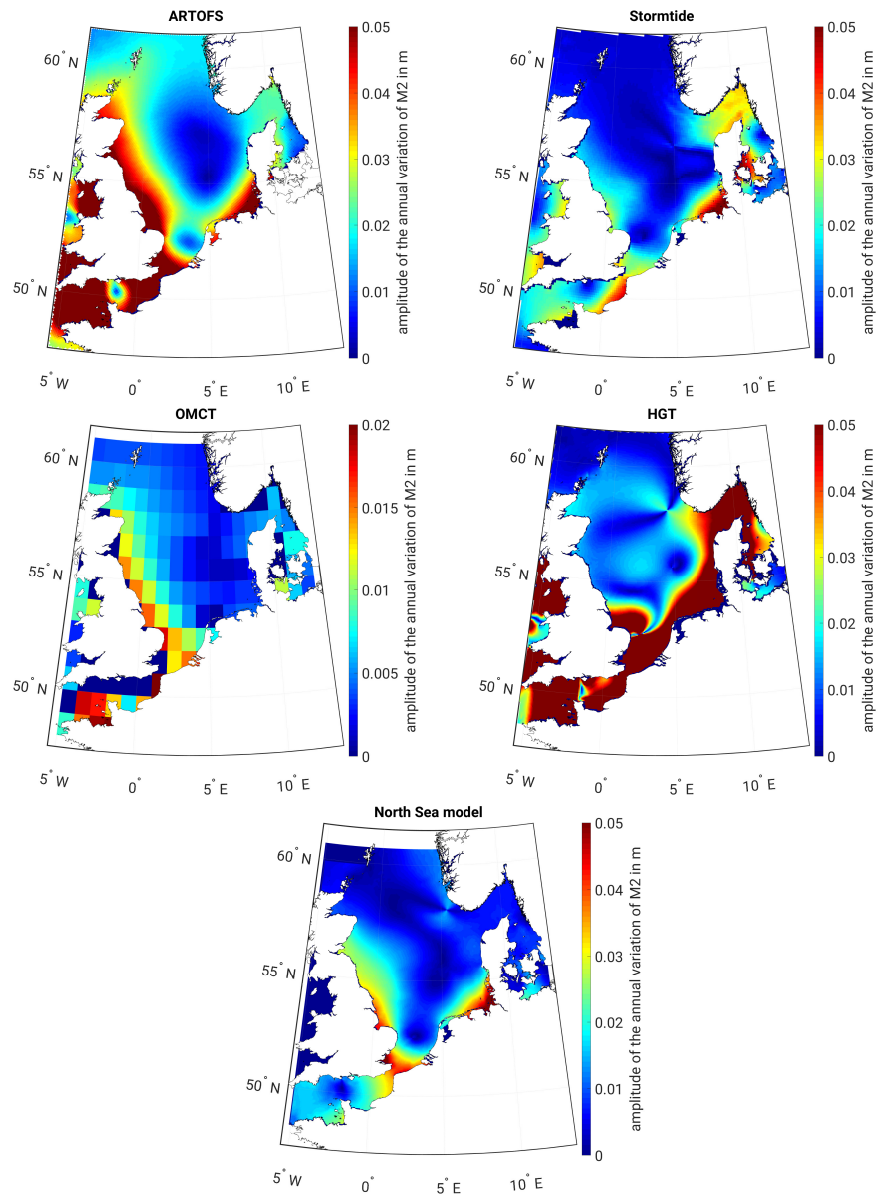
Fig. 8.3. Amplitude of the annual variation of the M2 amplitude from ARTOFS (top left), Stormtide (top right), OMCT data set with changed ice drag (centre left), HGT (centre right) and the North Sea model (bottom). Please note that the dark blue colours close to the coasts can be due to land grid points which have zero amplitude. Also, note the different colour scale for OMCT; the amplitudes are also in a range of centimetres but only half of the amplitudes of the other models.
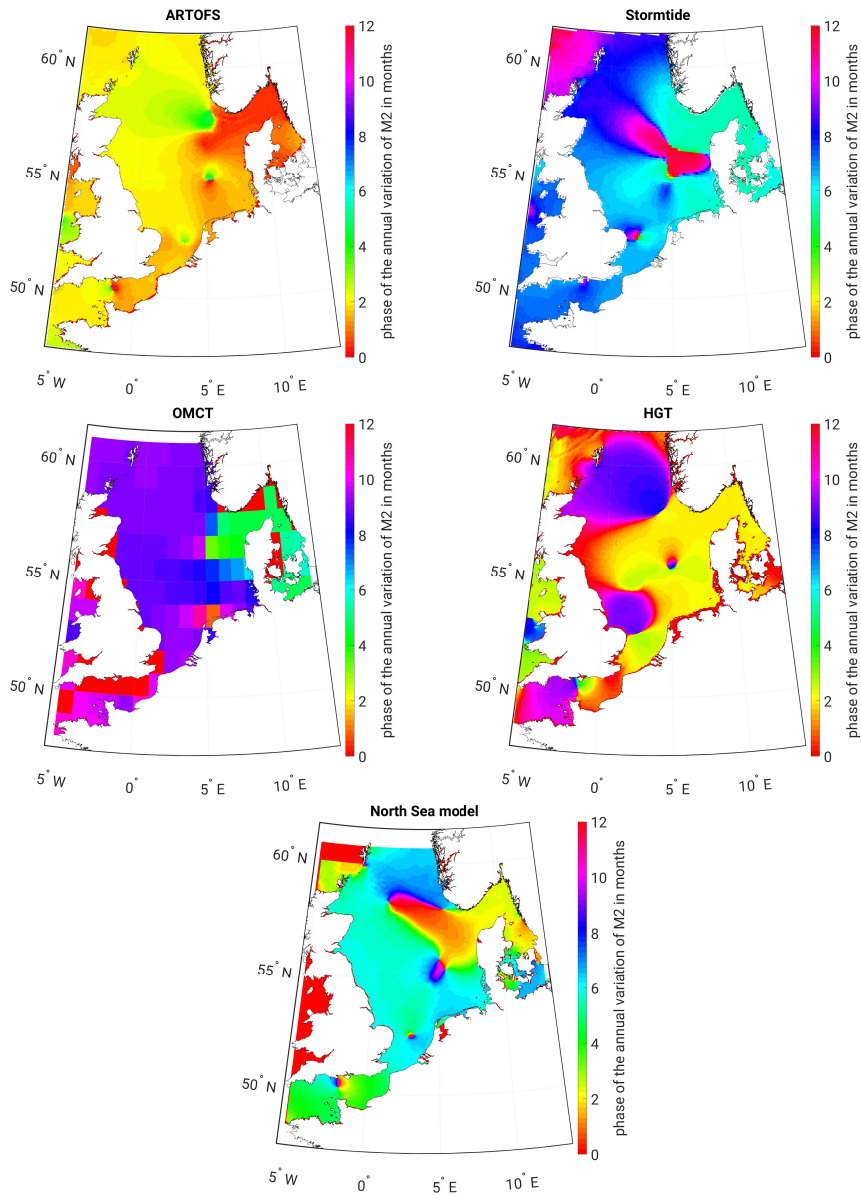
Fig. 8.4. Greenwich phase of the annual variation of the M2 amplitude in months from ARTOFS (top left), Stormtide (top right), the OMCT data set with changed ice drag (centre left), HGT (centre right) and the North Sea model (bottom). Please note that the red colours close to the coasts can be due to land grid points which have zero phase.

Syowa and TIGO Concepción (see section 5.1). As ARTOFS and the North Sea model (see sections 8.2.1 and 8.2.5) are restricted to certain regions only, those stations which are close to coastal areas of the models are used. The station at Onsala is exceptional because the SG is located extremely close to the coast (about 250 m). Therefore, it is probably strongly influenced by the oceans. This makes the ocean loading calculation challenging, because the local coast line is not known well enough, and also the Green's functions for short distances have to be very accurate. The influence of these effects is discussed in appendix F. Onsala is therefore mainly taken into account to show how large these influences can be.

In most cases, the mean values (stationary part, see sections 3.1.2 and 4.2.2) are subtracted from the curves in order to compare the temporal variations of the tidal parameters. They are given in Tabs. E.1 to E.5 in appendix E. In the following sections 8.2.1 to 8.2.5 it is only checked whether the stationary part (mean value) of the tidal parameters increases with respect to the theoretical values of $\delta = 1.16$ and $\phi = 0°$ (see section 4.2.2). The stationary part of the tidal parameter is discussed in more detail in section 8.2.6.2.

As mentioned in section 4.2, the variations of the tidal parameters are compared regarding the order of magnitude of the variation (between 10^{-3} and 10^{-4} for the gravimetric factor and between 0.1° and 0.01° for the phase, of course depending on the regarded station) and the periods of the variation.

8.2.1. ARTOFS

The ARTOFS model is described in section 5.2.2.3. The calculation of the gravity loading time series is given in section 3.2. The investigation follows the concepts described in sections 4.1.2 and 4.2.2.

Fig. 8.5 shows the result for BFO as an example. Most striking is the step at the beginning of 2012 in both tidal parameters. At that time the model run was restarted due to an update of the tides at the open boundaries of the model given by TPX (see section 5.2.2.3, L. Liu and A. Mehra, pers. comm.). The tides at the boundaries are obviously important for the M2 amplitudes in the SSH in the whole model. The amplitudes and phases of the M2 harmonic in the model have changed significantly.

As mentioned in section 4.2.2, the ocean loading is expected to increase the mean value of the tidal parameters. Because of the step, no mean values are calculated for the results from synthetic data MWA, but all gravimetric factors are lower than 1.16. The phase is about 2° which fits to the value for the measured data.

As the interest is on the AVM2, the step was corrected in all cases with the corresponding function in TSoft (van Camp and Vauterin, 2005) and the mean values were subtracted. The results for BFO are shown in Fig. 8.6 in comparison to the results from measurements. The tidal parameters obtained for the other stations close to the model region are given in Fig. E.8 in appendix E. The example in Fig. 8.6 shows that the correction of the step can be inaccurate, because the exact date of the restart was not provided by the modellers and in this example the step occurs at the same time as an increase of the phase. Therefore, the step in the phase is difficult to estimate. Due to the window length of 90 days the step has to occur in this time span. The step is estimated for the gravimetric factor and
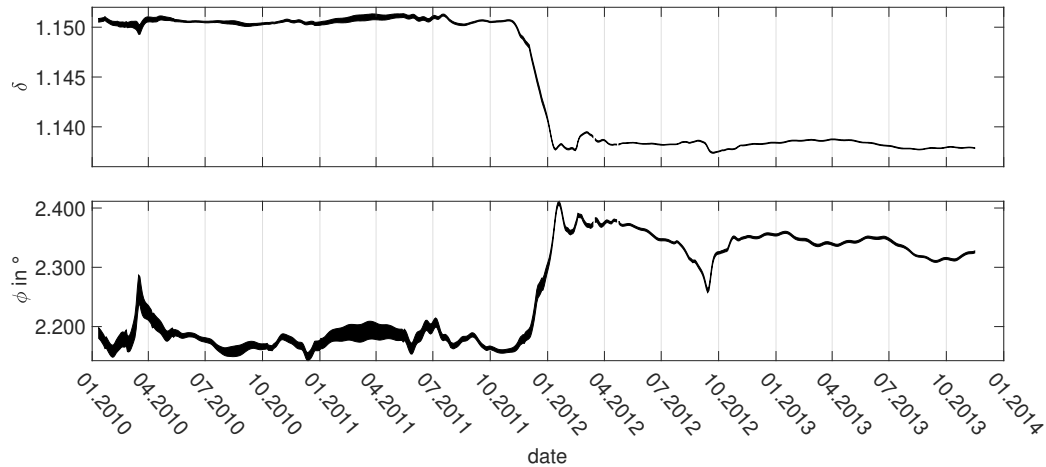
Fig. 8.5. Variation of the M2 tidal parameters obtained with loading from the ARTOFS model and synthetic Earth tides at the station BFO. The upper panel shows the gravimetric factor and the lower panel the phase in degree.

the same parameters are used for the correction of the phase. However, it remains unsure whether the increase of the variation of the phase after the beginning of 2012 is caused by an increase of the annual variations of the M2 amplitude in the SSH or by an inaccurate estimation of the step. As I only discuss the order of magnitude of the AVM2, this has no influence on the interpretation.

An AVM2 is visible in the tidal parameters obtained from ARTOFS but also short-term variations of a few months length, e.g. at the beginning of 2010, which do not seem to have a periodic character. They can be caused by the measurements which are nudged during the modelling (see section 5.2.2.3) or they can be artefacts from the open boundaries due to the model's restriction to the North Atlantic. In a test where a subset of the model, for example the North Sea, in some distance to the open boundaries is used for the loading calculation, the short-term variations are smaller by about 90% than in the curves shown in Fig. 8.6, whereas the AVM2 of the North Sea subset explains between 30% to 50% of the AVM2 obtained from the whole ARTOFS model. This indicates that the open boundaries may at least partly be the origin of the short-term variations.

As the interest is on the AVM2, the results shown in Fig. 8.6 are filtered with a Butterworth low-pass filter with a corner frequency of $\frac{1}{0.5 \text{ years}}$ in Tsoft, in order to eliminate the short-term variations. The filtered results are shown in Fig. 8.7. The dominating period of the time-dependent tidal parameters is annual and the amplitude of the variation is of the same order of magnitude as the results obtained from measurements. For the European stations, the results of the synthetic data MWA are delayed a few months relative to the results from measurements, but there are similarities in the shape of the variation. For example in 2010, the amplitude of the annual variation of the gravimetric factor obtained from measured
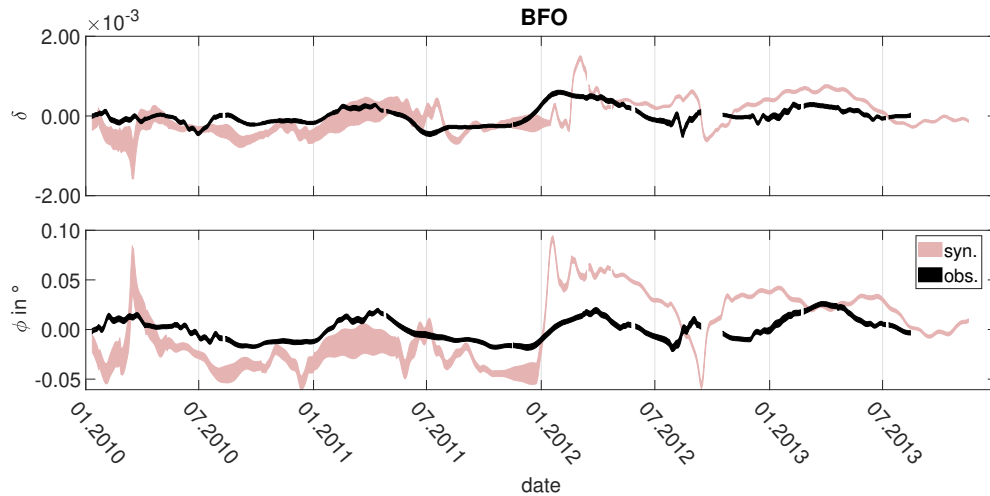
Fig. 8.6. Tidal parameters of wave group M2 at BFO obtained from measurements (black) and synthetic data calculated with ARTOFS (light pink).

data is small at BFO and Moxa compared to the following years. A small amplitude of the gravimetric factor in 2010 is also observed in the results from the synthetic data MWA. At the stations considered here, the annual variation of the M2 amplitude at the ocean model grid points add up to a loading signal in gravity that causes an AVM2 of the correct order of magnitude.

The results for Cantley and Onsala from synthetic data MWA also show an AVM2 but the variation is much larger than the variation in the results from measurements. In contrast to the tidal parameters from the European stations, the AVM2 from synthetic data MWA at Cantley leads the AVM2 from measured data by several months. Merriam (1995) discusses a strong influence of the Bay of Fundy on the SG measurements at Cantley. The Bay of Fundy is not included in the ARTOFS model (see, e.g., Fig. 5.2). Additionally, the amplitudes of the AVM2ssh from the Stormtide model (see Fig. 8.1) show that large amplitudes occur at the Canadian islands which are also not included in ARTOFS. Therefore, the model is probably not able to describe the AVM2 realistically. Please note that high amplitudes in the oceans do not necessarily mean high amplitudes at the gravimeter. Depending on the phase of the annual variation the contributions of the different grid points will add up or cancel each other. Therefore, the consideration of areas of high amplitudes could reduce the AVM2. It cannot be excluded that the same happens at Onsala, as close areas, e.g. the Norwegian Sea and the Baltic Sea, are not included in ARTOFS. However, these regions do not show as high amplitudes of the AVM2ssh as for example the Canadian Islands. As described above, the results from the SG in Onsala are influenced by effects which occur due to the SG's proximity to the coast (see appendix F).
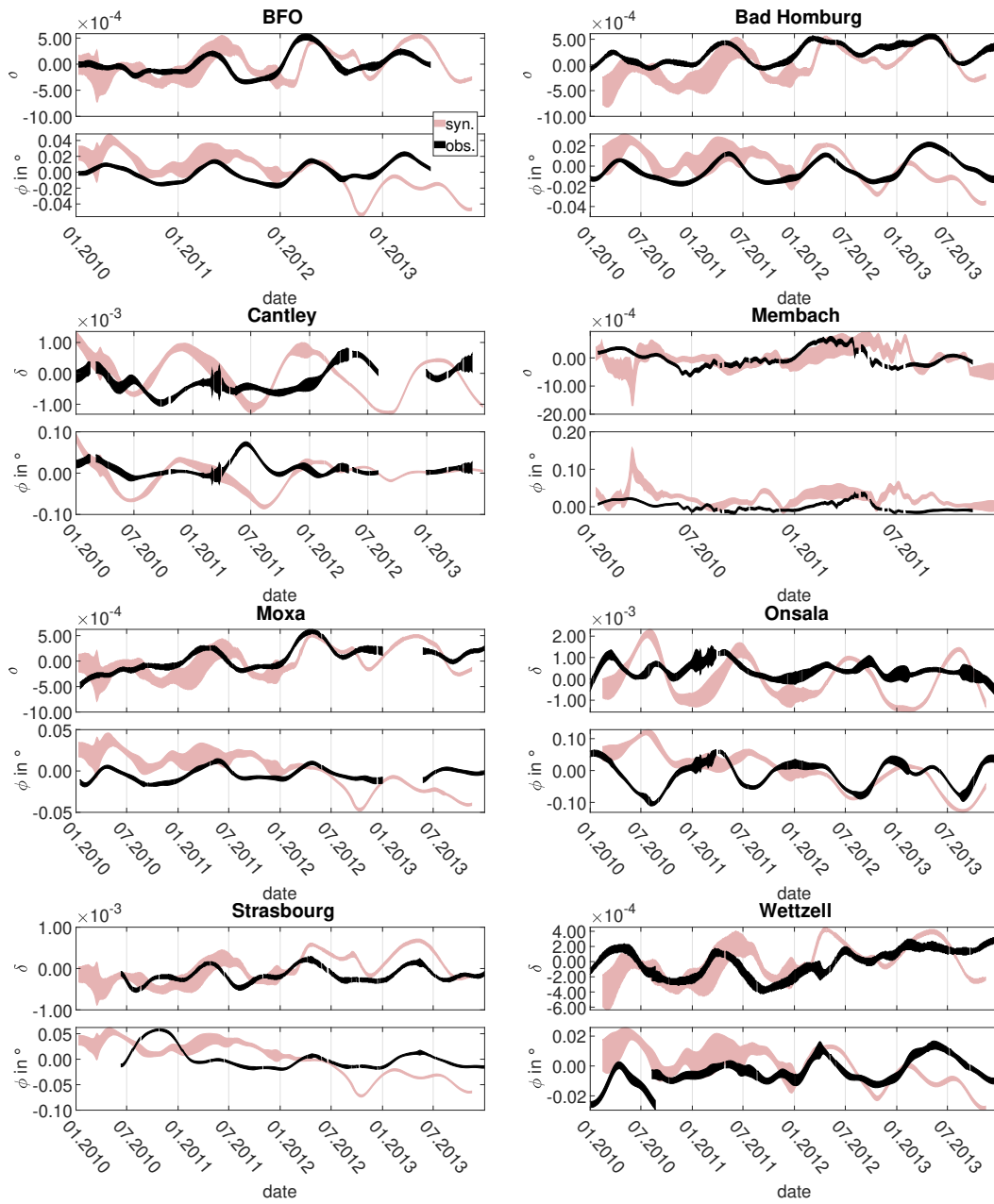
Fig. 8.7. Tidal parameters of wave group M2 at BFO, Bad Homburg, Cantley, Membach, Moxa, Onsala, Strasbourg and Wettzell obtained from measurements (black) and synthetic data calculated with ARTOFS (light-pink) filtered with a low pass Butterworth filter with corner frequency of $\frac{1}{0.5 \text{ years}}$.

8.2.2. Stormtide

For Stormtide, as mentioned in section 5.2.2.4, amplitudes and phases of M2 and its annual variation are available, as well as the SSH values they were obtained from. In the first part of the section, the synthetic data MWA results for both representations of the model output are compared. As the SSH values are only available for 1954 to 1957, the comparison with results from measurements is only done with the synthetic data MWA based on the amplitude and phase representation.

8.2.2.1. Comparison of the tidal parameter variations obtained with SSH and amplitude and phase representation

The loading calculations were done for the years 1954 until 1956, as mentioned in section 5.2.2.4. In the 1950s, Earth tide gravity observations were only available from spring gravimeters whose accuracy is not high enough (Torge, 1989) for the amplitude of the annual variation of M2 in gravity, which is about 0.1 $\frac{\text{nm}}{\text{s}^2}$. The meteorological forcing in Stormtide is climatological and does therefore not necessarily represent the conditions between 1954 and 1956. Hence, the results cannot be directly compared to the results from measurements. However, the AVM2 presented in section 6 in Fig. 6.2 show that the amplitudes of the variation differ only slightly from year to year. The amplitudes in the 1950s should have the same order of magnitude as in the periods regarded here (see Tab. 5.2).

A comparison of the results obtained from SSH with the results of the amplitude and phase representation can show whether the consideration of only few frequencies in the loading can have a significant effect on the AVM2.

The calculation of the ocean loading from Stormtide is done as described in section 3.2. The amplitudes and phases for M2 and the annual variation are used for calculating the SSH as given by equation 5.3. Fig. 8.8 shows the temporal variations of the tidal parameters obtained with synthetic data calculated with the SSH and the amplitudes and phases from Stormtide. The standard deviation for the parameters obtained with loading calculated from amplitudes and phases are very small, because the loading time series contains M2 and its annual variation only. The loading at these frequencies is the only deviation from the analysis model, therefore the residuals, on which the standard deviations are based (see equation 3.9), are very small.

For both representations of the Stormtide model, the loading of Stormtide increases the tidal parameters, as is expected due to the results from observations, but there are significant differences in the stationary parts of both curves. This will be discussed in section 8.2.6.2. The phase obtained with the SSH shows an increase at the beginning of 1954. As 1954 was the first year which was used after the spin-up period of the model (also by Müller et al. 2014), this could be caused by the spin-up if it was not completely finished. However, as it affects only 1.5 months at the beginning of the time series, the results in this period were cut out. Then the mean values are subtracted in order to compare the variations. The tidal parameters in Fig. 8.9 obtained with the amplitude and phase representation have a
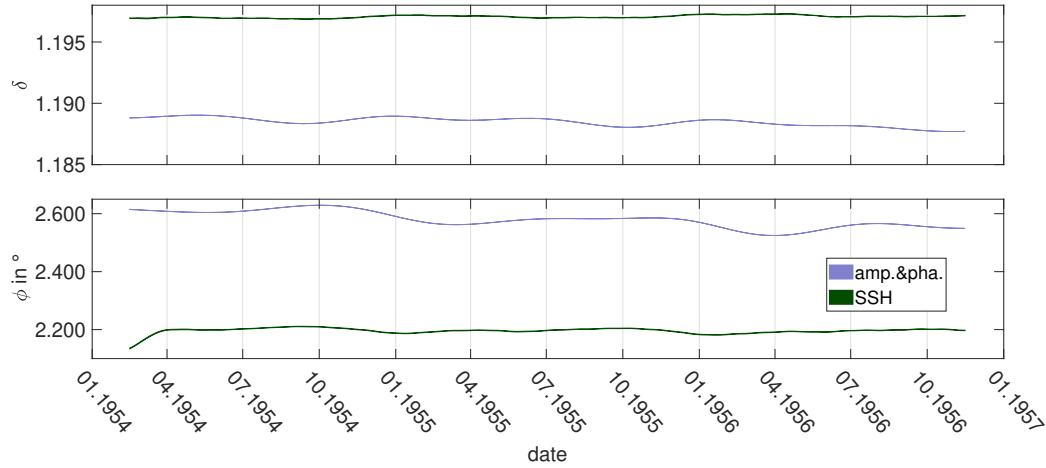
Fig. 8.8. M2 tidal parameters obtained with loading calculated based on the SSH (dark green) and the amplitudes and phases (blue) from the Stormtide model at the station BFO. The upper panel shows the gravimetric factor and the lower panel the phase in degree.
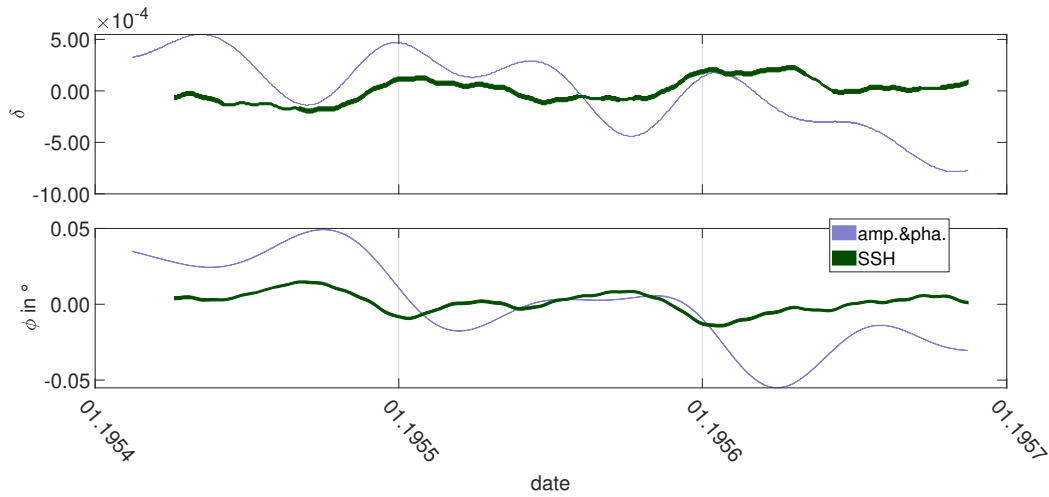
Fig. 8.9. Variation of the M2 tidal parameters (AVM2) obtained with loading calculated based on the SSH (dark green) and the amplitudes and phases (blue) from the Stormtide model at the station BFO. The mean values were subtracted. The upper panel shows the gravimetric factor and the lower panel the phase in degree.

trend, which is not observed for the results obtained with SSH. However, there are also long-periodic variations of the tidal parameters, of, e.g., 8.8 years, possible (Meurers et al., 2016), which would appear as a trend in a short time span (few years). Therefore, it has to be proven whether the apparent trend can be confirmed as a trend or as a long-periodic variation with tidal periods, of, for example, 8.8 years or 18.6 years (see Tab. 2.1). A 20 years long data set is calculated and analysed. The observed variation has a period of 18.6 years with an amplitude of about $2 \cdot 10^{-3}$ in the gravimetric factor and an amplitude of about $0.1°$. The apparent trend in Fig. 8.9 is a short part of this variation.

In the tidal catalogue a harmonic at the frequency of $f_{M2} - \frac{1}{18.6 \text{ years}}$ is found with an amplitude of about 12.4 $\frac{\text{nm}}{\text{s}^2}$ at BFO. It has the number 9323 in the Hartmann-Wenzel catalogue (Hartmann and Wenzel, 1995a,b) and it is named with this number in the following. There are also other harmonics with the same frequency and with $f_{M2} + \frac{1}{18.6 \text{ years}}$, but they have only very small amplitudes and, thus, probably have no significant influence. By adding the loading only for M2, $\alpha 2$ and $\beta 2$, the amplitude ratios and phase differences of the 9323 harmonic to the other harmonics is changed with respect to the assumed amplitude ratios and phase differences in the analysis model. A variation of 18.6 years can only be caused by M2 and 9323 and the order of magnitude of the 18.6-years-variation indicates that harmonics with larger amplitudes than $\alpha 2$ and $\beta 2$ are needed to explain the variation. A synthetic data MWA with wave groups in which M2 and the 9323 harmonic are separated in different wave groups is made. Then the long-periodic variation of the M2 parameters vanishes. Obviously, the apparent trend in Fig. 8.9 is an artefact caused by the consideration of only single frequencies in the frequency band of the M2 wave group.

In order to compare the variations with shorter periods both results, the tidal parameters obtained with synthetic data MWA and from MWA of measured data, are filtered with a high-pass filter (corner frequency $f = 0.0015$ cpd, Tsoft). These results are shown in Fig. 8.10. The filtered tidal parameters obtained with both model representations have similar periods (annual and semi-annual), but with significant differences. The results from SSH show a clear AVM2 and a small semi-annual component, whereas the semi-annual variation is much stronger in the results from the amplitude and phase representation. Additionally, the results obtained with amplitudes and phases are about 1.5 times the amplitudes of the variations obtained with the SSH. This is again due to the fact that only the M2 frequency and the frequencies in a distance of $\frac{1}{1 \text{ year}}$ are taken into account in the loading which changes the amplitude ratio and phase difference with other harmonics. Probable candidates for causing variations of about semi-annual periods would be $\gamma 2$ and $\delta 2$. The frequency $f_{\gamma 2} = 1.92741671$ cpd is in a frequency distance of $\Delta f = \frac{1}{205.8 \text{ d}}$ and $f_{\delta 2} = 1.93774935$ cpd in a distance of $\Delta f = \frac{1}{182.6 \text{ d}}$. This is checked by a synthetic data MWA with the amplitude and phase representation data with a changed wave grouping. $\gamma 2$ is excluded from the M2 group by extending the N2 group and reducing the frequency range of the M2 group. The same is done for $\delta 2$ which is moved that way to the L2 group. This results in the tidal parameters shown in pink in Fig. 8.10. They are much closer to the results from the SSH. The semi-annual variation of the M2 parameters from the amplitude and phase representation is therefore an artefact as well, caused by the consideration of only few frequencies in the loading. The remaining differences are probably due to the small
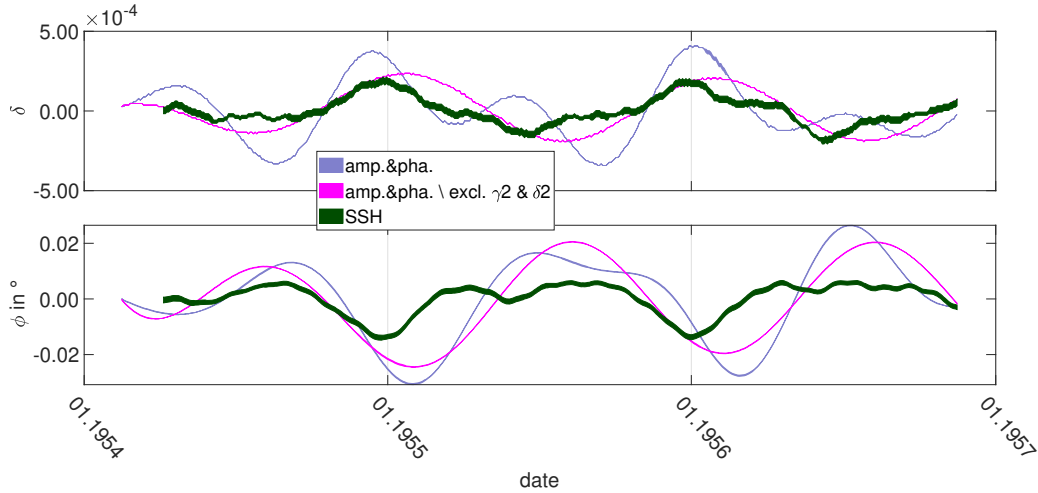
Fig. 8.10. Variation of the M2 tidal parameters obtained with loading calculated from the Stormtide model at the station BFO, based on the SSH (dark green), the amplitudes and phases (blue) and also with the amplitudes and phases but obtained in an MWA with different wave groups. $\gamma 2$ and $\delta 2$ are excluded from the M2 wave group (pink). All curves are high-pass filtered with a corner frequency of $f = 1.5 \cdot 10^{-3}$ cpd. Please note that later on a corner frequency of $f = 1 \cdot 10^{-3}$ cpd is used; this is not possible here because the time series is too short. The upper panel shows the gravimetric factor and the lower panel the phase in degree.

semi-annual components in the results obtained from SSH which cannot be represented by the amplitude and phase representation. These tests show that considering the full frequency range of the loading is of advantage for the results of MWA.

In Fig. 8.11 the variations obtained with the SSH and the amplitudes and phases with the M2 wave group that excludes $\gamma 2$ and $\delta 2$ are compared to the results obtained from measurements. The AVM2 from measured data are larger than the AVM2 obtained from synthetic data MWA. Especially the maximum in the gravimetric factor at the beginning of 2012 is about three times larger than the maxima of the gravimetric factor from synthetic data MWA, but also the other extrema are twice as large as the results from synthetic data. However, they are of the same order of magnitude. The variation of the phase resulting from synthetic data MWA based on SSH are smaller than the results from measurements. The phase variations contain a semi-annual component that is not visible in the results from measurements. Compared with the results from synthetic data MWA based on the amplitude and phase representation ($\gamma 2$ and $\delta 2$ excluded), the variations are similar.

It has to be mentioned that there is a bias in the amplitudes and phases obtained for the Stormtide model. The SSH values are sampled at the 50th minute of every hour, but in the analysis program, described in section 3.3, it is assumed, that the SSH is sampled at the full hour. This would cause a phase shift of M2 of about $4.8305°$. The influence on
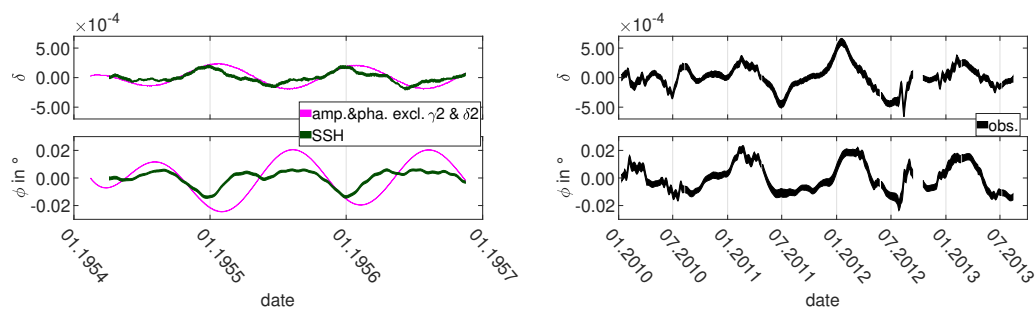
Fig. 8.11. Left: Variation of the M2 tidal parameters obtained with loading calculated from the Stormtide model at the station BFO, based on the SSH (dark green) and the amplitudes and phases but obtained in an MWA with different wave groups. $\gamma 2$ and $\delta 2$ are excluded from the M2 wave group (pink). Right: Results from measured data. All curves are high-pass filtered with a corner frequency of $f = 1.5 \cdot 10^{-3}$. Please note that later on a corner frequency of $f = 1 \cdot 10^{-3}$ cpd is used; this is not possible here because the time series is too short. The scaling of the axes is identical in both plots.

the annual variations is tested by the calculation of a loading time series with correction of the phase shift during the computation. This loading time series is investigated with synthetic data MWA and the results are compared to the results shown above. Differences in the variations are observed but they are only of the order of magnitude of 10^{-5} in the gravimetric factor and of $10^{-4\circ}$ in the phase. As the information about the phase shift was not available from the beginning and the difference is small compared to the AVM2 which is discussed here, I decided not to correct the phase shift.

8.2.2.2. Comparison of the variations obtained with synthetic data to variations obtained with measurements

The analyses in section 8.2.2.1 show that Stormtide loading calculated from amplitudes and phases produces an annual variation of the correct order of magnitude at BFO. Here the comparison is done for different stations. As shown in the previous section the long-periodic and the semi-annual variations occur due to the consideration of only few frequencies in the loading. To remove the long-periodic variation the results are high-pass filtered with a corner frequency of $\frac{1}{1000 \text{ d}}$. For this comparison, the measured data were filtered as well.
I did not try to remove the semi-annual variation because I wanted to avoid filtering close to the annual periods. An adjustment of the analysis model (e.g. excluding $\gamma 2$ and $\delta 2$ from the M2 wave group) would also be possible, but the semi-annual variation is much smaller than the long-periodic variation and, therefore, does not hinder the comparison of the results from synthetic data MWA and from measured data. Besides, there are similarities with the results from measurements, which is discussed below. The filtered results are shown in Fig. 8.12 for the European stations and Fig. 8.13 for the global stations. The unfiltered results are presented in appendix E. For all European stations the variation of the tidal

European stations
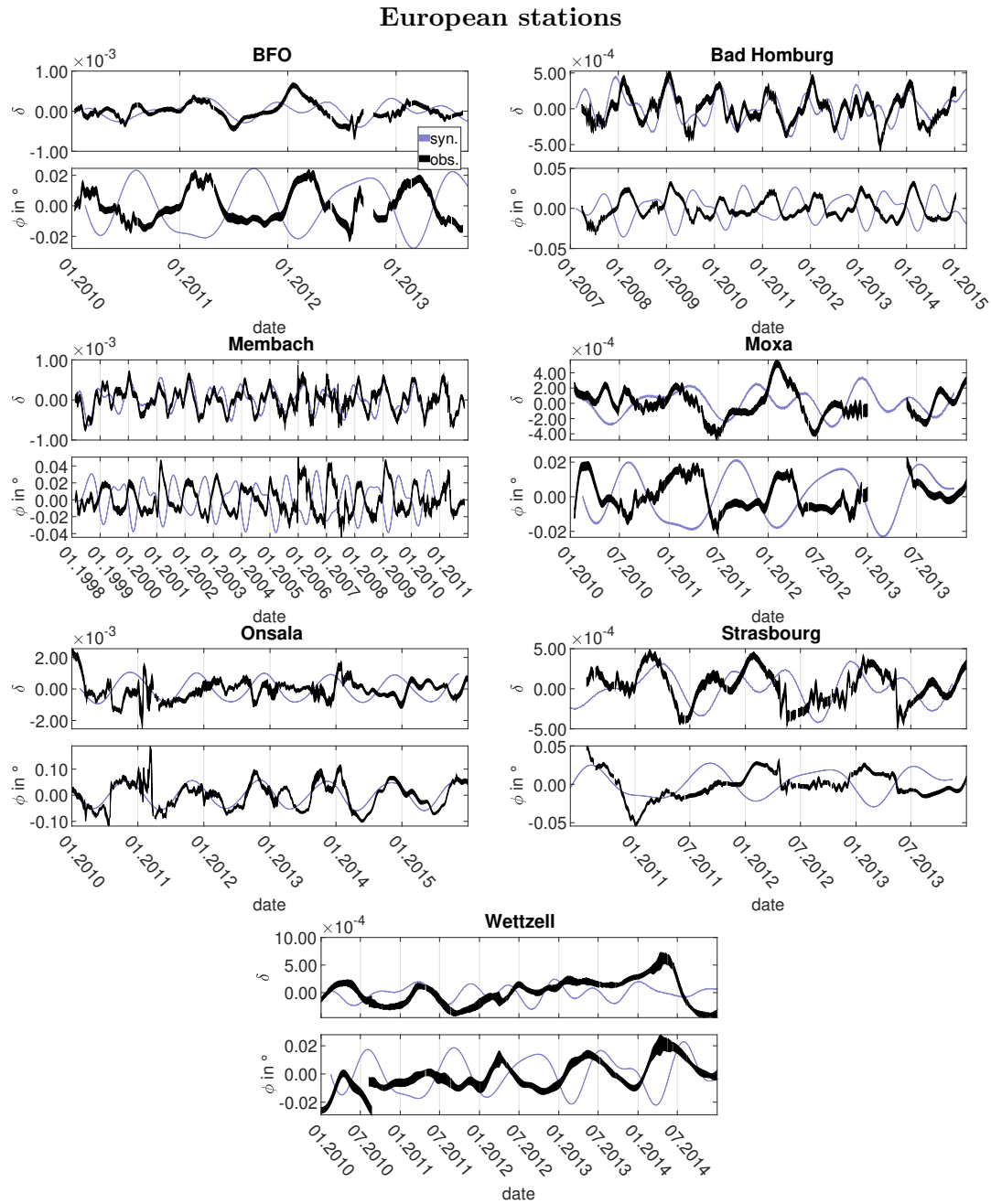
Fig. 8.12. Tidal parameters of wave group M2 at BFO, Bad Homburg, Membach, Moxa, Onsala, Strasbourg and Wettzell obtained from measurements (black) and synthetic data calculated with Stormtide (blue), high-pass filtered with a corner frequency of $\frac{1}{1000\,\mathrm{d}}$.

parameters from measured and synthetic data shows an annual variation in the same order of magnitude. The variations of the gravimetric factors from the synthetic data MWA are a few months delayed to the results from measurements. There are semi-annual components in the variation of the gravimetric factor from measured data that show similarities to the synthetic data MWA results. As shown in section 8.2.2.1 the semi-annual variation in synthetic data is an artefact due to the usage of only the M2, $\alpha 2$ and $\beta 2$ frequencies in the loading. The results from measured data which contain the loading of the frequencies M2 $\pm \frac{1}{0.5\text{years}}$ indicate that the loading at these frequencies is not as strong as for the M2 frequency. This deviation from the analysis model could happen either by a reduction of these harmonics by loading contributions or large loading signals at the M2 frequency.

In contrast, the phases have a smaller semi-annual component than the gravimetric factors but are much more shifted, about 6 months, relative to the measurements' results. The tidal parameters at Onsala again behave differently. The phase from synthetic data MWA is only slightly shifted and leads the results from measurements. The gravimetric factor is shifted stronger, by almost 6 months.

An AVM2 of the correct order of magnitude is also visible for the global stations in Fig. 8.13. The tidal parameters at Canberra and Concepción, the phase of Kamioka and the gravimetric factor of Sutherland have a similar behaviour for the results from both data sets. In the phase at Sutherland from measured data the semi-annual component is strong which cannot be described by the amplitude and phase representation. The phase at Sutherland from synthetic data MWA has a stronger annual component than the results from measurements. The results for Syowa also have a similar behaviour, but the synthetic results lead the measurement results by about three months. For Cantley the variations of the parameters obtained from the measurements are about twice the variations from synthetic data, the similarity is not as high as at the other stations. Here, the vicinity to the Bay of Fundy (Merriam, 1995) probably is a problem because it has a significant influence on the SG, but it is a complex shelf area that can be a challenge in ocean modelling (M. Müller, B. K. Arbic, M. Thomas, J. Saynisch, pers. comm.).

This comparison shows that the annual variations in the SSH predicted by Stormtide add up to an annual variation in gravity which causes an AVM2 of the correct order of magnitude at most SG stations, but the parameters from synthetic data are shifted in time relative to the results from measurements.

8.2.3. OMCT

In this section the results from the OMCT model are presented. First, the tidal parameters obtained from the loading calculations based on the SSH and the OBP are compared. Then the results for the different data sets listed in Tab. 5.3 in section 5.2.2.5 are shown in the second part of the section. At last, the results are compared for different stations. All data sets and the information about them were provided by J. Saynisch.
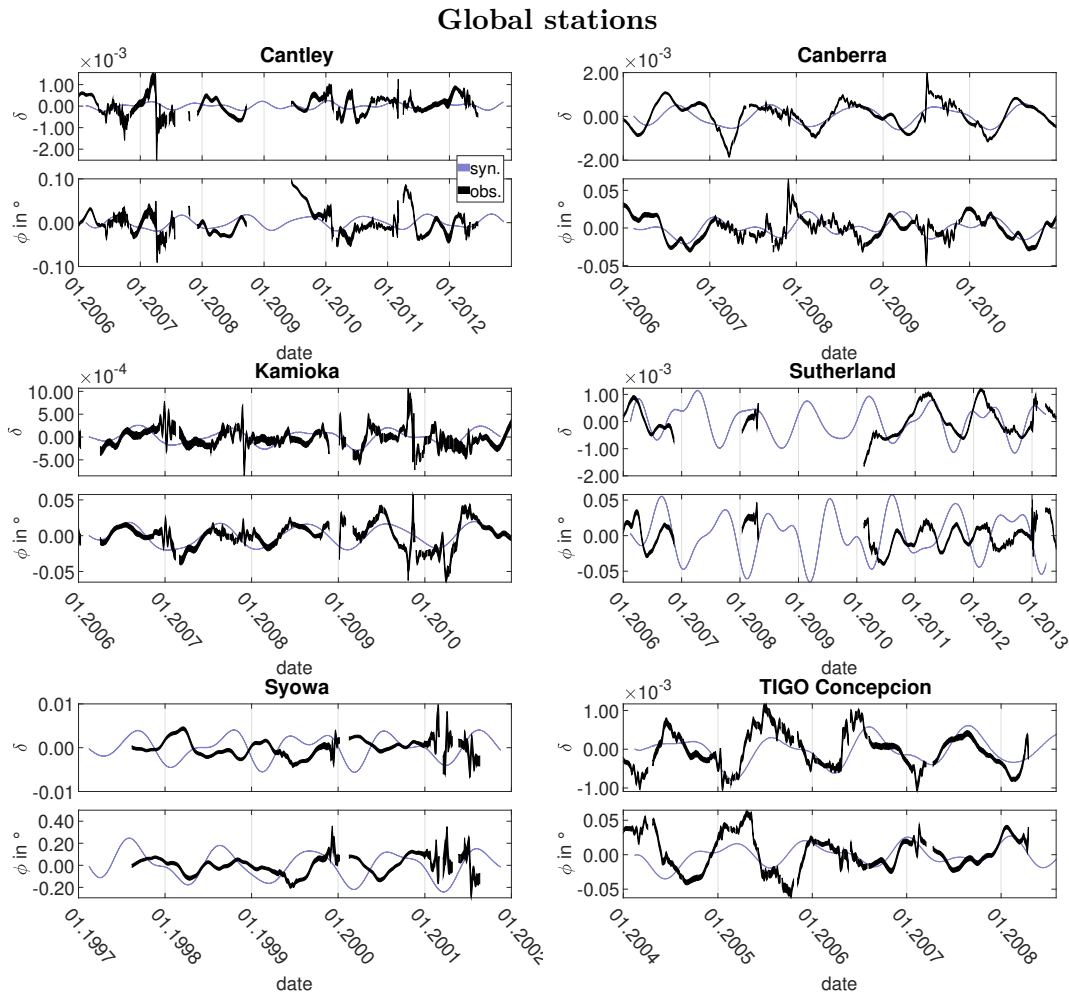
Fig. 8.13. Tidal parameters of wave group M2 at Cantley, Canberra, Kamioka, Sutherland, Syowa and TIGO Concepción obtained from measurements (black) and synthetic data calculated with Stormtide (blue), high-pass filtered with a corner frequency of $\frac{1}{1000 \text{ d}}$.

8.2.3.1. Comparison of results achieved with SSH and OBP

The loading from the OMCT model is calculated as described in section 5.2.2.5 and analysed with MWA as described in section 3.1.2. Here, the first original data set (see Tab. 5.3) is used. The results are given in Fig. E.10 in appendix E. The mean values of the gravimetric factors are higher than 1.16 and the phases are larger than 0°. An increase of the stationary part of the tidal parameters is expected (see section 4.2.2) due to the results from measurements (see Fig. 6.2) if the model describes the stationary M2 amplitude realistically. The stationary parts of the tidal parameters are discussed in section 8.2.6.2. In order to compare the variations, the mean values were subtracted from the curves. This is shown in Fig. 8.14.
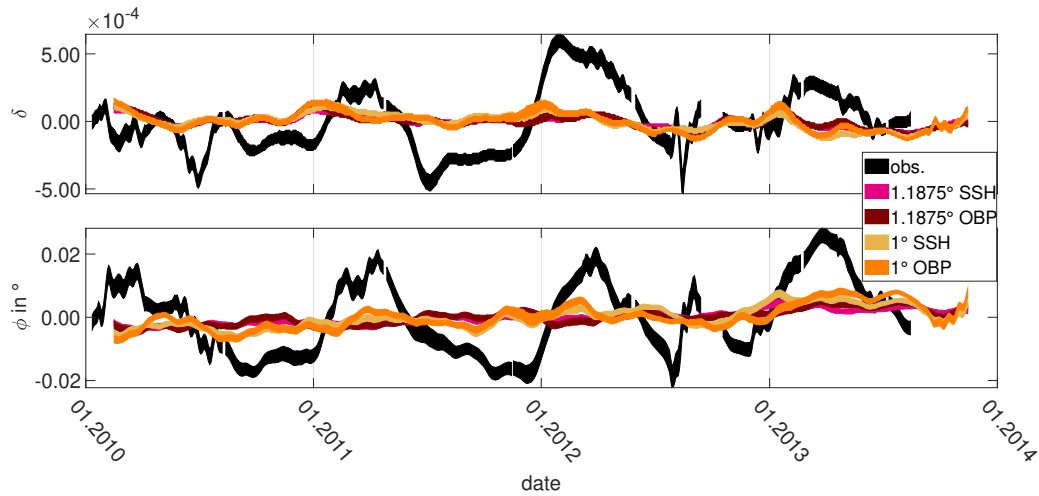
Fig. 8.14. Variations of the tidal parameters of the M2 wave group obtained with the OMCT data set for the station BFO. The results from measurements are shown in black. The curve in pink was obtained with the SSH data set and the curve in dark red with the OBP data set of 1.875° resolution. The curve in light orange was estimated from the synthetic data calculated from the 1° SSH and the curve in orange from synthetic data calculated from the corresponding OBP. The upper panel shows the gravimetric factor and the lower panel the phase in degree.

The variations of the tidal parameters obtained with the different OMCT versions and output do not differ much. For the model with the 1.875° grid the variations are within the standard deviation. The results for the 1° model show slightly larger differences in some parts of the curves, but as the model does not show variations of the order of magnitude observed for measurements, it is unreasonable to discuss differences so small. Therefore, the SSH are used when discussing the variations in the following sections, as the comparison with the loading calculations from other models based on SSH is more consistent.

8.2.3.2. Comparison of SSH results with different properties

The AVM2 from synthetic data MWA are an order of magnitude smaller than the variations obtained with measured data (see Figs. 8.15 and 8.16). As the AVM2 in Fig. 8.14 is slightly larger for the results obtained with the 1° grid model, this version is used for the comparison. The light orange curves in Figs. 8.15 and 8.16 show results of synthetic data MWA for different stations. For the European stations the variations are about an order of magnitude smaller than the variations observed for the results from measurements, as shown for BFO in Fig. 8.14. The exception is Onsala, where the variations of the gravimetric factor are twice the variations observed for the measured data from Onsala and the variations of the phase are of the same order of magnitude. As mentioned before, the gravimeter at Onsala
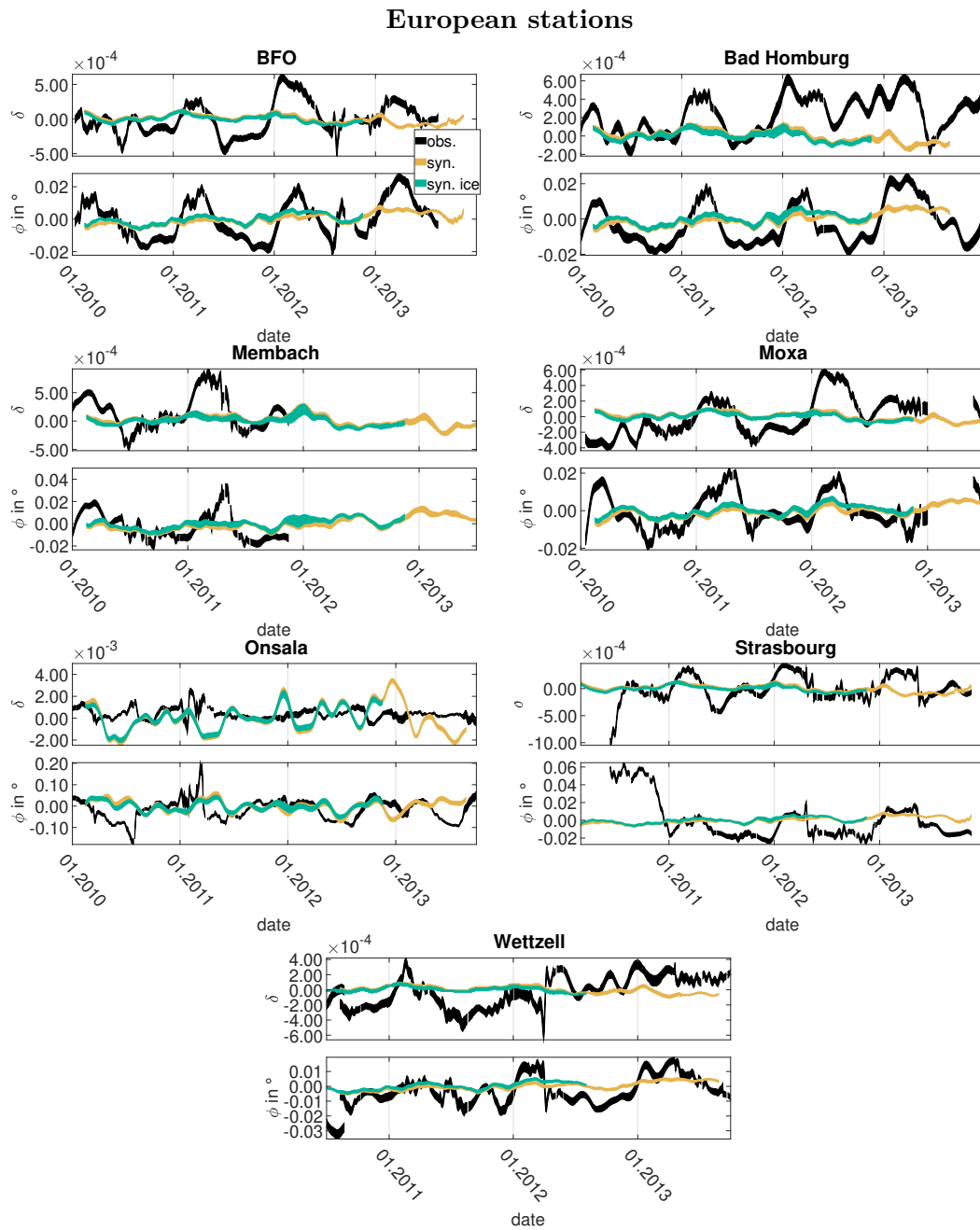
Fig. 8.15. Tidal parameters of wave group M2 at BFO, Bad Homburg, Membach, Moxa, Onsala, Strasbourg and Wettzell obtained from measurements (black), synthetic data calculated with the original version of OMCT (light orange) and the version with a changed ice drag (green).

is very close to the coast and the OMCT model has a low spatial resolution. However, the results in section F.2 show that the variation of the tidal parameters obtained from the loading calculation with SPOTL, which is more accurate for the stations close to the coasts than the simplified loading calculation, is even higher. The large difference between the results shown here and the SPOTL results implies that for Onsala, there is a strong influence of the effects which are neglected in the simplified loading calculation. As the AVM2 obtained with the SPOTL loading calculation is much larger than the results from measurements, it has to be concluded that the model predicts too high M2 amplitudes for ocean areas whose loading influences the gravity at Onsala significantly.

For the variations at the globally distributed stations a similar result is observed as for the European stations. The variations of the tidal parameters from synthetic data are about an order of magnitude lower than the results from measured data. Only the gravimetric factor at Concepción is of the same order of magnitude as the results from measurements. The comparison with the SPOTL calculations in appendixF.2 shows that this is just by chance and due to the fact that the simplified loading calculation is not accurate enough for the station, because the station is located relatively close to the coast and the 1° grid of OMCT is probably too coarse to describe the coast line accurately. This version of OMCT does not describe an AVM2 of the correct order of magnitude.

In order to investigate the reasons why the model does not produce annual variations although it should be possible with the implemented physics, another data set with a changed formulation of the ice drag was used. As Müller et al. (2014) emphasise that a more realistic description of the ice drag is important for a realistic occurrence of the annual variations, their description of the ice drag was implemented in OMCT. These results are shown in green in Figs. 8.15 and 8.16. There is not much difference between the original version and the version obtained with a changed ice drag. Only for some stations there are differences larger than the standard deviation. The changed ice drag results in a very small increase of the variations, at least at some stations, but it is still an order of magnitude too small. Thus, it is concluded that the change of the ice friction description in OMCT has no significant benefit.

As ARTOFS produces an AVM2 which is similar to the results observed for measurements and it nudges a lot of measured data sets, two new data sets with OMCT were calculated with different degree of nudging (high nudging tenfold stronger than low nudging, see section 5.2.2.5). The results for BFO are presented in Fig. 8.17. There is no significant difference between the different nudging versions and the original OMCT version. Therefore, I desisted from continuing this test for other stations. The strongest difference is between the result from the 1.875° to the 1° version.

Of course there are many other parameters available that could influence the occurrence of the annual variation, which were not tested. However, summarising the results described above, they show that the different properties that are tested (ice drag, nudging) do not affect the results much. This indicates that there has to be another reason for the fact that the AVM2 does not occur with OMCT. The fact that the variation is slightly stronger for 1° may be a hint that the model resolution is relevant here. Especially the vertical resolution has to be high enough to resolve the processes which cause the annual variations
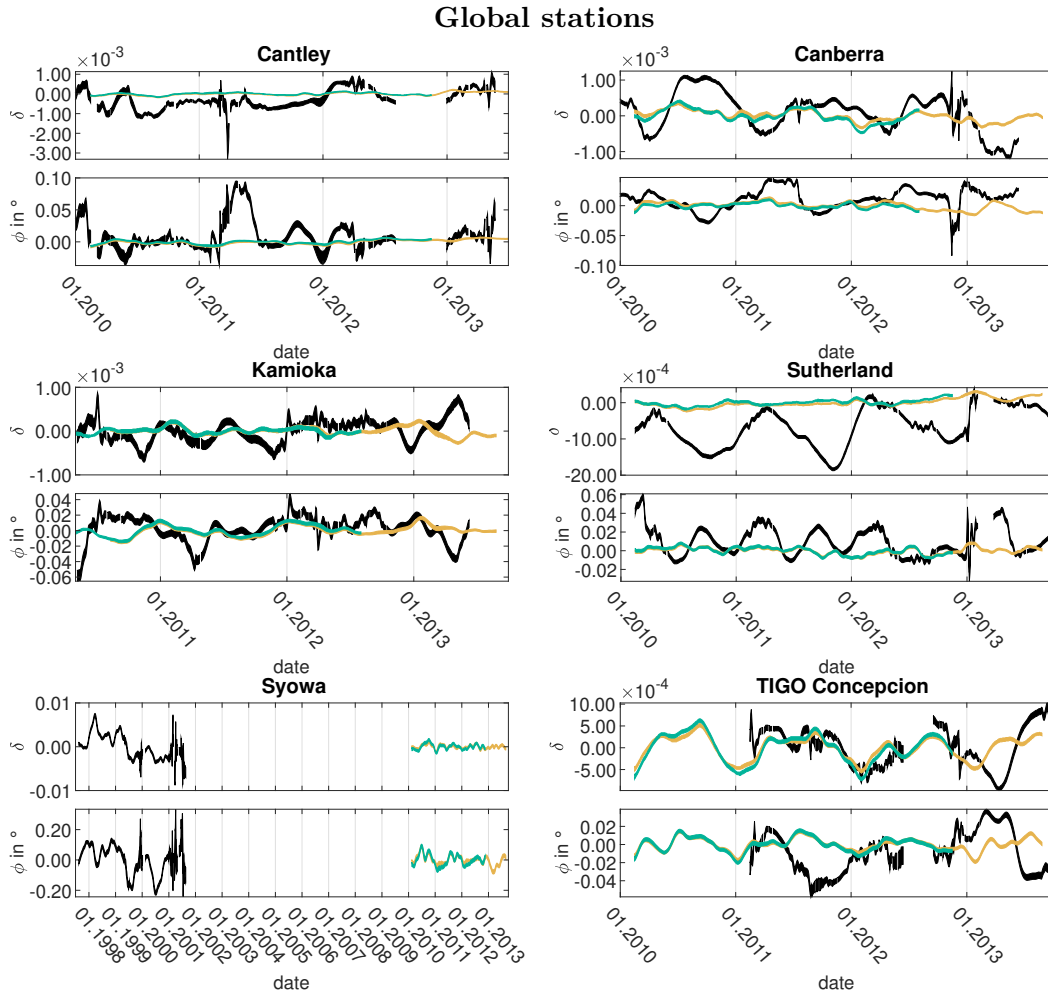
Fig. 8.16. Tidal parameters of wave group M2 at Cantley, Canberra, Kamioka, Sutherland, Syowa and TIGO Concepción obtained from measurements (black), synthetic data calculated with the original version (light orange) and the version with a changed ice drag (green). Please note that the apparent offset of the tidal parameters at Sutherland is due to the calculation of the mean value for a longer time span. The results also show a small long-periodic trend (Schroth et al., 2018); therefore, the part of the curve shown here is below zero. As described in section 7.3.1, the results from Kamioka used here were obtained with correcting the data with Atmacs.
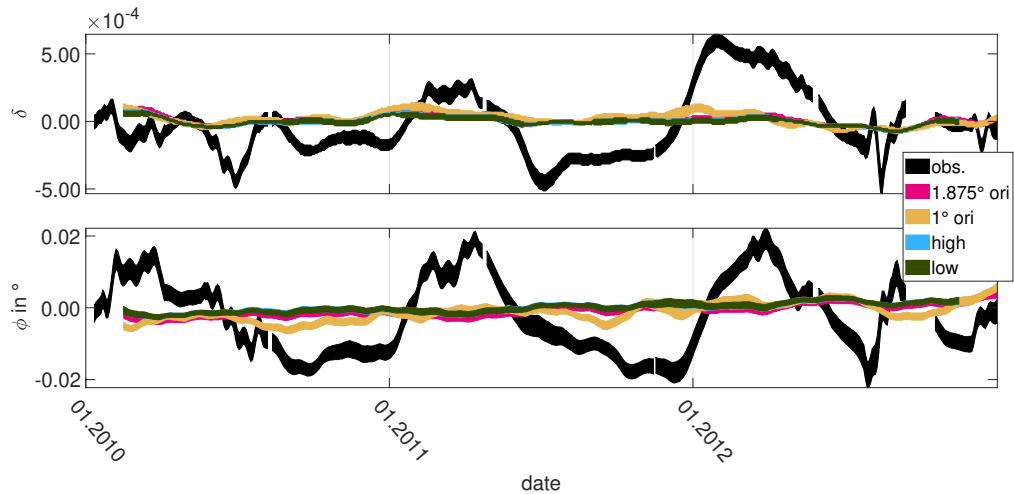
Fig. 8.17. Variations of the tidal parameters of the M2 wave group obtained with the OMCT data sets for the station BFO. The results from measurements are shown in black. The pink curve was obtained with the SSH data set of 1.875° resolution. The light orange curve was estimated from the synthetic data calculated from the 1° version, the blue curve is the result with high and the dark green curve the result with the low nudging data set. The upper panel shows the gravimetric factor and the lower panel the phase in degree.

(M.Müller, pers. comm.). The 20 vertical layers in the 1° version probably cover the related effect better than the 13 layers in the 1.875° version.

8.2.4. HGT

The results for the HGT model were obtained with the synthetic data MWA (see section 4.2.2). In the first part of the paragraph the results for the total and nonsteric SSH are discussed. In the second part the results for the different stations are compared.

8.2.4.1. Comparison of results from total and nonsteric SSH

The results for BFO with loading calculations based on total and nonsteric SSH are shown in Fig. 8.18. Unfortunately, the HGT data sets and the measured data only overlap in 2010. The stationary parts of the tidal parameters from synthetic and measured data are close to each other. It is not necessary to remove the mean value in order to see the variation. The AVM2 caused by the HGT model is larger than in the results from measurements. The tidal parameters obtained with synthetic data MWA show a long-periodic behaviour which is due to the harmonic in a frequency distance of $\frac{1}{18.6\text{years}}$ (9323) (see section 8.2.2.1). In this case only a few harmonics are taken into account in the forcing, which does not contain the 9323 harmonic. Its effect is corrected with a constant value (B. K. Arbic, J. Shriver, pers. comm.). As this harmonic is taken into account in the analysis, it causes a long-periodic
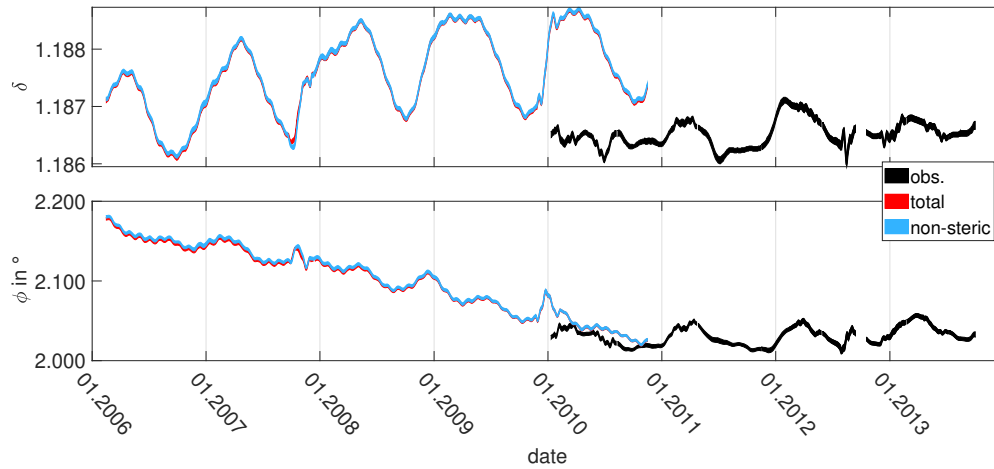
Fig. 8.18. Variations of the tidal parameters of the M2 wave group obtained with the HGT data sets for the station BFO. The results from measurements are shown in black. The curve in red was obtained with the total SSH and the curve in dark red with the nonsteric SSH. The upper panel shows the gravimetric factor and the lower panel the phase in degree.

variation. This was tested in the same way as described for Stormtide (see section 8.2.2.1). As soon as the 9323 harmonic is excluded from the M2 group, the long-periodic variation vanishes.

The results from total and nonsteric SSH show no significant differences. The steric effects, as described in HGT, have only very small effects on gravity. For reasons of consistency the total SSH is used in the following.

8.2.4.2. Results for different stations

The results for the different stations are shown in Figs. 8.19 and 8.20. As mentioned in the previous section, the tidal parameters show a long-periodic behaviour which is due to the harmonic in a frequency distance of $\frac{1}{18.6 \text{ years}}$. Therefore, the results are filtered with the same high-pass filter with $f_c = 0.001$ cpd that was used for Stormtide.

For all European stations, except for Onsala, the model produces a clear, annual variation of the M2 gravimetric factor of about $8 \cdot 10^{-4}$. This is approx. twice the variation observed from measurements. The phase also has a semi-annual component, the amplitude of the variation is about $0.15°$, which is slightly smaller than the variations obtained from measurements. The loading calculation is based on the SSH. It potentially can contain all frequencies, but the model is forced only with a few harmonics. These harmonics do not contain the harmonics with a frequency distance of $\frac{1}{0.5 \text{ years}}$. If this frequency is not forced by some other mechanism in the model, it is missing in the loading which can result in the semi-annual
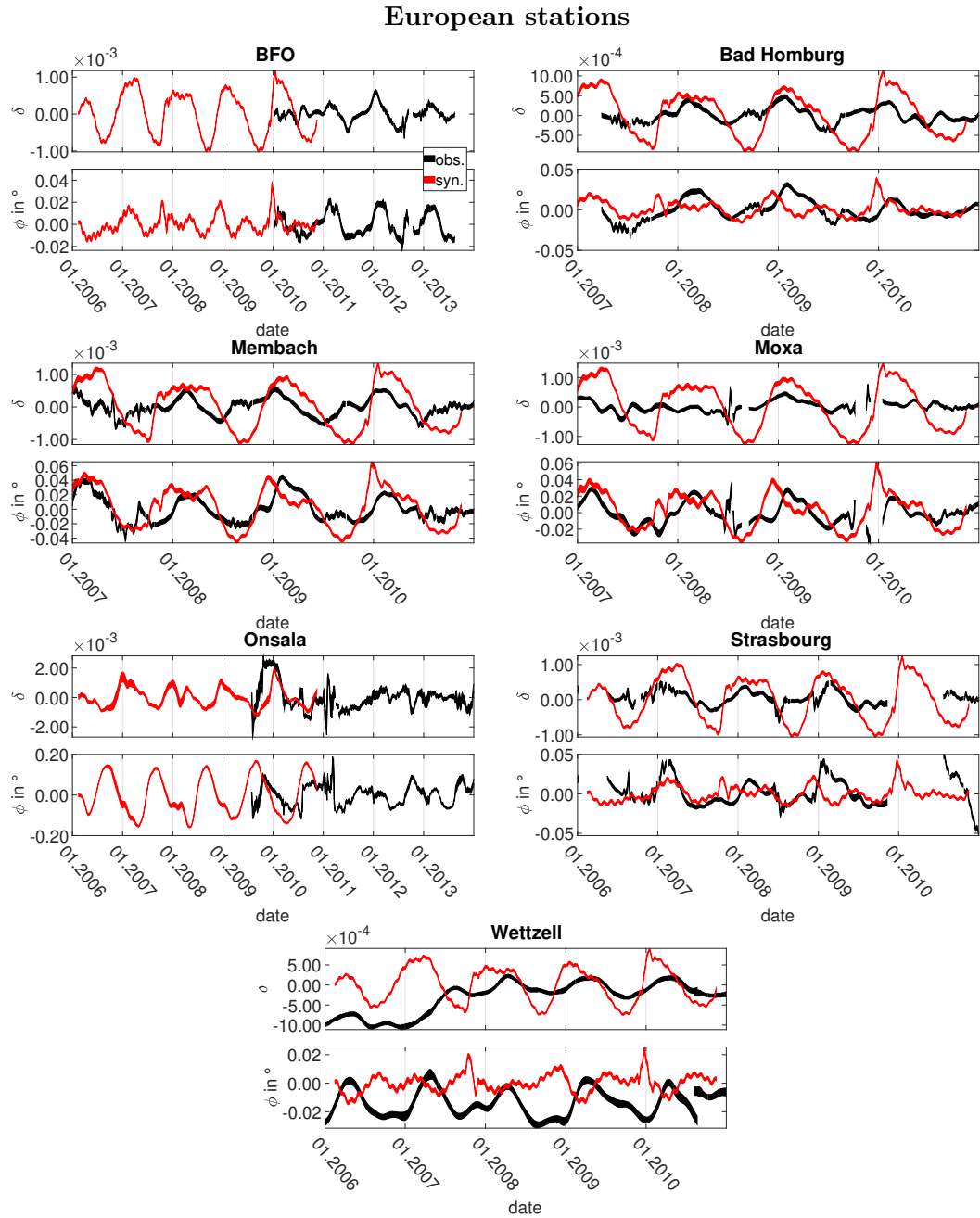
Fig. 8.19. Tidal parameters of wave group M2 at BFO, Bad Homburg, Membach, Moxa, Onsala, Strasbourg and Wettzell obtained from measurements (black) and synthetic data calculated with HGT (red), high-pass filtered with a corner frequency of $\frac{1}{1000 \text{ d}}$.
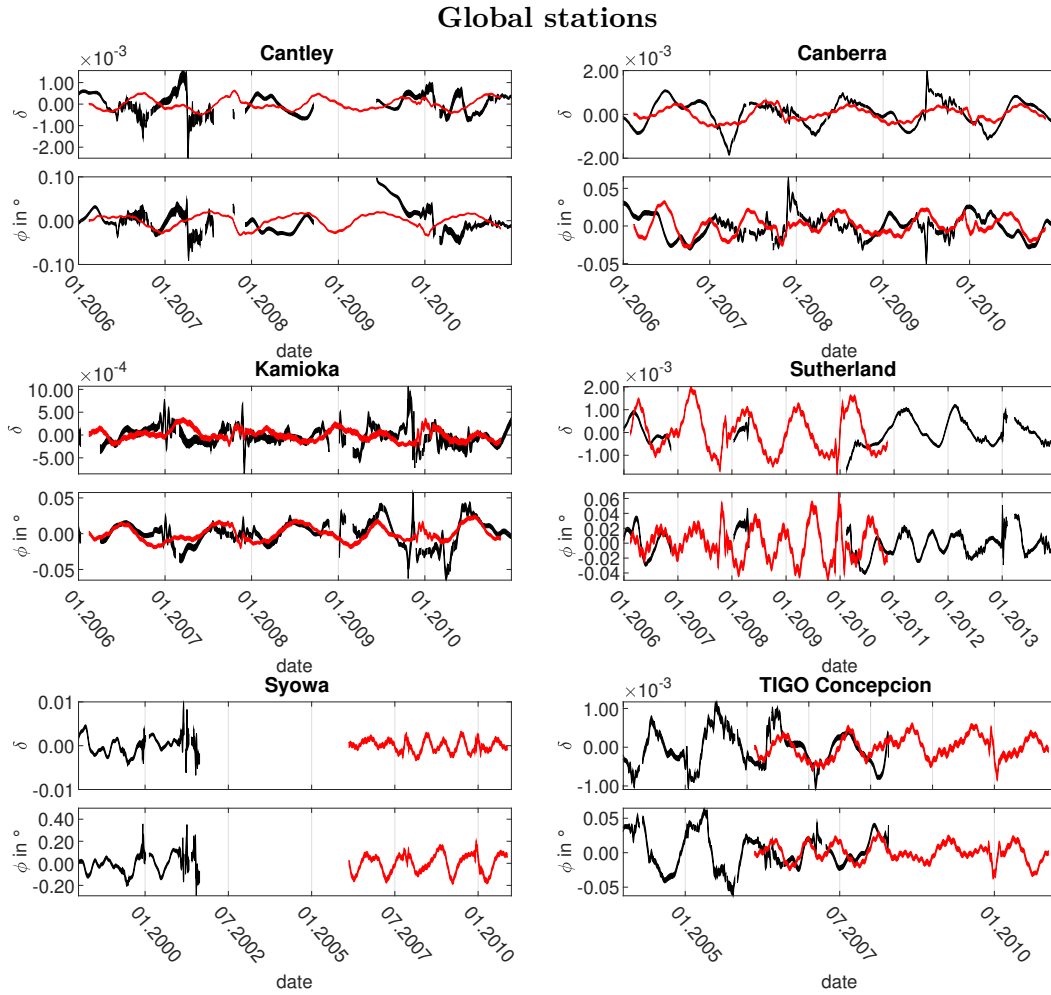
Fig. 8.20. Tidal parameters of wave group M2 at Cantley, Canberra, Kamioka, Sutherland, Syowa, TIGO Concepción obtained from measurements (black) and synthetic data calculated with HGT (red), high-pass filtered with a corner frequency of $\frac{1}{1000\ \mathrm{d}}$.

variation different from the semi-annual variations observed with measured data. The right panel of Fig. 8.25 in section 8.2.6.1 shows the spectra of the loading time series calculated with the different ocean models for BFO in a small frequency band around M2. At the frequencies $f_{M2} - \frac{1}{182.6\ \mathrm{d}} = 1.92679792$ cpd and $f_{M2} + \frac{1}{182.6\ \mathrm{d}} = 1.93774932$ cpd no signals are visible. This indicates that the discussed signal is not present in the loading.

At Onsala the annual variation is dominating. The variation of the gravimetric factor is only slightly larger than the variation observed with measurements while the variation of the phase has about twice the size of the variation observed with measurements.

At Sutherland in Fig. 8.20 the variations caused by the model are about 1.5 times larger than the variations from measurements. In this case the semi-annual variations of the phase

fit well for both data sets. The AVM2 observed for Kamioka have about the same size for synthetic and measured data. For all the other stations the variations of the tidal parameters from measured data are larger than the variations obtained with the model. In all cases the variations are of about the same order of magnitude as the results from measurements. For example, in the gravimetric factor at Strasbourg, Canberra, and Concepción the extrema occur at similar times. For some stations short-periodic variations occur for which no reason was found. The Hann window was also used in these cases. However, the variations are small and do not influence the significance of the AVM2. Therefore, this issue was not investigated further.

8.2.5. North Sea model

One might expect that a regional high-resolution model is able to describe the AVM2ssh in the ocean areas close to the station more accurately than a global model. If it is assumed that the ocean areas close to the SG station are mainly responsible for the AVM2 observed at a station, the AVM2 obtained with such kind of model should be closer to the results from observations. The North Sea model (see section 5.2.2.7) is used for investigating this for the European stations. The loading was calculated as described in section 3.2. Fig. 8.21 shows the results. As the North Sea is only a very small part of the global oceans, it cannot be expected that the mean values are close to the stationary parts of the tidal parameters from measurements (see sections 8.2.1 and 8.2.6.2). All mean values are discussed in detail in section 8.2.6.2 and are given in Tabs. E.1 to E.5 in appendix E. For the following discussion, the mean values are subtracted. Please note that I refer to the ocean area as 'North Sea'. If the ocean model is meant, the term 'North Sea model' is used. The results of the synthetic data MWA are similar for all three stations and do not show an AVM2. The results from sections 8.2.1 to 8.2.4 show that the Central European stations behave similar. It is unlikely that another European station shows an AVM2 in a synthetic data MWA with the North Sea model. Therefore, no further stations were investigated.

These results are surprising because the amplitudes of the AVM2ssh from the North Sea (see Fig. 8.3) are similar to the results from Stormtide in the North Sea. Two interpretations of this are possible: First, the North Sea is, although it is close to the regarded stations and shows high amplitudes of the AVM2ssh, an area too small and does not contribute significantly to the AVM2. Second, the amplitudes of the AVM2ssh from the North Sea model may not sum constructively.

In order to investigate which of the two possibilities applies in this case, a part of the Stormtide model (amplitude and phase representation) which has about the same size as the North Sea model is used for synthetic data MWA. The results are shown in Fig. 8.22. Stormtide was chosen for this test because the computation is much faster than for the other models. For the amplitude and phase representation the area which is used has to be cut out only once, whereas for the SSH of Stormtide or the other models the area needs to be cut out for every time step. The results for the North Sea cutout from the Stormtide model show an annual variation of about $8 \cdot 10^{-5}$ for the gravimetric factor and $0.002°$ for the phase, which is approx. 10% of the variations caused by the total model. This shows
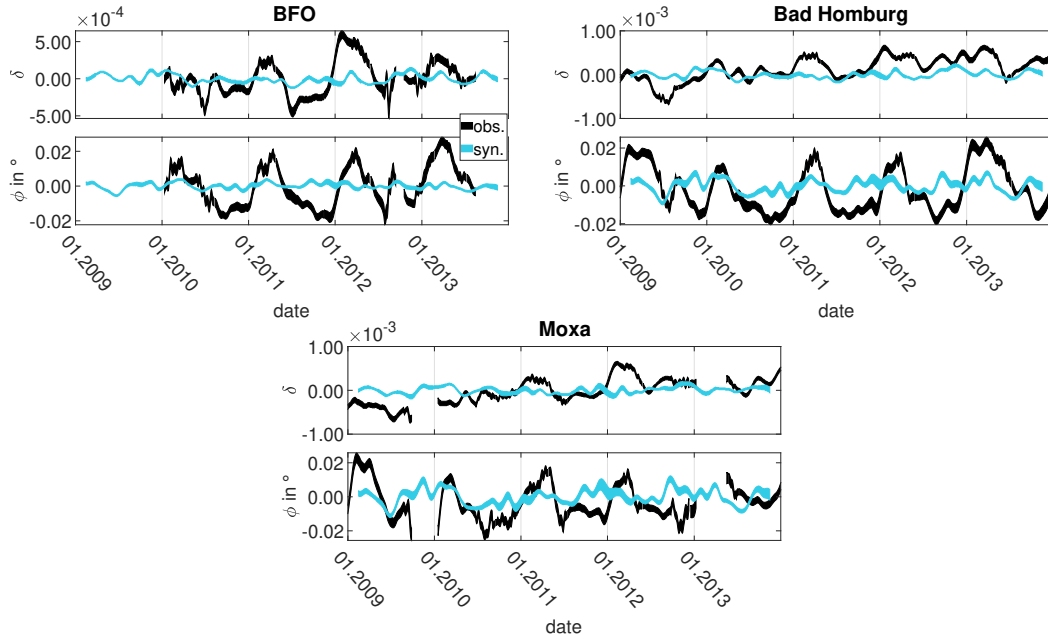
Fig. 8.21. Variations of the tidal parameters of wave group M2 at BFO, Bad Homburg and Moxa obtained from measurements (black) and synthetic data calculated with the North Sea model (turquoise). The mean values were subtracted.
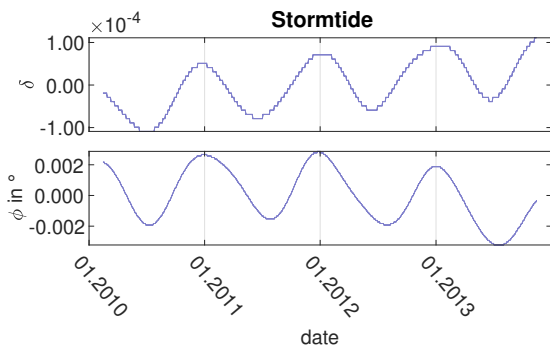
Fig. 8.22. Variation of the tidal parameters at BFO from synthetic data based on the North Sea cutout from the Stormtide model. The time span is chosen similar to the time span the North Sea model SSH are available for.
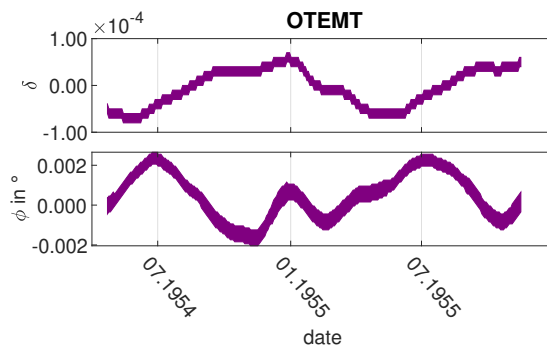
Fig. 8.23. Result from the synthetic data MWA for BFO with the barotropic OTEMT model for North Sea, Skagerrak and Kattegat forced with Stormtide SSH at the boundaries. The time span of the SSH values from OTEMT in this case depend on the availability of the Stormtide SSH.

that the North Sea produces a significant AVM2, although it is not enough to fully describe the AVM2 obtained with measurements. The variation obtained with a synthetic data MWA of the North Sea model is of the same order of magnitude, but shows no clear annual periodicity. The results in Fig. 8.21 show short-periodic variations of a few months length which can potentially cover an AVM2. However, even low-pass filtering with a frequency of $\frac{1}{0.5 \text{ years}}$ does not result in an AVM2. This means that the amplitudes of the AVM2ssh of the North Sea model do not add up constructively.

A test with the OTEMT model (Ocean Tide Equations Main program time-dependent, H.-G. Scherneck) can give a hint on the reason for this result. In the following paragraph a short introduction to the OTEMT model is given, as it is not described or used in any other part of this thesis.

OTEMT is based on the formulation of the equations of motion and mass conservation (see equations 5.1 and 5.2 in section 5.2.2.1) by Wübbe and Krauss (1979) and Wübbe (1979) and advice by W. Zahel (H.-G. Scherneck, pers. comm.). An area which covers the North Sea, the Skagerrak and the Kattegat is considered. The model has no atmospheric forcing and is barotropic. No vertical changes of the ocean water properties are possible. Therefore, it cannot produce an AVM2ssh (see chapter 1.1) on its own. This is shown by model runs with the standard forcing of the model at the boundaries with 46 harmonics (11 from TPXO7.2, Egbert and Erofeeva 2002; amplitude ratios from the Tamura tidal catalogue, Tamura et al. 1991, assumed for the others). $\alpha 2$ and $\beta 2$ are not among those 46 harmonics. Neither an AVM2ssh nor an AVM2 of the correct order of magnitude occurred. From the OTEMT model output, SSH time series at specified grid points and a loading time series for BFO were stored. The loading signal is computed with the programs used for the Ocean Loading Provider website (see section 8.2.6.2) with modifications due to the restricted size of the model (H.-G. Scherneck, pers. comm.).

In the model run discussed in the following, the model is forced at the boundaries with the Stormtide SSH. In the first step, it is tested whether an AVM2ssh can be observed in the SSH predicted by OTEMT. Unfortunately, the SSH values are only available for certain grid points, as mentioned above. MWA of the SSH time series at these grid points with ETERNA (see sections 3.1.1 and 3.1.2) can show whether an AVM2ssh of the correct order of magnitude occurs, even if it does no allow to represent the distribution of the AVM2ssh in the model area. The results are shown Fig. 8.24. Tab. 8.1 gives the positions of the grid points from which the SSH time series are used.

At all four grid points, variations of the amplitudes and phases occur which are of the same order of magnitude as the results from the amplitudes of annual variations predicted by Stormtide (see section 8.1). Even at the NSE grid point which is far from the boundaries the amplitude of the AVM2ssh is still about half a centimetre. As the variations of the M2 amplitude shown in Fig. 8.24 cannot be caused by the OTEMT model, they have to be caused by the AVM2ssh in the Stormtide SSH which are used for the forcing at the boundaries. Four grid points are of course not sufficient to show the amplitude distribution of an area of the size of the North Sea, but the results described above indicate that the AVM2ssh occurs in the whole model area and not only close to the boundaries.

The results in Fig. 8.23 show that synthetic data MWA with the OTEMT model at BFO
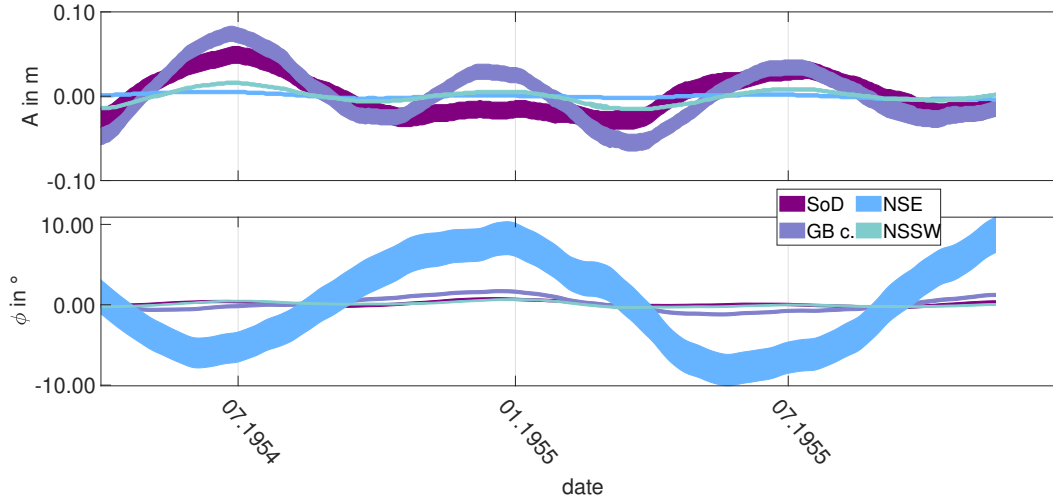
Fig. 8.24. Variations of the M2 amplitude in metres and the phase lead in degree at four different grid points of the OTEMT model. The position of the grid points are given in Tab. 8.1. Please note that in contrast to the Greenwich phase lags in section 8.1 the phase lead here is relative to the local potential.

name	lat in °	lon in °	description
Strait of Dover (SoD)	51.053	1.563	centre of the strait, close to the shortest distance between coast lines
German Bight coast (GB c.)	53.963	8.348	close to the coast and mouth of Elbe, Wadden Sea area
North Sea East (NSE)	55.541	5.076	distant from the coast, in the East of the North Sea
North Sea South West (NSSW)	53.272	3.167	distant from the coast, in the South West of the North Sea

Table 8.1. Latitudes and longitudes in degree of the four grid points whose results are shown in Fig. 8.24

results in an AVM2. The AVM2 is of the same order of magnitude as the AVM2 of the North Sea cutout from the Stormtide model in Fig. 8.22. The tidal parameters are given for different time spans, but the investigations in section 8.2.2.1 show that the AVM2 from the Stormtide amplitude and phase representation in the 1950s and between 2009 and 2013 do not differ much.

Although OTEMT does not contain the mechanisms causing the AVM2ssh, the forcing of AVM2ssh (with the Stormtide SSH) at the boundaries leads to a distribution of the variations that add up constructively at BFO in the correct order of magnitude. This does not happen for the North Sea model. It includes the phenomena causing the temporal variations, but has only 11 harmonics as forcing at the boundaries, which do not describe the annual variations (see section 5.2.2.7). Sündermann and Pohlmann (2011) state that the tides in the North Sea are dominated mainly by the tides in the Atlantic. If it is assumed that $\alpha 2$ and $\beta 2$ behave similar to M2, then $\alpha 2$ and $\beta 2$ in the North Sea are significantly influenced by $\alpha 2$ and $\beta 2$ in the neighbouring regions. The information about $\alpha 2$ and $\beta 2$ in the neighbouring regions is not included in the North Sea model, but in OTEMT (with forcing with Stormtide SSH at the boundaries). This would explain the results of the synthetic data MWA with these models. They indicate that modelling on a large (global) scale or information about the annual variations at the boundaries of the model are important for the occurrence of the AVM2 at an SG station.

It remains unclear how large the contribution of the generation of the AVM2ssh within the area of the North Sea is. In my opinion, the large amplitudes of the AVM2ssh in the North Sea model SSH (see Fig. 8.3) cannot be neglected. Further investigations will be necessary for estimating how large both contributions, the generation within the North Sea area and the forcing at the boundaries, are.

8.2.6. Comparison of results

In the previous part of the chapter the results from the different ocean models were presented. Here these results are compared. In the first section a direct comparison of the loading time series is made. In the second part the stationary parts are compared and in the third part the focus is on the temporal variations.

8.2.6.1. Comparison of the loading time series

In sections 8.2.1 to 8.2.5 the results for the tidal parameters obtained with the different ocean models are presented. All loading time series should in principle represent the same effects, but it is shown in these sections that the tidal parameters obtained with the ocean models differ significantly. The loading time series, therefore, also have to show clear differences. In the time domain, they will surely look very different, as for example the Stormtide loading time series calculated from the amplitude and phase representation does only contain the M2 frequency and its annual variation, whereas the others contain many tidal frequencies. Therefore, Fig. 8.25 shows the spectra of the loading time series for BFO. The spectra were calculated with *foutra* (see section 3.4), which normalises the amplitudes

in the spectrum such that they have the same amplitude as the time domain signal. As the tidal parameters obtained with OMCT did not differ much, whatever OMCT data set was used, the spectrum was calculated from the original 1.875° data set, as its length of 13 years is of advantage for the frequency resolution. In section 5.2.2.5 it is mentioned that the OMCT loading time series have a high mean value. This has no influence on the MWA, but in the spectrum the amplitude of more than 4000 $\frac{nm}{s^2}$ at 0 cpd hides the signals of interest. Therefore, the spectrum of the OMCT loading time series is only shown for frequencies higher than 0.0012 cpd. With the amplitude and phase representation in Stormtide, a loading time series of 13 years was calculated. A spectrum of loading obtained with Stormtide SSH is not shown, because with only three years length of the time series the frequency resolution is too low. Also for ARTOFS no spectrum is shown because the signals of interest are covered by artefacts, probably due to the change in the tidal amplitudes, which also causes the step in the tidal parameters (see section 8.2.1). If only a part of the data set, before or after the step, were used, these data sets would be too short (about 2 years) for a sufficient frequency resolution. The spectrum on the left side of Fig.8.25 shows that M2 has the highest amplitude (except for the constant contribution in OMCT mentioned above), the amplitude itself is different from model to model. They fit well to the distribution of the gravimetric factors shown in Fig. 8.26 in section 8.2.6.2.
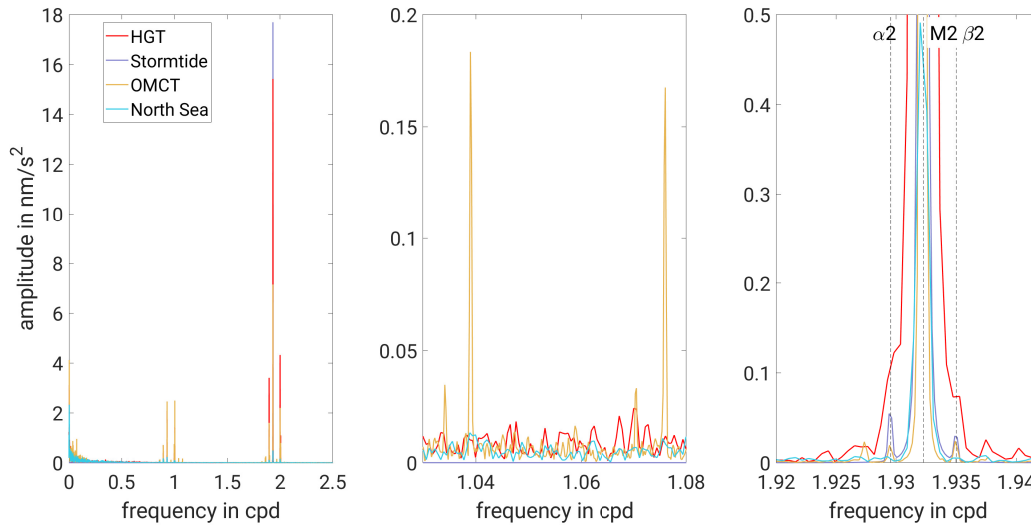
Fig. 8.25. Left: Spectra of the loading time series calculated for BFO with Stormtide in blue, HGT in red, OMCT in light orange and the North Sea model in cyan, between 0 and 2.5 cpd. There is almost no signal at higher frequencies. Please note that for OMCT the spectrum at frequencies lower than 0.0012 cpd is not shown because the loading has a large mean value, whose signal in the spectrum would cover the rest of the signal due to the range of the y-axis. Middle: Small frequency band around J1 and OO1. Right: Small frequency band around M2, the M2, $\alpha 2$ and $\beta 2$ frequencies are marked.

The M2 amplitude in the Stormtide loading is the highest, just as the mean value of the gravimetric factor is the highest. Both values are in the middle for HGT and the lowest for OMCT. The amplitudes cannot be compared in absolute values to the gravimetric factors without additional information about the phase. The phase can be taken, for example, from the stationary tidal parameters estimated with tidal analysis. As the stationary tidal parameters are discussed in the following section 8.2.6.2 anyway, this is not discussed in detail here.

For the spectrum from the North Sea model it is not expected that its amplitude reaches the same order of magnitude as the others, because it covers only a small part of the global ocean, but here also M2 has the largest amplitude.

At the semi-diurnal frequencies the amplitudes of HGT are larger than those of OMCT. It is the other way round for the diurnal harmonics. Here, OMCT has the higher amplitudes. A closer look at the spectrum in the centre panel of Fig. 8.26 shows that OMCT contains signals that are not present in HGT, for example at the J1 or the OO1 frequency where one would expect a signal at least due to astronomical forcing. This shows that a forcing with ephemerides is of advantage when the complete tidal spectrum is needed in the gravity loading.

In the right panel of Fig. 8.25 only a small part of the frequency axis around M2 is chosen. The annual variation of the gravimetric factor cannot be seen directly in the spectrum, because both, $\alpha 2$ and $\beta 2$, contribute to the annual variation and their phase leads have to be taken into account. However, the spectra show that in the loading from HGT and Stormtide, which both produce an AVM2, the signals at the $\alpha 2$ and the $\beta 2$ frequency have higher amplitudes than the neighbouring frequencies, whereas their signals in the North Sea model loading vanish in the noise. The resolution of the 5-years-long HGT time series is not good enough to display $\alpha 2$ and $\beta 2$ as separate peaks, but the shape of the spectrum indicates that there are signals at the corresponding frequencies. The spectrum from OMCT shows that the loading contains small contributions at $\alpha 2$ and $\beta 2$, but whereas the $\beta 2$ amplitude is almost as high as in the Stormtide loading, the $\alpha 2$ signal is smaller by about two-thirds. Stormtide and HGT predict a higher amplitude for $\alpha 2$ than for $\beta 2$, but OMCT shows an opposite behaviour. Therefore, their amplitude ratio is different to their ratio in the loading from HGT and Stormtide and cannot cause an annual variation in the correct order of magnitude.

The comparison of the spectra of the loading time series fit to the results obtained with synthetic data MWA. HGT and Stormtide, which show an AVM2, also have strong contributions of $\alpha 2$ and $\beta 2$ in the loading, whereas OMCT, which shows only a small AVM2, and the North Sea model, which shows no AVM2, have only small signals at $\alpha 2$ and $\beta 2$ frequencies. Moreover, the relative heights of the M2 amplitudes in the models behave similar to the mean values of the tidal parameters discussed in the next section.

8.2.6.2. Comparison of the stationary part of the tidal parameters

In this section, the stationary parts of the tidal parameter obtained with the different ocean models (see sections 8.2.2 to 8.2.4) are compared to results obtained with measurements and
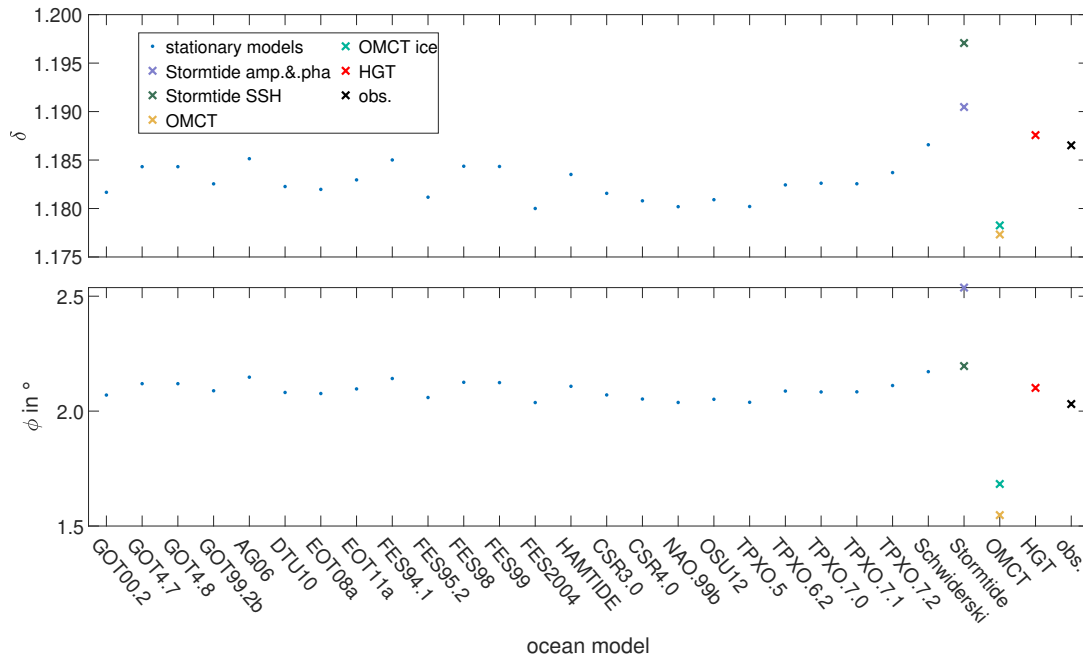
Fig. 8.26. Top: Gravimetric factors obtained with altimeter models[9] (blue) and the non-stationary models Stormtide with the calculation based on amplitudes and phases (light blue) and SSH (dark green), the original 1° (light orange) and the changed ice drag version (green) from OMCT and HGT (red) in comparison to the results from measurements. Bottom: Same for the phase. No standard deviations are shown here because they are of an order of 10^{-5} for the gravimetric factor and 10^{-3} for the phase and would be almost invisible.

with loading calculations based on altimeter models. This comparison shows if the stationary M2 predicted by the non-stationary ocean models is close to results from observations and models which were especially designed for the prediction of the stationary tides. The latter values are obtained from the Ocean Loading Provider[9](OLP) by H.-G. Scherneck and M. S. Bos. It takes into account the same effects as SPOTL (see section 3.2), which are neglected in my simplified loading calculation. The loading values obtained from OLP are used for calculating the resulting tidal parameters assuming a gravimetric factor $\delta = 1.16$ and phase $\phi = 0°$ for the solid Earth (see section 4.2.2). They are given with the results for the nonstationary models in Fig. 8.26. ARTOFS and the North Sea model are not shown here. Due to their limitation to certain areas, they cannot provide reasonable mean values. Several issues have to be considered for the comparison. They can cause differences of the mean values which are not due to the ocean model. These issues are discussed first in this section, starting with those that can cause differences between the results from the

---

[9] http://holt.oso.chalmers.se/loading/index.html (05.07.19)

stationary and the nonstationary models.

The loading calculations for the stationary models were made with a different program (OLP). It takes into account different effects and is based on different Green's functions compared to the simplified loading calculation. The calculation based on different Green's functions in appendix F.1.2.2 shows that there can be a difference in the tidal parameters due to the usage of Green's functions calculated for different Earth models of about $2 \cdot 10^{-3}$ in the gravimetric factor and about $0.025°$ in the phase.

The mean values obtained with the SPOTL-based loading calculations in appendix F.2 differ from the results with the simplified loading calculation at most $2 \cdot 10^{-3}$ in the gravimetric factor and about $0.02°$ in the phase for OMCT. Only for Onsala, the differences are larger because it is close to the coast where the simplified loading calculation is highly inaccurate. This difference contains the influence of the neglected effects (e.g. coastlines, extent of grid cells, see section 3.2) and the usage of different Green's functions (based on Gutenberg-Bullen model, Agnew 2012). The difference obtained with SPOTL is similar to the difference which is obtained in the test with the Green's functions based on different Earth models. As an upper limit of accuracy shall be estimated, I assume that, by chance, this SPOTL difference is only caused by the neglected effects and not influenced by differences in the Green's functions. Below, it is therefore completely added to the error range.

Additionally, the mean values obtained from the time-dependent tidal parameters depend on the length of the time series. An integer number of periods of the variation will result in a mean value which is close to the results from the tidal analysis, otherwise it can deviate from this value by less or equal to the variation amplitude. The maximal deviation caused by this issue can be of an order of 10^{-4} in the gravimetric factor and $0.01°$ in the phase.

An error that will cause differences between the tidal parameters obtained with the ocean model and the results from measured data is the assumption of a gravimetric factor $\delta = 1.16$ and a phase $\phi = 0°$ for the solid Earth. The calculation of the resulting tidal parameters is based on this assumption and it cannot be tested whether it is an appropriate measure of the solid Earth response to tidal forcing. This has to be considered when comparing the results obtained with the different ocean models to the result obtained with measured data. If it is assumed that the established, theoretical tidal parameters are close to the real Earth response, the value of 1.16 for the gravimetric factor deviates from the Earth model results by up to $1 \cdot 10^{-3}$ (Dehant et al. 1999, see also appendix B).

If it is assumed that all differences estimated above add up, this will result in a difference for the gravimetric factor of $5.1 \cdot 10^{-3}$ and for the phase of $0.06°$. The results from the stationary models vary in a similar range of about $5 \cdot 10^{-3}$ (gravimetric factor) and $0.1°$ (phase lead). Therefore, differences of this order of magnitude between the results from stationary and nonstationary models or nonstationary models and measurements are not interpreted.

If the mean values obtained with measured data are taken as the true values and the errors in the range which was estimated previously in this section, about $\pm 5 \cdot 10^{-3}$ in the gravimetric factor and $\pm 0.1°$ in the phase, then most of the results from the stationary models and the results from HGT are within the error range. The HGT model describes

the stationary part of M2 equally well as the stationary models, which is remarkable as HGT does not use any kind of nudging or assimilation (B. K. Arbic, pers. comm.).

For OMCT additionally the interpolation to hourly values (see appendix F.3) causes mean values which are too low by $1.4 \cdot 10^{-3}$ to $2.5 \cdot 10^{-3}$ for the gravimetric factor and $0.14°$ for the phase. This cannot explain the differences between the tidal parameters of the stationary models and the mean values from OMCT, though.

For both Stormtide data sets (SSH and amplitude and phase representation), only one of both tidal parameters is within this range. The results with the SSH data set have a phase lead within the error range but the gravimetric factor is too large. For the amplitudes and phases it is vice versa. The difference between the Stormtide results are caused by the artefacts that occur in the synthetic data MWA with the amplitude and phase representation of the model (see section 8.2.2.1) and the phase shift caused in the harmonic analysis, due to the sampling of the SSH at the 50th minute of every hour which is not taken into account in every analysis (see section 8.2.2.1). Both effects combined explain the difference in the mean values.

The results for the stationary part of M2 obtained in the harmonic analyses (see section 8.1 and appendix E) fit to the results discussed here. The amplitudes and phase lags from the HGT model have a high similarity to the results from HAMTIDE. Similarities also exist for the other models, but more differences are visible.

All mean values of the tidal parameters shown in sections 8.2.1 to 8.2.5 are given in Tabs. E.1 to E.5 in appendix E. The loading calculations with stationary ocean models for the other stations (Baker and Bos, 2003; Boy et al., 2003) correspond to the results obtained for MWA. In most cases a similar behaviour as for BFO occurs. The results obtained with HGT are usually close to the results from measurements. The results for Stormtide tend to have higher mean values. OMCT shows values too small for the European stations, whereas for the other stations there is no obvious pattern. As the stationary part is not the main issue of this study, I did not further investigate the differences of the results for the different stations.

As mentioned above, ARTOFS and the North Sea model cannot produce reasonable stationary tidal parameters, as they are restricted to certain areas. The North Sea model increases the gravimetric factor only slightly for BFO and reduces it slightly for Moxa and Bad Homburg, the phase leads have small negative values (see Tabs. E.1 to E.5 in appendix E). For ARTOFS, the mean values of the gravimetric factors are smaller for all stations except for Cantley, Onsala, and the part of the tidal parameters for Moxa after the step (not shown in this thesis). The phase leads are about $2°$ for the European stations and about $-0.1°$ for Cantley which is similar to the results from measurements. The influence of the spatial restriction on the stationary tidal parameters could, for example, be further investigated by cutting out similar areas from the global models, in order to check whether their loading causes similar stationary parts of the tidal parameters. This is not done here, as the focus of this thesis is on the temporal variations of the tidal parameters.

8.2.6.3. Comparison of the temporal variations of the tidal parameters

In this section the AVM2 obtained from ARTOFS, Stormtide and HGT loading (see sections 8.2.1, 8.2.2 and 8.2.4) are compared. The results for OMCT and the North Sea model are not shown here because they cause only small or no AVM2. The tidal parameters in the previous sections obtained with ARTOFS are low-pass filtered, whereas high-pass filtering is used for the HGT and Stormtide results. For the comparison in Figs. 8.27 and 8.28 the results are band-pass filtered with a lower frequency of $\frac{1}{1000 \text{ d}}$ and higher frequency of $\frac{1}{0.5 \text{ years}}$ (see sections 8.2.1 and 8.2.2.1). Except for the fact that all three models cause an AVM2 of the correct order of magnitude, the results from the synthetic data MWA look very different. For the European stations the AVM2 produced by ARTOFS represents the behaviour of the results from measured data better than the other two models, for example in the varying heights of the amplitudes from year to year. This can be seen for example in the results from BFO or Bad Homburg. However, this does not hold for every station as, for example, the phase leads from measured data at Strasbourg behave differently from the results from synthetic data MWA with ARTOFS. ARTOFS and HGT are very similar models (B. K. Arbic, pers. comm.), but HGT produces much larger amplitudes for the tidal parameters at the European stations. The nudged, measured data is probably of advantage in ARTOFS.

These observations fit to the amplitude of the AVM2ssh obtained with harmonic analyses (see section 8.1). The amplitude of the AVM2ssh is larger for HGT and ARTOFS than for Stormtide, just as the annual variation of the gravimetric factors of HGT and Stormtide. There are two possibilities why ARTOFS shows annual variations of the gravimetric factor of a similar order of magnitude as Stormtide, although it covers only a part of the global ocean. One possibility is that the AVM2ssh in ARTOFS are in the correct order of magnitude and the model covers the area with the significant contributions for the European stations. In this case, the rest of the global oceans would have no significant contribution at those stations. The second possibility is that the amplitudes of the AVM2ssh in ARTOFS are too large and the annual variation of the gravimetric factor is of the correct order of magnitude because of the model's restriction. In section 8.3 the contribution of different ocean areas to the total loading signal is discussed. This will show which possibility is appropriate.

The extrema in the results from HGT and ARTOFS occur close (in time) to those in the measured data. In contrast, the results achieved with Stormtide have one tidal parameter that fits to the results from measurements (mainly the gravimetric factor) and are only slightly shifted (see section 8.2.2.2); whereas the other parameter (mainly the phase lead) is shifted by approx. 6 months.

At Cantley (see Fig. 8.28), the results from all three synthetic data MWA are very different compared to the results obtained with measurements. This indicates that the ocean areas influencing the gravity at Cantley are not properly described by the ocean models. This is most likely the region of the Canadian islands and Greenland, which is difficult to model. In the following section the influence of different ocean areas is studied and the region dominating the loading signal can be identified.
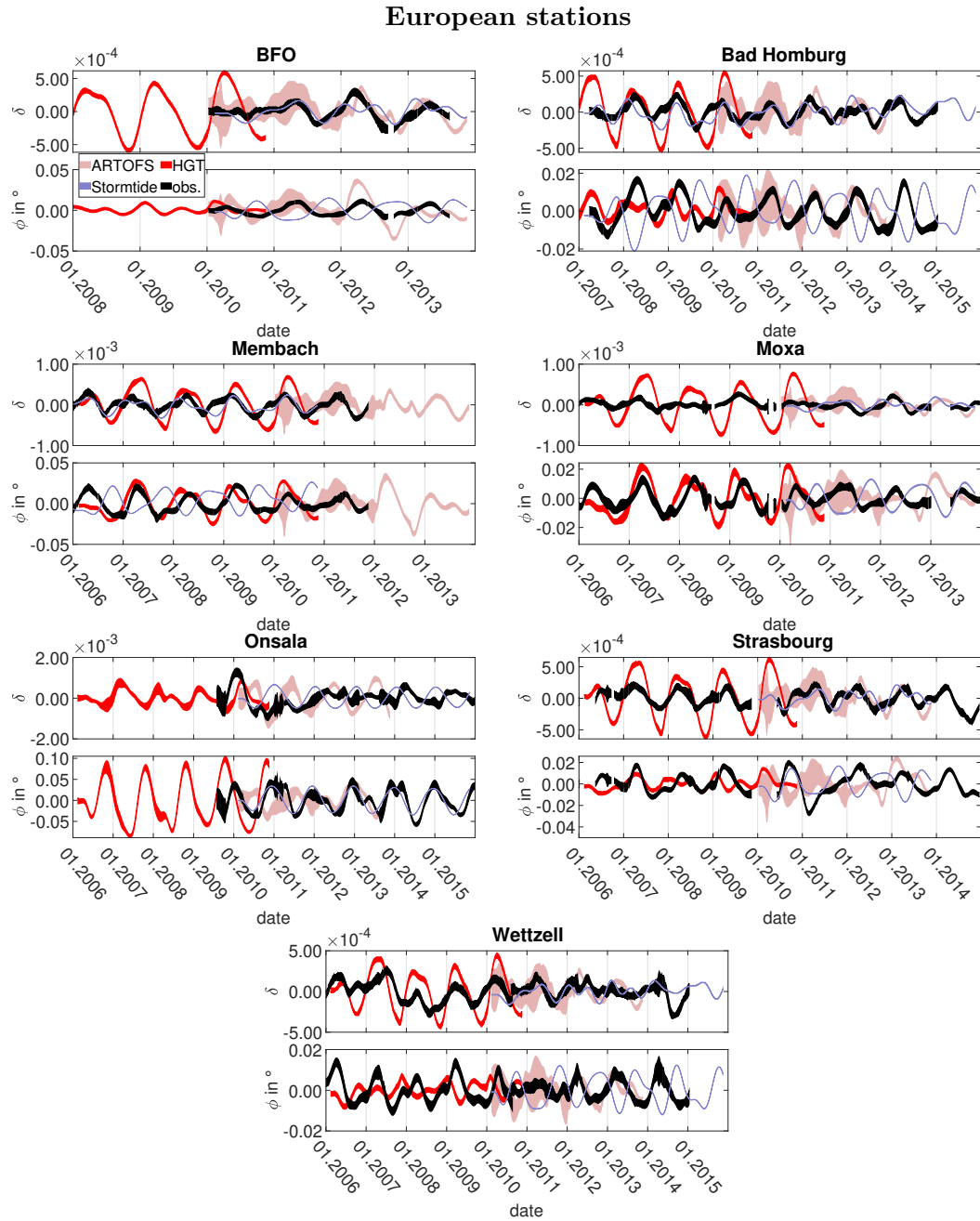
Fig. 8.27. Tidal parameters of wave group M2 at BFO, Bad Homburg, Membach, Moxa, Onsala, Strasbourg and Wettzell obtained from measurements (black) and synthetic data calculated with with ARTOFS (light pink), Stormtide (blue) and HGT (red), band-pass filtered between $\frac{1}{1000 \text{ d}}$ and $\frac{1}{0.5 \text{ years}}$. Note that the line thickness of the gravimetric factor at BFO, Strasbourg and Wettzell is higher than it would be due to the standard deviations for a better visibility. The maximum number of digits in ETERNA is 5, therefore the standard deviation has to be smaller than 10^{-5}.

125
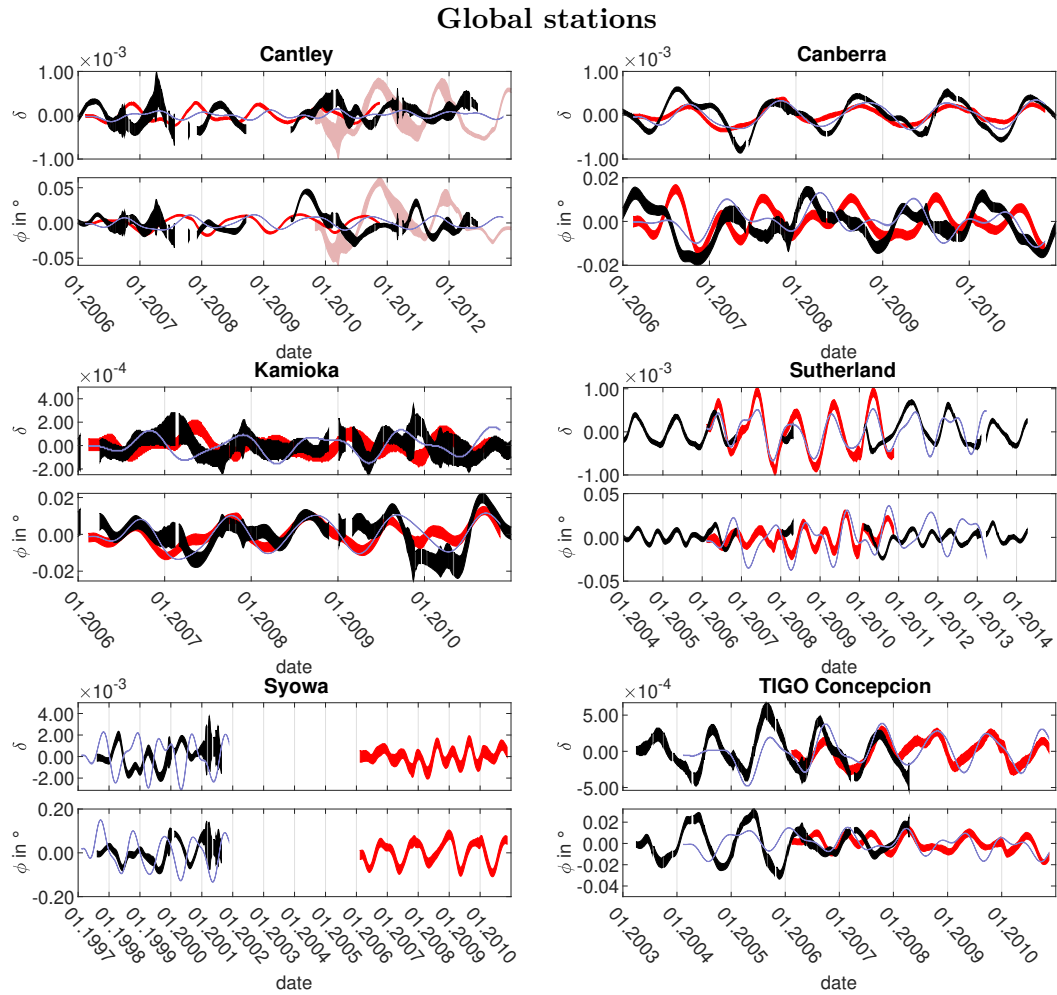
Fig. 8.28. Tidal parameters of wave group M2 at Cantley, Canberra, Kamioka, Sutherland, Syowa and TIGO Concepción obtained from measurements (black) and synthetic data calculated with with ARTOFS (light pink), Stormtide (blue) and HGT (red), band-pass filtered between $\frac{1}{1000\text{ d}}$ and $\frac{1}{0.5\text{ years}}$. Note that the line thickness of the gravimetric factor at Cantley, Canberra, Kamioka and TIGO Concepción is higher than it would be due to the standard deviations for a better visibility. The maximum number of digits in ETERNA is 5, therefore the standard deviation has to be smaller than 10^{-5}.

8.3. Contribution of different ocean areas to the total loading signal

The largest amplitudes of the AVM2ssh occur in coastal areas, as shown by Müller et al. (2014) and by the results in Figs. 8.1 to 8.4 in section 8.1 and E.1 in appendix E.1. On the other hand, the open oceans, where the AVM2ssh has only a very small amplitude, cover large areas whose contribution could also sum to a large amplitude in gravity.

In order to investigate which regions have to be taken into account to describe the AVM2 at a certain station sufficiently well, the gravity amplitude of the annual variation at every single grid point is calculated. Equation 2.13 is used, but the values are not integrated over the Earth's surface. The amplitude of the AVM2ssh is used as SSH. The resulting gravity value is therefore the maximum contribution to the annual variation of the M2 amplitude in gravity of that grid point. In the following, it is referred to as maximum contribution or maximum gravity signal. These maximum contributions are used as thresholds for synthetic data MWA. Only grid points are taken into account whose maximum gravity contribution exceeds the threshold. By comparing the AVM2 obtained with the whole model to the AVM2 obtained with the thresholds, the grid points can be found whose gravity contributions have to be taken into account. Plotting the necessary grid points on a map will show which ocean regions are important for the station under consideration.

This test was done with Stormtide, because it covers the whole globe and causes an AVM2 of the correct order of magnitude in the synthetic data MWA. The stations BFO, Cantley, Canberra, Kamioka, Moxa, Sutherland and TIGO Concepción are used. As the results in the previous section 8.2 showed a very similar behaviour for the Central European stations, I chose BFO and Moxa as representatives. A comparison between both can show whether differences in the grid point distribution of the European stations are observable. BFO and Moxa, from those European stations used for synthetic data MWA in section 8.2, are the station pair with the largest distance to each other. Onsala is not used because it behaves differently than the other European stations and the loading calculation is not as accurate due to the location close to the coast (see appendix F).

Figs. 8.29 to 8.32 show the distribution of grid points exceeding the corresponding threshold, the results of the corresponding analyses are given in Fig. E.12 in appendix E and in Fig. 8.33, in which the mean values were subtracted.

At BFO, Moxa and Sutherland the results in Fig. 8.33 show that at least all grid points whose maximum gravity signal exceeds $10^{-6}\frac{\text{nm}}{\text{s}^2}$ are needed to get variations of the tidal parameters which are similar to the results of the whole model. The differences in the tidal parameters obtained with the $10^{-6}\frac{\text{nm}}{\text{s}^2}$ threshold and the global model are about 10%. For BFO, Moxa and Sutherland the points with maximum gravity signals above the $10^{-6}\frac{\text{nm}}{\text{s}^2}$ threshold are concentrated at a region close to the station and on the coastal areas, but both are not restricted to close vicinity of the stations. For BFO, for example, the complete area between Europe and Greenland and large parts of the eastern North Atlantic and even coastal areas of Indonesia have a significant contribution.

The distribution of grid points for BFO and Moxa (see Fig. 8.29) show differences in
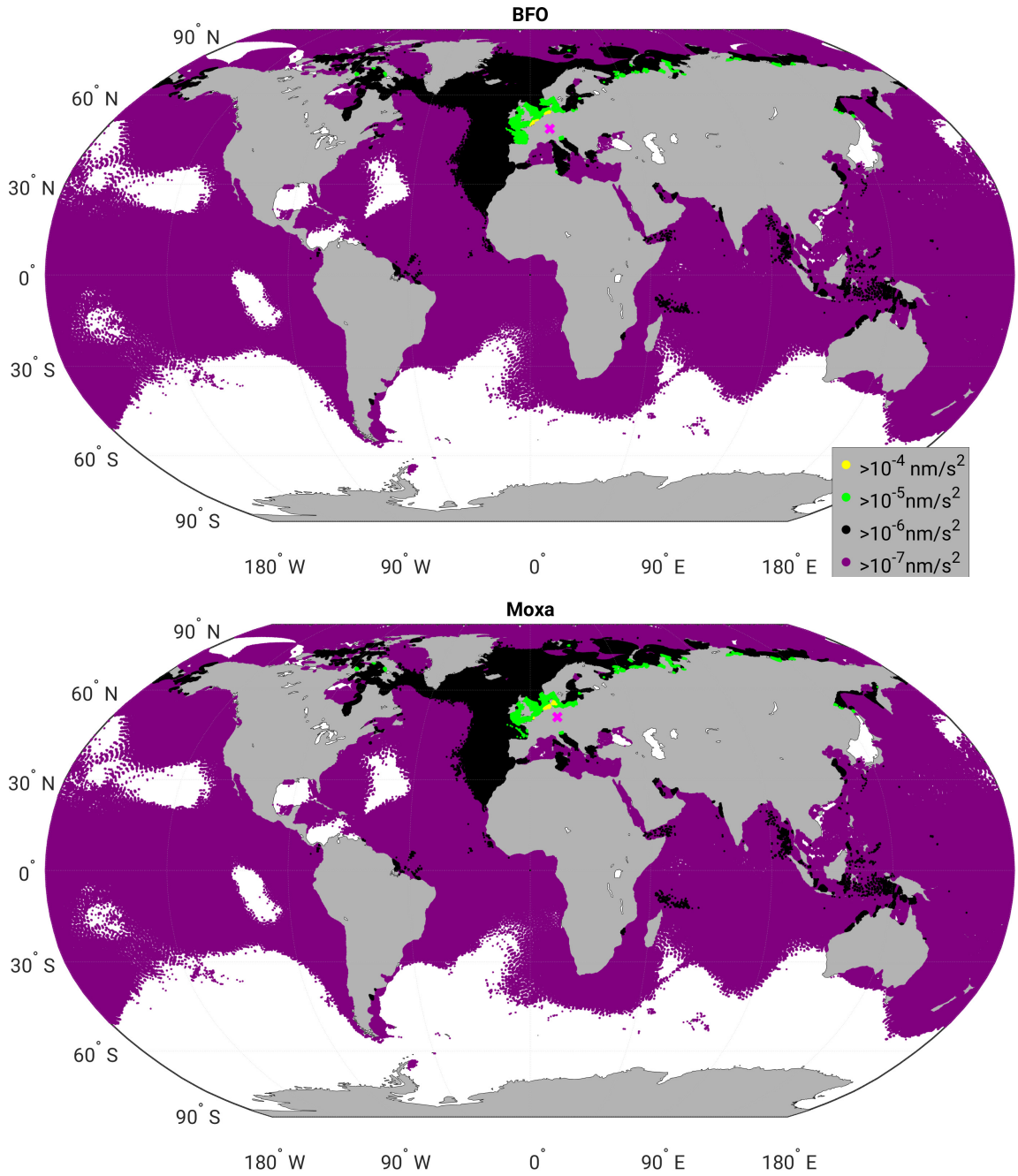
Fig. 8.29. Maps of Stormtide grid points whose gravity contribution exceeds the threshold $10^{-4}\frac{\text{nm}}{\text{s}^2}$ in yellow, $10^{-5}\frac{\text{nm}}{\text{s}^2}$ in green, $10^{-6}\frac{\text{nm}}{\text{s}^2}$ in black and $10^{-7}\frac{\text{nm}}{\text{s}^2}$ in purple at the stations BFO and Moxa. Depending on the results shown in Fig. 8.33, not all thresholds are used at all station. The pink cross shows the position of the stations. The pink cross shows the position of the station.
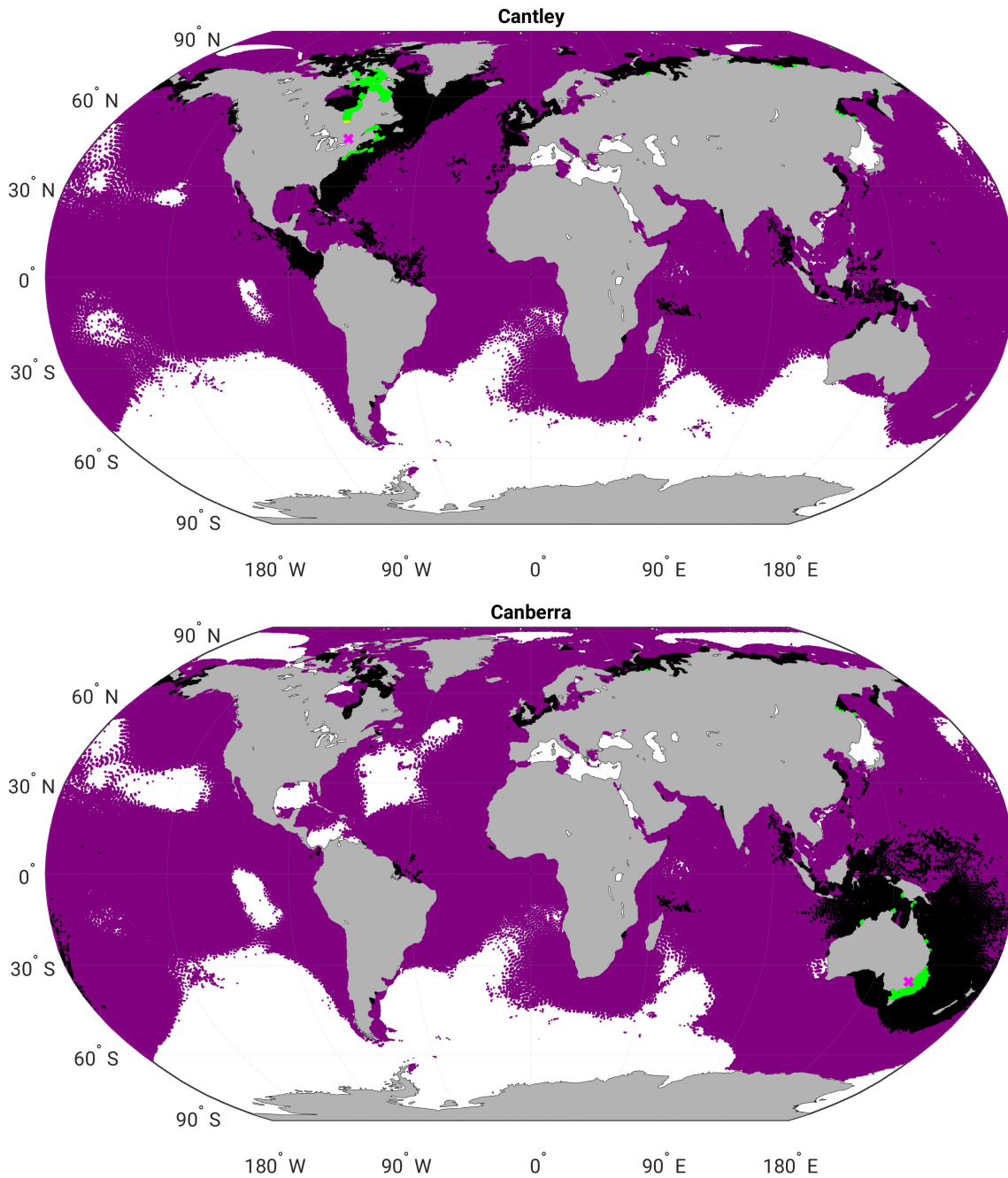
Fig. 8.30. Maps of Stormtide grid points whose gravity contribution exceeds the threshold $10^{-4}\frac{\text{nm}}{\text{s}^2}$ in yellow, $10^{-5}\frac{\text{nm}}{\text{s}^2}$ in green, $10^{-6}\frac{\text{nm}}{\text{s}^2}$ in black and $10^{-7}\frac{\text{nm}}{\text{s}^2}$ in purple at the stations Cantley and Canberra. Depending on the results shown in Fig. 8.33, not all thresholds are used at all stations. The legend is given Fig. 8.29. The pink cross shows the position of the station.
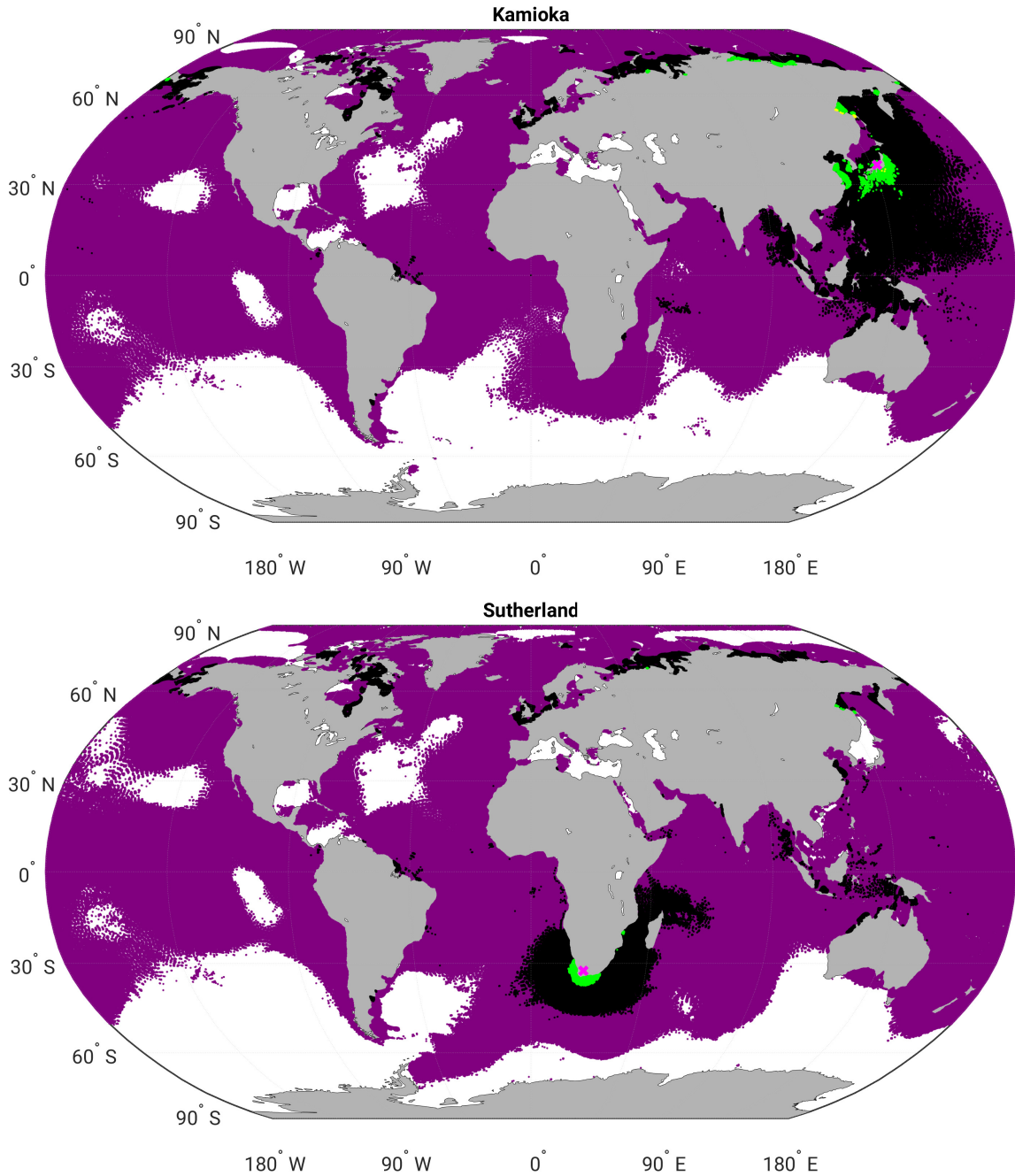
Fig. 8.31. Maps of Stormtide grid points whose gravity contribution exceeds the threshold $10^{-4}\frac{\text{nm}}{\text{s}^2}$ in yellow, $10^{-5}\frac{\text{nm}}{\text{s}^2}$ in green, $10^{-6}\frac{\text{nm}}{\text{s}^2}$ in black and $10^{-7}\frac{\text{nm}}{\text{s}^2}$ in purple at the stations Kamioka and Sutherland. Depending on the results shown in Fig. 8.33, not all thresholds are used at all stations. The legend is given Fig. 8.29. The pink cross shows the position of the station.
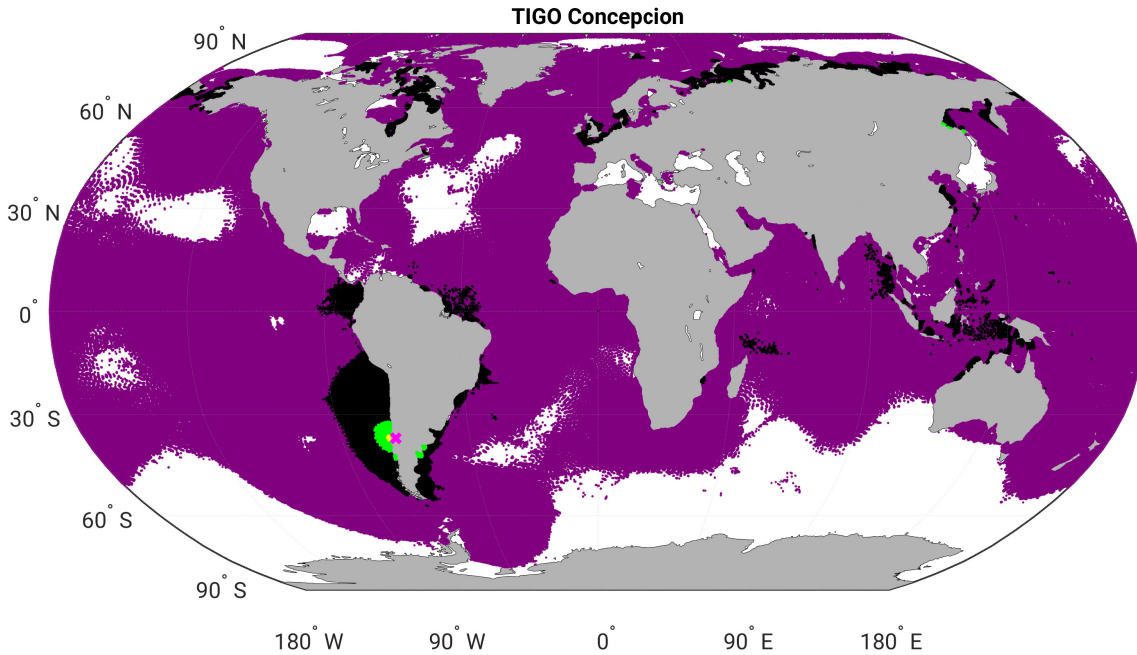
TIGO Concepcion

Fig. 8.32. Map of Stormtide grid points whose gravity contribution exceeds the threshold $10^{-4}\frac{\text{nm}}{\text{s}^2}$ in yellow, $10^{-5}\frac{\text{nm}}{\text{s}^2}$ in green, $10^{-6}\frac{\text{nm}}{\text{s}^2}$ in black and $10^{-7}\frac{\text{nm}}{\text{s}^2}$ in purple at the station TIGO Concepción. The legend is given Fig. 8.29. The pink cross shows the position of the station; it was moved about 2° inland, because the cross covered the yellow grid points.

the Mediterranean Sea and around Svalbard. This, however, does not cause observable differences in the tidal parameter variation (see Fig. 8.33).

Reaching the same level of similarity (a difference of approx. 10% of the tidal parameters obtained with a threshold data set and the whole model) at Cantley, Canberra, Kamioka and TIGO Concepción requires a synthetic data MWA for which all grid points whose maximum contribution exceeds a threshold of $10^{-7}\frac{\text{nm}}{\text{s}^2}$ are taken into account. This means that many contributions which exceed $10^{-6}\frac{\text{nm}}{\text{s}^2}$ have to cancel each other and do not sum constructively. The grid points which are above the $10^{-7}\ \frac{\text{nm}}{\text{s}^2}$ threshold and needed at Cantley, Canberra, Kamioka and TIGO Concepción cover almost all the Atlantic and the Pacific Ocean. This shows that the loading signal causing the temporal variations of the M2 tidal parameters has its origin in ocean areas all over the globe.

The grid points with maximum contributions exceeding the $10^{-7}\frac{\text{nm}}{\text{s}^2}$ threshold in Figs. 8.29 and 8.31 (Sutherland) are plotted in order to see whether their distribution is different from the other stations, but no obvious difference is visible. The $10^{-7}\frac{\text{nm}}{\text{s}^2}$ threshold grid points cover of course slightly different areas due to the location of the stations, but the general pattern is the same.

At Sutherland and Canberra no maximum contributions are found that exceed $10^{-4}\frac{\text{nm}}{\text{s}^2}$.
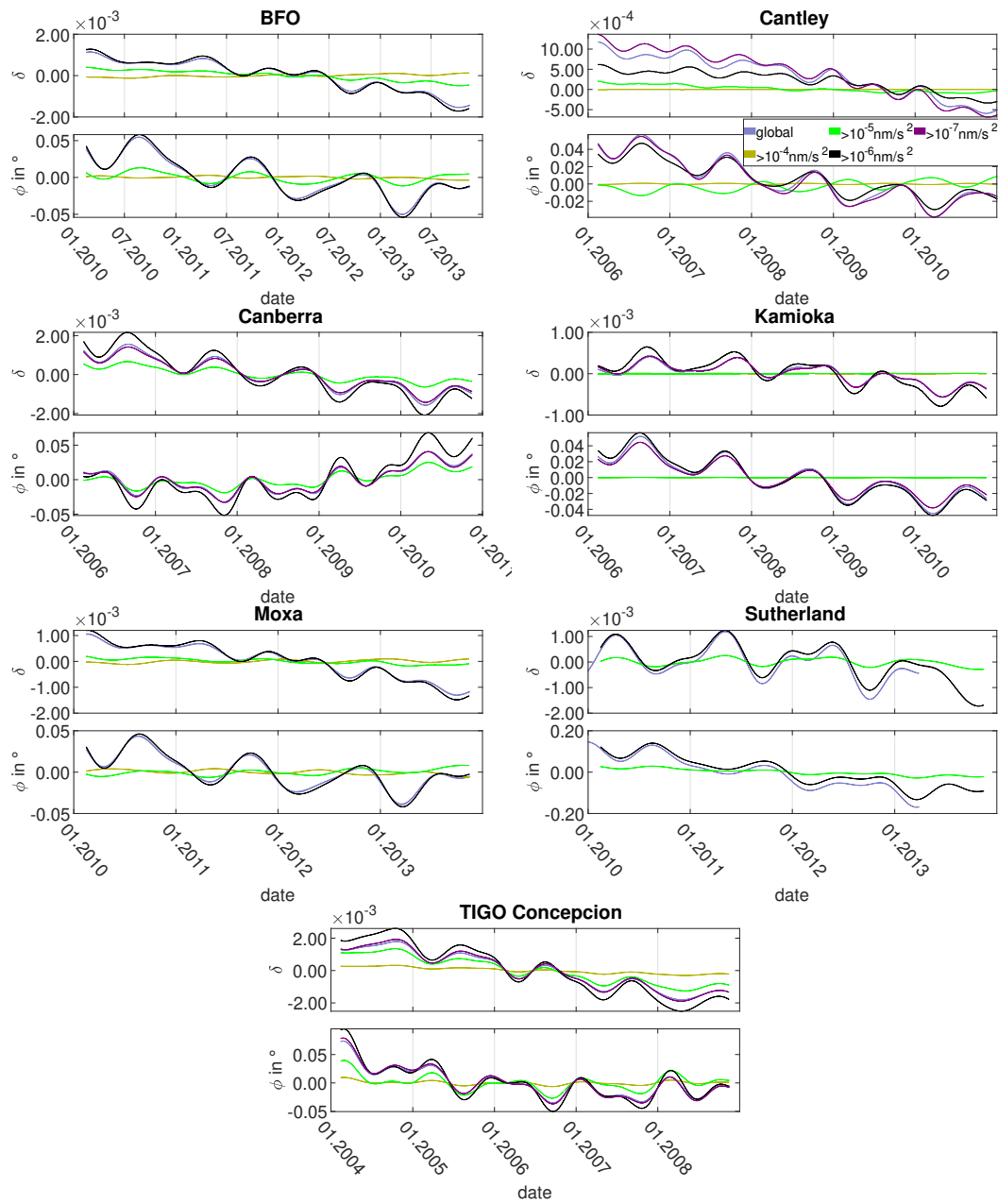
Fig. 8.33. Results of the synthetic data MWA based on Stormtide grid points that exceed the threshold $10^{-4}\frac{\text{nm}}{\text{s}^2}$ in yellow, $10^{-5}\frac{\text{nm}}{\text{s}^2}$ in green, $10^{-6}\frac{\text{nm}}{\text{s}^2}$ in black and $10^{-7}\frac{\text{nm}}{\text{s}^2}$ in purple as well as the results for which the complete model was used in blue at the stations BFO, Cantley, Canberra, Kamioka, Moxa, Sutherland and TIGO Concepción. The mean values were subtracted.

station	$> 10^{-4}\frac{nm}{s^2}$		$> 10^{-5}\frac{nm}{s^2}$		$> 10^{-6}\frac{nm}{s^2}$		$> 10^{-7}\frac{nm}{s^2}$	
	pts.	$\cdot 10^{-3}\%$	pts.	$\%$	pts.	$\%$	pts.	$\%$
BF	166	2.98	8619	0.16	**174564**	**3.14**	-	
CA	48	0.86	10162	0.18	155712	2.80	**2410015**	**43.36**
CB	0	0	6451	0.12	222834	4.01	**2815878**	**50.66**
KA	65	1.17	7716	0.14	225853	4.06	**2318720**	**41.71**
MO	251	4.51	8102	0.15	**172818**	**3.11**	-	
SU	0	0	5056	0.09	**169751**	**3.05**	-	
TC	151	2.72	5458	0.09	129491	2.33	**2967392**	**53.38**

Table 8.2. Number of grid points (absolute value and percentage) that exceed a certain threshold at the stations BFO, Cantley, Canberra, Kamioka, Moxa, Sutherland and TIGO Concepción. The total number of ocean grid points (number of points on land subtracted from the total grid) is 5558633. The values needed to explain 90% of the variation obtained with the global model are written in bold.

This investigation shows that the North Sea model, described in section 5.2.2.7 and investigated in section 8.2.5, even if the annual variations would add up realistically, cannot explain the annual variations of the tidal parameters at the European stations, since it covers only a small fraction of the ocean regions, contributing significantly to the AVM2 at the European stations. ARTOFS (see section 5.2.2.3) covers approx. half of the areas which have a significant contribution to the total signal at the European stations. The fact that it nevertheless shows an AVM2 of the same order of magnitude as the measured data indicates that the second possibility, discussed in section 8.2.6.3, holds for ARTOFS: The AVM2ssh in the model is too large and the AVM2 from synthetic data MWA fit to the results from measurements due to the restriction of the model area.

Tab. 8.2 shows the number of grid points whose maximum contribution exceeds a certain threshold. The number of grid points for a certain threshold differs from station to station but is of the same order of magnitude. Cantley is an exception because it has fewer grid points with maximum contributions exceeding $10^{-4}\frac{nm}{s^2}$ and more exceeding $10^{-5}\frac{nm}{s^2}$. The variations caused by the $10^{-4}\frac{nm}{s^2}$ threshold grid points in Fig. 8.33, which are about 0.003% (depending on the station, less for Cantley) of all the ocean grid points, can reach up to 25.5% tidal parameter variation, depending on the station and the tidal parameter. Although their contribution has to be cancelled out by the contributions from other grid points, as the variations they cause have the opposite sign of the variations caused by the total model, these very few, but close grid points have a large influence on the total variation at BFO, Moxa and TIGO Concepción.

The stationary parts from the tidal parameters (see Fig. E.12 in appendix E) obtained with the thresholds behave differently to the corresponding AVM2. The results from BFO

obtained with the 10^{-6} $\frac{\text{nm}}{\text{s}^2}$ threshold differ by less than 20% in the phase from the results obtained with the global model and less than 1% in the gravimetric factor. For the European stations, this observation indicates that the same regions contribute significantly to the stationary and the nonstationary part of the M2 loading. Meurers et al. (2016) report similar observations. This is supported by the distributions of the amplitudes of the annual variation (see Fig. 8.1) and of M2 (see Fig. E.3) from Stormtide which are large in approx. the same region. However, there must be significant differences as the 10^{-6} $\frac{\text{nm}}{\text{s}^2}$ threshold grid points do not give an equally good result for the stationary M2 as for its annual variation.

In contrast, synthetic data MWA with the 10^{-7} $\frac{\text{nm}}{\text{s}^2}$ threshold in Cantley causes similar annual variations but the mean value of the phase still differs by about 50% from the result of the global model. Of course, the thresholds were defined for the amplitudes of the annual variations and therefore do not have to hold for the stationary M2 amplitude. In this case, the significant contributions to the tidal parameters for the stationary and the nonstationary part of M2 originate from different ocean areas.

8.4. Discussion

This section contains a combined discussion of the results presented in the previous sections (see sections 8.1 to 8.3).

The results of the synthetic data MWA with ARTOFS are discussed with respect to the results for the North Sea model. The synthetic data MWA with the North Sea model and OTEMT (see section 8.2.5) indicate that the forcing of the AVM2ssh at the model boundaries (if the model is restricted to a certain area) is important. In principle, ARTOFS suffers from the same problem as the North Sea model. There is no information about the AVM2ssh at the boundaries, as it is also driven by only a few harmonics. I think this might be compensated by the nudging of different measured data sets, but further investigations are needed for verification. These findings indicate that models restricted to an area need additional information about the AVM2ssh. This can be information about the amplitudes and phases of the AVM2ssh at the boundaries or information about the amplitudes and phases in the model area. With this comparison it is not possible to conclude which of both possibilities leads to better results as these possibilities have not been tested with the same model.

The analysis of the North Sea model in section 5.2.2.7 showed that the synthetic data MWA can be a valuable tool to evaluate the nonstationary response of the oceans to tidal forcing. From the harmonic analysis of the SSH (see section 8.1) one would probably have expected that the model produces realistic annual variations, but the synthetic data MWA showed that the amplitudes do not add up constructively. Additionally, the variations caused by ARTOFS, Stormtide and HGT, as mentioned before, differ a lot from each other and from the results obtained with measurements, which indicates that the models contain the principle mechanisms but do not yet describe the annual variations of the M2

amplitude realistically. I would not (yet) recommend correcting measured gravity data with these models due to the strong differences (see e.g. section 8.2.6.3). However, if ocean modellers would be interested in developing their models towards a realistic representation of the causing mechanisms, MWA of SG data and synthetic data MWA could provide observational data that have advantages over tide gauges and satellite altimetry data. The study on the contributing grid points in section 8.3 shows that, depending on the station, the oceans contribute on a global scale significantly to the observed signal. Due to the high accuracy of SGs, these small SSH variations on a centimetre to millimetre level can be monitored through their loading globally (at least with several SGs). The temporal variations of the tidal parameters obtained from SG data do not suffer from low spatial or temporal resolution. Additionally, with MWA also a temporal behaviour of the loading, which is probably not perfectly harmonic, can be observed.

A disadvantage is the difficulty to get information on a certain ocean area from gravity data, as the investigations in section 8.3 on the influence of different ocean areas and in section 8.2.5 on the North Sea model show. Therefore, using SG data additionally to tide gauges and satellite altimetry data could be useful, as the latter two provide information that can be spatialised to certain areas.

Another influence that is considered in different sections is the influence of a varying density of the ocean water. The synthetic data MWA with the OBP and the SSH from OMCT (see section 8.2.3.1) and the total and nonsteric SSH (see section 8.2.4.1) from HGT both resulted in only very small or no significant differences. The considered quantities that are compared for the models (SSH/OBP for OMCT and total/nonsteric SSH for HGT) do not represent exactly the same effects. The OBP contains the density variations of the whole water column, in contrast to the SSH for which a constant density is assumed, whereas the nonsteric SSH excludes only density variations which are caused by steric effects. However, as mentioned above, both cases result in almost no difference in the AVM2. A similar observation is made in a test for which different density values were used in synthetic data MWA analyses of ARTOFS data, which is described in appendix F.1.1. This indicates that density variations of the ocean water have only a small influence on the temporal variations of the M2 tidal parameters. They are not significant on the level of accuracy regarded here.

Artefacts are observed when not all tidal frequencies are included in the loading. This is for example shown for HGT (see section 8.2.4). The model is forced with only eight harmonics which causes variations of the tidal parameters of M2 that are not observed in the results from measurements. The spectra in section 8.2.6.1 additionally show that some tidal lines in other frequency bands than M2 are missing. Their loading cannot be studied. Therefore, for MWA as well as for tidal analysis it is of advantage to use an ocean model forced with ephemerides. Stormtide has this kind of forcing, but the representation in amplitudes and phases for M2 and its annual variation also produces variations of the tidal parameters which are not present in the results from measurements (see section 8.2.2.1). The loading can then contain only the regarded frequencies, which also causes artefacts. A loading calculation based on SSH data should therefore be preferred to calculations based

on amplitude and phase representation.

8.5. Summary of the chapter

In this chapter it is shown that nonstationary, nonlinear ocean models can, through their loading, produce an AVM2 of the same order of magnitude as the AVM2 obtained from measured SG data. This is a strong indication for the nonstationary ocean loading as cause for the AVM2. Three out of the five ocean models used here, ARTOFS, Stormtide and HGT, cause annual variations of the tidal parameters. The similarity to the results from measurements differs from station to station and from model to model. For the Central European stations, the synthetic data MWA with ARTOFS shows a similar shape as the results from measurements. The AVM2 observed at the same stations with the synthetic data MWA of HGT are larger than the results from measurements. The results obtained with Stormtide have a similar amplitude as the results from measurements, but are shifted relative to the measurements' results. For the other stations no general statement can be made, except for the occurrence of variations of the correct order of magnitude. Their characteristics have to be regarded for every station individually.

The harmonic analysis at the beginning of the chapter showed that all five models produce an AVM2ssh of the expected order of magnitude, but whereas ARTOFS, Stormtide, HGT and the North Sea model showed similar distributions of the amplitudes, the results for OMCT differ in their distribution. They possess also only half the amplitude of the other models. The phase lags of all models have similar patterns, but show differences in their distribution on a regional scale and the dominating value. Without further information it is not possible to decide whether one is more realistic than another.

The synthetic data MWA of OMCT showed only small variations which did not change for model versions with different properties in the ice drag or the nudging. The largest difference occurs between the $1.875°$ (13 vertical layers) and $1°$ (20 vertical layers) version. As the resolution (especially the vertical) is crucial for the occurrence of the AVM2ssh and it is an obvious difference to the other models, it is concluded that the OMCT grid is most likely too coarse to predict the AVM2ssh correctly.

The synthetic data MWA of the North Sea model also did not result in AVM2 of the correct order of magnitude. The harmonic analysis of the SSH showed that the model is able to produce AVM2ssh of the correct order of magnitude, but they do not sum to an annual variation of the M2 amplitude in gravity and do not cause an AVM2. In contrast, the barotropic OTEMT model driven by Stormtide SSH at the boundaries produces AVM2 of the correct order of magnitude, even if it does not contain the mechanisms generating the AVM2ssh. This indicates that the forcing of the AVM2ssh at the boundaries of the model is important. ARTOFS also lacks this information, but shows annual variations of the correct order of magnitude which is probably due to the nudging of measured data sets. The harmonic analysis of the ARTOFS SSH results in high amplitudes of the AVM2ssh, whereas the investigations of the ocean areas contributing significantly to the AVM2 at a certain station indicate that only half of the area which contributes significantly at the Central European stations is included in the model. This indicates that the amplitudes of

the AVM2ssh in ARTOFS are too large and show the correct order of magnitude of the AVM2 because of the models' restriction to the North Atlantic.

The study with ocean models forced differently (harmonics or ephemerides) and with different ways of presenting the output (SSH, amplitudes and phases) showed that it is advantageous to have all tidal frequencies in the forcing and in the output upon which the loading calculation is based. A forcing with ephemerides and the output as SSH should be preferred for studying the loading.

In the last part of the chapter it was investigated with the help of Stormtide which regions of the ocean contribute significantly to the AVM2 observed at a certain station. At some stations, BFO, Moxa and Sutherland, all ocean grid points whose maximum gravity contribution exceeds $10^{-6}\frac{\text{nm}}{\text{s}^2}$ are needed to reach about 90% of the variation of the total model. For the other stations all grid points with a maximum contribution exceeding $10^{-7}\frac{\text{nm}}{\text{s}^2}$ are necessary for the same level of similarity. In the first case ($10^{-6}\frac{\text{nm}}{\text{s}^2}$ threshold), the regions of significant distributions are located in ocean basins close to the station but also at shelf regions with large amplitudes of the AVM2ssh all over the globe. For the latter case ($10^{-7}\frac{\text{nm}}{\text{s}^2}$ threshold), the grid points with significant contributions are distributed over almost the entire globe. This shows that for an accurate description of the AVM2 a global distribution of the annual variation of the M2 amplitude in the SSH is needed and a regional model like the North Sea model is insufficient.

On the one hand, regarding the results of the synthetic data MWA, the ocean models do not describe the annual variations of the M2 amplitude accurately enough yet to correct gravity measurements. On the other hand, the results showed that SG measurements can observe variations of the SSH in the centimetre to millimetre range accurately. SG measurements can therefore be an additional observation of such effects in the oceans; they do not suffer from temporal or spatial aliasing and thus, they are useful for the evaluation of the ocean models.

Chapter 9.

Influence of atmosphere and oceans on other wave groups

In this chapter results and observations from other wave groups are presented.
The influence of the oceans on other wave groups than M2 can only be studied with OMCT or the SSH output of Stormtide because these are the only models driven by ephemerides. The other models which are driven by single harmonics cause artefacts (see sections 8.2.2 and 8.2.4) or do not contain the regarded harmonics, as shown in section 8.2.6.1.

9.1. Influence of the oceans and the atmosphere on the tidal parameters of O1

As mentioned above, Stormtide and OMCT are used for this investigation. Depending on the mechanisms that cause the effects responsible for the variations of the O1 tidal parameters, OMCT has the disadvantage that the model may be too coarse to represent the corresponding effects, as was discussed for the AVM2 (see section 8.2.3.2); but for other effects it is not too far from results obtained from measurements, as the comparison of the stationary parts of the tidal parameters shows (see section 8.2.6.2). Stormtide has a finer grid, but the SSH was calculated for the 1950s and therefore a comparison with results from SG data is difficult.

The results of the synthetic data MWA with the two different 1° OMCT data sets (original and with changed ice drag, see section 8.2.3.2) are given in Fig. 9.1. From the stations used in chapter 8, those stations are chosen that show some kind of similarity in the O1 tidal parameters. The variations of the O1 tidal parameters obtained with OMCT have larger amplitudes than the AVM2 from OMCT (see section 8.2.3.2). They are smaller than the variations obtained from measurements but of the same order of magnitude. For Bad Homburg and Sutherland the combined analyses with OMCT and Atmacs (*atmacs*, see section 7.3.2), as described in section 7.4, are shown additionally. At Bad Homburg the shape of the variations changes but still has the same order of magnitude and periodicity, whereas at Sutherland the variation obtained with OMCT and Atmacs is twice as large as the variation of the tidal parameters obtained with measurements. The similarity is low and one might be sceptical whether there is similarity at all. However, the similar
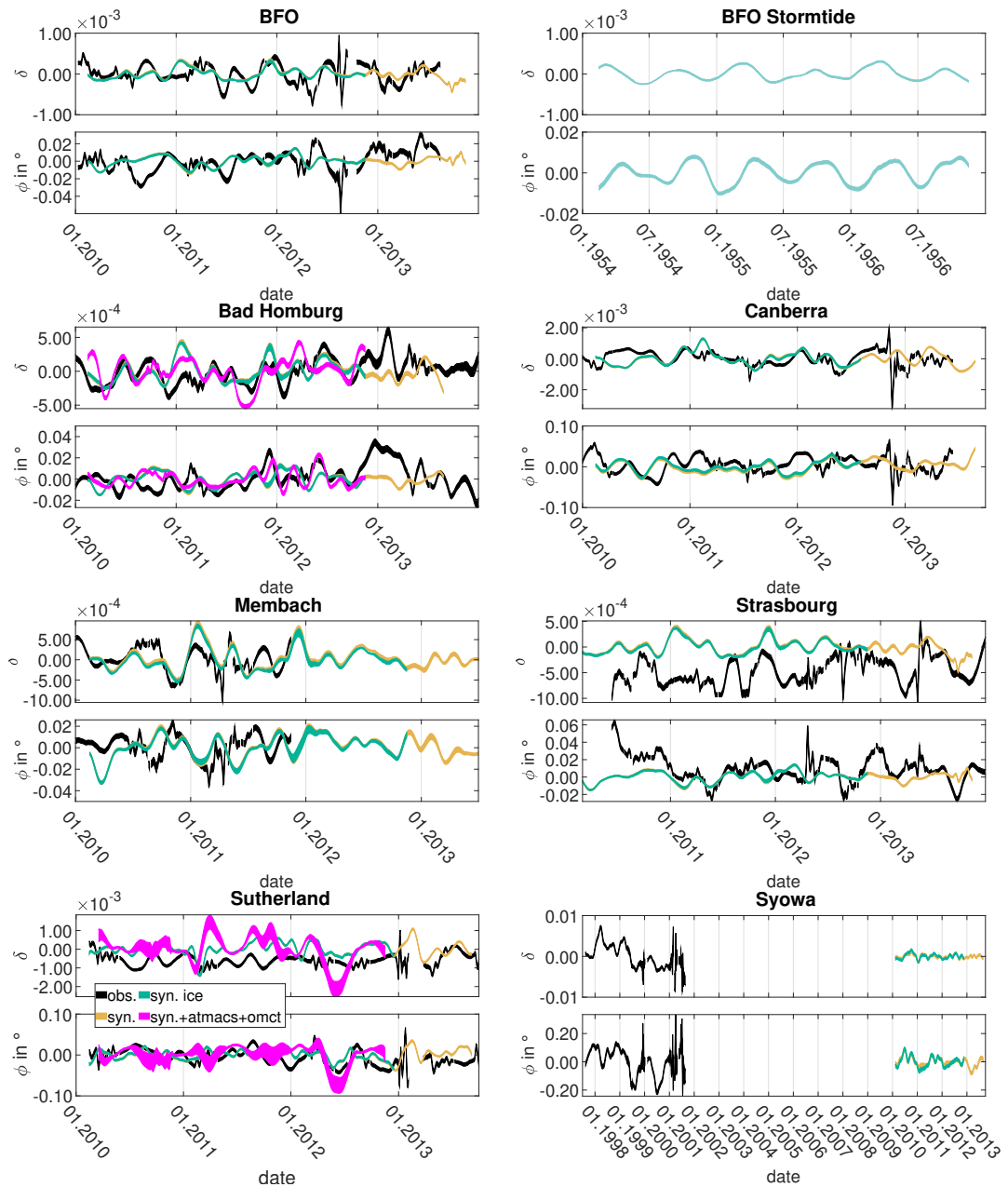
Fig. 9.1. Tidal parameters of wave group O1 at Cantley, Canberra, Kamioka, Sutherland, Syowa and TIGO Concepción obtained from measurements (black), synthetic data calculated with the original OMCT version (light orange), the version with a changed ice drag (green) and Atmacs in combination with the OMCT version with a changed ice drag (pink, Bad Homburg and Sutherland only). Please note that the apparent offset of the tidal parameters at Strasbourg is due to the calculation of the mean value for a longer time span. The first panel on the right shows the result of the synthetic data MWA with the Stormtide SSH at BFO on the same y-scales as the result for OMCT in first panel on the left.

140

periods occurring for OMCT at these stations and also the similarity of the shape of the gravimetric factors at Bad Homburg and Canberra as well as of the phases of Syowa could, in my opinion, be a hint that there is an influence of the oceans and maybe also from the atmosphere at O1. The result for Stormtide shows a semi-annual variation which is not observed for the results obtained with measurements. This may indicate that a realistic, meteorological forcing is of advantage, in contrast to the climatological forcing in Stormtide. Baker and Alcock (1983) show that there is a harmonic in tide gauge data close to O1 which deviates from the expected amplitude in the analysis model. The frequency distance of this harmonic and O1 would cause a variation of shorter period (2 to 4 weeks) that cannot be correctly represented by an MWA with 90 days window length. In addition, the scale of the corresponding figure in the publication by Baker and Alcock (1983) is not fine enough to estimate this frequency precisely.

Of course, this comparison is subjective and the similarities are low. Therefore, further investigations will be necessary to ensure that the similarities are not just by chance.

9.2. Higher-degree harmonics

In this section the influence of the higher-degree harmonics in the wave groups is discussed. The first part focuses on how different assumptions for higher-degree harmonics in the analysis model change the variation of the tidal parameters of the corresponding wave groups. The influence of the oceans is discussed in the second part. Schroth et al. (2018) identified degree 3, 4 and 5 harmonics in the wave groups Q1, M1, 2N2, N2 and L2 which probably cause variations. These wave groups are discussed here.

9.2.1. Influence of different model assumptions on the wave groups containing higher-degree harmonics

As described in section 1.1, different theoretical values are available for the degree 3, 4 and 5 harmonics. The difference of the tidal parameters from the WDZ model used in ETERNA 3.4 (Dehant, 1987) to the values computed by Dehant et al. (1999) is not large enough to explain the observed variations in the wave groups mentioned above. Nevertheless, an MWA is performed for the measurements from BFO with a modified version of ETERNA which uses additionally to the more recent FCN model (D1999, see section 7.1) modified, theoretical gravimetric factors of the higher-degree harmonics. The results are shown in Fig. 9.2. Except for the phase of N2 in a short period in October 2010, the tidal parameters for the two different Earth models do not differ by more than one standard deviation. This is expected due to the small differences between the theoretical values used here. The variation of the tidal parameters has to be caused by other effects.

9.2.2. Influence of the oceans

Meurers et al. (2016) observe variations of the tidal parameter of M2 of 8.8 years which are most likely caused by harmonics of degree 3. In tidal analyses of a long data set
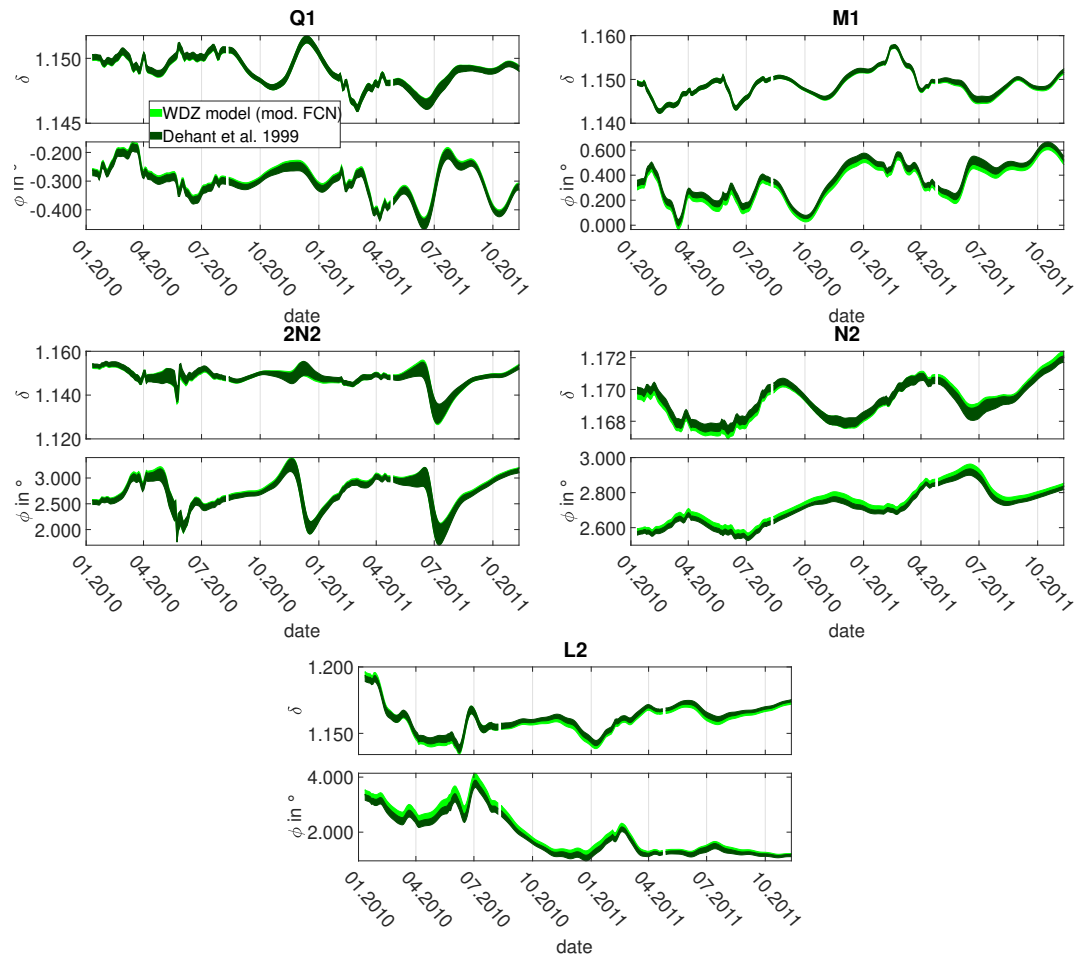
Fig. 9.2. Tidal parameters of the wave groups Q1, M1, 2N2, N2 and L2 at BFO, obtained with MWA based on different ETERNA versions. In green the results are shown for which the WDZ model with the modified FCN model was used, the results in dark green were obtained with the theoretical values by Dehant et al. (1999) and modified FCN.

(long enough to separate these harmonics from M2), they found tidal parameters for these harmonics which are much closer to the expectations of the analysis model than in case of the harmonics of degree 2. This shows that the ocean loading for semi-diurnal degree 3 harmonics is much smaller than for degree 2 harmonics of similar frequency. The loading of the harmonics of different degree then automatically changes the amplitude and phase difference of the harmonics with respect to the expectations for body tides in the analysis model and therefore leads to variations of the tidal parameters.

From the description of the tidal forcing of the ocean models given by Thomas et al. (2001) I conclude that the harmonics of degrees higher than two are not included in the tidal forcing. The tidal parameters obtained from synthetic data MWA with OMCT and Stormtide
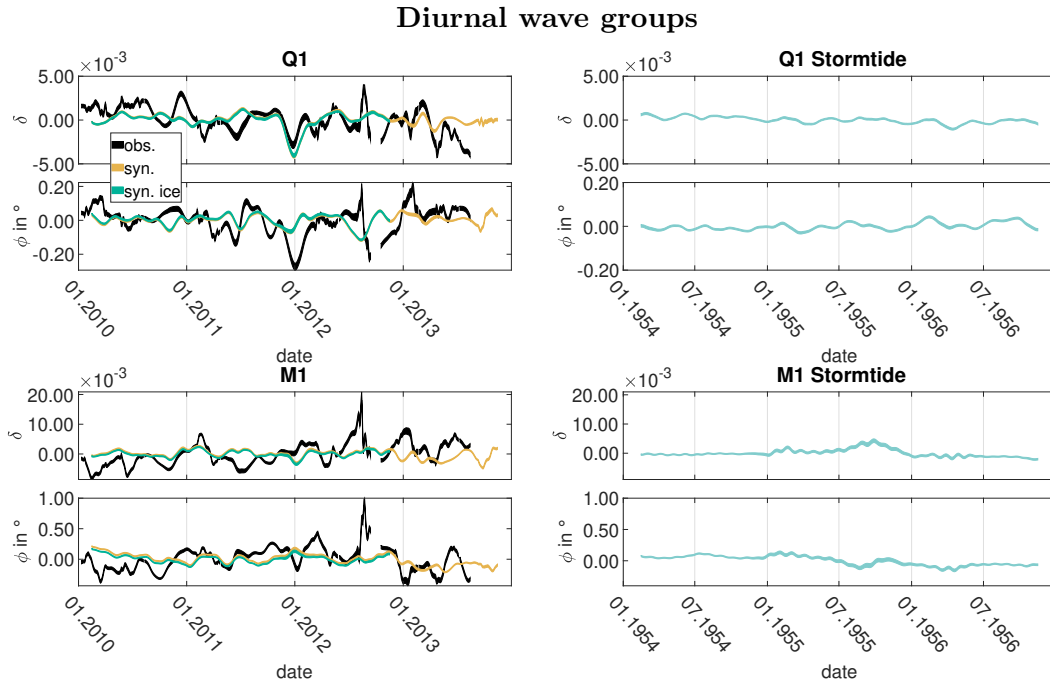
Fig. 9.3. Left: Tidal parameters of wave groups Q1 and M1 at BFO from measurements (black), from synthetic data MWA of the original OMCT version in yellow and the version with OMCT ice drag in green. Right: Tidal parameters of wave groups Q1 and M1 at BFO from synthetic data MWA with Stormtide SSH. The y-scales were set to the same values as for the plots with OMCT.

SSH should therefore show variations of the tidal parameters of the regarded wave groups. These two ocean models are used for the reasons given at the beginning of section 9. The results for BFO are shown in Figs. 9.3 and 9.4. The variations of the tidal parameters of the diurnal wave groups for OMCT differ a lot from the results from measurements. They have the same order of magnitude and the same variation periods, but the shapes of the curves are different. The behaviour is similar to that of O1 described in section 9.1. Schroth et al. (2018) observed a variation of 8.8 years in those wave groups. If this variation period occurs due to the consideration of ocean loading, it can probably not be seen on these short time scales. The time span for which the ocean model data is available is too short for studying this influence. The results show smaller variations and for M1 also show a different periodicity. It is uncertain whether the variations of the diurnal wave groups are caused by the oceans. The similarity of the tidal parameters of the semi-diurnal wave groups obtained with OMCT and the results from measured data are much higher than in the case of the semi-diurnal wave groups. The variation of the gravimetric factor of 2N2 obtained with OMCT is only half the size of the results from measurements, but the phase and the tidal parameters of N2 and L2 fit very well to the variations obtained

Semidiurnal wave groups
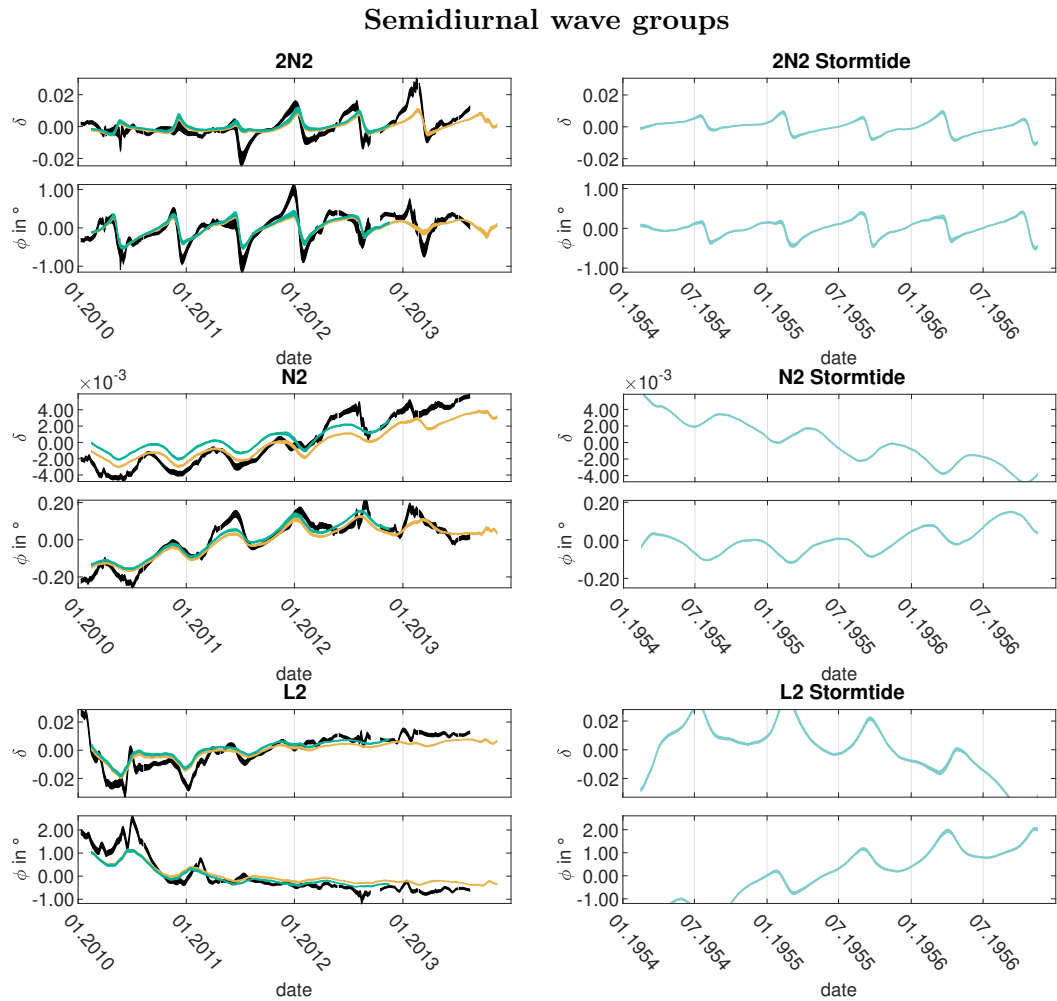
Fig. 9.4. Left: Tidal parameters of wave groups 2N2, N2 and L2 at BFO from measurements (black), from synthetic data MWA of the original OMCT version in yellow and the version with OMCT ice drag in green. Right: Tidal parameters of wave groups 2N2, N2 and L2 at BFO from synthetic data MWA with Stormtide SSH. The y-scales were set to the same values as for the plots with OMCT.

with measurements. All periods (0.56 years, 8.8 years, Schroth et al. 2018) occurring in the tidal parameters estimated from SG data are also present in the results with OMCT. The results for Stormtide have the same periodicity and are of the same order of magnitude. The differences in the shape and the larger variation of the L2 tidal parameters are probably due to the different time spans the model data cover. In particular, the L2 parameters show strong variations with a complex character (e.g. Schroth et al. 2018).

As mentioned above, the higher-degree harmonics are not included in the ocean models; therefore, they are not present in the loading time series. The fact that the tidal parameters

obtained from measurements and synthetic data are nevertheless very similar means that the load of the higher-degree harmonics in the measurement data must be close to zero. These results fit to the results shown by Meurers et al. (2016), mentioned above. The variations of 2N2, N2 and L2 can be explained by a very small loading due to the degree 3, 4 and 5 harmonics in contrast to the large loading at the degree 2 harmonics.

9.3. S2

The S2 period is exactly 12 hours. In the atmosphere there is also an S2 radiation tide due to effects caused by the heating of the Sun. In fact, the semi-diurnal atmospheric tide is larger than the diurnal (Volland, 1997). Klügel and Wziontek (2009) mention that the influence of the S2 atmospheric tides on the tidal parameters is small because the S2 amplitude is large. However, this difference can cause variations of the S2 tidal parameters as it changes the amplitude ratio and phase difference with the other harmonics in the wave group. For discussing this issue, the results for S2 are shown in Fig. 9.5. The measured data are corrected with Atmacs (*direct method*) and Atmacs with replacement of the modelled by the measured air pressure (*replacement method*), see section 7.3.1. The results are different from station to station. At Bad Homburg, Strasbourg and Wettzell, the *direct method* reduces the variation of the tidal parameters by up to 50%, whereas the usage of the locally measured air pressure (with and without Atmacs) causes large semi-annual variations with an amplitude of about $2 \cdot 10^{-3}$ for the gravimetric factor and about $0.1°$ for the phase. It is unlikely that this is caused by a physical effect, as it would mean that there would be a S2 signal present in the measured air pressure that is not present in gravity. This is unlikely as pressure changes are usually associated with mass redistribution which would cause gravity changes at the SG in most cases; further investigations will be necessary to exclude that these results are caused by technical issues.

At Kamioka and Sutherland, there are only small differences between the three time series. The usage of the *replacement method* for the data from Canberra reduces the variation of the tidal parameters while the *direct method* increases the variation to about double amplitude. The variation of the tidal parameters at Onsala has the same amplitude in all three cases, only the shape of the curves differ. A part of the semi-annual variations of the S2 parameters can probably be explained by the loading of the atmosphere which is not completely removed by the adjustment of the locally measured air pressure, but there must be another cause for the remaining variations.

This cause may be the loading of the oceans. The S2 amplitude in the oceans deviates from the amplitude expected from gravitational forcing only by about 17% (Kantha and Clayson, 2000). In order to investigate the influence of the oceans, the tidal parameters of S2 obtained with synthetic data MWA with Atmacs and OMCT (see section 7.4) are shown in Fig. 9.6. The results from measurements and the synthetic data MWA with Atmacs are shown in comparison. Except for Onsala where OMCT again causes variations too large, the combination of Atmacs and OMCT produces a semi-annual variation of the S2 tidal parameters. At Bad Homburg the combined usage of the OMCT and Atmacs enhances the semi-annual character; at Kamioka and Sutherland the variations are twice the variation
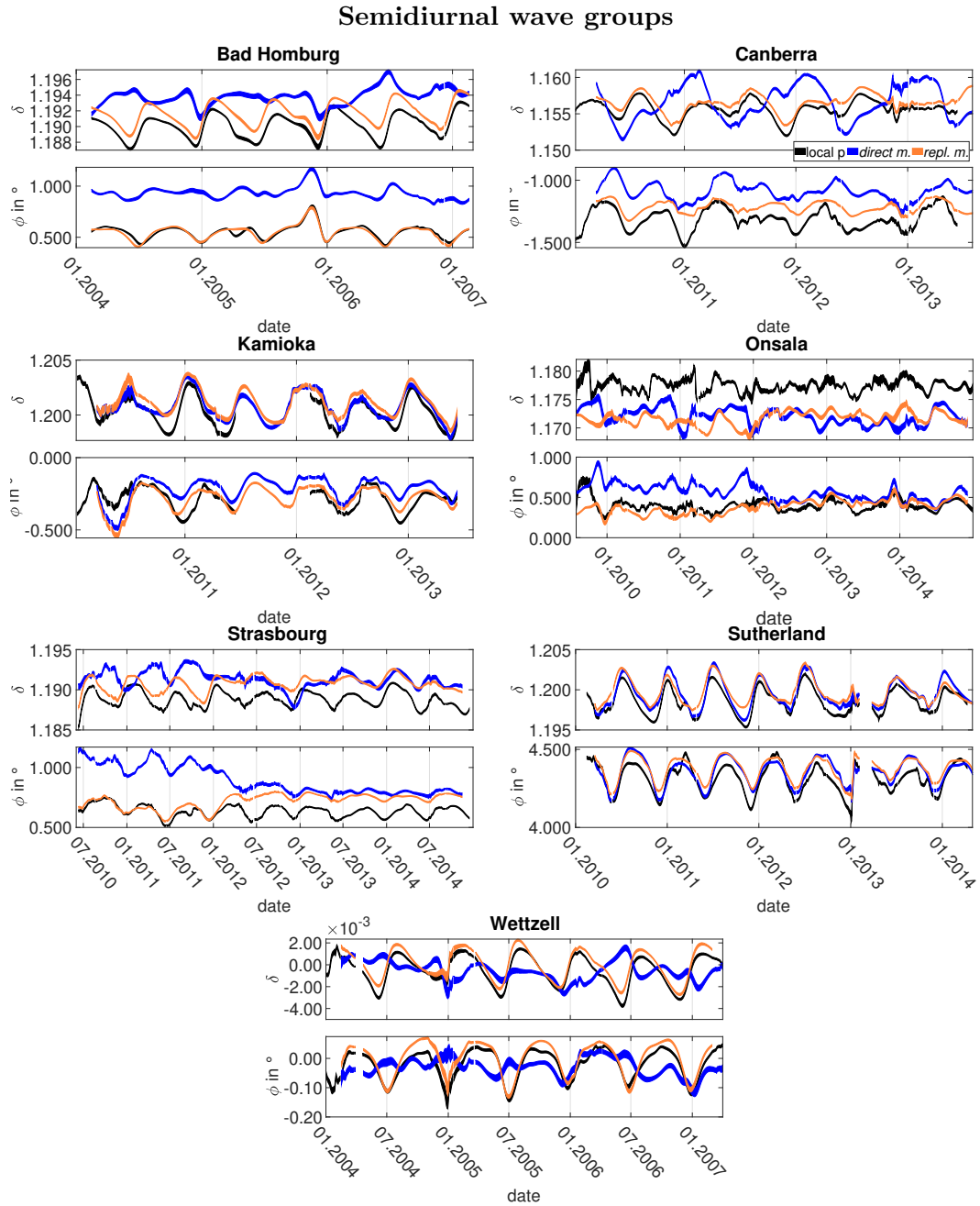
Fig. 9.5. Tidal parameters of wave group S2 at Bad Homburg, Canberra, Kamioka, Onsala, Strasbourg, Sutherland and Wettzell from measurements and adjustment of the measured air pressure (*local p*, black), correction with Atmacs (*direct method*, blue) and correction with Atmacs in which the modelled air pressure was replaced by the measured air pressure (*replacement method*, orange).

Semidiurnal wave groups
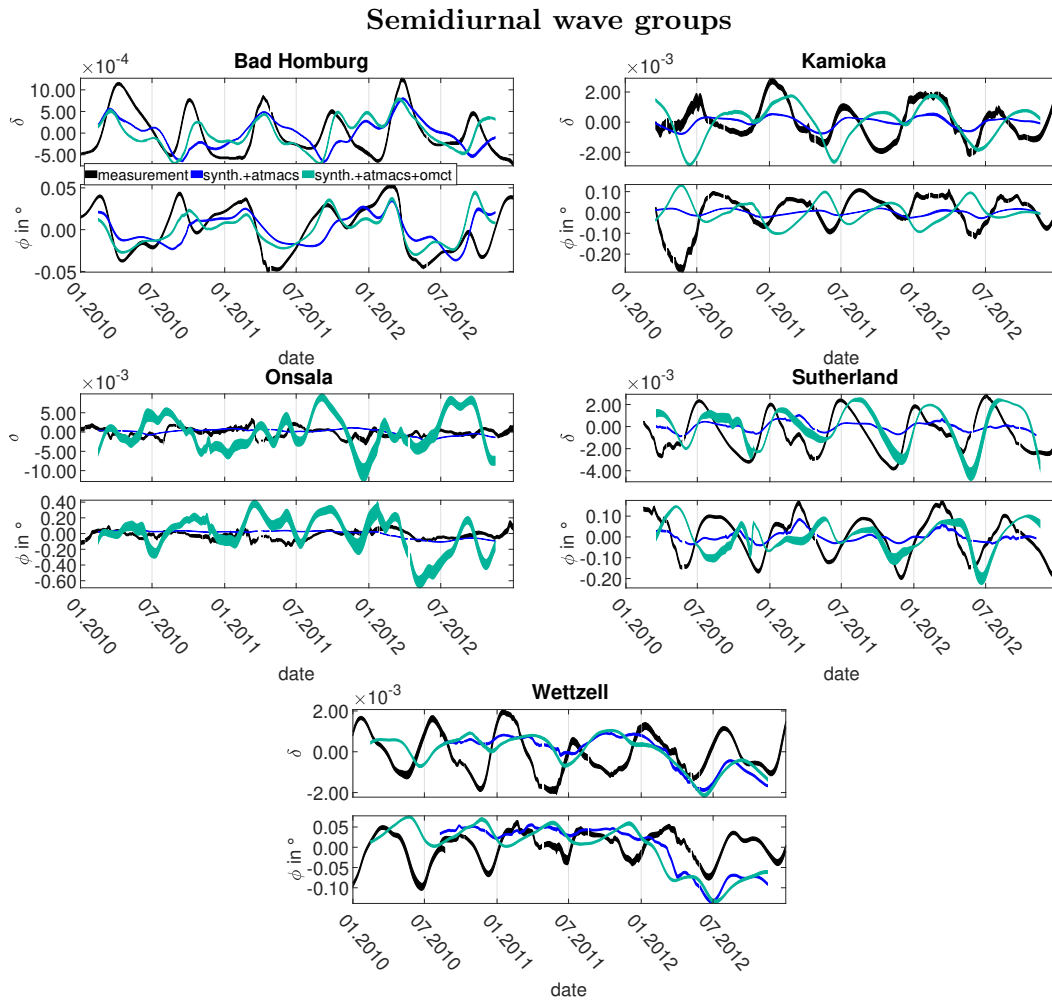
Fig. 9.6. Tidal parameters of wave group S2 at Bad Homburg, Kamioka, Onsala, Sutherland and Wettzell from measurements and adjustment of the measured air pressure (*local p*, black), synthetic data MWA with Atmacs (blue) and synthetic data MWA with Atmacs and OMCT (green).

obtained with only Atmacs, which indicates that oceanic and atmospheric loading at the S2 frequency is of comparable order of magnitude at these stations. For Wettzell, there is no high similarity between synthetic data MWA results and results from measurements, but the usage of OMCT and Atmacs together causes a slightly higher semi-annual variation. However, except for the Sutherland results, the variations obtained with synthetic data MWA have only half the size of the variations obtained with measurements. The tidal parameters from synthetic data MWA are shifted by a few months relative to the results from measurements. These results indicate that oceanic and atmospheric loading cause the variations of the S2 tidal parameters. However, further studies are needed to show whether

Atmacs and OMCT simply do not describe the atmosphere and ocean correctly, or whether additional effects are involved here, especially regarding the increase of the variations at Bad Homburg, Strasbourg and Wettzell when the measured air pressure is used in the correction for atmospheric loading.

9.4. Summary of the chapter

Synthetic data MWA with OMCT, and for two stations with Atmacs and OMCT, result in variations of the O1 tidal parameters that are of the same order of magnitude as the variations of the measurement results with the same frequencies. However, the shapes of the curves differ. This may indicate that the oceans (and maybe the atmosphere) have an influence at O1, but further investigations are needed.

The tidal parameters of the wave groups Q1, M1, 2N2, N2 and L2 which contain higher-degree harmonics do not change significantly when different theoretical tidal parameters (Dehant et al., 1999) are assumed in the tidal analysis. This was expected because of the small difference between the new theoretical values and the original ones (Dehant, 1987). The ocean loading is of larger influence, which is tested with a synthetic data MWA with OMCT. There are no obvious similarities for Q1 and M1, but the variations of 2N2, N2 and L2 are explained well in value of the amplitudes, periods and shape of the curves. The fact that higher-degree harmonics are not included in the OMCT forcing means that the variations of the 2N2, N2 and L2 tidal parameters are caused by very small loading contributions of harmonics with higher degree.

For S2, it can be shown that, at least at some stations, the correction with Atmacs leads to a reduction of the variations of the S2 tidal parameters. Synthetic data MWA show that the S2 tidal parameters are influenced by the atmosphere and the oceans in a comparable order of magnitude.

Chapter 10.

Conclusions

In this chapter the conclusions obtained from the investigations described in chapters 7 to 9 are presented.

K1

For the K1 wave group it was hypothesised that the FCN model used in ETERNA as well as atmospheric and oceanic loading cause variations of the tidal parameters. These hypotheses were formulated as questions in section 1.2. The answers are given in the following.

- Is a part of the variation caused by the outdated FCN model used in the analysis? Can the variations be reduced if a better description of the FCN is used?
  The outdated model with a resonance period of $T_{FCN} = 459.25$ si. d. (WDZ, Dehant 1987) is replaced in ETERNA 3.4 by a more recent FCN model with a resonance period of $T_{FCN} = 431.37$ si. d. (D1999, Dehant et al. 1999), which is close to estimations of the FCN period from VLBI (Krásná et al., 2013). The comparison of the results obtained with both FCN models shows that usage of the D1999 model reduces the variations of the tidal parameters by up to 40%. The more recent FCN model fits the measured data better than the outdated model does.

The remaining variation of the tidal parameters has annual and semi-annual periods. In addition to the questions asked in the introduction, the question arises which harmonics contribute significantly to the variation of the tidal parameters. For identifying the harmonics with significant contributions, synthetic body tide data sets were calculated for BFO with tidal parameters following the analysis model, except for one smaller wave group within the K1 group (sub-group). The tidal parameters of this sub-group were set in a way that the amplitude ratio and phase difference of that particular wave group to K1 was the same as in the measured data (tidal parameters of the sub-groups obtained in a tidal analysis of the whole data set). The largest variation occurred for S1 with an annual period and the second largest for P1 with a semi-annual period. This shows that the S1-to-K1 and P1-to-K1 amplitude ratios and phase differences deviate from the expectations of the analysis model and cause the main part of the variation of the K1 tidal parameters. $\Psi 1$ and $\phi 1$ have only

a minor contribution to the total variation.

The large variation caused by S1 leads to the following questions:

- Can a part of the variation be explained by atmospheric loading contributions at the S1 frequency? Can the variation be reduced if the contributions from the atmosphere are corrected?
  The influence of the atmosphere at the S1 frequency is studied with Atmacs. Through corrections of the measurements with Atmacs combined with the measured air pressure the variation of the tidal parameters is reduced by about 50% at most of the stations. Synthetic data MWA with Atmacs causes an annual variation of the K1 tidal parameters of the correct order of magnitude. This shows that a part of the annual variation of K1 is caused by atmospheric loading.

- Is there an evidence that the oceans contribute to the observed variation?
  Both, Atmacs and ocean loading calculated with OMCT, were used in a synthetic data MWA. Ocean loading at the S1 frequency due to radiation tides contributes to the annual variation. Loading at the P1 frequency could cause a semi-annual variation. The results allow no clear conclusion. For some stations the variation obtained with synthetic data MWA with both data sets is closer to the results from measurements but the difference between the results from Atmacs and from Atmacs and OMCT is small. In those cases in which the results with both data sets are closer to the measurement results the variation gets a stronger semi-annual contribution which indicates that the loading at least from OMCT particularly contributes at the P1 frequency.

From the results described above I conclude that the variation of the K1 tidal parameters is dominated by the deviation of the amplitude ratios and phase differences of S1-to-K1 and P1-to-K1 and can partly be explained by an inappropriate model for the FCN and loading contributions by the atmosphere at the S1 frequency. The influence of ocean loading has to be further investigated.

All investigations are described in detail in chapter 7.

M2

In the M2 wave group the loading effect of annual variations of the M2 amplitude in the oceans is expected to cause the annual variations of the tidal parameters. This influence was studied by synthetic data MWA with nonlinear, time-stepping ocean models (ARTOFS, Stormtide, OMCT, HGT and the North Sea model). The results of the synthetic data MWA are used in the following for answering the questions regarding M2 (see section 1.2).

First, harmonic analyses from the models' output (SSH) are made in which the satellite harmonics of M2, $\alpha 2$ and $\beta 2$, are also estimated. The amplitudes and phases of $\alpha 2$, $\beta 2$ and M2 are used for calculating the annual variations of the M2 amplitude (Stormtide results provided by M. Müller). That way it can be checked whether an AVM2ssh of the expected order of magnitude occurs in the ocean models. All models show amplitudes of the annual variation in the same order of magnitude. The amplitudes of the AVM2ssh from OMCT are only approximately half the size of the amplitudes from Stormtide and the North Sea model. The large amplitudes in OMCT are similarly distributed as in the other models but in some regions no significant AVM2ssh is observed where Stormtide and the analysed part of HGT predict large amplitudes. The analysed part of HGT and ARTOFS show, in the small parts they overlap, a similar distribution of large amplitudes of the AVM2ssh but the amplitudes are twice the amplitudes in Stormtide. The phases of the AVM2ssh look different, but similar patterns like the number of amphidromic points and their approximate location can be observed. Without a comparison to observations, it is not possible to decide whether one of those phase patterns is more realistic than another. The harmonic analyses of the different models' output show that all of them produce annual variations of the M2 amplitudes, although with differences in size and distribution of the amplitudes and phases. The fact that the annual variations occur in the model output does not necessarily mean that they sum constructively in gravity. Therefore, the next questions are:

- Do gravity loading time series computed with SSH from nonstationary ocean models cause annual variations of the M2 gravimetric factor and phase?
  The results of three of the five models used in the thesis (ARTOFS, Stormtide and HGT) show annual variations of the M2 tidal parameters. For OMCT and the North Sea model very small or no variations are observed.

- If annual variations are caused by these loading time series, are they of the correct order of magnitude compared to the results from measured data? Do they have a similar character?
  The time-dependent tidal parameters obtained with synthetic data MWA of AR-TOFS, Stormtide and HGT are of the same order of magnitude as the results from measurements. The AVM2 differ in shape. For ARTOFS and Stormtide there are similarities of the shape of the tidal parameters at some stations, but the curves are shifted by some months relative to the results from measurements. In contrast, the tidal parameters obtained with HGT are in phase with the tidal parameters obtained with measurements, but at many stations the amplitudes of the variations are up to three times larger than the amplitudes of the variations obtained from measured data. These results indicate that the model describes the responsible effects in general but not in a realistic way.
  For OMCT annual variations occur which are an order of magnitude lower than in the results from measured data. The North Sea model results show variations which have the same order of magnitude as expected for the variations caused by the North

Sea, but, as mentioned above, they have no annual periodicity.

The ocean models used here account for the same physical effects (even if the implementation is different). However, this does not result in similar variations of the tidal parameters for all models and leads to the following question.

- Are there evidences why an ocean model shows or does not show annual variations of the M2 amplitude?
  Several OMCT data sets with changes of the model properties were used, but the synthetic data MWA did not result in significant differences in the tidal parameter variations. The largest differences occur between model versions of different spatial resolution. The variations are slightly larger in the 1° version (20 vertical layers) compared to the 1.1875° version (13 vertical layers). These results indicate that the OMCT grid is too coarse to describe the processes causing the variations of the M2 amplitude in the oceans.
  For the North Sea model no clearly annual variation is observed. In contrast, a barotropic model without meteorological forcing but forced with Stormtide SSH at the boundaries (Ocean Tide Equations Main program time-dependent, OTEMT), shows annual variations of the M2 amplitude in the SSH which sum up to an annual variation of the M2 amplitude in gravity. The synthetic data MWA with OTEMT results in temporal variations of the M2 tidal parameters of the correct order of magnitude. These results indicate that the tides at the model boundaries have a significant contribution which is missing in the North Sea model because it is only driven at the boundaries by 10 harmonics which do not contain the annual variation of M2. The fact that ARTOFS does not suffer from the same problem is probably due to the nudging of several measured data sets.
  Another parameter that was investigated is the density of the ocean water. The comparison of synthetic data MWA of SSH and OBP from OMCT as well as nonsteric and total SSH from HGT and a test with two different densities in the loading calculation with ARTOFS showed that the influence of a varying density on the tidal parameters is small compared to other effects.
  The consideration of only few harmonics in the forcing, as in HGT, or in the output, as for the amplitudes and phases for the annual variation of the M2 amplitude from Stormtide, causes artefacts in the variation of tidal parameters. Using the full tidal spectrum in forcing and output of the models is of advantage for synthetic data MWA.

The harmonic analyses mentioned above show that the large amplitudes of the AVM2ssh occur mainly in shelf areas, which are only a small part of the global oceans. In contrast, the amplitudes of the AVM2ssh in the open ocean are small but cover large areas. Therefore, the next questions is:

- Which ocean areas contribute significantly to the variations of the gravimetric factor and phase?
  The investigation of which model areas have a significant influence at different stations was made with Stormtide. It shows that, depending on the station, all grid points where the gravity contribution of the annual variation of the M2 amplitude exceeds a threshold of $10^{-6}\frac{\text{nm}}{\text{s}^2}$ or $10^{-7}\frac{\text{nm}}{\text{s}^2}$ are needed to reach about 90% of the variation caused by the total model. The distribution of the necessary grid points shows that the annual variations of the M2 amplitudes in the oceans on a regional to global scale contribute significantly, depending on the regarded station.
  This shows that MWA of SG data and synthetic data MWA of ocean model data can be used to evaluate how ocean models represent the effects causing the annual variations of M2 amplitudes in the oceans. In contrast to satellite and tide gauge data, SG measurements do not suffer from spatial and temporal aliasing and allow a global observation (at least with several SGs). The disadvantage of this approach is that the influence of certain areas cannot be easily separated.

From the occurrence of annual variations of the M2 tidal parameter in synthetic data MWA with the afore mentioned ocean models, it is concluded that the annual variations resulting from MWA of measured SG data are caused by ocean loading. The ocean models describe the causing effects in general, but not realistically. There are indications that the model resolution and, for models which are restricted to a certain area, information about the annual variations at the model boundaries are important. It is shown that the ocean loading has to be taken into account on a global scale, because also areas far from the SG station contribute significantly.
The complete description of all related investigations is given in chapter 8.

Other wave groups

For the other wave groups the results are summarised as follows.

- Is there an evidence for atmospheric and oceanic loading as causes for the variations of the O1 gravimetric factor and phase?
  The influence of the ocean loading on O1 was investigated with synthetic data MWA of OMCT and the Stormtide SSH. The OMCT results vary with similar periods and have the correct order of magnitude but have a different shape from the results from measurements. Therefore, it remains uncertain whether there is an influence of ocean loading on the O1 tidal parameters.

- Can the variations of the S2 gravimetric factor and phase be caused by atmospheric loading?
  At S2 frequency it could be shown that both, the atmospheric and the oceanic loading, cause variations of the S2 tidal parameters.

- Does a more recent model for the Earth's admittance (Dehant et al., 1999) reduce the variations which are most likely caused by higher-degree harmonics?

For wave groups which are probably influenced by higher-degree harmonics (Q1, M1, 2N2, N2 and L2), it is shown that presuming of other theoretical tidal parameters based on more recent Earth models (Dehant et al., 1999) has no significant influence on the tidal parameter variations.

- Does the ocean loading cause variations of the tidal parameters of Q1, M1, 2N2, N2 and L2?
  The influence of ocean loading was tested with synthetic data MWA with OMCT and Stormtide SSH. Very similar variations of the 2N2, N2 and L2 tidal parameters occur, especially for OMCT for which output is available for the same time span as the measured data. The variations of these tidal parameters can be explained by the missing forcing of higher-degree harmonics in OMCT. Therefore, these harmonics are not included in the loading. The similarity with the results from measured data leads to the conclusion that the loading of these harmonics in measurements has to be much smaller than the loading of the harmonics of degree 2 even if they have similar frequencies. The tidal parameters of Q1 and M1 behave differently and show a similar behaviour as O1.

This is described in detail in chapter 9.

Chapter 11.

Outlook

For most of the studied models the AVM2ssh occur with the same order of magnitude but do not describe the variations realistically. An interesting question is whether this could be improved. A possibility to improve the ocean models' description of the AVM2ssh can be the usage of data assimilation methods. In some cases the variations obtained with ARTOFS seem to be closest to the variations observed for measurements. As output from that model without data assimilation was not available, it was not possible to estimate the influence of assimilation. A more recent version of HGT uses data assimilation, but up to now only one year of data are available. With this study it remains unclear which properties of the ocean models are necessary to describe the effects of the AVM2ssh correctly. The causing mechanisms were studied by Müller et al. (2012), but even the Stormtide model does not explain the variations of the tidal parameters realistically. Therefore, a systematic study of the relevant properties based on a comparison of the model output with data from tide gauges and satellite altimetry as well as variations of the tidal parameters of M2 may help in understanding and improving the description of the corresponding processes. This should include a study on how much the pattern of the AVM2ssh in a certain region (e.g. the North Sea) depends on the distribution of the AVM2ssh in the surrounding areas and how large the contribution of the AVM2ssh is which is generated in this region.

Other scientific measurements which need ocean tide correction would benefit from these improvements as the corrections would be more precise. On a long-term perspective it would of course be desirable if gravity data could be corrected for the annual variation of the M2 amplitude and other effects causing variations.

In principle all types of models could be evaluated with synthetic data MWA, of course with respect to the effects they potentially capture. For example, the loading of radiation tides can be measured by SGs. Radiation tides most likely cause the variations of the K1 and S2 tidal parameters. The variations are therefore additional observational data of the radiation tides in the oceans and the atmosphere.

The influence of atmosphere was of course already investigated many times, but as far as I know never with MWA. MWA has the advantage that it potentially represents for example the annual variability of the radiation tides which otherwise will end in the residuals and can probably not be seen. However, the investigation of atmospheric effects requires a high-quality description for the ocean loading, as there are ocean loading contributions at all tidal frequencies.

Acknowledgements

I would like to thank all the people who supported me during my time as PhD student, in particular:

- Malte Müller for the support allowing my stay at the Norwegian Meteorological Institute, Norway.

- Rosemary Morrow for the support allowing my stay at the Laboratoire d'Etudes en Géophysique et Océanographie Spatiales, France.

- the participants of the Arbeitskreis Geophysik Geodäsie for the helpful discussions and inspiration.

- Thomas Grombein for the LaTeX template this thesis is based on.

- Thomas Bohlen for providing my office at the Geophysical Institute.

- Claudia Payne and Martina Pfersching for the administrative support.

- Petra Knopf and Thomas Hertweck for the IT support.

- the Landesgraduiertenförderung Baden-Württemberg and the German Research Foundation (Deutsche Forschungsgemeinschaft, WE2628/4-1) for funding the project as well as Thilo and Sabine Schroth for funding me and, thus indirectly funding the project.

- the Graduate School for Climate and Environment at KIT for funding my stays at the Onsala Space Observatory, Norwegian Meteorological Institute and Laboratoire d'Études en Géophysique et Océanographie Spatiales.

Bibliography

Agnew, D. C. (2005): Earth Tides: An Introduction. Lecture Note. Scripps Institution of Oceanography. URL: `https://www.unavco.org/education/professional-development/short-courses/course-materials/strainmeter/2005-strainmeter-course-materials/tidenote.pdf` (visited on 2019-06-05).

Agnew, D. C. (2009): Earth Tides. In: *Treatise on Geophysics.* Ed. by G. Schubert and T. Herring. Vol. 3. Amsterdam, Boston: Elsevier B.V. Chap. 3.06, pp. 163–195.

Agnew, D. C. (2012): SPOTL: Some Programs for Ocean-Tide Loading. Technical Report. Scripps Institution of Oceanography. URL: `http://igppweb.ucsd.edu/~agnew/Spotl` (visited on 2015-06-24).

Arbic, B. K., Richman, J. G., Shriver, J. F., Timko, P. G., Metzger, E. J. and Wallcraft, A. J. (2012): Global modeling of internal tides within an eddying ocean general circulation model. *Oceanography* 25(2):20–29. DOI: `10.5670/oceanog.2012.38`.

Arbic, B. K., Wallcraft, A. J. and Metzger, E. J. (2010): Concurrent simulation of the eddying general circulation and tides in a global ocean model. *Ocean Modelling* 32:175–187. DOI: `10.1016/j.ocemod.2010.01.007`.

Baines, P. (1982): On internal tide generation models. *Deep-Sea Research* 29(3A):307–338.

Baker, T. F. and Alcock, G. A. (1983): Time variation of ocean tides. In: Kuo, J. T. (ed.) Proceedings of the Ninth International Symposium on Earth Tides, Stuttgart: E. Schweizerbart´sche Verlagsbuchhandlung, pp. 341–350.

Baker, T. F. and Bos, M. S. (2003): Validating Earth and ocean tide models using tidal gravity measurements. *Geophysical Journal International* 152:468–485.

Bartels, J. (1957): Gezeitenkräfte. In: Flügge, S. (ed.) Handbuch der Physik, vol. 48: Geophysik : 2. Geophysics 2. Berlin: Springer.

Beaumont, C. and Berger, J. (1974): Earthquake prediction: modification of the Earth tide tilts and strains. *Geophysical Journal of the Royal Astronomical Society* 39:111–121.

Bonatz, M. (1967): Der Gravitationseinfluss der Bodenfeuchte. *Zeitschrift für Vermessungswesen* 92:135–139.

Boy, J.-P., Gegout, P. and Hinderer, J. (2002): Reduction of surface gravity data from global atmospheric pressure loading. *Geophysical Journal International* 149:534–545.

Boy, J.-P., Llubes, M., Hinderer, J. and Florsch, N. (2003): A comparison of tidal loading model using superconducting gravimeter data. *Journal of Geophysical Research* 108(B4). DOI: `10.1029/2002JB002050`.

Boy, J.-P., Longuevergne, L., Boudin, F., Jacob, T., Lyard, F., Llubes, M., Florsch, N. and Esnoult, M.-F. (2009): Modelling atmospheric and induced non-tidal oceanic loading contributions to surface gravity and tilt measurements. *Journal of Geodynamics* 48:182–188.

Bützler, C. (2018): Drift des supraleitenden Gravimeters SG056 am BFO. German. Drift of the Superconducting Gravimeter SG056 at BFO. Bachelor's thesis. Karlsruhe Institute of Technology (KIT). URL: https://publikationen.bibliothek.kit.edu/1000082191/7834583.

Calvo, M., Hinderer, J., Rosat, S., Legros, H., Boy, J.-P., Ducarme, B. and Zürn, W. (2014): Time stability of spring and superconducting gravimeters through the analysis of very long gravity records. *Journal of Geodynamics* 80:20–33. DOI: 10.1016/j.jog.2014.04.009.

Corkan, R. (1934): An annual pertubation in the range of tide. *Proceedings of the Royal Society of London A* 144:537–559.

Dahlen, F. A. and Tromp, J. (1998): Theoretical global seismology. 14. Princeton University Press, Princeton, New Jersey. ISBN: 0-691-00116-2.

Dehant, V. (1987): Tidal parameters for an inelastic earth. *Physics of the Earth and Planetary Interior* 49:97–116.

Dehant, V., Defraigne, P. and Wahr, J. M. (1999): Tides for a convective Earth. *Journal of Geophysical Research* 104:1035–1058.

Dietrich, G., Kalle, K., Krauss, W. and Siedler, G. (1975): Allgemeine Meereskune, Eine Einführung in die Ozeanograohie. 3. Gebrüder Borntraeger. ISBN: 3-443-01016-4.

Dobslaw, H., Flechtner, F., Bergmann-Wolf, I., Dahle, C., Dill, R., Esselborn, S., Sasgen, I. and Thomas, M. (2013): Simulating high-frequency atmosphere-ocean mass variability for dealiasing of satellite gravity observations: AOD1B RL05. *Journal of Geophysical Research: Oceans* 118(7):3704–3711. DOI: 10.1002/jgrc.20271.

Doodson, A. T. (1921): The harmonic development of the tide generating potential. *Proceedings of the Royal Society of London A* 100:305–329.

Egbert, G. D. and Erofeeva, S. Y. (2002): Efficient Inverse Modeling of Barotropic Ocean Tides. *J. Atmos. Oceanic Technol.* 19:183–204. DOI: 10.1175/1520-0426(2002)019<0183:EIMOBO>2.0.CO;2.

Egbert, G. D., Erofeeva, S. Y. and Ray, R. D. (2010): Assimilation of altimetry data for nonlinear shallow-water tides: Quarter-diurnal tides of the Northwest European Shelf. *Continental Shelf Research* 2010. DOI: 10.1016/j.csr.2009.10.011.

Farrell, W. E. (1972): Deformation of the Earth by surface loads. *Review of Geophysics* 10(3):761–797. DOI: 10.1029/RG010i003p00761.

Foreman, M. G. G. (2004): Manual for tidal heights analysis and prediction. Pacific Marine Science Report 77-10. Patricia Bay, Sidney: Institute of Ocean Sciences.

Foreman, M. G. G. and Henry, R. F. (1989): The harmonic analysis of tidal model time series. *Advances in Water Resources, 3* 12:109–120. DOI: 10.1016/0309-1708(89)90017-1.

Foreman, M. G. G. and Neufeld, E. T. (1991): Harmonic tidal analysis of long time series. *International Hydrographic Review, 1* 68:85–108.

Foreman, M. G. G., Walters, R., Henry, R., Keller, C. and Dolling, A. (1995): A tidal model of eastern Juan de Fuca Strait and the southern Strait of Georgia. *Journal of Geophysical Research* 100:721–740.

Gräwe, U., Holtermann, P., Klingbeil, K. and Burchard, H. (2015): Advantages of vertically adaptive coordinates in numerical models of stratified shelf seas. *Ocean Modelling* 92:56–58. DOI: `10.1016/j.ocemod.2015.05.008`.

Hartmann, T. and Wenzel, H.-G. (1995a): Catalogue HW95 of the tide generating potential. *Bulletin d'Information des Marées Terrestres* 123:9278–9301.

Hartmann, T. and Wenzel, H.-G. (1995b): The HW95 tidal potential catalogue. *Geophysical Research Letters* 22(24):3553–3556. DOI: `10.1029/95GL03324`.

Hinderer, J., Crossley, D. and Warburton, R. J. (2007): Gravimetric Methods - Superconducting Gravity Meters. In: *Geodesy*. Ed. by G. Schubert. Vol. 3. Treatise on Geophysics. Elsevier B.V. Chap. 3.04, pp. 65–120. DOI: `10.1016/B978-044452748-6.00172-3`.

Huess, V. and Andersen, O. B. (2001): Seasonal variation in the main tidal constituent from altimetry. *Geophysical Research Letters* 28(4):567–570. DOI: `10.1029/2000GL011921`.

Jentzsch, G. (1997): Earth tides and ocean tidal loading. In: *Tidal phenomena*. Ed. by H. Wilhelm, W. Zürn and H.-G. Wenzel. Vol. 66. Lecture notes in earth sciences. Berlin: Springer, pp. 145–171. ISBN: 3-540-62833-9. DOI: `10.1007/BFb0011461`.

Kang, S., Foreman, M. G. G., Lie, H. J., Lee, J.-H., Cherniawsky, J. and Yum, K.-D. (2002): Two-layer tidal modeling of the Yellow and East China Seas with application to seasonal variability pf the M2 tide. *Journal of Geophysical Research: Oceans* 107. DOI: `10.1029/2001JC000838`.

Kantha, L. H. and Clayson, C. A. (2000): Chapter 6 - Tides and Tidal Modeling. In: *Numerical Models of Oceans and Oceanic Processes*. Ed. by L. H. Kantha and C. A. Clayson. Vol. 66. International Geophysics. Academic Press, pp. 375–492. DOI: `10.1016/S0074-6142(00)80011-X`. URL: `http://www.sciencedirect.com/science/article/pii/S007461420080011X`.

Klügel, T. and Wziontek, H. (2009): Correcting gravimeters and tiltmeters for atmospheric mass attraction using operational weather models. *Journal of Geodynamics* 48:204–210.

Krásná, H., Böhm, J. and Schuh, H. (2013): Free core nutation observed by VLBI. *Astronomy and Astrophysics* 555:A29. DOI: `10.1051/0004-6361/201321585`.

Kroner, C. (2001): Hydrological effects on gravity data of the Geodynamic Observatory Moxa. *Journal of the Geodetic Society of Japan* 47(1):353–358.

Majewski, D., Liermann, D., Prohl, P., Ritter, B., Buchhold, M., Hanisch, T., Paul, G., Wergen, W. and Baumgardner, J. (2002): The operational global icosahedralhexagonal grid point model GME: description and high resolution tests. *Monthly Weather Review* 130:319–338.

Mathews, P. M., Harring, T. and Buffet, B. (2002): Modeling of nutation and precession: New nutation series for nonrigid Earth and insights into the Earth's interior. *Journal of Geophysical Research* 107(B4):ETG 3-1 –ETG 3-26. DOI: `10.1029/2001JB00016510.1029/2000JB000056`.

Mehra, A. and Rivin, I. (2010): A Real Time Ocean Forecast System for the North Atlantic Ocean. *Terrestrial, Atmospheric and Oceanic Sciences* 21(1):211–228. DOI: `10.3319/TAO.2009.04.16.01(IWNOP)`.

Melchior, P. (1966): Diurnal Earth tides and the Earth's liquid core. *Geophysical Journal of the Royal astronomical Society* 12:15–21. DOI: `10.1111/j.1365-246X.1966.tb03097.x`.

Mellor, G. L. (1996): Introduction to Physical Oceanography. Springer. ISBN: 1-56396-210-1.

Merriam, J. B. (1995): Non-linear tides observed with the superconducting gravimeter. *Geophysical Journal International* 123:529–540.

Meurers, B. (2004): Investigation of temporal gravity variations in SG-records. *Journal of Geodynamics* 38:423–435.

Meurers, B., Van Camp, M., Francis, O. and Pálinkáš, V. (2016): Temporal variation of tidal parameters in superconducting gravimeter time-series. *Geophysical Journal International* 205:284–300. DOI: `10.1093/gji/ggw017`.

Mukai, A. and Fujimori, K. (2001): Elastic constants in fault zone determined using strain changes obtained at an 800 m borehole. *Journal of the Geodetic Society of Japan* 47:470–475.

Müller, M. (2012): The influence of changing stratification conditions on barotropic tidal transport and its implications for seasonal and secular changes of tides. *Continental Shelf Research* 47:107–118. DOI: `10.1016/j.csr.2012.07.003`.

Müller, M., Cherniawsky, J. Y., Foreman, M. G. G. and von Storch, J.-S. (2012): Global M2 internal tide and its seasonal variability from high resolution ocean circulation and tide modeling. *Geophysical Research Letters* 39. DOI: `10.1029/2012GL053320.2012`.

Müller, M., Cherniawsky, J. Y., Foreman, M. G. G. and von Storch, J.-S. (2014): Seasonal variation of the M_2 tide. *Ocean Dynamics* 64:159–177. DOI: `10.1007/s10236-013-0679-0`.

Munk, W. H. and Cartwright, D. E. (1966): Tidal spectroscopy and prediction. *Phil. Trans. Roy. Soc. London* 259(1105):533–581.

Munk, W. H. and Hasselmann, K. (1964): Super-resolution of Tides. In: *Studies on Oceanography, Hidaka Memorial Volume, Tokyo (1964)*, pp. 339–344.

Na, S.-H. and Baek, J. (2011): Computation of the Load Love Number and the Load Green's Function for an Elastic and Spherically Symmetric Earth. *Journal of the Korean Physical Society* 58(5):1195–1205. DOI: `10.3938/jkps.58.1195`.

Olsson, P.-A., Scherneck, H.-G. and Ågren, J. (2009): Effects on gravity from non-tidal sea level variations in the Baltic Sea. *Journal of Geodynamics* 48:151–156. DOI: `10.1016/j.jog.2009.09.002`.

Omura, M., Otsuka, S., Fujimori, K. and Yamamoto, T. (2001): Tidal strains observed at a station crossing the Otsuki fault, Kobe, Japan, before the 1995 Hyogoken-Nanbu earthquake. *Journal of the Geodetic Society of Japan* 47(1):441–447.

Peters, J. and Beaumont, C. (1987): Tidal and secular tilt from an Earthquake zone:thresholds for detection of regional anomalies. *Earth and Planetary Science Letters* 84:263–276. DOI: `10.1016/0012-821X(87)90091-4`.

Riccardi, U., Rosat, S. and Hinderer, J. (2011): Comparison of the Micro-g LaCoste gPhone-054 spring gravimeter and the GWR-CO26 superconducting gravimeter in Strasbourg

(France) unsing a 300-day time series. *Metrologia* 48:28–39. DOI: 10.1088/0026-1394/48/1/003.

Sato, T., Tamura, Y., Matsumoto, K., Imanishi, Y. and McQueen, H. (2004): Parameters of the fluid core resonance inferred from superconducting gravimeter data. *Journal of Geodynamics* 38:375–389. DOI: 10.1016/j.jog.2004.07.016.

Schindelegger, M., Einšpigel, D., Salstein, D. and Böhm, J. (2016): The Global S1 tide in Earth's Nutation. *Survey in Geophysics* 37:643–680. DOI: 10.1007/s10712-016-9365-3.

Schroth, E. (2013): Analyse von Gezeitenregistrierungen des Supraleitenden Gravimeters SG-056. German. Analysis of tidal recordings of the superconducting gravimeter SG-056. urn: nbn:de:swb:90-466565. Supervisors: T. Forbriger, M. Westerhaus. Diplomarbeit. Karlsruhe Institute of Technology (KIT). URL: http://nbn-resolving.org/urn:nbn:de:swb:90-466565.

Schroth, E., Forbriger, T. and Westerhaus, M. (2018): A catalogue of gravimetric factor and phase variations for twelve wave groups. *KIT Scientific Working Papers* 101. ISSN: 2194-1629.

Schüller, K. (1976): Ein Beitrag zur Auswertung von Erdgezeitenregistrierungen. German. A contribution to the analysis of Earth tide measurements. PhD thesis. Bonn.

Schüller, K. (2015): Theoretical Basis for Earth Tide Analysis with the New ETERNA-ANA-V4.0 Program. *Bulletin d'Information des Marées Terrestres* 149:12024–12061.

Schulzweida, U. (2018): Climate data operators (CDO) User Guide, Version 1.9.3. URL: https://code.mpimet.mpg.de/projects/cdo/embedded/cdo.pdf.

Stammer, D., Ray, R. D., Andersen, O. B., Arbic, B. K., Bosch, W., Carrère, L., Cheng, Y., Chinn, D. S., Dushaw, B. D., Egbert, G. D., Erofeeva, S. Y., Fok, H. S., Green, J. A. M., Griffiths, S., King, M. A., Lapin, V., Lemoine, F. G., Luthcke, S. B., Lyard, F., Morison, J., Müller, M., Padman, L., Richman, J. G., Shriver, J. F., Shum, C. K., Taguchi, E. and Yi, Y. (2014): Accuracy assessment of global barotropic ocean tide models. *Revies of Geophysics* 52:243–282. DOI: 10.1002/2014RG000450.

Steele, M., Morley, R. and Ermold, W. (2001): A global hydrography with a high quality Arctic Ocean. *Journal of Climate* 14:2079–2087.

Steppeler, J., Doms, G. and Schättler, U. (2003): Meso-gamma scale forecasts using the nonhydrostatic model LM. *Meteorology and Atmospheric Physics* 1(4):75–96.

Sündermann, J. and Pohlmann, T. (2011): A brief analysis of North Sea physics. *oceanologia, 3* 53:663–689. DOI: 10.5697/oc.53-3.663.

Taguchi, E., Stammer, D. and Zahel, W. (2014): Inferring deep ocean tidal energy dissipation from the global high-resolution data-assimilative HAMTIDE model. *Journal of Geophysical Research Oceans, 7* 119:4573–4592. DOI: 10.1002/2013JC009766.

Tamura, Y., Sato, T., Ooe, M. and Ishiguro, M. (1991): A procedure for tidal analysis with a Bayesian information criterion. *Geophysical Journal International* 104:507–516.

Thomas, M., Sündermann, J. and Maier-Reimer, E. (2001): Consideration of ocean tides in an OGCM and impacts on subseasonal to decadal polar motion excitation. *Geophysical Research Letters* 28(12):2457–2460. DOI: 10.1029/2000GL012234.

Torge, W. (1989): Gravimetry. de Gruyter, Berlin. ISBN: 3-11-010702-3.

Van Camp, M. and Vauterin, P. (2005): Tsoft: graphical and interactive software for the analysis of time series and Earth tides. *Computers and Geosciences* 31:631–640.

Voigt, C., Förste, C., Wziontek, H., Crossley, D., Meurers, B., V. Pálinkáš, V., Hinderer, J., Boy, J.-P., Barriot, J.-P. and Sun, H. (2016): Report on the Data Base of the International Geodynamics and Earth Tide Service (IGETS). *Scientific Technical Report STR – Data* 16/08. DOI: `doi.org/10.2312/GFZ.b103-16087`.

Volland, H. (1997): Atmospheric Tides. In: Wilhelm, H., Zürn, W., and Wenzel, H.-G. (eds.) Tidal phenomena, *Lecture notes in earth sciences*, vol. 66. Berlin: Springer, pp. 221–246. ISBN: 3-540-62833-9. DOI: `10.1007/BFb0011464`.

Wahr, J. M. (1981): Body tides on an elliptical, rotating, elastic and oceanless earth. *Geophysical Journal of the Royal astronomical Society* 64:677–703.

Wang, H., Xiang, L., Jia, L., Jiang, L., Wang, Z., Hu, B. and Gao, P. (2012): Load Love numbers and Green's functions for elastic Earth models PREM, iasp91, ak135, and modified models with refined crustal structure from Crust 2.0. *Computers & Geosciences* 49:190–199. DOI: `10.1016/j.cageo.2012.06.022`.

Wang, R. (1997): Tidal Response of the Solid Earth. In: Wilhelm, H., Zürn, W., and Wenzel, H.-G. (eds.) Tidal phenomena, *Lecture notes in earth sciences*, vol. 66. Berlin: Springer, pp. 27–57. ISBN: 3-540-62833-9. DOI: `10.1007/BFb0011456`.

Warburton, R. and Goodkind, J. (1977): The influence of barometric-pressure variations on gravity. *J. Geophys. Res.* 48:281–292.

Wenzel, H.-G. (1996): The nanogal software: Earth tide data processing package ETERNA 3.30. *Bulletin d'Information des Marées Terrestres* 124:9425–9439.

Wenzel, H.-G. (1997a): Analysis of Earth Tide Observations. In: Wilhelm, H., Zürn, W., and Wenzel, H.-G. (eds.) Tidal phenomena, *Lecture notes in earth sciences*, vol. 66. Berlin: Springer, pp. 59–75. ISBN: 3-540-62833-9. DOI: `10.1007/BFb0011457`.

Wenzel, H.-G. (1997b): Eterna 3.40, Manual. Black Forest Observatory, Universtät Karlsruhe. Karlsruhe.

Wenzel, H.-G. (1997c): Tide-Generating potential for the Earth. In: Wilhelm, H., Zürn, W., and Wenzel, H.-G. (eds.) Tidal phenomena, *Lecture notes in earth sciences*, vol. 66. Berlin: Springer, pp. 9–26. ISBN: 3-540-62833-9. DOI: `10.1007/BFb0011455`.

Westerhaus, M. and Zschau, J. (2001): No clear evidence for temporal variations of tidal tilt prior the 1999 Izmit and Düzce earthquakes in NW-Anatolia. *Journal of the Geodetic Society of Japan* 47(1):448–455.

Westerhaus, M. (1997): Tidal tilt modification along an active fault. In: *Tidal phenomena*. Ed. by H. Wilhelm, W. Zürn and H.-G. Wenzel. Vol. 66. Lecture notes in earth sciences. Berlin: Springer, pp. 311–339. ISBN: 3-540-62833-9. DOI: `10.1007/BFb0011469`.

Wübbe, C. (1979): Die zweidimensionalen Seiches der Ostsee. German. The two-dimentisonal seiches of the Baltic Sea. Diploma. Christian Albrechts University Kiel. DOI: `doi:10.3289/IFM_BER_64`.

Wübbe, C. and Krauss, W. (1979): The two-dimentisonal seiches of the Baltic Sea. *Oceanolgica Acta* 2(4):435–446.

Wziontek, H. (2016): Verification of transfer function of co-located Superconducting Gravimeters in time and frequency domain. In: 18. International Symposium on Geodynamics and Earth Tides, Trieste.

Zürn, W. (1997): The Nearly-Diurnal Free Wobble-Resonance. In: Wilhelm, H., Zürn, W., and Wenzel, H.-G. (eds.) Tidal phenomena, *Lecture notes in earth sciences*, vol. 66. Berlin: Springer, pp. 95–109. ISBN: 3-540-62833-9. DOI: 10.1007/BFb0011459.

Zürn, W., Forbriger, T. and Widmer-Schnidrig, R. (2008): Magnetfeldeinflüsse auf Doppelkugel-Supraleitgravimeter. In: Arbeitskreis Geophysik Geodäsie, Hirschegg.

Appendix A.

Glossary

A.1. Definitions

- analysis model: The analysis model is a model for solid Earth tides. It is used in tidal analysis (see section 3.1.1) and defines the theoretical tidal parameters depending on the degree and frequency (in case of FCN, see section 2.2.4 and 7.1) of the harmonic. Tidal analysis is based on the assumption that the Earth responds equally to forcing of harmonics of similar frequency. Thus, the amplitude ratios and phase differences of the harmonics on one wave group are kept constant. The amplitude ratios and phase differences are defined by the analysis model. This is the important issue with respect to this thesis, because as soon as the amplitude ratios and phase differences deviate from the values predicted by the analysis model, variations of the tidal parameters occur in the MWA.

- body tides: Body tides or solid Earth tides, these terms are used as synonyms in this thesis, denote the gravity tides that would be measured on an elliptical, rotating, elastic Earth without oceans and atmosphere.

- constituent: This term is used only in section 3.3 because Foreman (2004) defines the term 'constituent group'. In this case, constituent has the same meaning as harmonic, but as it is sometimes understood differently it is not used in other sections of this thesis.

- Earth tides: Earth tides in the context of this thesis means the tidal signal as measured at an SG station, containing the contributions of body, ocean and radiation/atmospheric tides.

- ETERNA: program package for tidal analysis and solid earth tide prediction (Wenzel, 1996).

- frequency distance: With frequency distance the difference of the frequency of two tidal harmonics is meant. Typically, one of these harmonics is a large amplitude harmonic defining a wave group and satellite harmonics within the same wave group. If the regarded harmonics cause a variation of the tidal parameters the variation frequency is equal to the frequency distance.

- harmonic: A harmonic is a cosine function which describes the tidal forcing at a certain frequency. Its amplitude and phase is given by the tidal catalogue (see 2.2.2).

- harmonic analysis/tidal analysis: Harmonic analysis is used for ocean tides (see section 3.3) and tidal analysis for Earth tides (see section 3.1.1). They use the same methods but differ in details in their practical implementation.

- line: Synonym for harmonic.

- loading: In this thesis loading is regarded as the combined effects in gravity of the deformation of the solid Earth and the Newtonian attraction due to a surface load.

- mean value of the tidal parameters: The term mean value is used as synonym for the stationary part of the tidal parameters. See below.

- satellite harmonic: A satellite harmonic is a harmonic whose frequency is close to the main harmonic of the wave group. Usually this term is used when the harmonic is the reason for a modulation of the tidal parameters of the wave group.

- solid Earth tides: See body tides.

- stationary/nonstationary model: By stationary model an ocean model is meant which describes the ocean tides by a set of amplitudes and phases for several harmonics. The amplitudes and phases cannot vary with time. A nonstationary ocean model allows temporal variations of the amplitudes of the harmonics. This can be done when the SSH is used as output or if amplitudes and phases for the variation are estimated. The SSH is used for most of the models available for this thesis and has the advantage that it can describe variations whose character is not perfectly harmonic.

- stationary/nonstationary part of the tidal parameters: The term stationary part of the tidal parameters means the part that can be described by a constant amplitude and phase. It can be estimated by the mean value of the time-dependent tidal parameters

or the tidal parameters estimated in a tidal analysis. The nonstationary part is the variation of the tidal parameters.

- synthetic data MWA: This approach is described in section 4.2. Synthetic data, the sum of synthetic body tides and the loading effect calculated for an ocean or an atmospheric model, are analysed with MWA and the results are compared to the results obtained from measured data.

- wave group: The concept of wave groups is used in tidal analysis. Due to the restricted frequency resolution (Munk and Hasselmann, 1964) the tidal parameters cannot be estimated for single harmonics. Instead, they are adjusted for wave groups which are sums of harmonics in a frequency band. It is assumed that the harmonics behave exactly as predicted by the analysis model. Their amplitude ratios and phase differences are kept constant during the adjustment in the tidal analysis.

A.2. Abbreviations

- ARTOFS: Atlantic real-time ocean forecast system (Mehra and Rivin, 2010)

- Atmacs: Atmospheric attraction computation service (Klügel and Wziontek, 2009)

- AVM2: annual variation of the M2 tidal parameters

- AVM2ssh: annual variation of the M2 amplitude in the oceans, represented by the sea surface height

- BFO: Black Forest Observatory

- cpd: cycles per day

- DWD: Deutscher Wetterdienst, German Weather Service

- FCN: Free Core Nutation

- FFT: fast Fourier transform

- HGT: HYCOM global tides model (Arbic et al., 2012; Arbic et al., 2010)

- IGETS: International Geodynamics and Earth Tide Service

- MWA: moving window tidal analysis

- OBP: ocean bottom pressure

- OLP: Ocean Loading Provider[10]

- OMCT: Ocean model for circulation and tides (Dobslaw et al., 2013; Thomas et al., 2001)

- OSO: Onsala Space Observatory

- OTEMT: Ocean Tide Equations Main program time-dependent, H.-G. Scherneck

- SNREI: Spherical symmetric, non-rotating, elastic, isotropic

- SG: superconducting gravimeter

- SPOTL: Some Programs for Ocean-Tide Loading

- si. d.: sidereal day

- TIGO: Transportable Integrated Geodetic Observatory

- SSH: sea surface height

- VK1: variation of the K1 tidal parameters

---

[10]http://holt.oso.chalmers.se/loading/index.html (05.07.2019)

Appendix B.

Detailed motivation of the choice of the gravimetric factor for the synthetic body tides

In section 3.1.3 it was mentioned that I used $\delta = 1.16$ for the gravimetric factors, which is close to values obtained for Earth models but not exactly the value obtained for a certain model calculation. The value of δ does not affect the temporal variations of the tidal parameters and is only of relevance for the stationary part of the tidal parameters, which is discussed as a side-product of the MWA for the wave group M2 in section 8.2.6.2. There, the mean values of the tidal parameters obtained from the synthetic data MWA with the nonstationary ocean models (see section 4.2.2) are compared to tidal parameters obtained with stationary ocean models (see section 8.2.6.2) and to the mean values from the results obtained from measurements. The results for the stationary ocean models were also obtained by assuming δ of the solid Earth to be 1.16. Therefore, the results can be directly compared.

The assumption of $\delta = 1.16$ is only of relevance for the comparison with results from measured data. Dehant (1987) and Wahr (1981) show calculations for solid Earth tidal parameters for different Earth models which differ by $1 \cdot 10^{-3}$. There is no possibility to prove which Earth model is describing the real Earth better, so I decided to use 1.16 for reasons of comfort, as the difference from 1.16 to the results obtained with the synthetic data MWA is easier to calculate than using 1.159 (Dehant, 1987) or 1.1617 (Dehant et al., 1999).

The latter value is in fact due to the assumption of a nonhydrostatic Earth. This computation was only available for one Earth model. Therefore, it would probably also be different in the same order of magnitude if the nonhydrostatic case was assumed for another Earth model. This indicates that the uncertainties due to the solid Earth are of an order of 10^{-3}. Please note that one of the values given by Dehant (1987) actually is 1.16. However, this value was not chosen because I believe the corresponding Earth model to be more realistic than the others.

Appendix C.

Data and models

time span	IGETS		corrected	
	'calibration factor'	time lag in s	'calibration factor'	time lag in s
	GWR CD029 lower sensor			
05.11.1998-30.09.1999	1.0017	8.000	1.0017	8.000
01.10.1999-20.03.2001	1.0017	5.000	1.0017	5.000
02.04.2001-31.12.2001	1.0017	0.000	1.0017	0.000
01.01.2002-31.12.2003	1.0017	5.000	1.0017	0.000
02.01.2004-16.04.2007	1.0017	40.000	1.0017	40.000
21.04.2007-31.12.2007	1.0000	14.931	1.0000	14.931
01.01.2008-31.12.2008	1.0017	40.000	1.0000	14.931
01.01.2009-06.10.2010	1.0000	14.931	1.0000	14.931
	GWR CD030 lower sensor			
26.06.2010-27.02.2005	1.0000	13.400	1.0000	9.000

Table C.1. 'Calibration factor' and phase lag in s for the station Wettzell, as given by IGETS and corrected (P. Wolf, H. Wziontek, pers. comm., Wziontek 2016)

Appendix D.

Temporal variations of the K1 tidal parameters

long periodic			diurnal			semi-diurnal and short periodic		
name	f_s in cpd	f_e in cpd	name	f_s in cpd	f_e in cpd	name	f_s in cpd	f_e in cpd
SA	0.001379	0.004107	Q1	0.501370	0.911390	2N2	1.470244	1.880264
SSA	0.004108	0.020884	O1	0.911391	0.947991	N2	1.880265	1.914128
MM	0.020885	0.054747	M1	0.947992	0.981854	M2	1.914129	1.950419
MF	0.054748	0.091348	P1	0.981855	0.998631	L2	1.950420	1.984282
MTM	0.091349	0.501369	S1	0.998632	1.001369	S2	1.984283	2.002736
			K1	1.001370	1.004107	K2	2.002737	2.451943
			$\psi 1$	1.004108	1.006845	M3M6	2.451944	7.000000
			$\phi 1$	1.006846	1.023622			
			J1	1.023623	1.057485			
			OO1	1.057486	1.470243			

Table D.1. Definition of wave groups, ordered by frequency, as given by Wenzel (1997b). Name of the wave group is given. f_s is the start and f_e the end frequency of the wave group in cpd.

	fine wave groups				MWA wave groups			
name	old FCN		new FCN		old FCN		new FCN	
	δ	$\Delta\delta$	δ	$\Delta\delta$	δ	$\Delta\delta$	δ	$\Delta\delta$
SA	6.23585	0.22546	6.23584	0.22546				
SSA	1.61590	0.00758	1.61590	0.00758				
MM	1.19642	0.00344	1.19642	0.00344				
MF	1.14659	0.00163	1.14659	0.00163				
MTM	1.13656	0.00807	1.13656	0.00807				
Q1	1.14888	0.00119	1.14888	0.00119	1.14899	0.00013	1.14896	0.00011
O1	1.14912	0.00024	1.14912	0.00024	1.14904	0.00002	1.14903	0.00002
M1	1.14960	0.00231	1.14960	0.00231	1.14871	0.00023	1.14866	0.00020
P1	1.14928	0.00054	1.14928	0.00054				
S1	1.22389	0.03284	1.22372	0.03284				
K1	1.13683	0.00017	1.13682	0.00017	1.13650	0.00002	1.13662	0.00001
ψ1	1.26711	0.02233	1.26662	0.02233				
ϕ1	1.17786	0.0121	1.17788	0.01217				
J1	1.15635	0.00296	1.15635	0.00296	1.15603	0.00031	1.15624	0.00027
OO1	1.15627	0.00453	1.15627	0.00453	1.15638	0.00050	1.15625	0.00044
2N2	1.15067	0.00548	1.15067	0.00548	1.14989	0.00061	1.14985	0.00053
N2	1.16945	0.00117	1.16945	0.00117	1.16945	0.00013	1.16945	0.00011
M2	1.18642	0.00023	1.18643	0.00023	1.18640	0.00003	1.18640	0.00002
L2	1.16452	0.00761	1.16472	0.00761	1.16532	0.00082	1.16533	0.00071
S2	1.18860	0.00050	1.18860	0.00050	1.18808	0.00005	1.18802	0.00005
K2	1.18938	0.00176	1.18938	0.00176				
M3M6	1.05948	0.01678	1.05948	0.01678	1.05909	0.0018	1.05909	0.00161

Table D.2. All gravimetric factors δ and their standard deviations $\Delta\delta$ from the tidal analyses described in section 7.1 of the data from BFO, with the finer wave grouping (see Tab. D.1) and the MWA groups as well as new and old FCN model.

	fine wave groups				MWA wave groups			
name	old FCN		new FCN		old FCN		new FCN	
	ϕ in °	$\Delta\phi$ in °	ϕ in °	$\Delta\phi$ in °	ϕ in °	$\Delta\phi$ in °	ϕ in °	$\Delta\phi$ in °
SA	143.5055	1.3470	143.5056	1.3470				
SSA	-35.2537	0.3225	-35.2536	0.3225				
MM	-1.0126	0.1651	-1.0126	0.1651				
MF	0.3670	0.0811	0.3670	0.0811				
MTM	-1.0160	0.4107	-1.0160	0.4107				
Q1	-0.3086	0.0595	-0.3086	0.0595	-0.3189	0.0063	-0.3412	0.0055
O1	0.0732	0.0121	0.0732	0.0121	0.0727	0.0012	0.0493	0.0011
M1	0.2705	0.1153	0.2706	0.1153	0.3455	0.0115	0.3164	0.0100
P1	0.1991	0.0267	0.1990	0.0267	0.2417	0.0008	0.2159	0.0007
S1	8.5540	1.5375	8.5441	1.5377				
K1	0.2495	0.0088	0.2484	0.0088				
ψ1	0.1491	1.0099	0.1814	1.0100				
ϕ1	-0.0498	0.5918	-0.0527	0.5918				
J1	0.1428	0.1468	0.1428	0.1468	0.0945	0.0155	0.0769	0.0136
OO1	0.0667	0.2246	0.0668	0.2246	0.0687	0.0249	0.0449	0.0217
2N2	2.7298	0.2726	2.7298	0.2726	2.7457	0.0304	2.7121	0.0266
N2	2.6901	0.0573	2.6901	0.0573	2.6926	0.0063	2.6475	0.0055
M2	1.9951	0.0112	1.9951	0.0112	1.9940	0.0012	1.9475	0.0011
L2	1.5809	0.3745	1.5809	0.3745	1.5997	0.0402	1.5428	0.0351
S2	0.6095	0.0239	0.6095	0.0239	0.5716	0.0027	0.5180	0.0023
K2	0.8179	0.0850	0.8179	0.0850				
M3M6	0.3770	0.9074	0.3770	0.9074	0.3427	0.0998	0.2687	0.0873

Table D.3. The same as Tab. D.2 for the phase leads ϕ and their $\Delta\phi$ in degree.
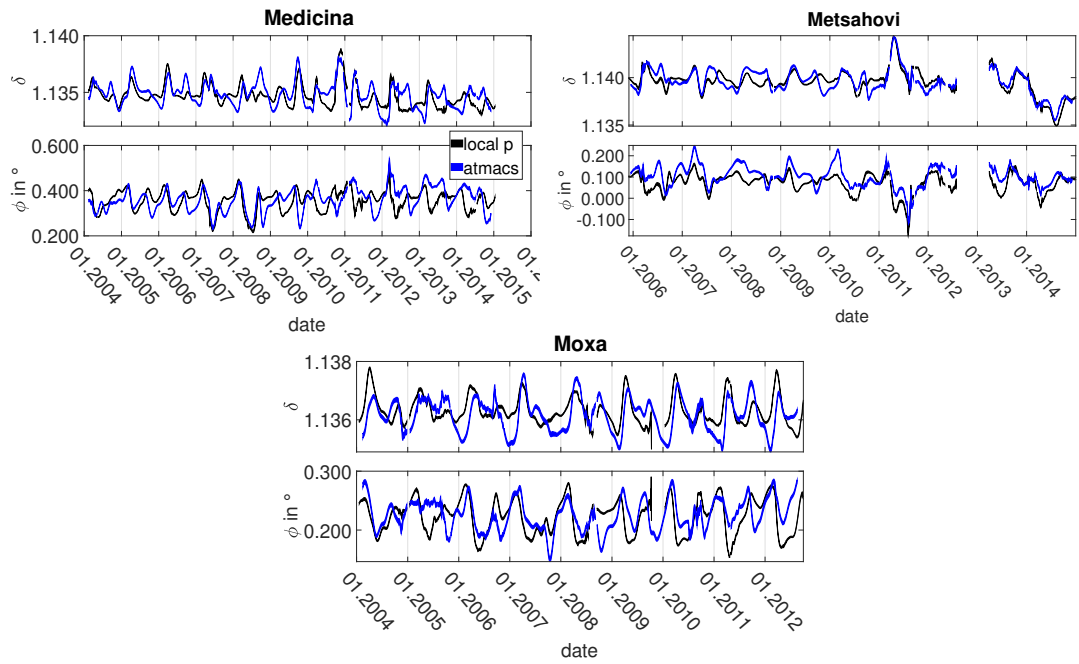
Fig. D.1. Tidal parameters (δ and ϕ) of wave group K1 at Medicina, Metsahovi and Moxa. The black curves are the tidal parameters of the measured data with the locally measured air pressure adjusted to the data. The blue curves are the results, when the SG data is corrected with the Atmacs model before the MWA.

Appendix E.

Temporal variations of the M2 tidal parameters

E.1. Description of the harmonic analyses of the HGT model

Harmonic analyses are made for all the available ocean models (see section 8.1). However, this was difficult for the HGT model. It has a very high spatial resolution of 4500×3289 grid points, which makes it impossible to analyse two years of data for the whole model at once on a standard desktop PC. Therefore, the model was analysed in small subsets. The following steps are needed for this approach: The HGT SSH is available in separate files for each time step. For the harmonic analysis the years 2009 and 2010 were used. First, the area of the corresponding subset is cut out from each data file, then the resulting 17520 separate subset files are merged to one data file. Afterwards the data can be analysed. The whole procedure takes almost 14.5 h for one subset when a subset size of 300×200 grid points is used. The cutout of the subsets is the most time-consuming step (approx. 14 h), therefore cutting out larger areas would be more efficient; however, I needed to use the computer for other issues at the same time and merging 17520 files of 300×200 grid points already slows down other programs. Therefore, this size of the subset is the compromise I decided to use. As far as I can see, only a small reduction of the overall computation time could be achieved, if only ocean grid points would be analysed in subsets that also contain land areas. This is not the case in the current stage. Subsets containing only land areas are left out.

The results are shown in Fig. E.1.

The stationary M2 amplitude and phase given in Fig. E.5 are also a result of this analysis. Alternatively, it would have been possible too parallelise the analyses which would have costed more afford in terms of preparing the parallelised analysis but has a smaller computation time. However, I chose the solution described above as it could be prepared very quickly and I could work on other tasks during the analysis.
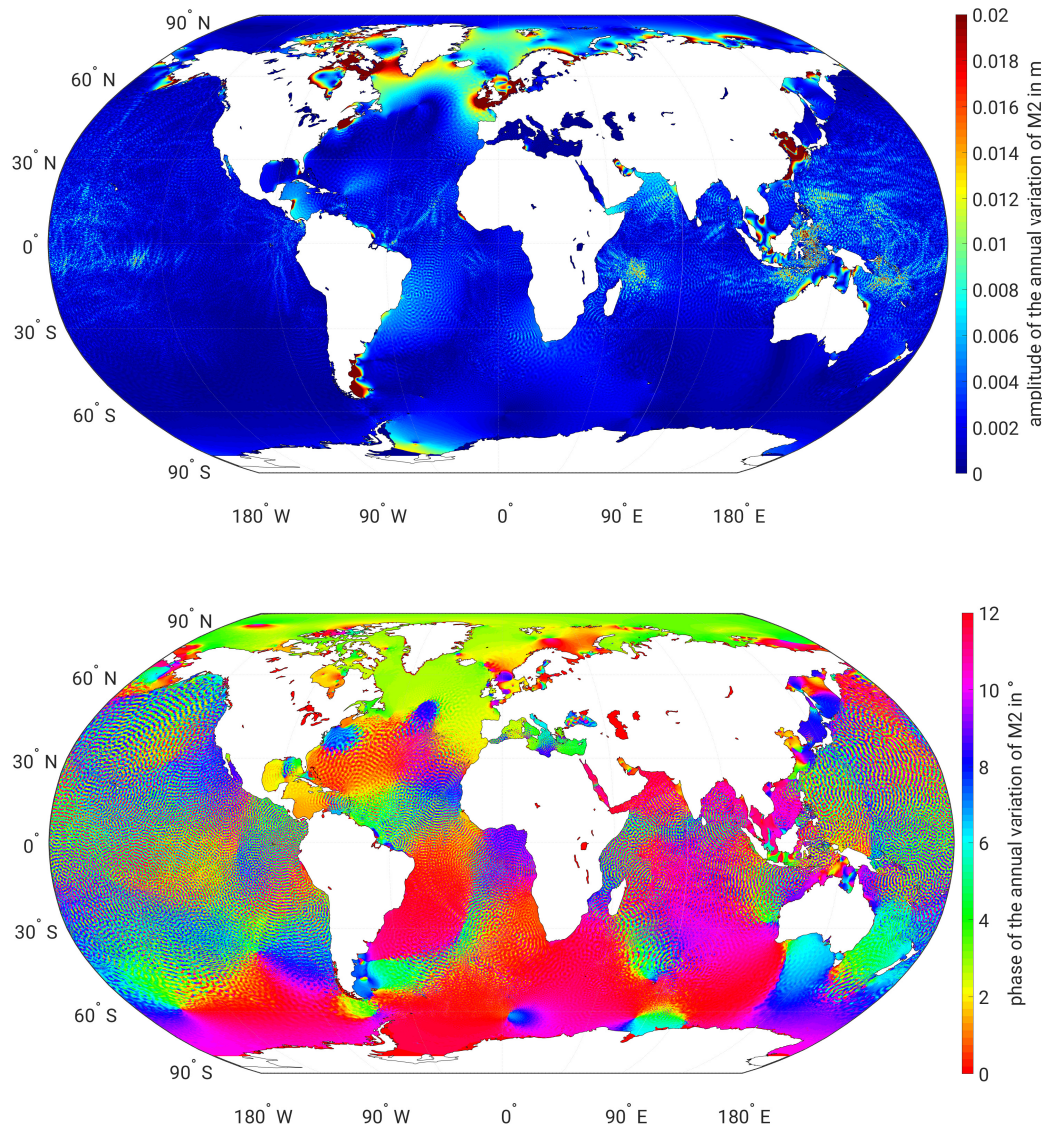
Fig. E.1. Top: Amplitude of the annual variation of M2 in metres. The maximal amplitude is about 0.3 m in a very small area, to make other patters visible, the colour scale is clipped at a maximum of 0.02 m. Bottom: Greenwich phases in months of the annual variation of the M2 amplitude from the HGT model.

E.2. Additional figures and tables for chapter 8
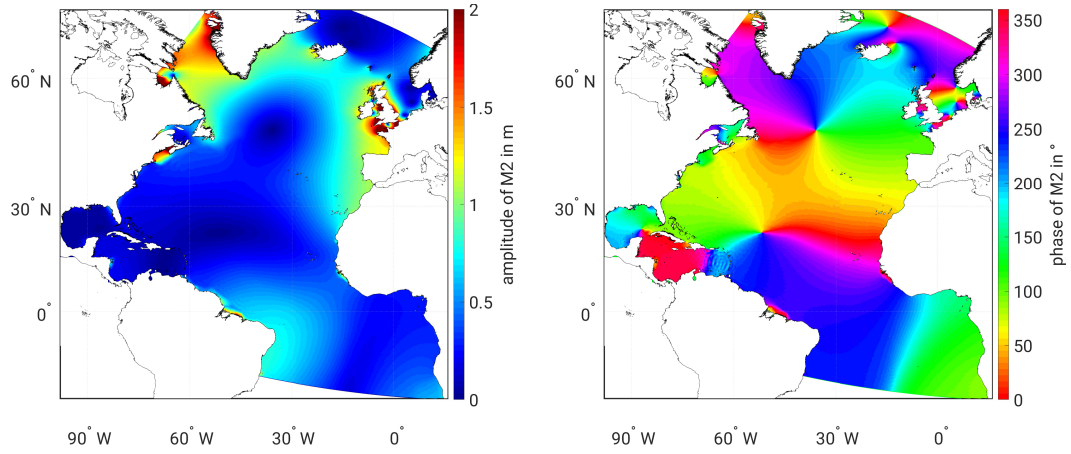
Fig. E.2. Left: Amplitudes in metres of M2 from the ARTOFS model. The colour scale is clipped at a maximum of 2 m. Right: Greenwich phases in degree of M2 from the ARTOFS model.
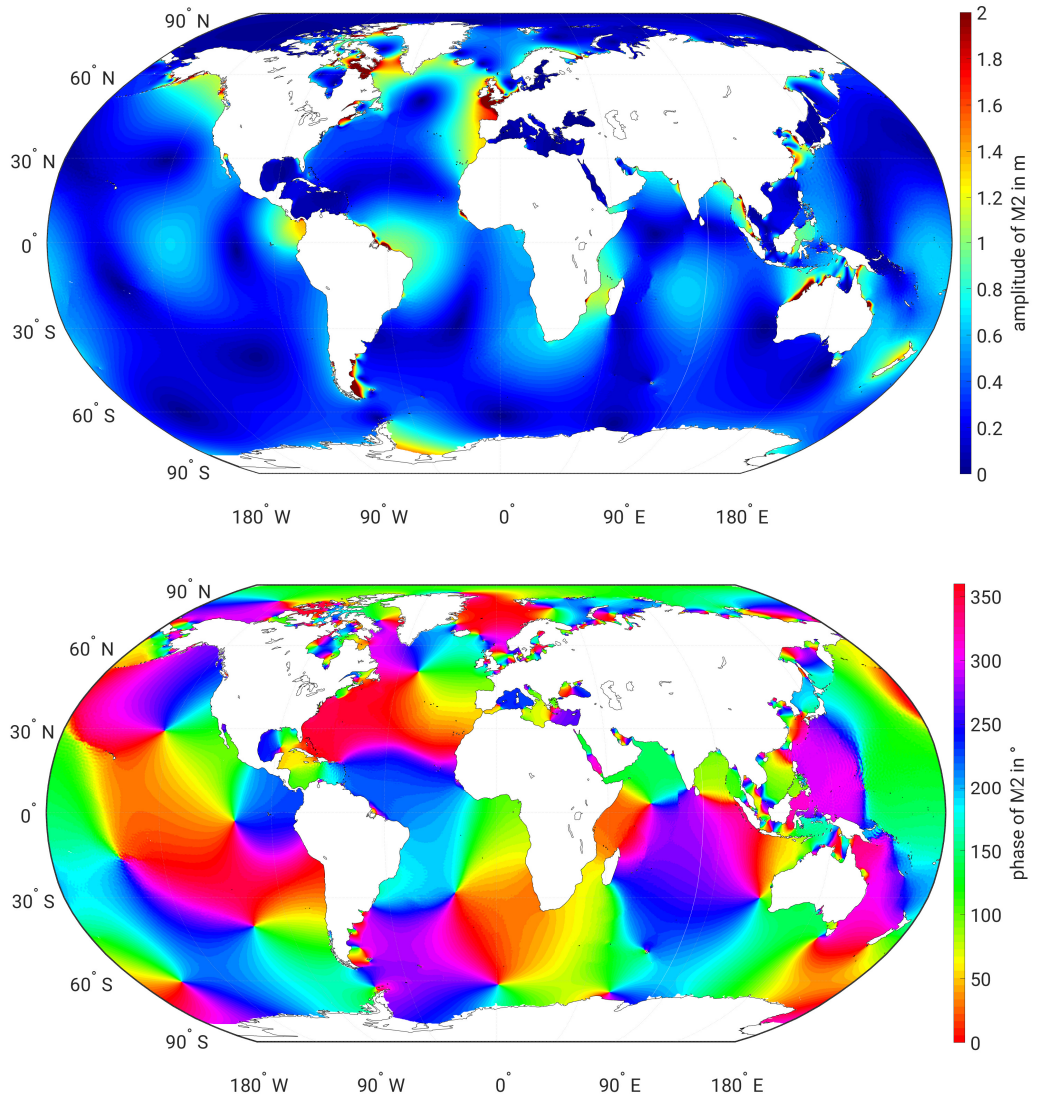
Fig. E.3. Top: Amplitudes in metres of M2 from the Stormtide model. The colour scale is clipped at a maximum of 2 m. Bottom: Greenwich phases in degree of M2 from the Stormtide model.
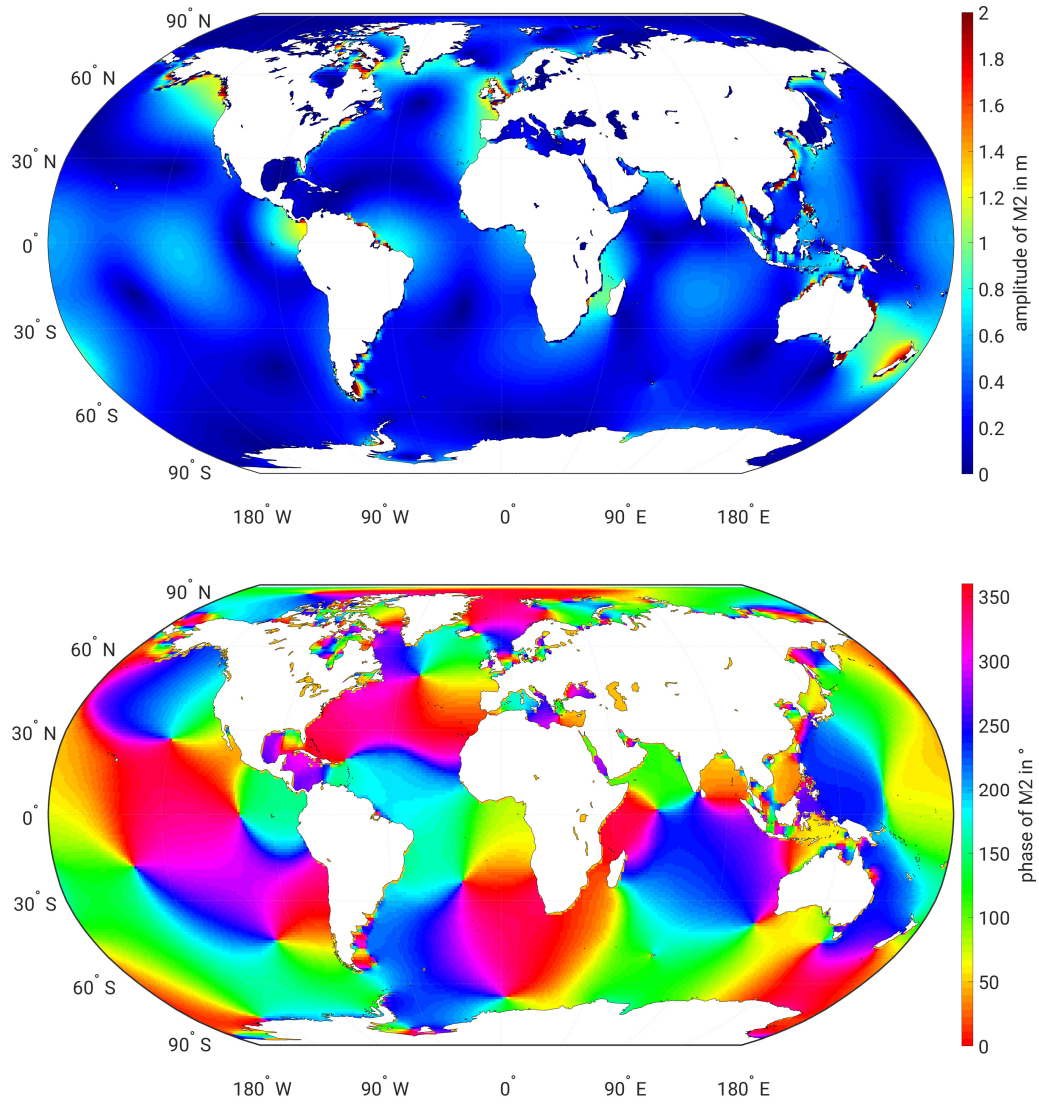
Fig. E.4. Top: Amplitudes in metres of M2 from the OMCT model. The colour scale is clipped at a maximum of 2 m. Bottom: Greenwich phases in degree of M2 from the OMCT model.
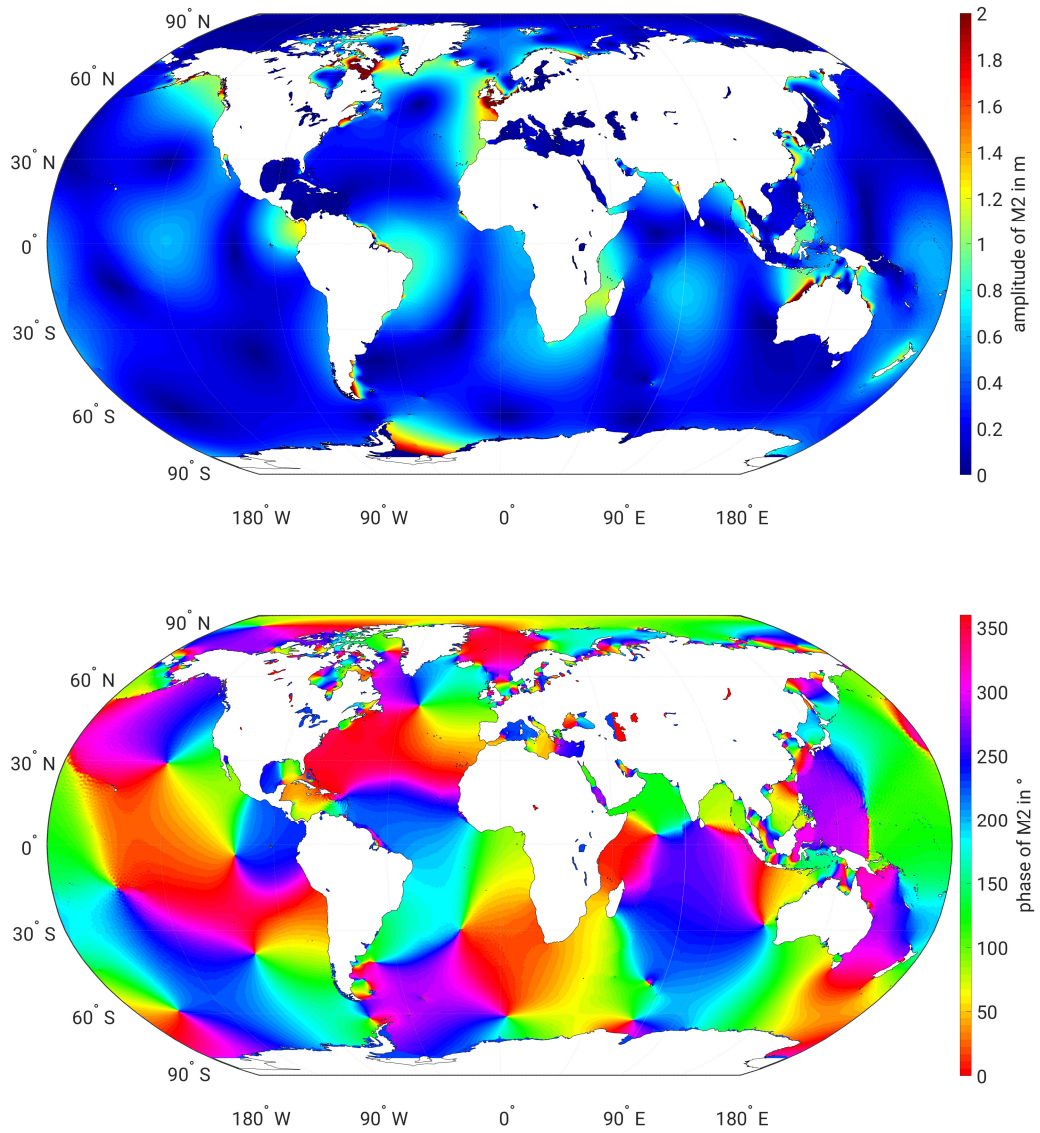
Fig. E.5. Top: Amplitudes in metres of M2 from the HGT model. The colour scale is clipped at a maximum of 2 m. Bottom: Greenwich phases in degree of M2 from the HGT model. Only a part of the model was analysed (see section E.1)
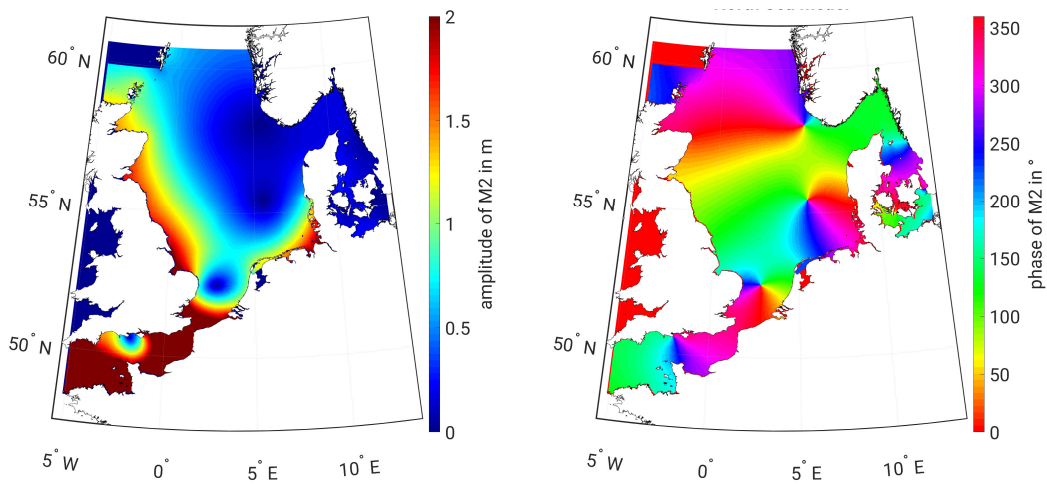
Fig. E.6. Left: Amplitudes in metres of M2 from the North Sea model. The colour scale is clipped at a maximum of 2 m. Right: Greenwich phases in degree of M2 from the North Sea model.
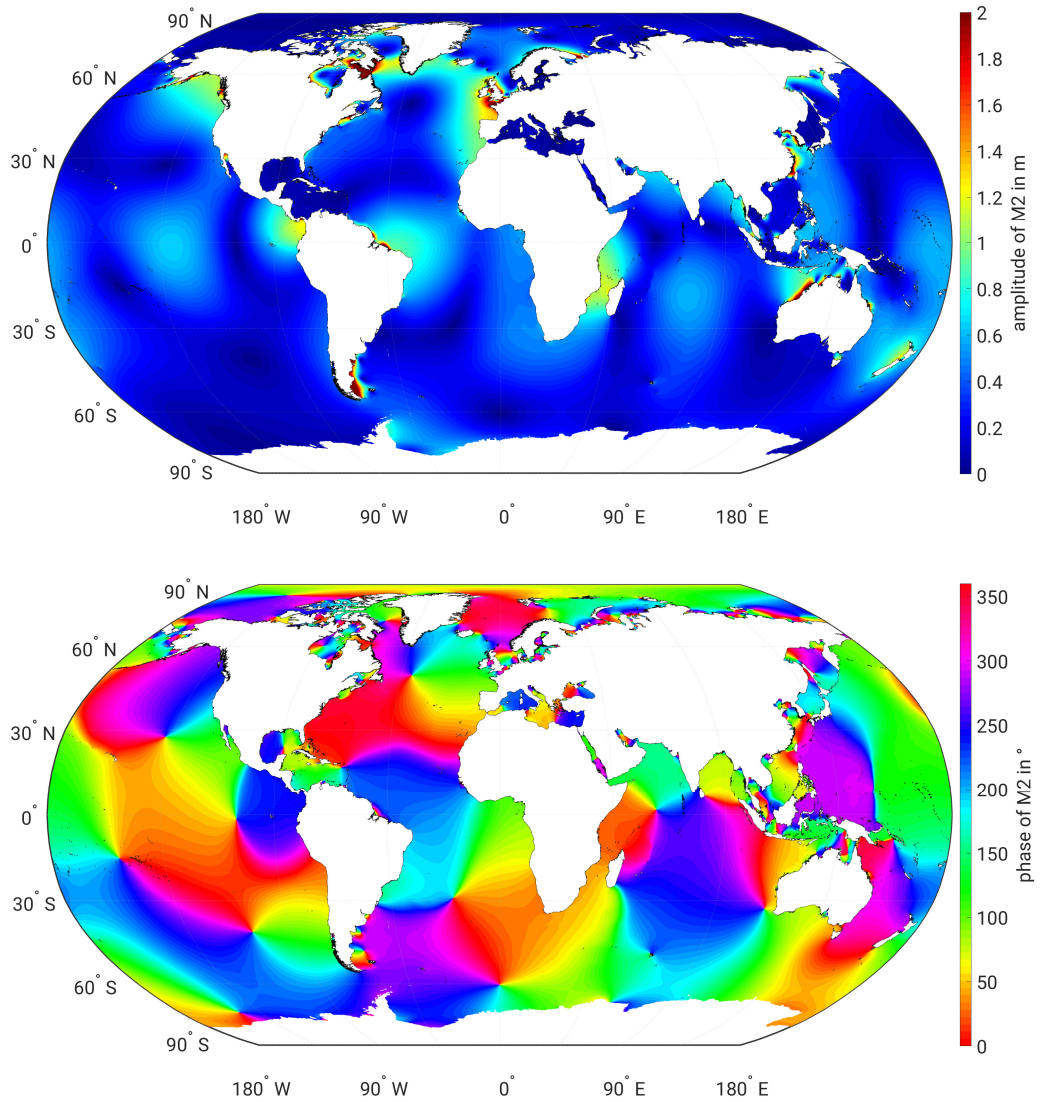
Fig. E.7. Top: Amplitudes in metres of M2 from the HAMTIDE model. The colour scale is clipped at a maximum of 2 m. Bottom: Greenwich phases in degree of M2 from the HAMTIDE model.
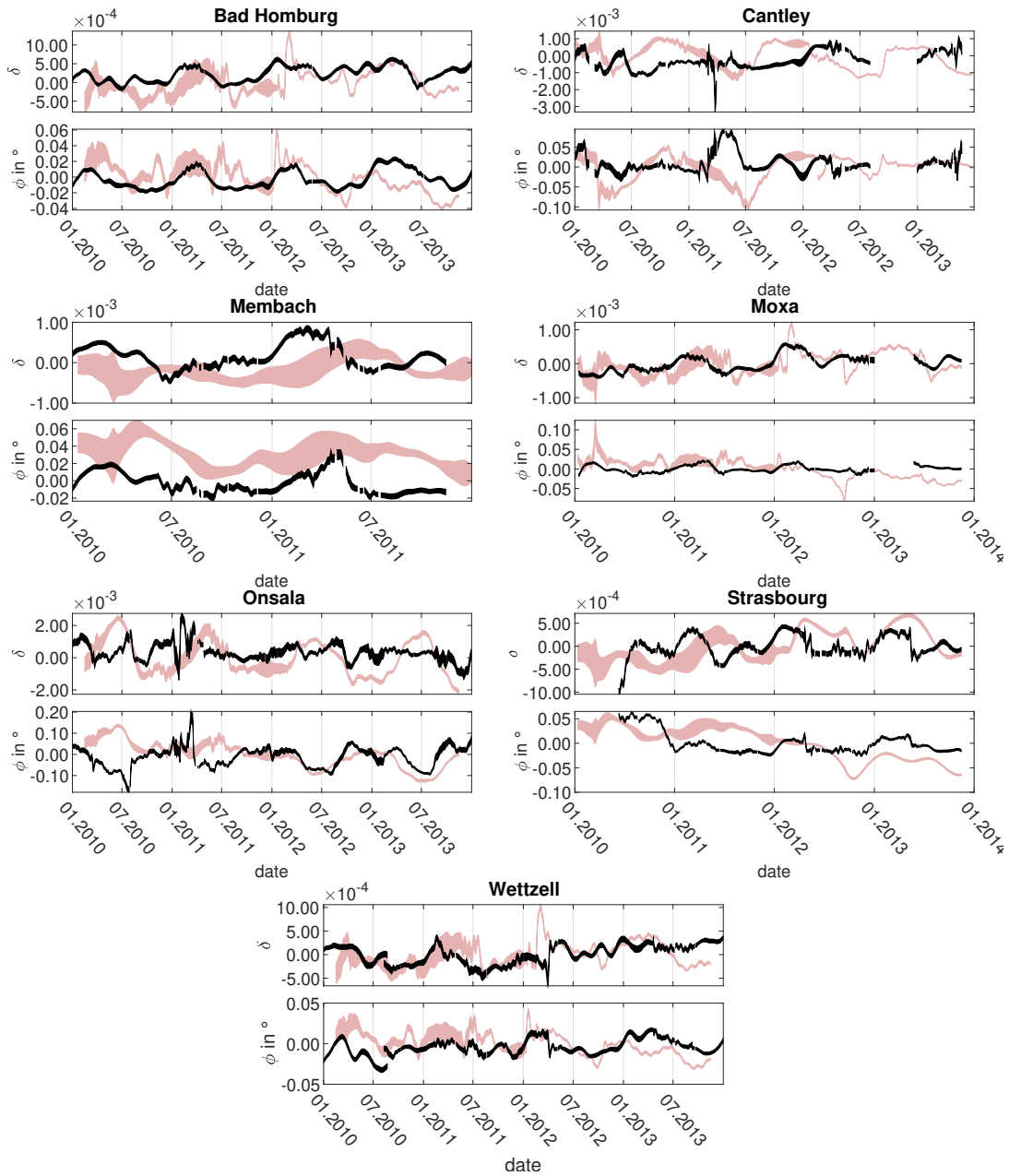
Fig. E.8. Tidal parameters of wave group M2 at BFO, Bad Homburg, Cantley, Membach, Moxa, Onsala, Strasbourg and Wettzell obtained from measurements (black) and synthetic data calculated with ARTOFS (light pink).
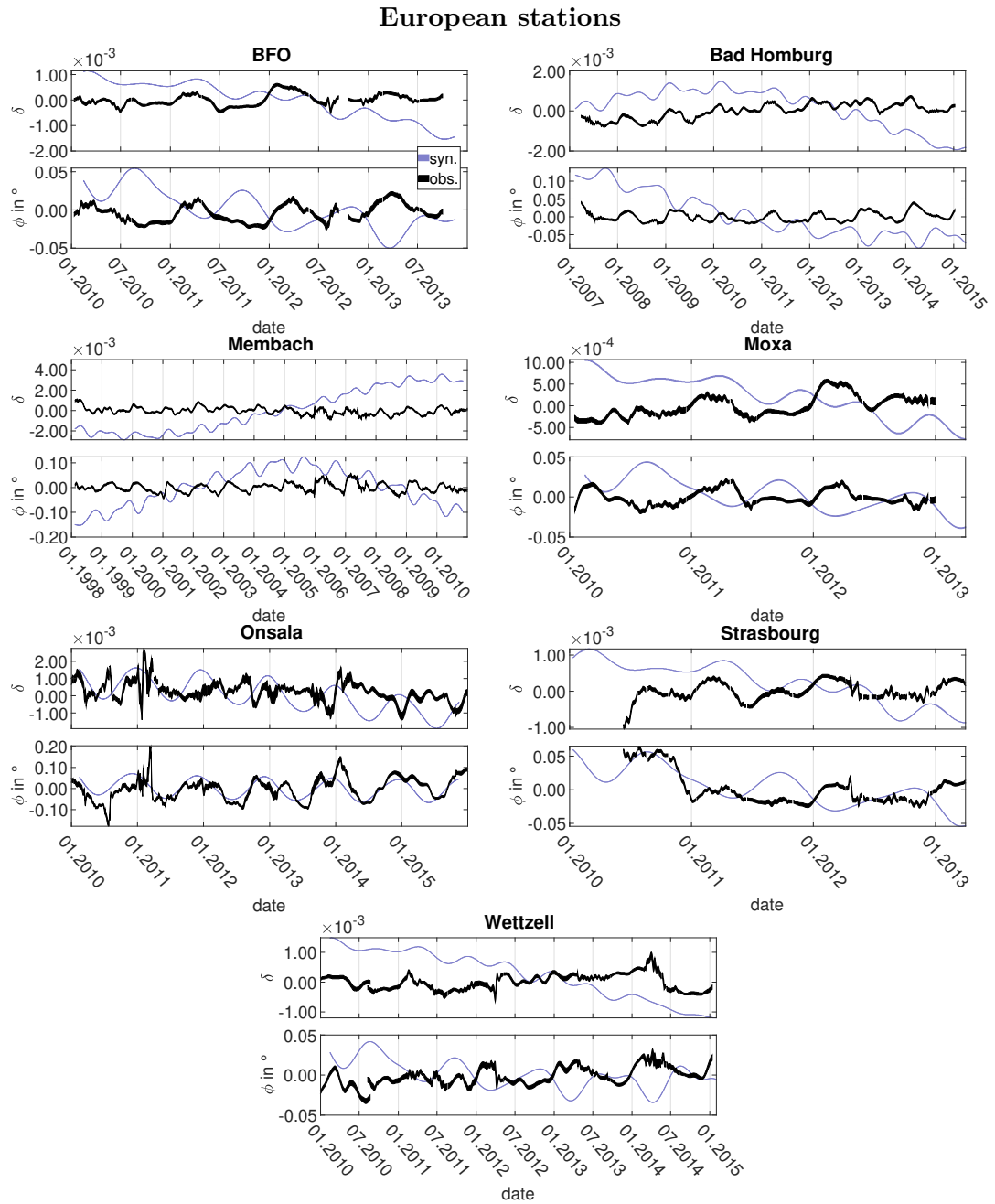
Fig. E.9. Tidal parameters (δ and ϕ) of wave group M2 at BFO, Bad Homburg, Membach, Moxa, Onsala, Strasbourg and Wettzell obtained from measurements (black) and synthetic data calculated with Stormtide (light purple).
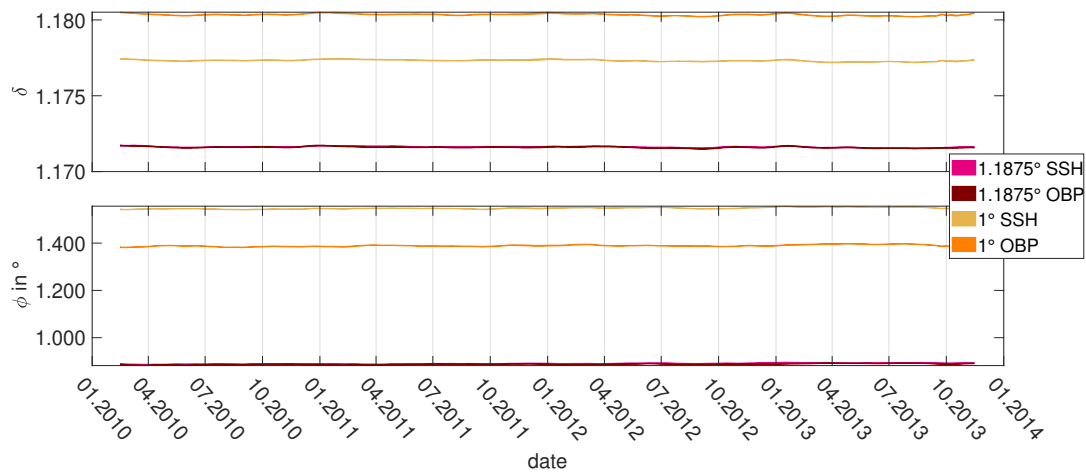
Fig. E.10. Tidal parameters of the M2 wave group obtained with the OMCT data set for the station BFO. The pink curve was obtained with the SSH data set and the dark red curve with the OBP data set of 1.875° resolution. The light orange curve was estimated from the synthetic data calculated from the 1° SSH and the orange from synthetic data calculated from the corresponding OBP. The upper panel shows the gravimetric factor and the lower panel the phase in degree.
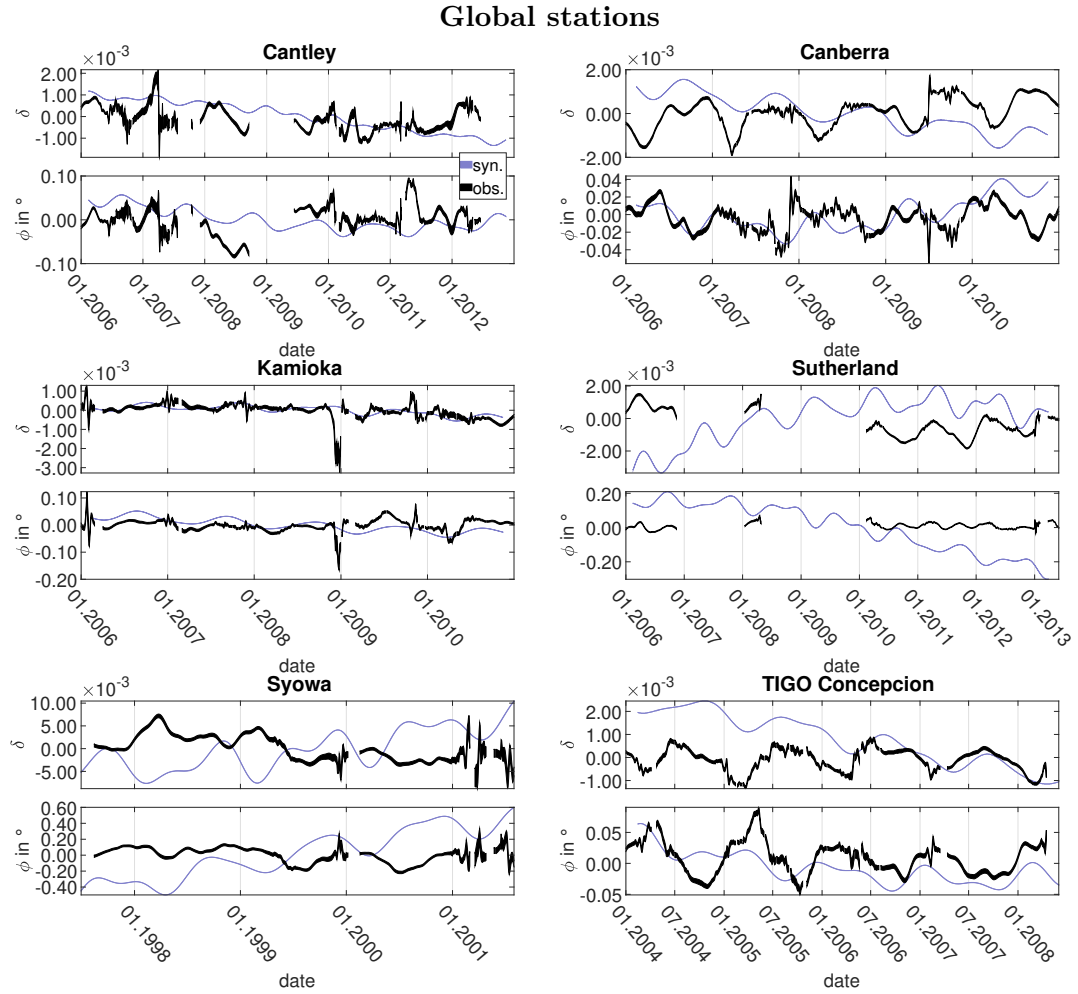
Fig. E.11. Tidal parameters (δ and ϕ) of wave group M2 at Cantley, Canberra, Kamioka, Sutherland, Syowa and TIGO Concepciòn obtained from measurements (black) and synthetic data calculated with Stormtide (light purple).

	BF		BH		CA	
	δ	$\Delta\delta$	δ	$\Delta\delta$	δ	$\Delta\delta$
ARTOFS	1.14446	0.00010	1.14888	0.00011	1.17686	0.00011
Stormtide	1.19047	$< 10^{-5}$	1.18943	$< 10^{-5}$	1.19420	$< 10^{-5}$
OMCT	1.17732	0.00002	1.17797	0.00002	1.19928	0.00002
OMCT ice	1.17826	0.00002	1.17912	0.00002	1.20051	0.00002
HGT	1.18757	0.00003	1.18858	0.00003	1.20051	0.00002
North Sea	1.16006	0.00002	1.15936	0.00003	-	-
obs.	1.18652	0.00005	1.18845	0.00005	1.20321	0.00011
	CB		KA		MB	
	δ	$\Delta\delta$	δ	$\Delta\delta$	δ	$\Delta\delta$
ARTOFS	-	-	-	-	1.14182	0.00013
Stormtide	1.18414	$< 10^{-5}$	1.18568	$< 10^{-5}$	1.18926	$< 10^{-5}$
OMCT	1.25220	0.00003	1.19769	0.00004	1.18059	0.00004
OMCT ice	1.26283	0.00003	1.19653	0.00004	1.18167	0.00004
HGT	1.17842	0.00004	1.18864	0.00005	1.18969	0.00005
North Sea	-	-	-	-	-	-
obs.	1.17868	0.00005	1.19060	0.00008	1.18784	0.00006

Table E.1. Mean values of the gravimetric factors δ of M2 and its standard deviations at the stations BFO (BF), Bad Homburg (BH), Cantley (CA), Canberra (CB), Kamioka (KA) and Membach (MB) obtained with synthetic data MWA with ARTOFS, Stormtide, two different types of OMCT data sets (see sections 5.2.2.5 and 8.2.3 for details), HGT and the North Sea model as well as MWA of the measured data sets (obs.). The mean values of the tidal parameters obtained with ARTOFS were calculated after the correction of the step (see section 8.2.1).

	MO		OS		ST	
	δ	$\Delta\delta$	δ	$\Delta\delta$	δ	$\Delta\delta$
ARTOFS	1.15569	0.00010	1.17267	0.00022	1.14300	0.00011
Stormtide	1.18984	0.00001	1.17408	0.00001	1.19121	$< 10^{-5}$
OMCT	1.17681	0.00002	1.15980	0.00021	1.17724	0.00002
OMCT ice	1.17804	0.00002	1.16533	0.00020	1.17815	0.00002
HGT	1.19953	0.00005	1.19246	0.00014	1.18827	0.00003
North Sea	1.15966	0.00003	-	-	-	-
obs.	1.18556	0.00008	1.18580/1.17873	0.00018/0.00013	1.18712	0.00023

	SU		SY		TC	
	δ	$\Delta\delta$	δ	$\Delta\delta$	δ	$\Delta\delta$
ARTOFS	-	-	-	-	-	-
Stormtide	1.16160	0.00001	1.70499	0.00003	1.17392	$< 10^{-5}$
OMCT	1.14511	0.00003	1.32076	0.00026	1.18354	0.00004
OMCT ice	1.14237	0.00003	1.31721	0.00027	1.19128	0.00004
HGT	1.16286	0.00009	1.46534	0.00050	1.14248	0.00006
North Sea	-	-	-	-	-	-
obs.	1.15704	0.00005	1.40271	0.00051	1.12482	0.00008

Table E.2. Mean values of the gravimetric factors δ of M2 and its standard deviations at the stations Moxa (MO), Onsala (OS), Strasbourg (ST), Sutherland (SU), Syowa (SY) and TIGO Concepción (TC) obtained with synthetic data MWA with ARTOFS, Stormtide, two different types of OMCT data sets (see sections 5.2.2.5 and 8.2.3 for details), HGT and the North Sea model as well as MWA of the measured data sets (obs.). For Onsala the results of the two differently preprocessed data sets from the station operators (1. values) and IGETS (2. values) (see sections 4.1.1 and 5.1 for details). The mean values of the tidal parameters obtained with ARTOFS were calculated after the correction of the step (see section 8.2.1).

	BF		BH		CA	
	ϕ in °	$\Delta\phi$ in °	ϕ in °	$\Delta\phi$ in °	ϕ in °	$\Delta\phi$ in °
ARTOFS	2.26061	0.00514	2.28897	0.00531	-0.10682	0.00537
Stormtide	2.53743	0.00014	2.57560	0.00013	-0.24316	0.00008
OMCT	1.54755	0.00099	1.49294	0.00118	-0.40988	0.00085
OMCT ice	1.68298	0.00100	1.62168	0.00119	-0.42120	0.00089
HGT	2.10109	0.00159	2.04973	0.00168	-0.27202	0.00138
North Sea	-0.07772	0.00080	-0.11590	0.00133	-	-
obs.	2.03085	0.00246	1.97525	0.00224	-0.49813	0.00522
	CB		KA		MB	
	ϕ in °	$\Delta\phi$ in °	ϕ in °	$\Delta\phi$ in °	ϕ in °	$\Delta\phi$ in °
ARTOFS	-	-	-	-	2.66410	0.00664
Stormtide	-2.37382	0.00013	0.29505	0.00009	3.30440	0.00016
OMCT	-2.67210	0.00150	1.71419	0.00177	1.66593	0.00196
OMCT ice	-2.89167	0.00153	1.89307	0.00174	1.81367	0.00193
HGT	-1.39314	0.00208	0.93557	0.00253	2.62879	0.00228
North Sea	-	-	-	-	-	-
obs.	-2.51936	0.00257	0.51708	0.00399	2.44079	0.00312

Table E.3. Mean values of the phase leads ϕ of M2 and its standard deviations at the stations BFO (BF), Bad Homburg (BH), Cantley (CA), Canberra (CB), Kamioka (KA) and Membach (MB) obtained with synthetic data MWA with ARTOFS, Stormtide, two different types of OMCT data sets (see sections 5.2.2.5 and 8.2.3 for details), HGT and the North Sea model as well as MWA of the measured data sets (obs.). The mean values of the tidal parameters obtained with ARTOFS were calculated after the correction of the step (see section 8.2.1).

	MO		OS		ST	
	ϕ in °	$\Delta\phi$ in °	ϕ in °	$\Delta\phi$ in °	ϕ in °	$\Delta\phi$ in °
ARTOFS	1.94436	0.00499	1.92493	0.01058	2.36765	0.00536
Stormtide	2.01392	0.00036	1.41734	0.00029	2.68657	0.00014
OMCT	1.23746	0.00106	-0.88544	0.01040	1.64264	0.00106
OMCT ice	1.33957	0.00106	-0.70238	0.01007	1.78533	0.00107
HGT	2.29626	0.00227	1.06531	0.00667	2.22947	0.00168
North Sea	-0.07336	0.00166	-	-	-	-
obs.	1.58303	0.00359	1.35866/1.29763	0.00881/0.00649	2.14548	0.00894

	SU		SY		TC	
	ϕ in °	$\Delta\phi$ in °	ϕ in °	$\Delta\phi$ in °	ϕ in °	$\Delta\phi$ in °
ARTOFS	-	-	-	-	-	-
Stormtide	6.37221	0.00029	9.04709	0.00104	-3.16880	0.00015
OMCT	4.42620	0.00131	-1.60224	0.01124	-1.81613	0.00179
OMCT ice	4.66734	0.00138	-2.12429	0.01159	-2.16986	0.00185
HGT	6.77866	0.00470	5.67862	0.01952	-3.00423	0.00303
North Sea	-	-	-	-	-	-
obs.	5.24763	0.00254	0.83320	0.02098	-2.30433	0.00389

Table E.4. Mean values of the phase leads ϕ of M2 and its standard deviations at the stations Moxa (MO), Onsala (OS), Strasbourg (ST), Sutherland (SU), Syowa (SY) and TIGO Concepción (TC) obtained with synthetic data MWA with ARTOFS, Stormtide, two different types of OMCT data sets (see sections 5.2.2.5 and 8.2.3 for details), HGT and the North Sea model as well as MWA of the measured data sets (obs.). For Onsala the results of the two differently preprocessed data sets from the station operators (1. values) and IGETS (2. values) (see section 4.1.1 and 5.1 for details). The mean values of the tidal parameters obtained with ARTOFS were calculated after the correction of the step (see section 8.2.1).

	δ	$\Delta\delta$	ϕ in °	$\Delta\phi$ in °
ARTOFS	1.15577	0.00008	1.74692	0.00417
Stormtide	1.18622	$< 10^{-5}$	1.81730	0.00010
OMCT	1.17660	0.00002	1.09301	0.00084
OMCT ice	1.17775	0.00002	1.18652	0.00083
HGT	1.18565	0.00003	1.55920	0.00126
North Sea	-	-	-	-
obs.	1.18545/1.18382	0.00005/0.00005	1.43437/1.41430	0.00249/0.00263

Table E.5. Mean values of the gravimetric factors δ and phase leads ϕ of M2 and their standard deviations at Wettzell obtained with synthetic data MWA with ARTOFS, Stormtide, two different types of OMCT data sets (see sections 5.2.2.5 and 8.2.3 for details), HGT and the North Sea model as well as MWA of the measured data sets. The data sets (obs.) of the two SGs CD029/CD030 (see section 5.1 for details) are given separately. The mean values of the tidal parameters obtained with ARTOFS were calculated after the correction of the step (see section 8.2.1).
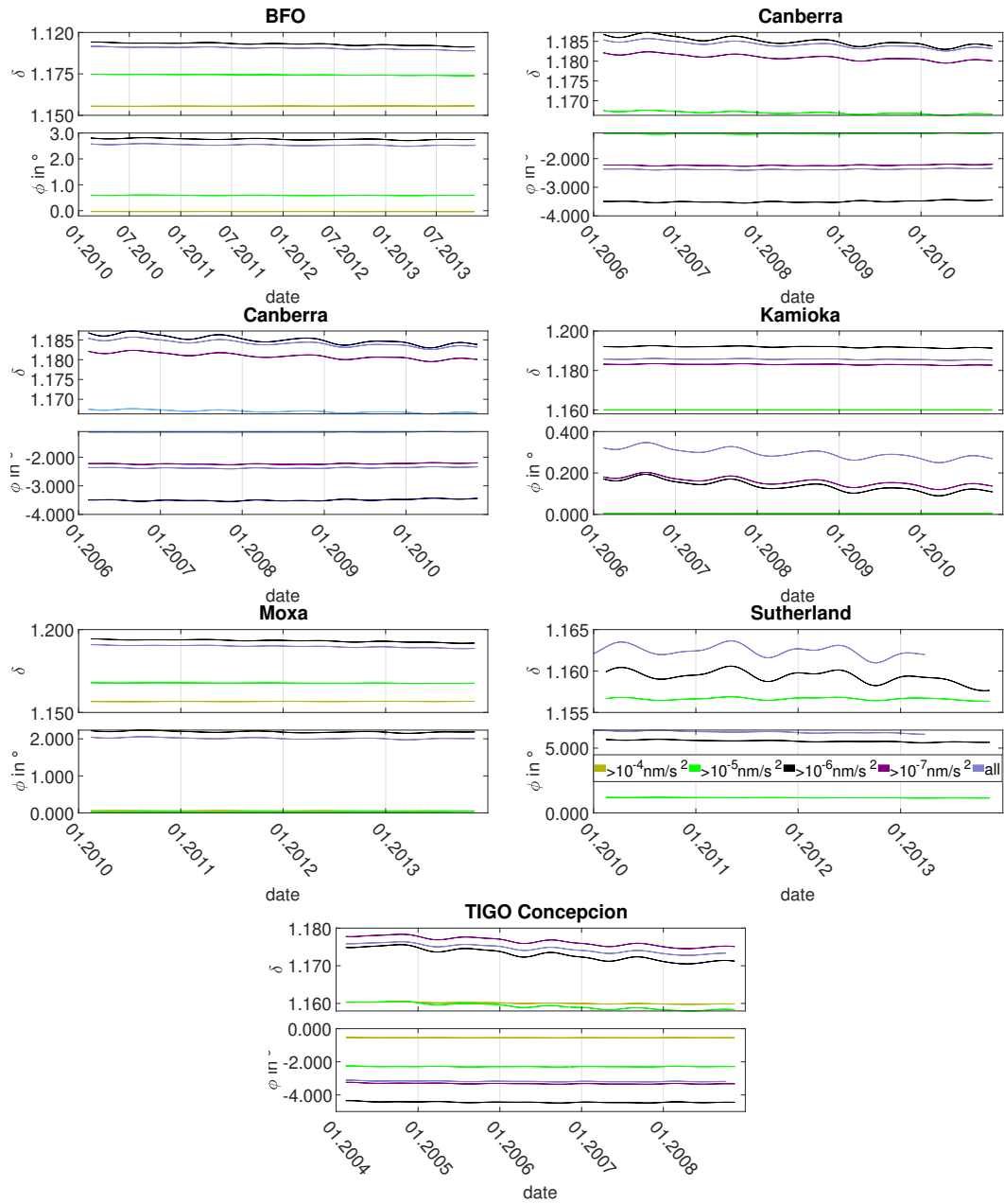
Fig. E.12. Results of the synthetic data MWA based on Stormtide grid points exceeding the threshold $10^{-4}\frac{\text{nm}}{\text{s}^2}$ in yellow, $10^{-5}\frac{\text{nm}}{\text{s}^2}$ in green, $10^{-6}\frac{\text{nm}}{\text{s}^2}$ in black and $10^{-7}\frac{\text{nm}}{\text{s}^2}$ in purple as well as the results for which the complete model was used in blue at the stations BFO, Cantley, Canberra, Kamioka, Moxa, Sutherland and TIGO Concepción.

Appendix F.

Accuracy of the loading calculation

In this chapter the accuracy of the loading calculation is studied.

F.1. Influence of the different quantities used in the loading calculation

The loading calculation is based on equation 2.13. It uses besides the SSH, the density, Green's functions and the area around the model grid points. The influence of assumptions made for these quantities on the resulting tidal parameters is investigated in this section.

F.1.1. Influence of density

In equation 2.13 the density is assumed to be constant. This is of course not the case for the real oceans. In a first step it is tested how much a constant but different density of $\rho = 1025 \ \frac{\text{kg}}{\text{m}^3}$ changes the tidal parameters compared to the value of $\rho = 1031 \ \frac{\text{kg}}{\text{m}^3}$ which was used for the investigations in chapters 7 to 9. These values were estimated from density distributions available for ARTOFS. A constant value for the density will not cause variations of the tidal parameters, but will probably show the maximal effect that can be reached by density, because density variations cannot cancel out each other in this case. The results of the synthetic data MWA with ARTOFS for both density values are given in Fig. F.1. As described in section 8.2.1, tidal parameters obtained from synthetic data MWA with ARTOFS contain a step. In this case, it is not corrected as only the offsets of the two curves are compared. There is no significant difference in the gravimetric factors. The difference in the phase is about $0.015°$, which is close to the amplitude of the phase variation. However, this is the maximal effect that occurs due to density variations. The effect of a varying density would most likely be smaller. Additionally, in this special case, the density change mainly influences the phase; in other cases the influence probably distributes equally on both tidal parameters. This depends on how the M2 loading signal superimposes with the M2 solid Earth tide, and will therefore change with time if the density varies.

The synthetic data MWA with the OBP from OMCT in section 8.2.3.1 and with the
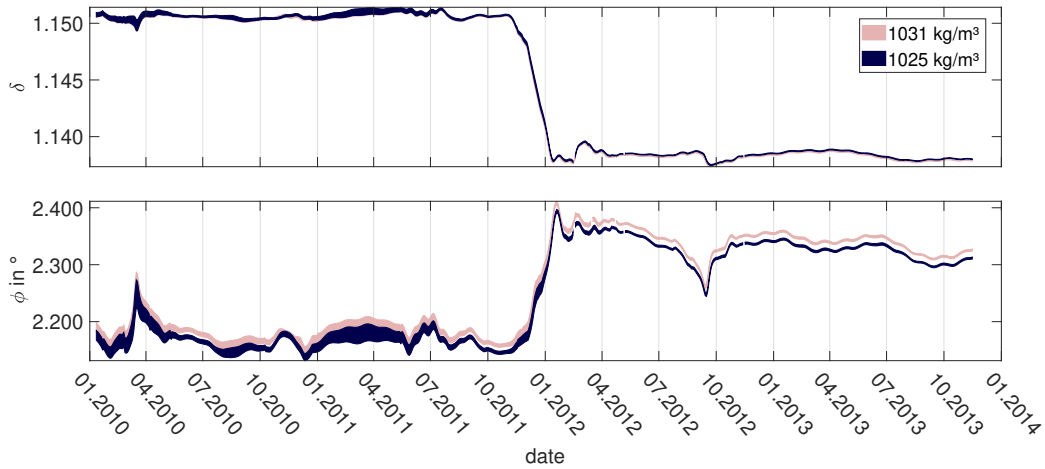
Fig. F.1. M2 tidal parameters obtained with synthetic data MWA for ARTOFS with a density of $\rho = 1025 \; \frac{\text{kg}}{\text{m}^3}$ shown in dark blue and $\rho = 1031 \; \frac{\text{kg}}{\text{m}^3}$ shown in light pink.

nonsteric and total SSH from HGT in section 8.2.4.1 also show that density variations have only a minor influence on the tidal parameters as they do not cause variations in the same order of magnitude as the variations of M2.

F.1.2. Influence of Green's functions

The Green's functions used in chapters 7 to 9 were taken from the publication by Na and Baek (2011). They are given for certain distances and they are interpolated to the required distances. The influence of the interpolation is studied in the first part of this section. In the second part the results are compared for the usage of different Green's functions as they depend on the Earth model they are based on. Both effects cannot cause variations of the tidal parameters.

F.1.2.1. Interpolation of Green's functions

As mentioned above, the Green's functions cannot produce variations of the tidal parameters because the Green's functions are not time-dependent. However, if the Green's functions are inaccurate they change how gravity contributions from different distances superimpose. Therefore, the accuracy of the interpolation of the Green's functions is estimated. It is assumed that the table given by Na and Baek (2011) interpolated to distances every $10^{-4}\,^\circ$, as is done in the loading calculation, is the correct description of the distance dependence of the Green's functions. Then every second value of the original (not interpolated) Green's functions is skipped and also interpolated to values every $10^{-4}\,^\circ$. The difference between both is an estimation made by interpolating the Green's functions. It is given in percent in Fig. F.2 (left) for linear interpolation and shape-preserving piecewise cubic interpolation (pchip),
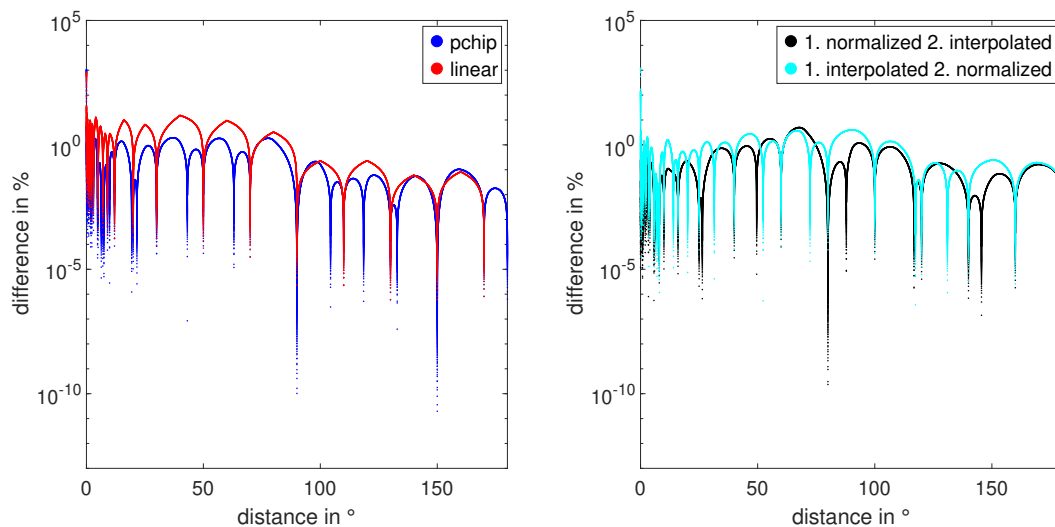
Fig. F.2. Left: Difference of the Green's functions over the distance between an SG and the position of the mass. Green's functions interpolated from only half of the values given by Na and Baek (2011) and interpolated from all values, both to distances every 10^{-4} °, for linear (red) and and shape-preserving piecewise cubic interpolation (pchip, blue). Right: Difference obtained with the same method, but for other Green's functions (H. Wang et al., 2012), which where first normalised and afterwards interpolated (black) and vice versa (cyan).

both based on the corresponding Matlab functions. The latter interpolation method has the advantage that it, in contrast to spline interpolation, avoids 'overshooting'.

For both cases very large differences in the range of 800% to 1000% occur for small distances (smaller than 0.1°). This indicates that the loading calculation for stations close to the coast, for example at Onsala, where Green's functions for short distances are needed, is inaccurate. However, the results in section 8.3 indicate that the short distances can have a significant influence on the variation of the tidal parameters, but they do not dominate the observed signal. The difference becomes smaller with increasing distance, but for the linear interpolation it is still about 7.5% at 62° distance. With the shape-preserving interpolation the difference is for distances larger than 0.2° smaller than 4%. Therefore, this interpolation was used for the loading calculations in chapters 7 to 9. Only certain grid points are wrong by about 4% and summed with the contributions of other grid points having a more precise Green's function. However, the difference of 4% is the maximum error for the Green's functions of those distances necessary for the calculation at most stations. This would mean that the loading signal was wrong by 4% as well. The influence on the tidal parameters will be an order of magnitude lower as the tidal parameters are estimated relative to the exciting tidal acceleration which is an order of magnitude higher than the loading. The influence of the Green's functions is further investigated in section F.2.

Another influence that was tested is the normalisation of the Green's functions (e.g. Jentzsch 1997; H. Wang et al. 2012) with distance d and Earth radius r ($10^{17}rd$) and its influence on the interpolation. On the right side of Fig. F.2 the differences which were obtained with the same method as described above, but in one case with Green's functions that were normalised before the interpolation, and in the second case vice versa. For short distances up to 12° the differences are by a factor of ten lower for the normalised than for the unnormalised Green's functions. Only for 67° the difference for the normalised Green's functions is about 1% larger than for the unnormalised Green's functions. The largest differences usually occur (except for the differences at very short distances) in the inflexion points of the distance-dependent Green's function curves. For the normalised Green's functions, at this point the gradient does not change as strongly as for the unnormalised Green's functions. Additionally, it is of advantage that the inflexion point is at larger distances where the Green's functions are small and the errors in percent do not represent large errors in absolute values. Therefore, in the loading calculation the Green's functions are normalised before the interpolation and the normalisation is removed afterwards.

The differences in the resulting tidal parameters of both effects, the normalisation and the interpolation method, are shown in Fig. F.3 in section F.1.2.2. The difference is about $2 \cdot 10^{-3}$ in the gravimetric factor and about 0.07° in the phase. There is no influence on the variations of the tidal parameters.

F.1.2.2. Green's functions based on different Earth models

As mentioned above, the Green's functions depend on the Earth model upon which their calculation is based. As this does not change with time, different Green's functions will not influence the variations of the tidal parameters, but they are relevant for the stationary part of the tidal parameters. Therefore, synthetic data MWA for Stormtide was made with the loading time series calculated for different Green's functions (H. Wang et al., 2012). The results are shown in Fig. F.3. The difference of the stationary parts is about $2 \cdot 10^{-3}$ in the gravimetric factor and about 0.025° in the phase. These values are regarded as the uncertainty due to the unknown properties of the solid Earth. There is no difference in the variation of the tidal parameters. As discussed in appendix B, there is no reason to regard an Earth model as a more realistic description of the solid Earth than another model. As some calculations were already made with the Na and Baek (2011) Green's functions, I decided to continue using them.

F.1.3. Influence of the approximation of model cell area

Another effect that influences the loading calculations is the calculation of the areas around the grid points. The areas around the grid points are approximated as rectangles (see section 3.2). They can overlap or they can have gaps between each other. The sum of the areas can therefore differ from the area the ocean model covers. The differences in the areas would only influence the stationary part of the tidal parameters.

The model area was calculated by summing the areas defined by the model grid points
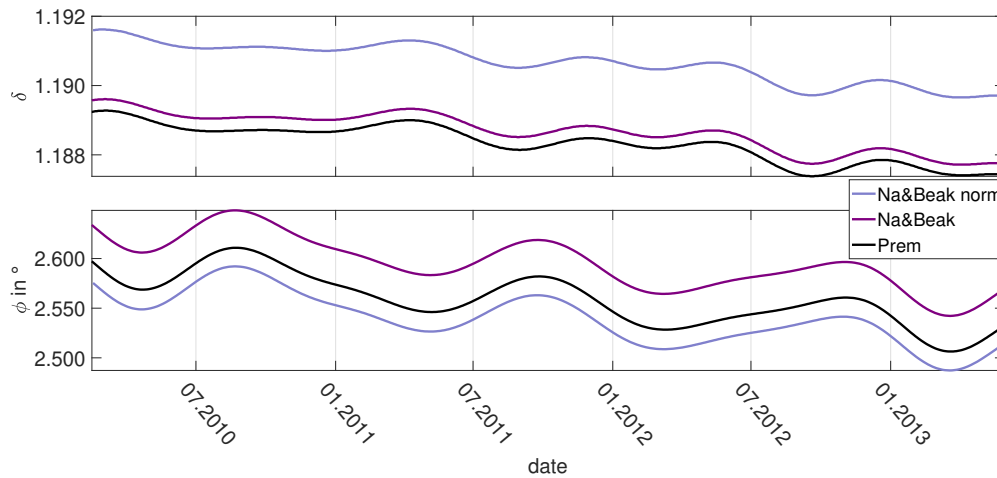
Fig. F.3. Tidal parameters of the M2 wave group (gravimetric factor δ, top; phase ϕ in degree, bottom) obtained from synthetic data MWA with Stormtide for the station BFO. The blue curve is obtained with the standard loading calculation described in section 3.2 (Green's function, Na and Baek 2011). The black curve is obtained with the same loading calculation procedure but under usage of PREM Green's functions (H. Wang et al., 2012). The purple curve is obtained with the Na and Baek (2011) Green's functions but linearly interpolated and not normalised before the interpolation (see section F.1.2.1). Please note that the line thickness is higher than the standard deviation for better visibility.

and compared to the approximated area. This is done exemplarily for Stormtide. Large differences can occur in particular for ARTOFS because it has a curvilinear grid, but as it is restricted to the Atlantic anyway, the stationary part of the tidal parameters is not interpreted.

Before the summation of the approximated areas, the half of each grid cell at minimum and maximum latitude of the grid has to be subtracted, as this is of course not part of the model grid. The area of the "true" Stormtide grid is $5.046 \cdot 10^8$ km^2 and the approximated area $5.048 \cdot 10^8$ km^2. The difference between both is about 0.04%. Thus, the loading contribution is wrong by 0.04%. As the influence on the tidal parameters will again be an order of magnitude lower (see section F.1.2.1), this is insignificant with respect to the differences discussed in, for example, section 8.2.6.2.

F.2. Comparison with SPOTL

As described in section 3.2, the loading calculation used in this thesis neglects some effects. They are implemented in higher developed programs like 'Some Programs for Ocean-Tide Loading' (SPOTL). In SPOTL, the intersection of model grid cells by coast lines, the extent of the grid cells (interpolation of SSH and Green's functions over the extent of the grid

cells) and the height of the gravimeter station above the sea level is taken into account. In order to ensure that the neglect of these effects does not affect the results significantly, the results obtained with the simplified loading calculations are compared to results obtained with SPOTL. As the computation time with SPOTL is significantly longer, this was tested for only two of the models: OMCT and HGT.

Olsson et al. (2009) studied the influence of the grid resolution of a disc load on the resulting gravity. The gravity value decreases rapidly for grids coarser than 1°. Of course, this also depends on the distance of the SG station from the coast, but as OMCT has a 1° resolution (or coarser, respectively), this is probably of significance for stations close to the coastline. HGT is used because it is the global model with the finest grid. I expect the results of the other models to lie between the results from OMCT and HGT. Additionally, the Green's functions are computed for the required distances in SPOTL (Agnew, 2012). This is more accurate than the interpolation in the simplified loading calculation. The comparison between SPOTL and the simplified version will show whether the effect mentioned above has a significant influence on the results.

For OMCT the calculation time of SPOTL was relatively short due to fewer grid points in the coarser grid. Even in this case the computation time for about 3 years of loading time series on a standard desktop PC increases from about 10 to 20 min (simplified loading calculation) to about 10 to 12 hours (SPOTL). Nevertheless, these calculations were done for 9 of the stations used in chapter 8.

For HGT, it was necessary to interpolate the model grid to equidistant grid points, because this is required by SPOTL. The smallest distance of the model grid points, 0.03°, was used for the interpolation. The difference between the loading time series, both calculated with the simplified loading calculation, on the original grid and the interpolated grid is about $0.01 \, \frac{\text{nm}}{\text{s}^2}$. For every HGT time step, the SSH values were interpolated to the equidistant grid before the loading calculation with SPOTL. The calculation of a loading time series for HGT of six months length takes about three weeks with SPOTL. The simplified calculation needs only about a day for several years of HGT data. Therefore, the SPOTL calculation was done for only 2 stations for 6 months of data. The station BFO was used because it is far from the coast, whereas Onsala is very close to the coast. The results are shown in Fig. F.6.

In Figs. F.4 and F.5 the results for OMCT are shown. The plots, showing also the stationary part of the tidal parameters are given in Figs. F.8 and F.9 at the end of the appendix. For most of the stations there are changes in the variations of the tidal parameters which are smaller than the standard deviation. The only exception is Onsala for which the variations of the tidal parameters are three times larger than the variations obtained with the simplified loading calculation. For Onsala, taking into account the effects of the coast line, the extension of the grid cells and the accuracy of the Green's functions' interpolation, is important. Of course, it cannot be distinguished whether one of those effects is of higher significance than the others. However, the variations of the tidal parameters were already too large for the simplified calculation (see section 8.2.3.2); with SPOTL the variations are even larger. This shows that the discussed effects neglected in the simplified loading calculation have a significant influence at Onsala. The variations of the tidal parameters
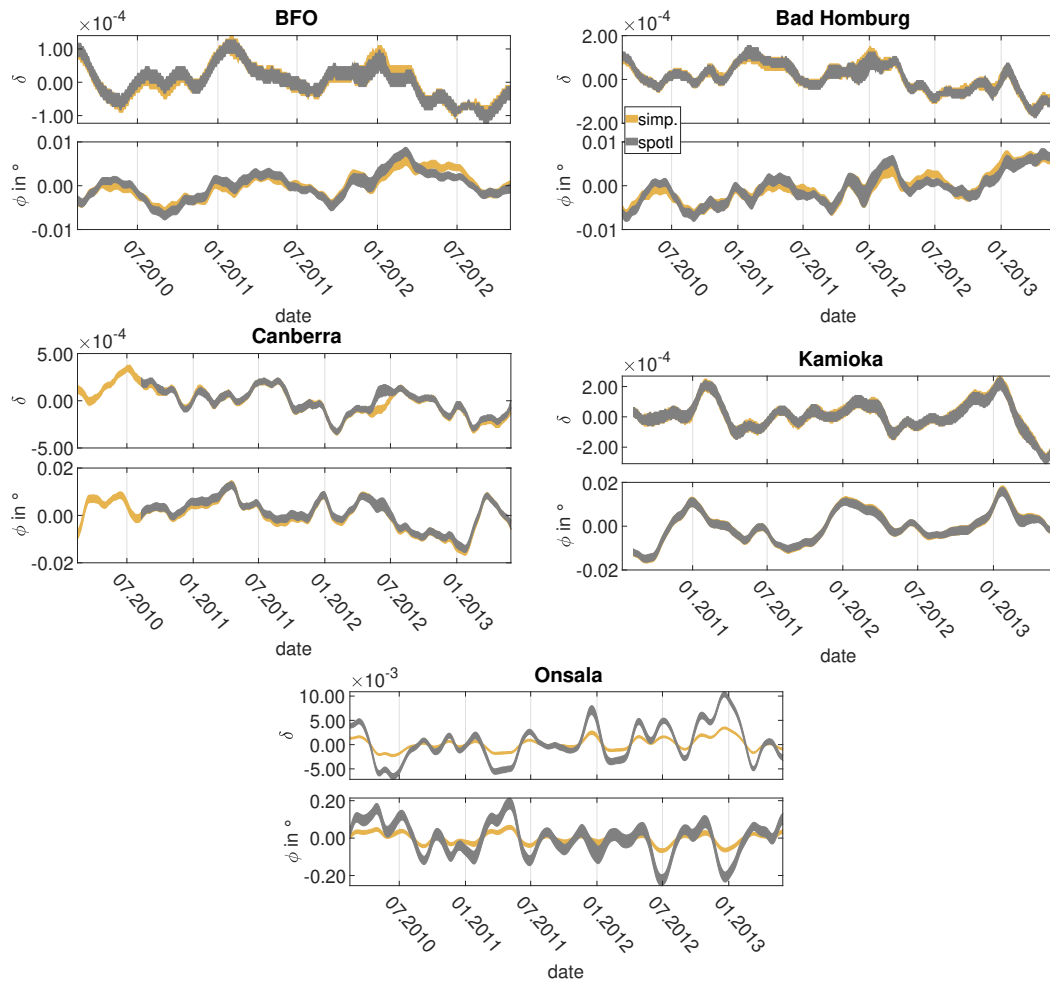
Fig. F.4. Variations of the tidal parameters of wave group M2 (gravimetric factor δ, top; phase ϕ in degree, bottom) at BFO, Bad Homburg, Canberra, Kamioka and Onsala obtained with synthetic data MWA for OMCT loading calculated with the simplified version (light orange) and with SPOTL (grey).

that are too large have to be caused by the OMCT model.

The differences in the stationary part (see Figs. F.8 and F.9) are significant with respect to the standard deviation. There is a tendency that stations which are close to the coast show larger differences in the results obtained for both loading calculation versions, e.g. Onsala and Syowa, whereas the differences are smaller at, for example, BFO and Wettzell. The calculation with SPOTL does not necessarily result in larger stationary parts of the tidal parameters. For the Central European stations, BFO, Bad Homburg and Wettzell as well as Canberra and Syowa the gravimetric factors are larger and the phases are smaller. At TIGO Concepción it is vice versa. Both parameters increase with the SPOTL calculation
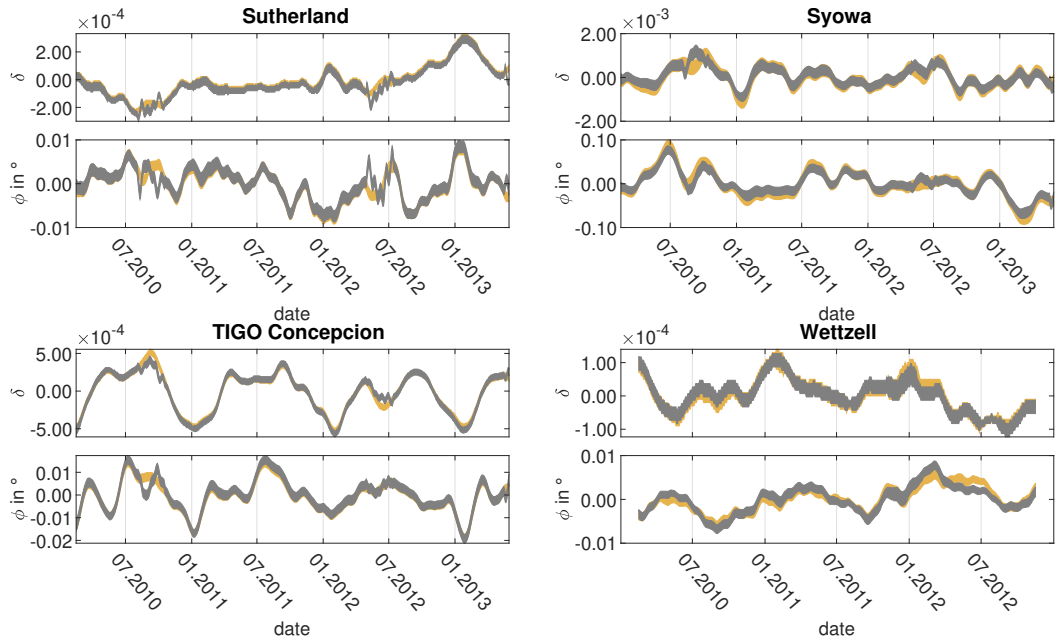
Fig. F.5. Variations of the tidal parameters of wave group M2 (gravimetric factor δ, top; phase ϕ in degree, bottom) at Sutherland, Syowa, TIGO Concepción and Wettzell obtained with synthetic data MWA for OMCT loading calculated with the simplified version (light orange) and with SPOTL (grey).

at Kamioka and Onsala, whereas the parameters decrease at Sutherland. As the main focus of this thesis is not on the stationary part of the tidal parameters, the causes for this observation are not studied further.

For HGT the results are given in Fig. F.6. For Onsala there is no significant difference in the tidal parameters for both loading calculation versions. This indicates that the differences which were obtained for OMCT are caused by the coarse OMCT grid. At BFO the variations do not change significantly, but there is a significant difference in the stationary part of the gravimetric factor of about $4.8 \cdot 10^{-4}$. There are several possible causes, but this issue was not investigated further.

These results show that the effects that were neglected in the simplified loading calculation do not influence the AVM2. For the stationary part, as for example discussed in section 8.2.6.2, they have to be considered.

F.3. Influence of interpolation of OMCT data sets to hourly values

As mentioned in section 8.2.3.1, the time axis of the OMCT SSH has to be interpolated to hourly values. Therefore, the influence of the interpolation on the resulting tidal parameters
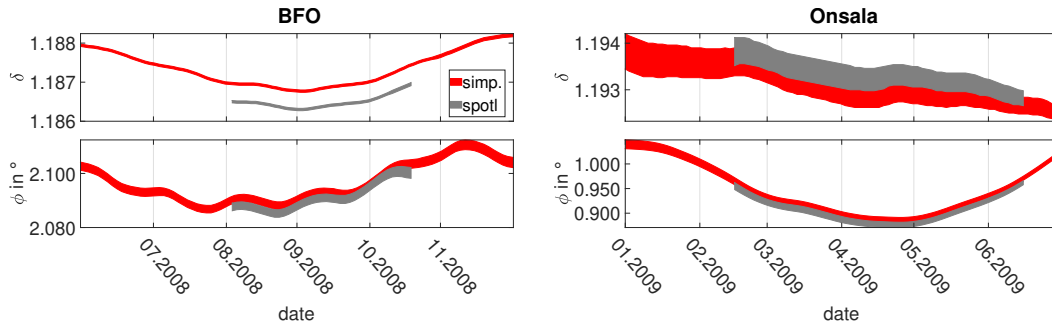
Fig. F.6. Tidal parameters of wave group M2 (gravimetric factor δ, top; phase ϕ in degree, bottom) at BFO and Onsala obtained with synthetic data MWA for HGT loading calculated with the simplified version (red) and with SPOTL (grey).

is estimated. The amplitudes and phases of M2 and the annual variation from Stormtide are used for calculating a loading time series with 2 h sampling. Then, this loading time series is interpolated to hourly values and analysed in a synthetic data MWA. The resulting tidal parameters are compared to the results of the synthetic data MWA for which the loading calculation was based on hourly Stormtide values. This comparison is shown in Fig. F.7. The stationary part of the gravimetric factors differs by $2.5 \cdot 10^{-3}$. There is no difference in the stationary part of the phase. The difference does not necessarily have to show up only in one of the tidal parameters. In another test a synthetic data MWA with Stormtide data calculated for 3 h sampling, interpolated to hourly values, was used. The difference between these results and the stationary part of the tidal parameters obtained with the hourly loading time series was $\delta = 1.7 \cdot 10^{-3}$ and $\phi = 0.14°$. This shows that the lower stationary tidal parameters obtained with OMCT (see sections 8.2.3.2 and 8.2.6.2) are partly caused by the interpolation.

There are only very small differences in the temporal variation of the tidal parameters. For the case shown in Fig. F.7 the variation of the phase obtained with the interpolated data set is significantly smaller with respect to the standard deviation. However, the difference is two orders of magnitude lower than the AVM2 which is far beyond the level of accuracy on which the AVM2 is discussed.
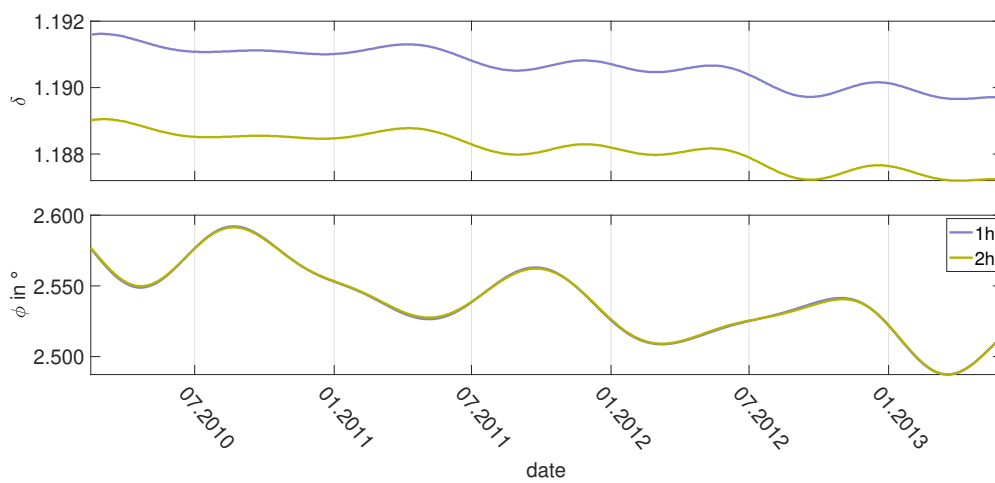
Fig. F.7. Tidal parameters of the M2 wave group (gravimetric factor δ, top; phase ϕ in degree, bottom) obtained from synthetic data MWA with Stormtide for the station BFO. The blue curve is obtained with a loading time series calculated for 1 h sampling. The yellow curve is obtained with a loading time series calculated for 2 h sampling and interpolated to hourly values. Please note that the line thickness is higher than the standard deviation for better visibility.
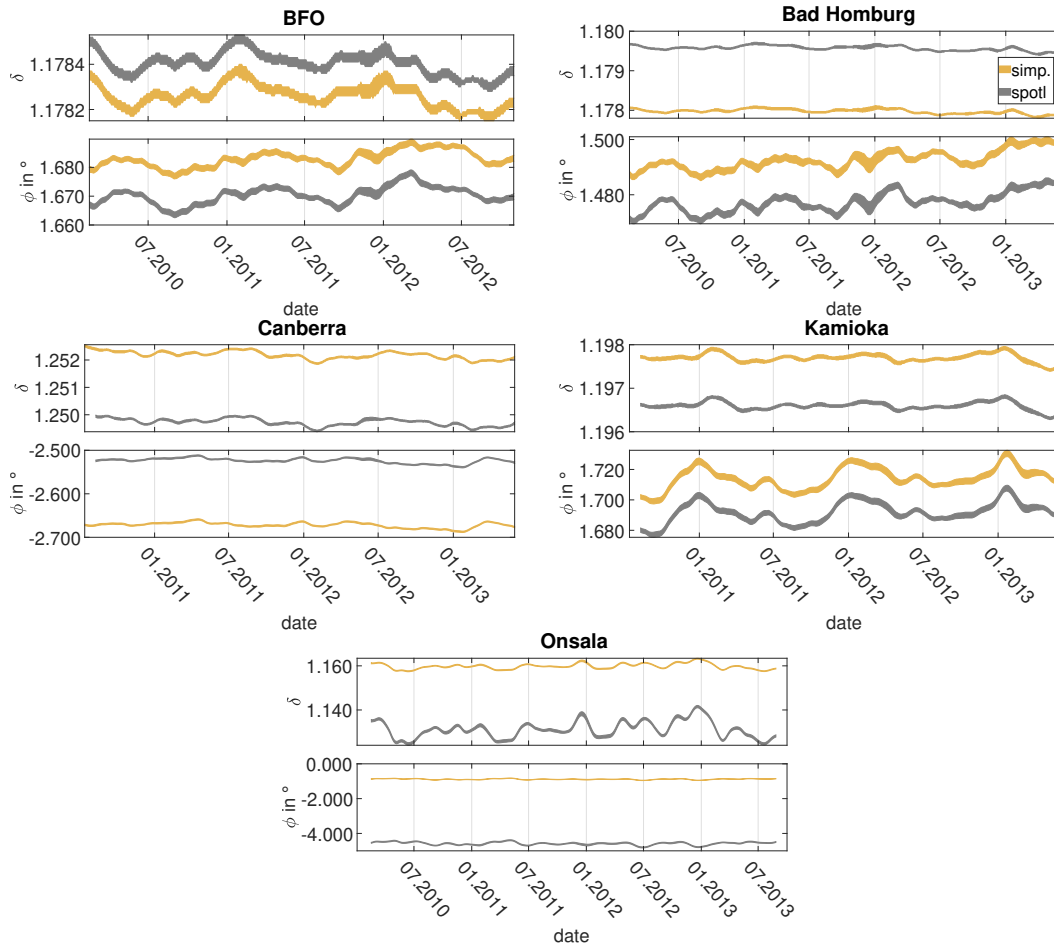
Fig. F.8. Tidal parameters of wave group M2 (gravimetric factor δ, top; phase ϕ in degree, bottom) at BFO, Bad Homburg, Canberra, Kamioka and Onsala obtained with synthetic data MWA for OMCT loading calculated with the simplified version (light orange) and with SPOTL (grey).

Fig. F.9. Tidal parameters of wave group M2 (gravimetric factor δ, top; phase ϕ in degree, bottom) at Sutherland, Syowa, TIGO Concepción and Wettzell obtained with synthetic data MWA for OMCT loading calculated with the simplified version (light orange) and with SPOTL (grey).